AN INVESTIGATION OF THE EFFECTS OF HIGH INTENSITY

IMPULSE LOADS ON SIMPLY SUPPORTED

REINFORCED CONCRETE BEAMS

By

JAMES NELSON INGRAM

Bachelor of Aerospace Engineering
The University of Kansas
Lawrence, Kansas
1966

Master of Science
The University of Kansas
Lawrence, Kansas
1970

Submitted to the Faculty of the Graduate College
of the Oklahoma State University
in partial fulfillment of the requirements
for the Degree of
DOCTOR OF PHILOSOPHY
July, 1976

AN INVESTIGATION OF THE EFFECTS OF HIGH INTENSITY

IMPULSE LOADS ON SIMPLY SUPPORTED

REINFORCED CONCRETE BEAMS

Thesis Approved:

Thesis Adviser

John E. Floyd

Donald E. Boyd

Dean of the Graduate College

964176

ii

ACKNOWLEDGMENTS

TABLE OF CONTENTS

LIST OF TABLES

LIST OF FIGURES

ix

NOMENCLATURE

A	acceleration, in./sec^2
A_s	tensile steel area, in.^{2}
b	beam width, in.
d	effective depth of tensile steel, in.
E	Young's modulus, psi
EI	beam flexural stiffness, lb-in.^{2}
f'_c	static concrete ultimate strength, psi
f'_{DC}	dynamic concrete ultimate strength, psi
f_{Dy}	steel yield stress under large strain rates, psi
f_y	steel yield stress under static loading, psi
g	unit of gravitational acceleration, 386 in./sec^2
i	total impulse, lb-sec
I	impulse per unit area, psi-ms
KE	kinetic energy, lb-in.
L	beam span, in.
m	beam mass per unit length, lb-sec^2/in.^{2}
ms	time in millisecond units, sec/1000
M	beam bending moment, lb-in.
M_b	beam mass, lb-sec^2/in.
M_y	beam yield moment, lb-in.
M'_u	static ultimate moment, lb-in.
$M'_u(D)$	static ultimate bending moment for damaged beam, lb-in.

$M_u'(T)$ theoretical ultimate bending moment, lb-in.

P_o peak reflected pressure, psi

P_{ult} beam static failure load

R_m maximum member resistance, lb.

t time, ms

t_d pressure loading duration, ms

T period of motion, ms/cycle

$T\emptyset$ tabulated data reference time

w weight of beam per unit length, lb/in.

W_p work performed on beams in forcing them from the yield to the failure displacement, kip-in.

X_G vertical distance between steel and concrete strain gages, in.

α ratio of dynamic to static ultimate compressive strength, f_{DC}'/f_C'

δ beam load point displacement during static load test, in.

δ_{max} load point displacement at beam failure, in.

δ_p plastic load point displacement, $_{max} - _y$, in.

δ_y maximum elastic load point displacement, in.

ε strain, in./in.

$\dot{\varepsilon}$ strain rate, in./in./sec

ε_C' static ultimate concrete strain, in./in.

ε_{DC}' ultimate concrete strain under dynamic loads, in./in.

μ ductility, ratio of maximum plastic to maximum elastic displacement

μ micro, 10^{-6} (unit prefix)

ρ steel reinforcing ratio, $A_s/(bd)$

ϕ curvature, rad/in.

CHAPTER I

INTRODUCTION

The development of analytical methods to predict survivability of complex structures has been enhanced by the digital computer. When accuracy of weapon placement was uncertain, the need for accurate determination of structural survivability to a single weapon was hardly justified when one considered possible weapon placement. However, with sophisticated weaponry, not only the size of the weapon but also its placement may be accurately specified. Furthermore, it is likely the impulse produced by the weapon will be due to high pressure over a small time increment, typical of chemical explosions.

In recent years considerable data has been developed on the response of complex structures to nuclear blast loading. A significant characteristic of the loading is the relatively large duration of the loading, as compared with fundamental frequencies of the structure. Furthermore, the nuclear blast can engulf the total structure. A chemical explosion, on the other hand, has a limited zone of influence and may be directed at a single critical structural member. Although the damage produced by the chemical explosive is very localized, the subsequent total structural damage may be as severe, by causing the failure of a critical structural member. This study is focused on chemical explosions, and the resulting structural damage to reinforced concrete beams.

1

To properly evaluate the survivability of a structure subjected to chemical explosions, one must study the survivability of the structural elements and the nature and location of the blast. Although a structure may survive the detonation of a weapon at the center of a wall or floor slab, the structure might collapse if the same weapon were detonated near a girder or column in the structure.

While many blast tests have been performed on reinforced concrete structures, little quantitative data have been obtained on the blast-structure interaction. To develop data of the phenomenon, the Warhead Effectiveness Branch, DLYW, of the Air Force Armament Laboratory, Eglin Air Force Base, Florida, entered into a contract in 1973 with Oklahoma State University to develop survivability data for reinforced concrete beams.

1.1 Objectives

Reinforced concrete beams, similar to those found in conventional office buildings or warehouses, were subjected to high intensity impulse loads and the structural response measured by accelerometers, load cells, and strain gages. The high intensity impulse was provided by spherical Pentolite suspended over the beams. Five different beams were studied and included a nominal beam, a nominal beam without shear reinforcement, a high strength concrete beam, a high strength steel beam and, finally, a beam with increased steel tensile reinforcement.

The first objective of these tests was to define the threshold failure impulse. By adjusting the standoff distance of the charge to the test item, it was possible to vary the impulse. Data from Goodman (1) were utilized to select the charge size for the desired range of impulse.

The second objective of the program was to generate basic test data for the evaluation of a numerical method (IMPBC), Reference (2), which was developed for nonlinear analysis of impulse loaded reinforced concrete beams.

Finally, an evaluation of the damage produced by the blast impulse was required. This quantity would be necessary to define survivability of the member.

1.2 Program Development

The work summarized in this report was conducted over a $3\frac{1}{2}$ year period at Oklahoma State University, Stillwater, Oklahoma, and Eglin AFB, Florida, from January 1973 until May 1976. The design and construction of the test beams and supporting frame were performed at Stillwater, Oklahoma, and shipped to Eglin AFB, Florida. The impulse test program conducted by Eglin AFB, began in May and was completed in September 1974. The explosive charges which generated the impulse were spherical Pentolite provided by the Naval Weapons Station, Yorktown, Virginia. Following the blast tests, the beams were returned to the Oklahoma State University, Stillwater, Oklahoma, for final damage inspection and static tests.

The analysis of test data began in February 1974 and continued through January 1976. Three tapes, containing 304 data files, were assembled by the Eglin AFB Computer Sciences Laboratory and forwarded to Oklahoma State University for processing and analysis. The Oklahoma State University Field Office, Eglin AFB, Florida, provided valuable assistance in the modification of the data tapes for compatibility with the OSU (Stillwater) IBM 360/65 computer system.

Data analysis was divided into five stages, conducted simultaneously whenever possible. First, pressure data were reviewed for reliability and accuracy. This was performed by the review of pressure-time curves and digitized data listings provided by Eglin AFB. Second, methods for the integration of accelerometer data were studied to provice a suitable integration technique to obtain beam velocity and displacement. Third, the strain data were processed and studied: load cell data to determine beam reactions and strain gage data to calculate curvature. Fourth, the evaluation of test damage was performed by the analysis of data from the final static test program. Finally, a correlation study was performed to compare test data with a digital computer simulation of the nonlinear structural response of reinforced concrete beams to impulse loading (IMPBC, Reference 2).

1.3 Program Results

In general, the data developed by these tests were very suitable for both the evaluation of computer program IMPBC and the definition of member damage. Only the acceleration data did not prove reliable for the analysis required in this work. Pressure data, from which the measured impulse was determined, indicated both pressures and impulses less than predicted by Goodman (1) for the detonation of spherical Pentolite. Consequently, the threshold impulse for member failure was not defined.

Laboratory static tests following the impulse tests provided a simple and reliable means for the estimation of damage. The method for damage assessment is based on an extension of a design procedure of Biggs (3) in which the impulse to produce failure is related to the static plastic work capacity of the member.

In this report, each type of data is presented and discussed. However, results for each test are not given due to similarity between test data and the quantity generated by this work. The general quality of the data is available for review in Appendix A. These curves were prepared by the Eglin AFB Computer Science Laboratory and present the data as a function of time. On the other hand, the results for test 11 have been presented in each chapter to illustrate instrument performance and analysis technique.

Finally, of the beams tested, the high strength concrete proved to be most durable while the one with the greatest strength, the beam with increased tensile steel, suffered the greatest damage. As a result of these tests, one must recommend high strength concrete with ductile steel reinforcement as the most suitable member to resist high intensity impulse loads.

CHAPTER II

PREVIOUS STUDIES OF IMPULSE LOADED

REINFORCED CONCRETE BEAMS

The response of impulsively loaded reinforced concrete beams is a function of several variables, among which are the strain rate, the material properties, and the cross section geometry. Under impulse loading, portions of a member experience high rates of change of curvature, which produces high strain rates in the steel and concrete. The net effect of high strain rates is to increase the strength and toughness of steel and the strength and crushing strain of concrete. These properties generally result in increased member strength and ductility. Thus, one requisite for understanding the impulse-related behavior of a reinforced concrete beam is knowledge of the strain rate behavior of the materials.

A number of studies of rapidly loaded reinforced concrete beams with both full- and model-sized specimens are reported. Although load application was primarily impact and controlled mechanical loading, more recent studies have used low-order explosive loading. The literature cited herein provides some information on both material and member behavior under dynamic to impulse loads. The literature describes various testing techniques and provides perspective for the evaluation of test results.

6

2.1 Strain Rate Effects on Steel Properties

The strain rates discussed in the literature are based on average rates, calculated from the strain at yield or ultimate and the elapsed time. Manjoine (4) investigated the effect of large strain rates on mild steel at temperatures varying from room temperature to 600°C. The stress-strain curves from the room temperature experiments are given in Figure 1 for strain rates which vary from 9.5×10^{-7} to 300/sec. It was concluded in this study that increased strain rates cause the lower yield point, the yield strain, the strain at which strain hardening began, and the ultimate strength to increase. The significant parameters-- yield stress, ultimate stress, total elongation, and ratio of yield to ultimate stress--are summarized in Figure 2 as a function of strain rate. The steel used in that study was a low-carbon, open-hearth, mild steel, not a reinforcing steel. However, for the purposes of this study, reinforcing steels were presumed to have similar characteristics.

The dynamic yield stress ratio, f_{Dy}/f_y, for reinforcing steel is presented in two studies, References (5) and (6). These ratios are shown in Figure 3 as a function of strain rate. Norris et al. (5) present results of an investigation of the effect of strain rate on structural and intermediate grade reinforcing steels while Allgood and Swihart (6) discuss results for intermediate and hard grade reinforcing steels.

A mathematical model of the relation between strain rate and dynamic yield stress ratio is given by Perrone (7):

$$f_{Dy}/f_y = 1 + (\dot{\varepsilon}/D)^{1/n} \tag{2.1}$$

where n and D are material dependent constants and $\dot{\varepsilon}$ is the strain rate.
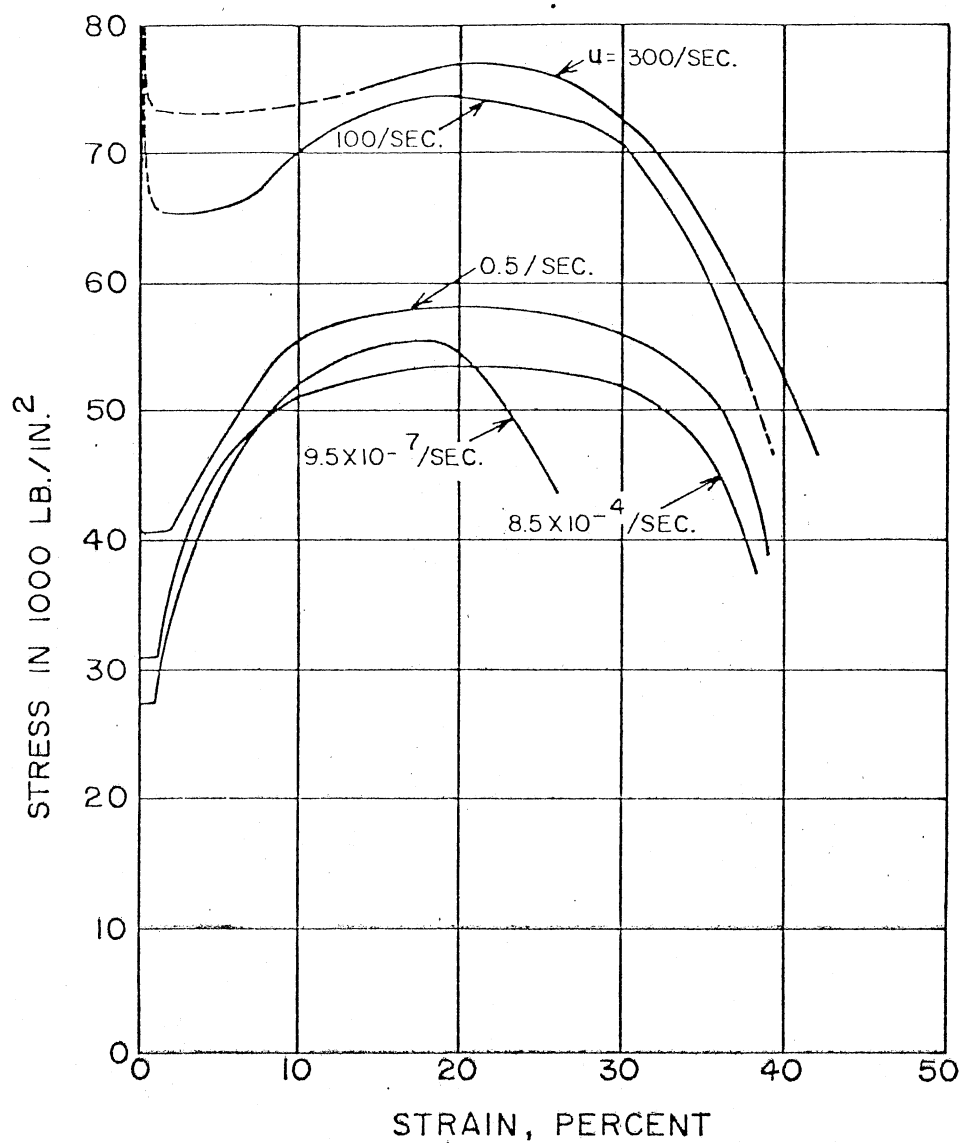
Figure 1. Stress-Strain Curves for Mild Steel for
Various Strain Rates (From Manjoine
(4))
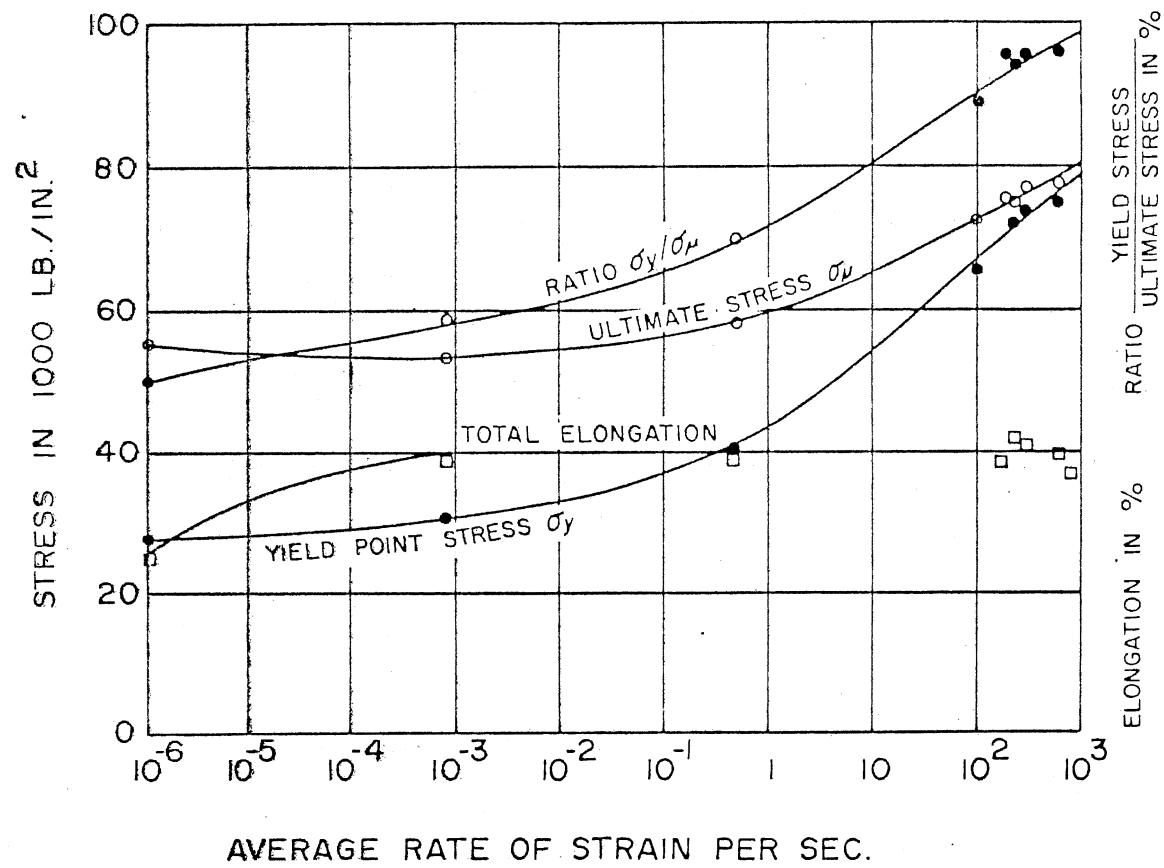
Figure 2. Influence of Strain Rate on Mild Steel Tensile
Properties (From Manjoine (4))

For mild steel these values are n = 5 and D = 40.4/sec. This equation is shown in Figure 3 along with data from References (4), (5) and (6). This model will be used to define steel properties for analytical studies of an impulse loaded reinforced concrete beam.

2.2 Strain Rate Effects on Concrete Properties

The effect of large compressive strain rates on concrete properties is to increase the ultimate strength, the strain at ultimate strength, and the absorbed strain energy. Watstein (8) tested 3 in. x 6 in. cylinders of 2000 and 6500 psi concrete at strain rates which varied from 10^{-6} to 10/sec. The test specimens were moist cured 25 days and air dried 3 days. Strain gages were applied to the cylinders and the specimen temperatures were elevated to 60°C for 4 hours to cure the gage adhesive. The specimens were tested at an age of 28 days. Watstein's results were presented as a function of both stress rate and strain rate. The latter form is most convenient for use in evaluating the data from the impulse tests presented in this work. In Figure 4 the ultimate dynamic strength of the specimens, f'_{DC}, is compared with the static strength, f'_C. The strain rates were averages based on the strain at ultimate stress and the elapsed time. The area under the dynamic stress-strain curves was integrated to yield work performed on the specimen per unit volume. These data are presented in Figure 5 as the ratio of the work under dynamic loading, W_D, to work under static loading, W_s, as a function of dynamic stress ratio, f'_{DC}/f'_C. This work function might be used to develop dynamic concrete stress-strain curves from static test data.
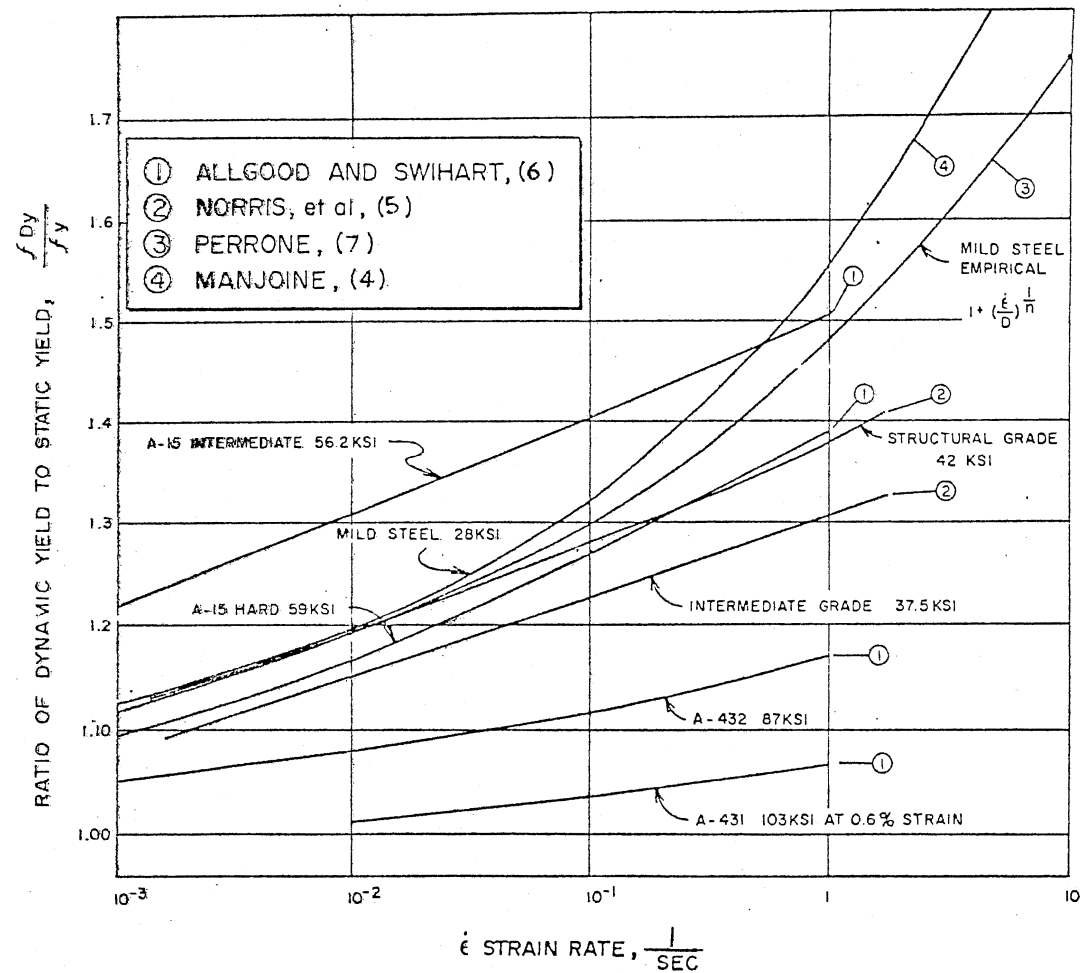
Figure 3. Influence of Strain Rate on Stress
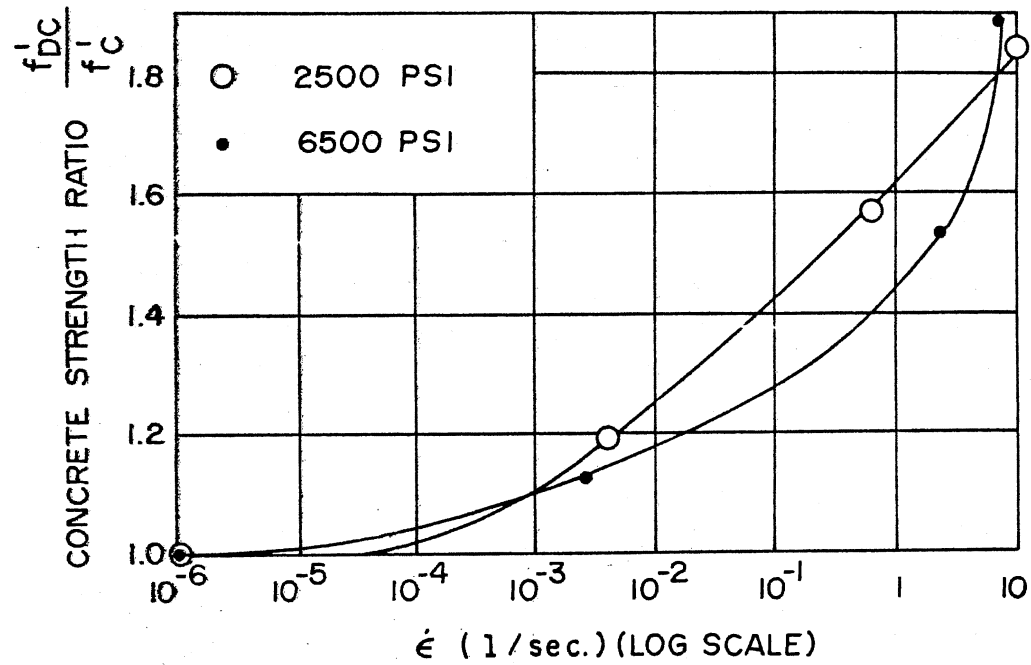
Figure 4. Influence of Strain Rate on Concrete
Cylinder Strength (From Watstein
(8))
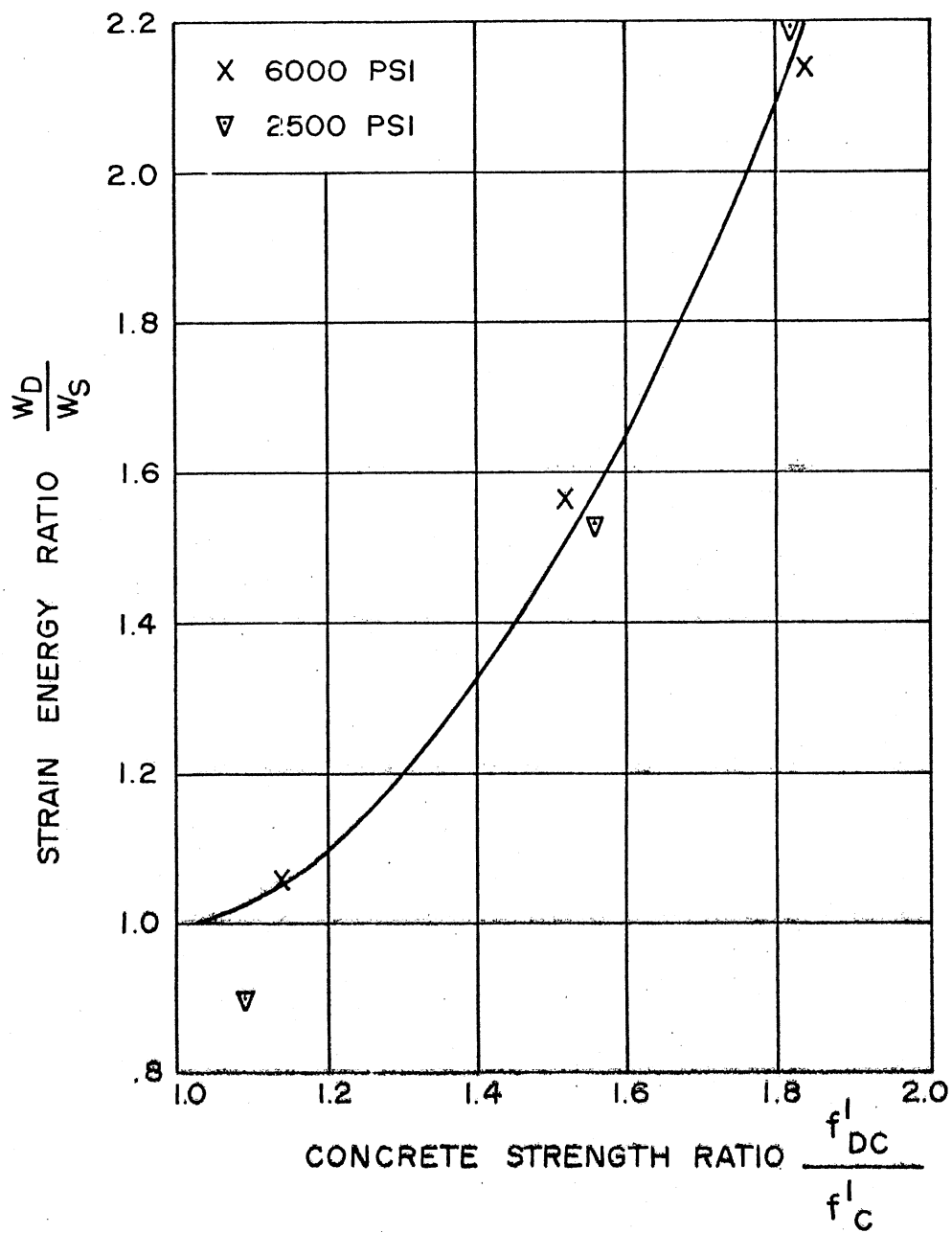
Figure 5. Relation Between Strain Energy Capacity
and Concrete Strength Ratio (From
Watstein (8))

Allgood and Swihart (6) presented results of tests performed at the Naval Civil Engineering Laboratory. The test specimens were noted as being low and high strength and were tested at two ages: 28 days and 49 days. The 28-day specimens were tested wet and the 49-day specimens were tested dry. Results of these tests as well as those of Watstein are shown in Figure 6 as a function of stress rate.

Atchley and Furr (9) tested 6 in. x 12 in. cylinders of three static strength levels: 2500, 3700 and 5000 psi. These cylinders were left in their molds for one day after casting, moist cured for seven days, and air dried for one day prior to testing. The resulting strength ratios, presented as a function of stress rate, appeared to approach a limiting value with increasing stress rate, a trend which contradicts the results shown in Figure 6. However, this may be due to the difference in the ages of the concrete specimens and the curing histories. Watstein reported an increase for the modulus of elasticity with strain rate; however, Atchley and Furr found no such tendency.

Basic work on strain rate effects on tensile strength of concrete is given by Keenan (10), who tested 4 in. x 8 in. split cylinders statically and dynamically at stress rates to 210,000 psi/sec. Tensile strains were measured with respect to time by strain gages perpendicular to the plane of splitting. The results of these tests are shown in Figure 7.

Fox (11) and Galloway and Rathby (12) performed rapid load tests on plain concrete beams to assess the effects of transient loads on the modulus of rupture. They reported, respectively, an average increase of 35%, and a range of increase of 0 to 66%. They did not mention, however, the effect of beam and fixture inertial reactions on the reported stress rates.
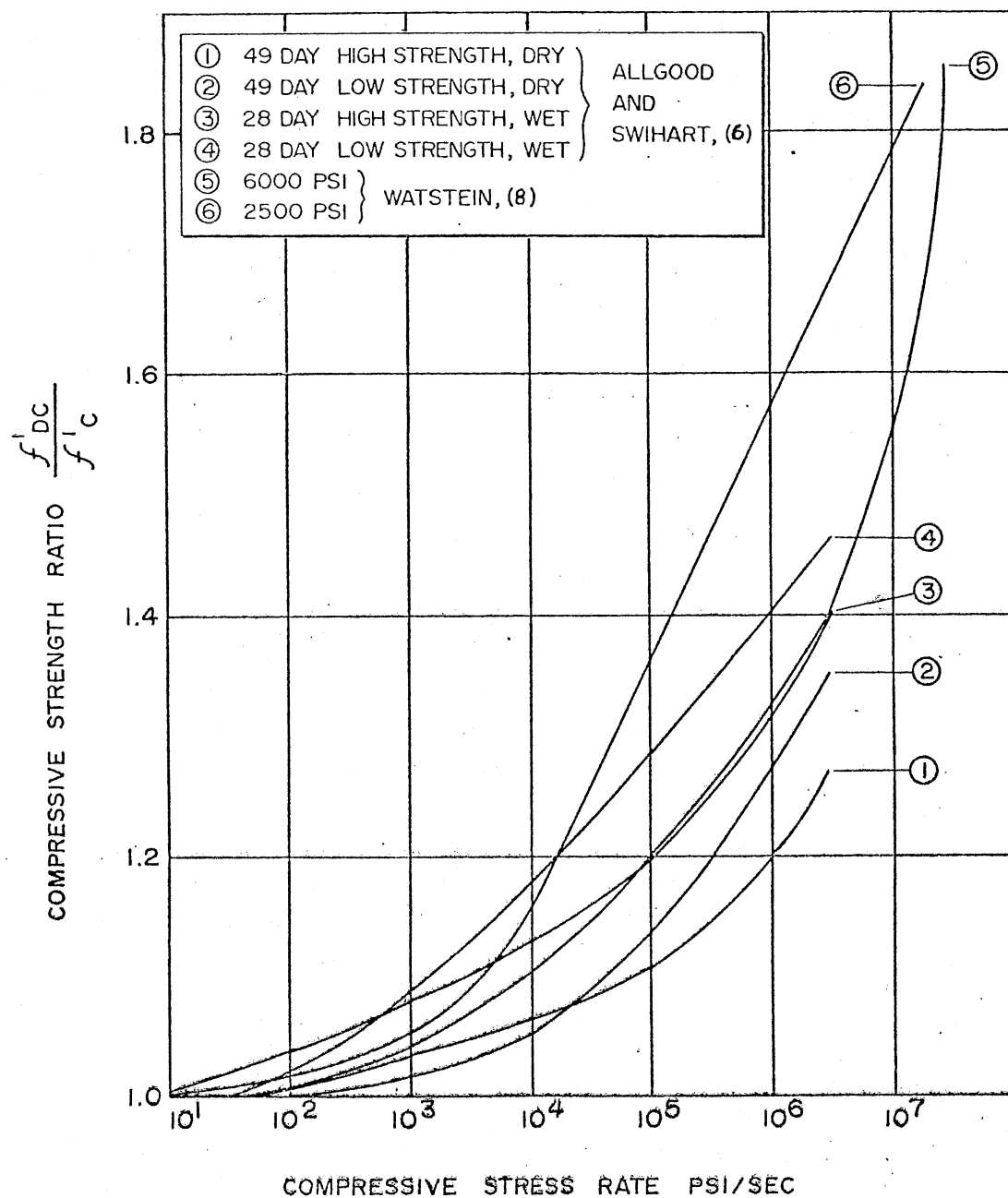
Figure 6. Comparison of Experimental Concrete Strength Ratios
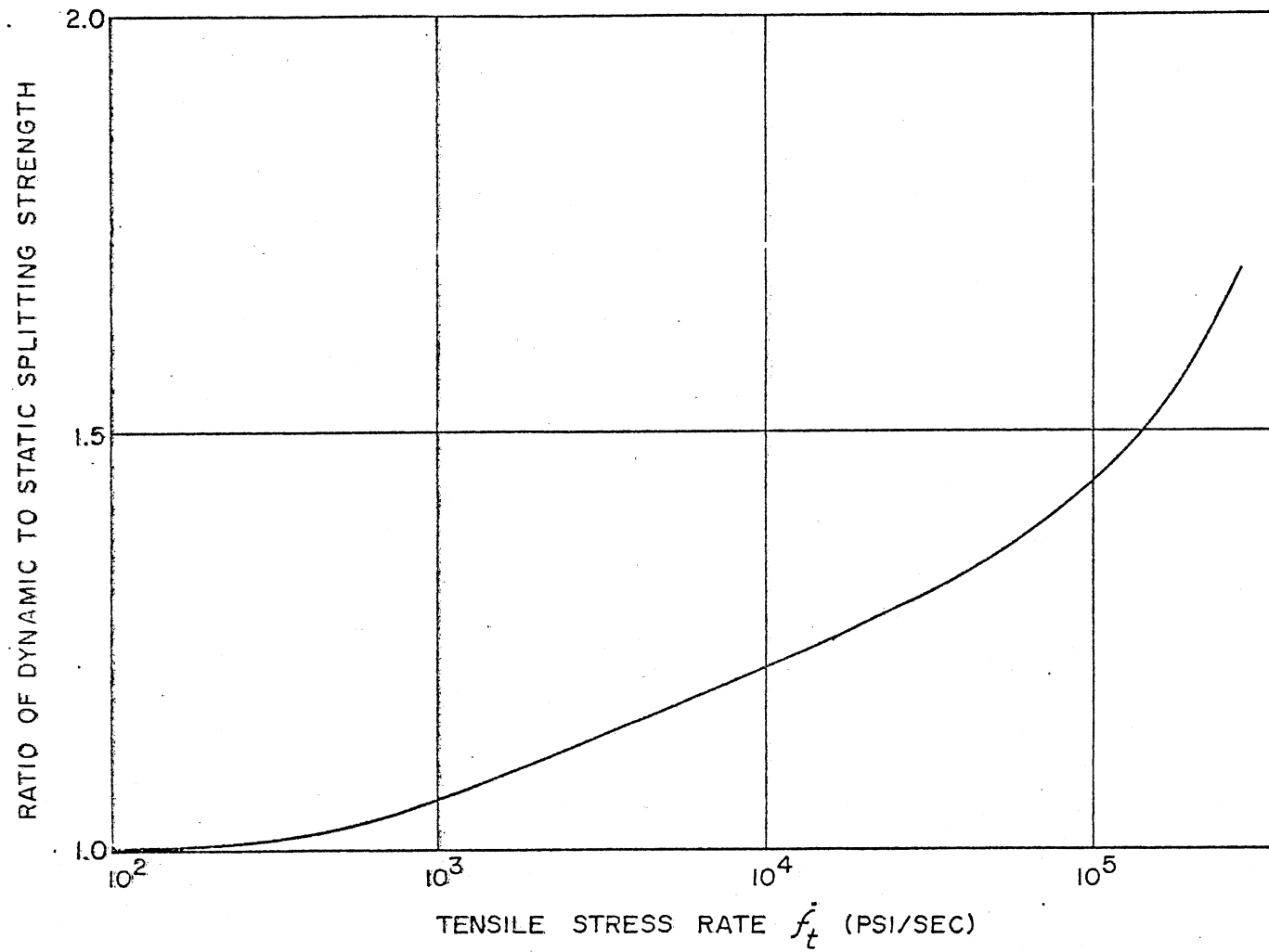
Figure 7. Influence of Stress Rate on the Tensile Splitting
Strength of Concrete Cylinders (From Keenan (10))

2.3 Research on Dynamically Loaded
Reinforced Concrete Beams

The literature reveals a limited number of studies of impulse loaded reinforced concrete beams. However, a number of studies have been performed on impact and rapidly loaded beams. This review is presented to establish the state of the art of dynamic load tests for reinforced concrete beams. The dynamic loading was achieved with three basic techniques: (1) impact, with falling weights; (2) mechanical, with release of stored energy through mechanisms; (3) impulse, with release of stored energy from chemical explosives.

2.3.1 Impact Loading

Mylrea (13) performed one of the early impact tests on very lightly reinforced beams. He used three grades of steel with yield strengths ranging from 45 ksi to 112 ksi, and two concrete strengths of 3 ksi and 6 ksi. The impact loads were provided by two drop hammers which weighed 540 and 2400 lbs. Mylrea found that the strength of the concrete had no effect on his results and that the lightly reinforced beams were very ductile. He concluded that the ductility of the reinforcing steel provided "an enormous reserve resistance to impact." He also concluded that for his tests the grade of steel did not significantly affect the resistance to impact. His test procedure was to repeatedly strike the beam until steel rupture occurred.

Kluge (14) performed impact tests on 6 ft by 2.5 ft slabs with thicknesses ranging from 1¼ to 7½ in. The investigation concerned the use of spiral reinforcement to increase the impact resistance of the

members. The slabs were supported in a vertical position, like pinned-
end beams, and were struck with a 1200 lb weight on a 12 ft pendulum
arm. The test procedure was to raise the weight to successively higher
starting points, 6 in. per increment, and to strike the slab repeatedly
until failure occurred. However, some specimens were subjected to a
single large impact for comparison with results from cumulative impact
tests. He concluded that the members would be up to three times more
resistant to a single large blow than to a succession of blows with in-
creasing magnitude.

Bate (15) reviewed the work performed on dynamically loaded beams
and found that: (1) beams reinforced with mild steels had greater
energy capacity than those reinforced with high strength steel; and (2)
the percentage increase in yield stress was greater for mild steel than
for cold worked, higher strength steels. Simms (16) performed tests
with a weight impacting the beam center. He formulated a damage evalu-
ation procedure with the potential energy of the weight being related,
through an empirically derived constant, to the work required to pro-
duce fracture of the steel.

2.3.2 Mechanical Loading

Early work with a mechanical controlled-load device was reported
by Hansen (17) of a gas-driven piston to load beams. The load was
applied to the center of the test specimens with typical rise times on
the order of 3 ms and load durations from 10 ms to 1 sec. The smallest
load durations, t_d, were the same order of magnitude as the beam funda-
mental period of oscillation, T. Hensen suggested that the concrete
and steel would withstand stresses which exceeded static failure and

yield stresses. Penzien and Hansen (18) extended the work to study the elastic behavior of simple structural elements under rapidly applied, relatively short duration loads.

Nordell (19), (20) performed static and dynamic load tests using equipment similar to that of Penzien and Hansen. The load was applied for a duration of approximately one second in a step-wise fashion, and repeated until the top concrete fibers showed signs of distress. Nordell found that the maximum dynamic resistance was approximately 30% greater than the static resistance. He also reported that for concentrated center loads, the development of a plastic hinge for dynamic loading was similar to that found for static loading but with a shorter hinge length.

Mavis and Richards (21) devised a test arrangement with two parallel beams joined at the ends by links. The beams were simultaneously center loaded in opposite directions. The loads were applied impulsively to the beams with a pair of spinning flywheels arranged so that they could transmit large forces to the beams. The object of this symmetrical arrangement was to subject pairs of beams, differing only in their grade of steel, to the same impulse loading and to compare responses. Two grades of steel were used: structural grade and hard grade with 39.7 and 75.8 ksi yield stress, respectively. The damage to the structural grade beams was always greater than that of the hard grade beams. Mavis and Richards did not mention that in such a test arrangement the beam which yielded first limited the maximum response on its pair-wise partner.

Mavis and Greaves (22) modified the loading method of Mavis and Richards to extend the study of the effect of steel grade on beam

durability. Instead of flywheels, they used preloaded springs with a parallel linkage arrangement to center load the beams. The beams were again connected pair-wise by linking their ends together. Release of a center restraint link rapidly transferred the load to the beams. Applied loads and end reactions were measured during the tests. Following the tests, selected segments of reinforcing steel were removed and plastic strain profiles were determined. The major conclusion was that hard grade steel was superior to intermediate grade steel in dynamically loaded reinforced concrete beams. This conclusion was disputed in a discussion of Mavis and Greaves' work by Balog et al. (23), who cited other research as well as experimental bias.

Shaw and Allgood (24) performed analytical studies of reinforced concrete beams utilizing a one-degree-of-freedom spring mass analog. The load-time function was triangular with various ratios of load duration to fundamental period t_d/T. They concluded that, for $t_d/T = .5$, reinforced concrete beams fabricated with structural grade steel had considerably greater dynamic load capacity than those with hard grade steel. Load capacity was almost equal for $t_d/T = 2.0$, and the hard grade steel began to show greater capacity for ratios above 2.0.

References (25) through (28) describe additional tests on reinforced concrete and prestressed beams using springs and third-point loading. The tests on prestressed beams are cited to indicate the logical extension of the test techniques to other fundamental member types.

2.3.3 Explosive Loading

Keenan (10) and Seabold (28) of the Naval Civil Engineering Laboratories investigated the dynamic shear strength of reinforced concrete beams. The specimens were loaded statically and dynamically in a blast simulator. Primacord detonated in the simulator produced the pressure loads. The pressures were on the order of 60 to 80 psi and remained constant on the specimen throughout the tests, producing long term step loads.

2.4 Discussion

From the available literature, a number of factors relative to the behavior of reinforced concrete members subjected to impulse loading have been presented. Both concrete and reinforcing steel are influenced by large strain rates. For concrete, the effect is for the stress and strain at crushing to increase with strain rate. This would cause corresponding increases in the curvatures at which a beam segment experiences concrete distress. For steel, large strain rates cause the yield stress to increase and consequently, the yield moment, M_y. The increase in dynamic yield stress relative to the static yield stress is larger for the intermediate and structural grade steels than for the high strength steels. These properties were verified by tests of the materials and reinforced concrete beams.

Material properties are presented as a function of average strain rates. There was no discussion of possible effects of variable strain rates; however, this phenomenon may be of significance. The initial strain rate in the steel reinforcement of an impulse loaded member

would generally be larger than the rate at yield. The question here is whether the dynamic yield stress would be an independent function of the initial rate, the rate at yield, or a rate between the two. Furthermore, the strain rate would decrease from the rate at yield to zero, as the member reaches its maximum displacement and motion momentarily ceases. It should be determined whether the resistance would remain at its dynamic yield value, or would approach the static yield value as the strain rate approaches zero. The implication of a rate dependent plastic stress level is that the dynamic yield moment of a section may be variable rather than constant.

Conflicting recommendations for the best grade of steel to use for rapidly loaded members were present in the literature. The proper perspective on the problem, as shown by later analysis, lay in the duration of the loading. A rapidly applied and sustained load would require maintenance of static strength to sustain the load. A very short duration impulse-type load would require the energy absorption capacities of the ductile beam. The former favored hard grade steel and the latter favored the ductile intermediate or structural grade steels. The beam tests showed that the beams would fail in one of two modes, shear or flexure. The opinion was expressed that flexural failure should be insured by using a sufficient amount of shear reinforcement. Splitting of the beams and subsequent bond failure were reported in some tests and further study of these problems was recommended. Furthermore, compression steel and confinement steel appeared to enhance beam ductility. By analogy with static tests, a significant increase in ductility and energy absorption capacity would be expected under dynamic loading, although specific studies were not made.

Except for the pendulum and flywheel tests, the duration of the applied loads was greater than the fundamental period of vibration of the beam. Excluding the blast simulator tests, the loads were applied as point loads to the center or third points of the beams.

The work presented in this report investigates the effect of a distributed-pressure load applied for a very short duration with respect to the fundamental period of vibration of the test specimen. The pressures anticipated were an order of magnitude greater than those produced in the blast simulator. The predicted pressure-time relationship was expected to be an exponential function, rather than the rapidly applied constant loads of the blast simulator and controlled load mechanisms, or the oscillating loads of the spring loaded mechanisms.

In general, the tests reported in the literature were conducted so as to drive the test specimens to destruction. If for a particular test the specimens were not destroyed, permanent displacement was noted and, in some cases, were reloaded until failure. The threshold of beam destruction was not identified in terms of required impulse. For the cases where the specimens were not destroyed, a quantitative damage assessment was not available.

CHAPTER III

TEST SPECIMENS

The objective of this investigation was to subject reinforced con-
crete beams to very short duration pressure loads, to study the blast-
structure interaction phenomena, and to assess the resulting damage.
Test specimens were fabricated to be representative of full-sized beams
used in typical building construction. They were prismatic, under-
reinforced, simply-supported beams with neither compression reinforce-
ment nor confinement steel in the center.

The primary aim of the tests was to subject a "nominal" beam to a
wide range of impulses to define the failure impulse, then modified
beams at selected impulses. The modified beams had the same physical
dimensions as the nominal beams, but different material and reinforcing
properties.

The beam response was measured by accelerometers mounted on the
lower beam surface and strain gages both on the concrete and reinforc-
ing steel. The beam was supported to permit the measurement of end
reaction loads by load cells.

The impulse loading was provided by the detonation of a spherical
Pentolite charge suspended above the beam. To restrict the impulse load
to the top surface of the beam, it was necessary to construct a test
fixture to provide side and bottom protection for the beam from the
blast load. This test fixture also protected the instrumentation. The
test fixture was inherently massive, a feature which limited its length

24

because of handling problems. Its size limitation controlled the length of the test specimens.

3.1 Beam Design

The physical test fixture constraints dictated a maximum beam length of ten feet. To select beam properties, the design method suggested by Biggs (3) was used, where the impulse for failure is related to the maximum beam resistance, R_m, and ductility, μ, by equating the maximum kinetic energy to the total static work capacity of the beam.

$$\mu = \frac{Y_{max}}{Y_y} = \frac{1}{2}\left(\frac{i^2\omega^2}{R_m^2} + 1\right) \tag{2.1}$$

where

Y_{max} = maximum displacement of beam center, in.;

Y_y = displacement of beam center at yield, in.;

i = total impulse applied to member, lb-sec;

ω = fundamental frequency of beam, rad/sec.

Failure was assumed to occur at a ductility ratio, μ, of 10, a quantity later evaluated by test to be 6.3. An 8 x 12 in. cross section with a pair of No. 6 40-grade bars was proposed. A dynamic strength ratio of 1.25 was assumed for the steel, which exhibited a nominal yield strength of 50 ksi. The factors above combined to yield estimates of R_m and ω, and predicted a failure impulse of 760 psi-ms. It was assumed that the value of μ = 10 was conservative and that the resulting value of 760 psi-ms was an upper limit. From Goodman (1) it was determined that 214 lb charge of spherical Pentolite would produce a suitable range of impulse. By adjusting charge standoff distance from 9.5 ft to 19.5 ft, the predicted impulse, I, varied from 778 to 279 psi-ms.

The overall geometry proposed above was found acceptable and was used to plan 16 test beams in five different configurations, Table I. Figure 8 shows the general beam dimensions as well as the details of reinforcing steel and the end support connection.

A steel end angle (L 6 x 6 x 3/8) was cast in the beam to provide a connection and bearing seat for the end support mechanism. The end angle also provided anchorage for the reinforcing bars to insure development of steel strength near the end of the beam.

3.2 Beam Instrumentation

Accelerometers, strain gages, and load cells were used to measure the response of the beam to the impulse loading. Three accelerometers were installed in each beam and the data were integrated to produce velocities and displacements. Each beam had four pairs of strain gages and consisted of one gage applied to the top of the steel bar and another to concrete near the top of the beam. Data from these pairs were used to calculate curvature. A pair was placed at each of the two quarter points and two pairs were placed at the center as shown in Figure 9. The quarter station instrumentation provided a check of symmetry, and provided greater reliability for quarter station data. This redundant strain gage arrangement was chosen to reduce the possibility of total data loss due to damage or data channel malfunction.

The concrete gages were applied to the beam sides approximately 1.6 in. below the top surface. Figure 10 shows a side view of a beam quarter point station and illustrates the placement of the concrete strain gage and its connecting lead wire, both of which were recessed. The cross section shows the steel gage installation with its lead wire passing up to a harness near the center of the beam. Also illustrated in this figure is the accelerometer housing with an accelerometer and

TABLE I

BEAM CONFIGURATION SCHEDULE

Beam Numbers	Beam Type	Design Parameters						
		f'_c ksi	f_y ksi	A_s in^2	ρ %	Shear Stirrups	Mix Design[1]	Water-Cement Ratio
2,3	High Strength Conc.	6	40	.88	1.04	Yes	1:1.85:2.93	.766
4,5	Increased steel area	3	40	2.00	2.39	Yes	1:3.60:4.75	.466
6,7	Increased steel strength	3	60	.88	1.04	Yes	1:3.60:4.75	.466
8,9	Shear stirrups removed	3	40	.88	1.04	No	1:3.60:4.75	.466
10-17	Nominal	3	40	.88	1.04	Yes	1:3.60:4.75	.466

[1]Weights "as stocked."

¢ Accelerometer Housing

2"

6-Spa. @ 5"=30"
Typ. ea. end

1-#3 Typ ea. end

7-#3 Typ.
ea. end

2-#6 or 2-#9

30" 30" 30"

120"

12"

2"

3" 3"

See Detail "A"
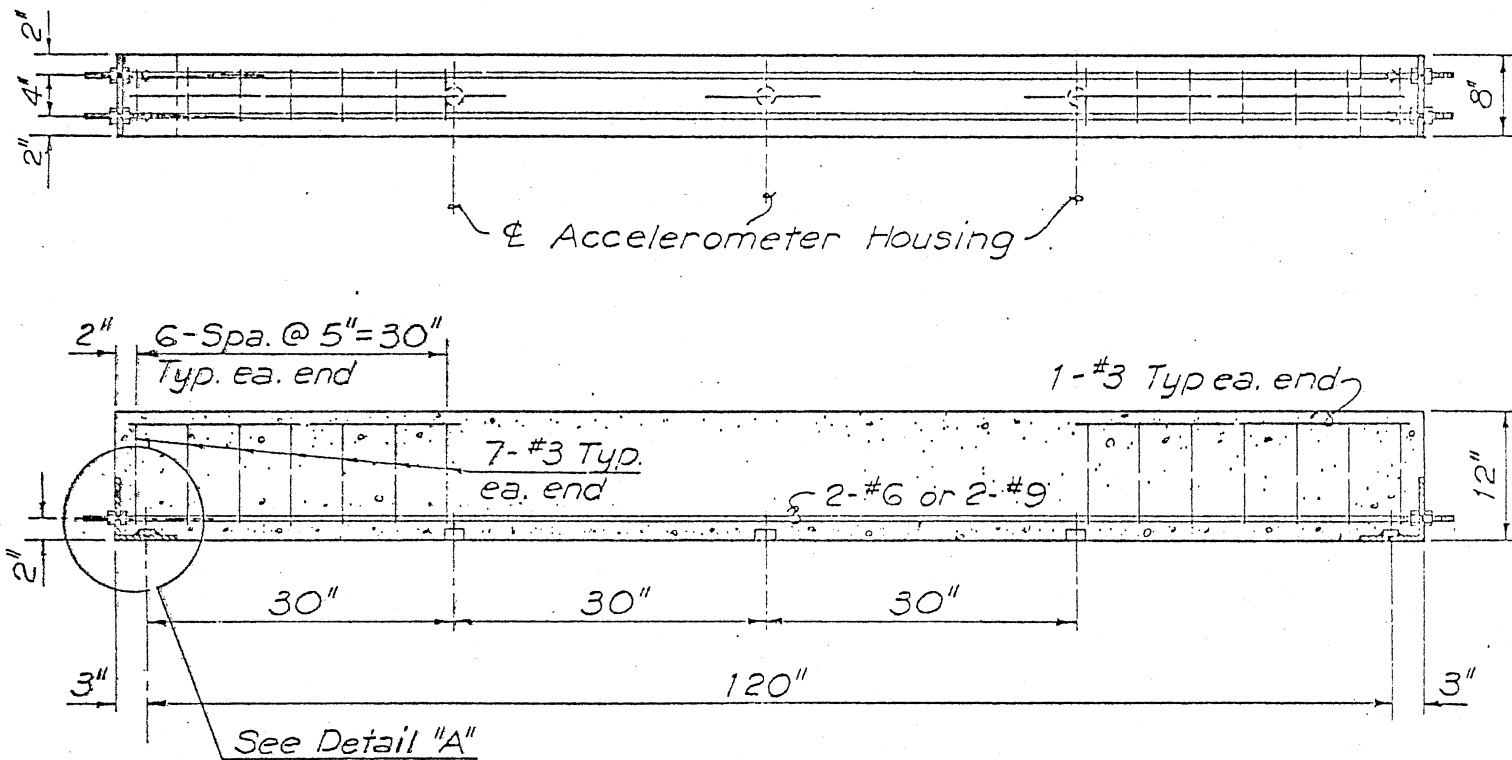
Figure 8. Test Beam Details
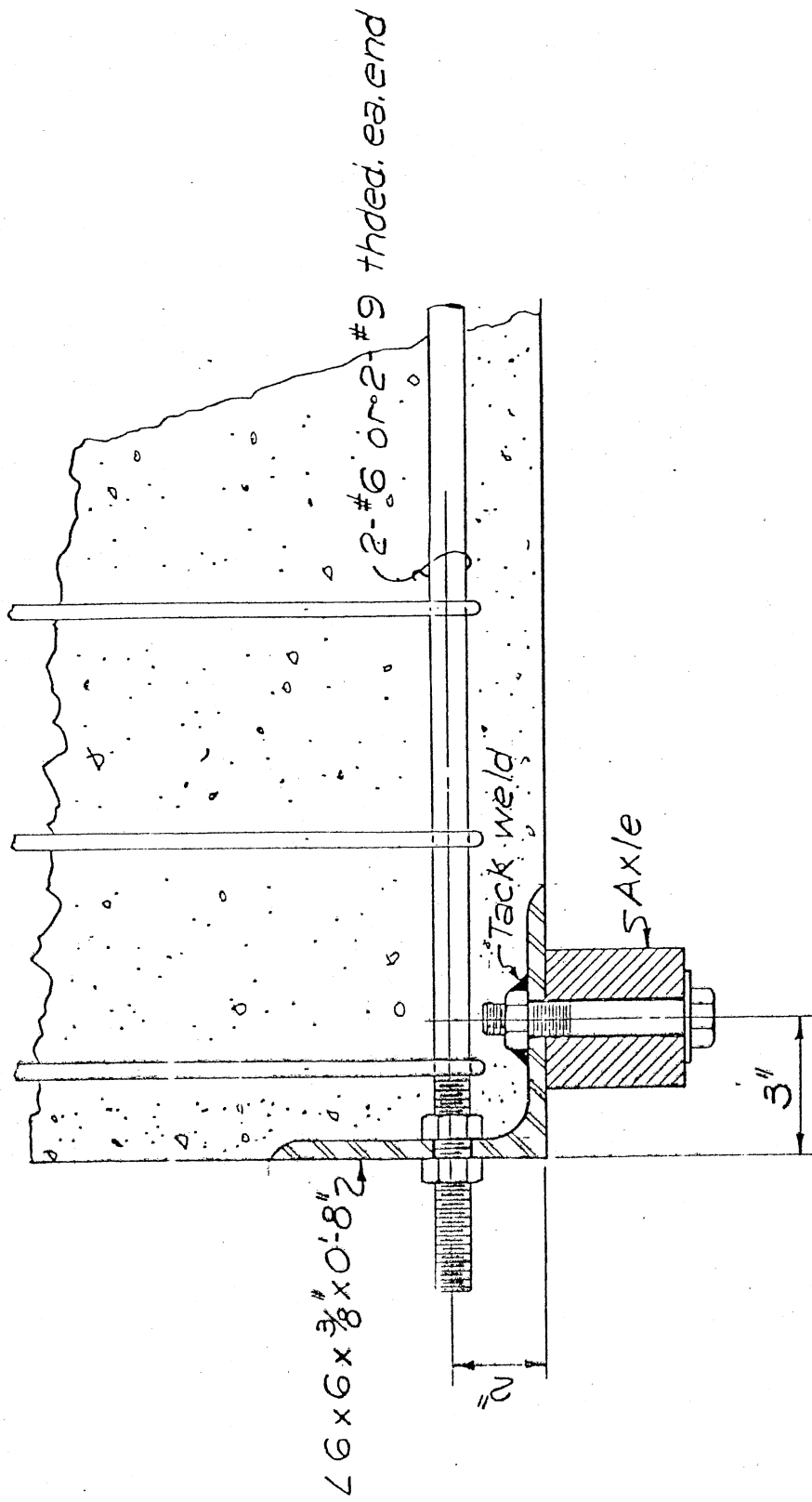
DETAIL "A"

Figure 8. (Continued)
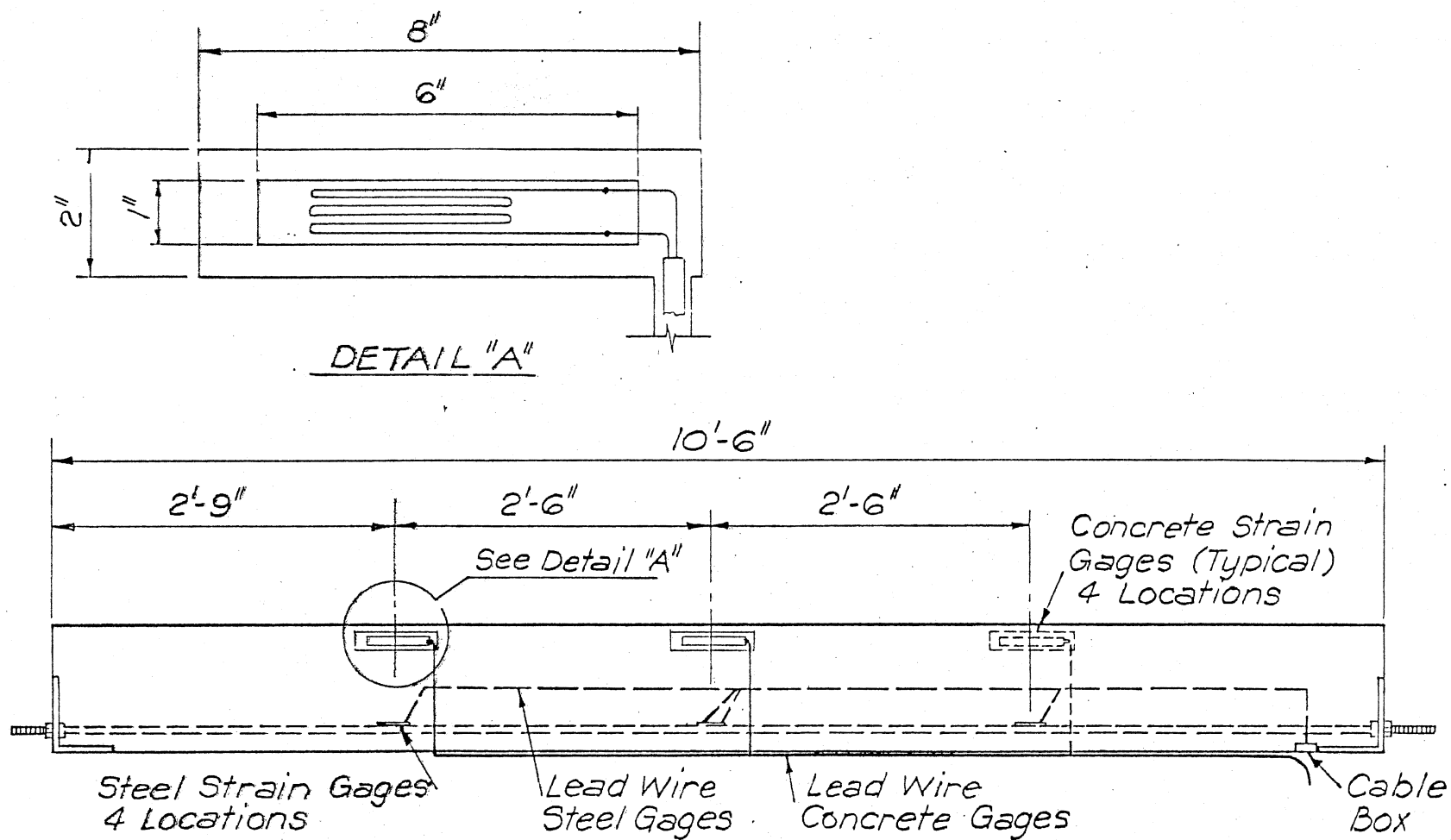
Figure 9. Strain Gage and Lead Wire Installation Details
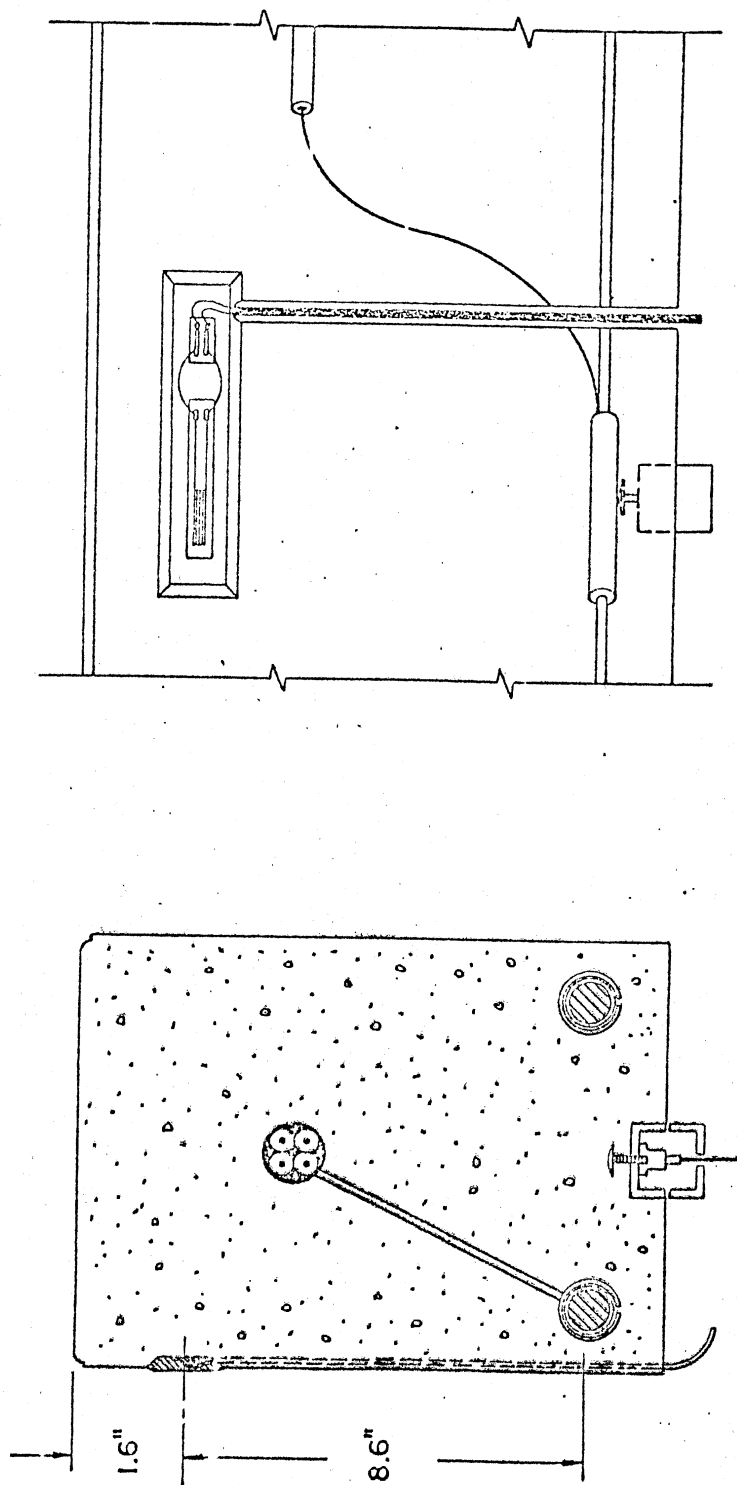
Figure 10. Typical Instrumentation at Beam Quarter Point

lead wire in place. The steel strain gage installation is illustrated in Figure 11.

3.3 Material Description

Material properties of the steel, fine aggregate, coarse aggregate, cement and concrete, are presented in this section. Static tensile test results for the reinforcing bars are given in Table II, along with applicable specifications. The coarse aggregate was 3/4 in. crushed limestone quarried at the Quapaw Quarry, Drumright, Oklahoma, while the fine aggregate Cimmaron River sand was taken at the Dolese Quarry, Guthrie, Oklahoma. Type I portland cement was manufactured by the Dewey Division of Martin-Marietta.

The aggregate properties analyzed were specific gravity, absorption capacity, and size gradation are given in Tables III and IV. These aggregates were used in a series of batch tests to develop a suitable mixture for the 3000 psi strength and the 6000 psi strength concretes. The resulting mixtures for these two strengths are shown in Table I.

The concrete properties for each beam are given in Table V. In addition to these data, the strain at ultimate load was recorded for a limited number of samples. For the 3 ksi concrete, the average strain, ε_c', from four samples, was 2230 μin./in., while a sample of 6 ksi concrete gave a value of 2100 μin./in. These data are required for the construction of the concrete stress-strain curves for dynamic loading.

TABLE II

REINFORCING STEEL STRENGTHS

Beam Number	Bar Size	f_y ksi	f_{ult} ksi	Percent Elongation	Specification
2,3,8-17	#6	51.95	82.85	22.15	A 615-72 Grade 40
6,7	#6	62.50	100.00	--	A 615-68 Grade 60
4,5	#9	50.50	81.80	24.00	A 615-72 Grade 40

TABLE III

FINE AGGREGATE SIZE GRADATION

	Fine Aggregate	
Size Gradation	% Retained	Σ % Retained
#4	.58	.58
#8	3.74	4.32
#16	11.79	16.11
#30	30.32	46.42
#50	39.87	86.30
#100	12.02	98.32
Pan	1.68	100.00

Specific gravity (bulk-SSD) = 2.61.

Absorption capacity = .46%.

TABLE IV

COARSE AGGREGATE SIZE GRADATION

	Coarse Aggregate	
Size Gradation	% Retained	Σ % Retained
1½"	0	0
1"	4.69	4.69
$\frac{3"}{4}$	40.41	45.10
$\frac{1"}{2}$	34.55	79.65
$\frac{3"}{8}$	10.95	90.60
#4	4.86	95.46
#8 (pan)	4.54	100.00

Specific gravity (bulk-SSD) = 2.79

Absorption Capacity = .90%

TABLE V

CONCRETE PROPERTIES--AS CAST

Beam	Water-Cement Ratio	Unit Weight lbs/ft^3	Entrapped Air, %	28 Day Strength f$'_c$,psi	f$'_{sp}$,psi	Strength at Test f$'_c$,psi	f$'_{sp}$,psi	Cord Modulus E$_c$,psi X 10^6
2	.437	154.88	2.5	5709	505	5865	413	5.636
3	.437	154.21	1.9	5765	432	5956	425	5.784
4	.714	153.92	2.1	3655	415	4351	372	4.753
5	.715	154.27	1.5	3496	392	3961	322	4.676
7	.719	153.75	1.6	3419	367	3821	343	4.595
8	.717	154.09	1.8	3466	362	3650	331	4.446
9	.714	152.87	2.0	3814	390	3899	346	5.023
10	.712	152.30	2.5	3767	382	3594	327	
11	.714	151.83	2.1	3707	389	3694	331	
12	.717	150.33	2.0	3655	369	3859	323	5.047
13	.711	155.20	1.3	3737	393			5.016
15	.715	150.54	4.3	3443	363	3882	345	4.557
16	.717	151.16	3.7	3738	386	4156	394	4.685

Note: Beam 10 and 11 modulus not taken.
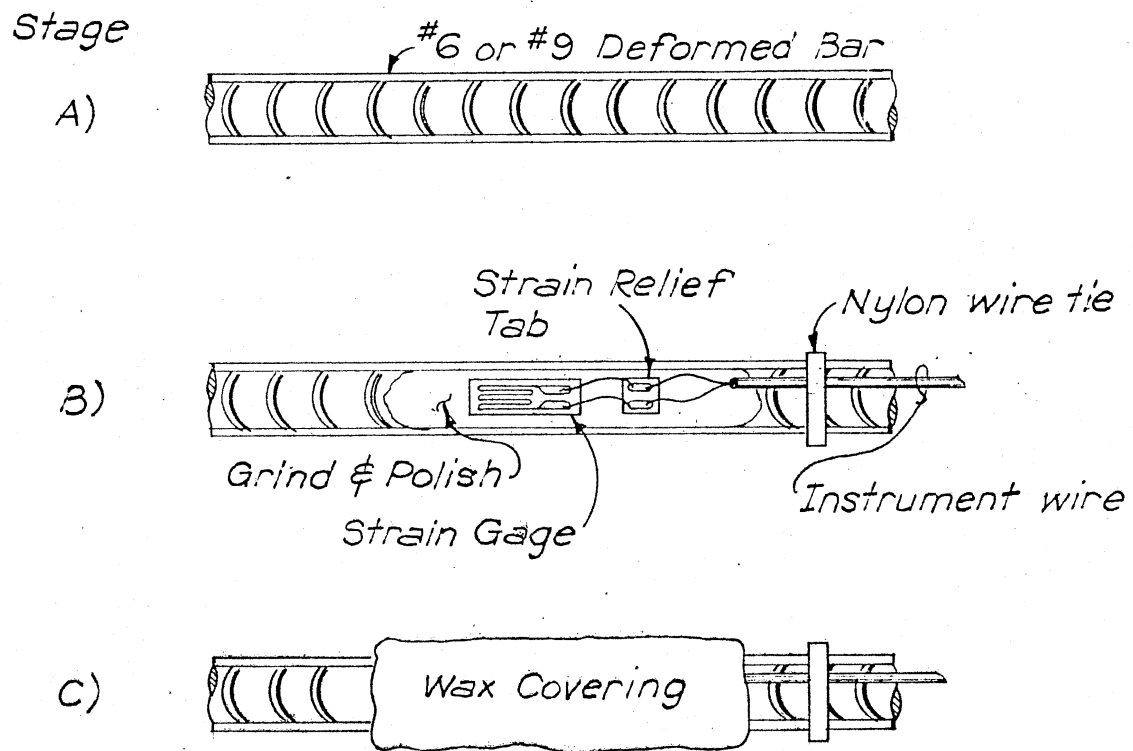
Figure 11. Typical Strain Gage Installation on Reinforcing Steel

3.4 Test Specimen Fabrication

Beam fabrication and instrumentation was performed in three stages:

1. Application of strain gages to the reinforcing bars;

2. Casting and curing beam and control cylinders;

3. Application of the concrete strain gages to the beams.

The beams were cast in a steel form to insure control of the beam dimensions. As cast, the beam cross sections were 8.2 in. wide and 12.2 in. deep. Each beam was cast in three four-inch lifts, with each lift a separate batch. Half of each lift was cast into control cylinders: four 6 in. x 12 in. cylinders and four 6 in. x 6 in. cylinders. The 12 in. cylinders were compressive strength specimens while the 6 in. cylinders were used for the Brazil indirect tensile strength test. Half of these cylinders were moist cured and were tested for ultimate strength at the age of 28 days. The other half were cured with the beam and were tested as soon after the beam field test as was practical. From the 28-day strength tests, strains of selected compression specimens were measured, and the corresponding stress-strain curves were used to compute representative moduli of elasticity. The modulus presented is a cord modulus measured in a stress range of 350 to 1400 psi to approximate the low stress portion of the stress-strain curve.

After casting, the beam and control cylinders were covered with wet burlap and a layer of plastic for about 16 hours. The beam and half of the control cylinders for each batch were removed from the forms and set aside to moist cure under wet burlap and plastic for 7 days, to be followed by drying in air. The remaining cylinders were placed in a moist cure room and were strength tested at 28 days.

CHAPTER IV

TEST PROGRAM

The physical test program extended from October 1973 through
November 1974 and was conducted in three phases. The initial tests were
conducted at Oklahoma State University, Stillwater, Oklahoma, and were
designed to check instrument performance and calibrate strain gages.
The second phase was conducted at Eglin AFB, Florida, from May through
September 1974, where the impulse tests were performed. Finally, the
beams were returned to Stillwater, Oklahoma for final tests and damage
evaluation.

4.1 Preliminary Static Load Tests

The preliminary static tests were conducted with the beams mount-
ed in a test fixture as shown in Figure 12. Static loads were applied
to develop a constant moment in the center 48 in. span of the beam.
Steel strains, concrete strains, and relative displacements of the con-
stant moment region were recorded. The purposes of these tests were:

1. To precrack the beam prior to application of the impulse loads
so its behavior would be similar to a beam with a prior service load
history;

2. To estimate the beam flexural stiffness in the constant moment
span; and
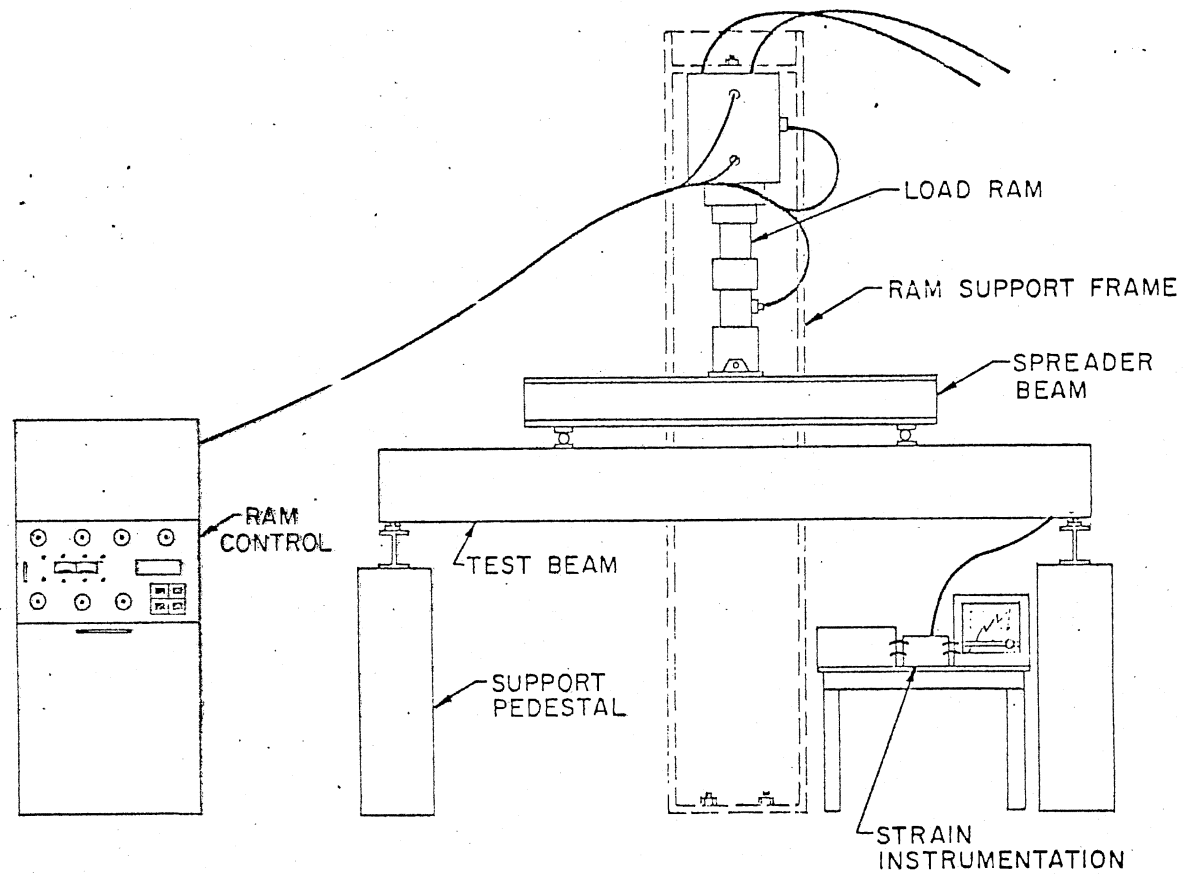
Figure 12. Beam Installed in Laboratory Test Fixture for
Preliminary Static Load Tests

3. To compare curvature calculated from steel and concrete strains with the measured center curvature.

The beams were cyclically loaded, from one to three cycles, with progressively larger maximum loads, as shown in Figure 13. In each cycle the load was increased to a peak value and then gradually decreased to zero. The maximum load was equal to or slightly larger than half the theoretical ultimate load. The preliminary load cycling was followed by a final load to a level of 40% of the theoretical ultimate. The data from this last cycle were used to estimate the flexural stiffness.

The center displacement, δ_c, was measured relative to points 20 in. on either side of the center with an electrical displacement transducer. The transducer signals and applied load were recorded continuously on an X-Y recorder. The loads were proportional to the center moments and the displacement was proportional to the center curvature. The load-displacement plots, with the proper scales, were moment-curvature plots, as shown in Figure 13. For a constant flexural stiffness, a beam segment of a length, ℓ, subjected to a constant moment, M, exhibits a center displacement relative to the segment ends of

$$\delta_c = \frac{M\ell^2}{8EI} = 200 \left(\frac{M}{EI}\right) \tag{4.1}$$

where $\ell = 20$ in.

Thus it was assumed that the average flexural stiffness, $(EI)_a$, and average curvature, ϕ_D, were related by:

$$\phi_D = \frac{\delta_c}{200} = \frac{M}{(EI)_a} \tag{4.2}$$

The slope of the last cycle, D (Figure 13), was used to calculate the average flexural stiffness and the results are given in Table VI.

TABLE VI

MEASURED FLEXURAL STIFFNESS

Beam	Measured Stiffness $lb/in.^2$
2	1.32×10^9
3	1.34×10^9
4	2.06×10^9
5	1.91×10^9
7	1.50×10^9
8	1.38×10^9
9	1.36×10^9
10	1.40×10^9
11	1.53×10^9
12	1.36×10^9
13	1.17×10^9
15	1.44×10^9
16	1.44×10^9
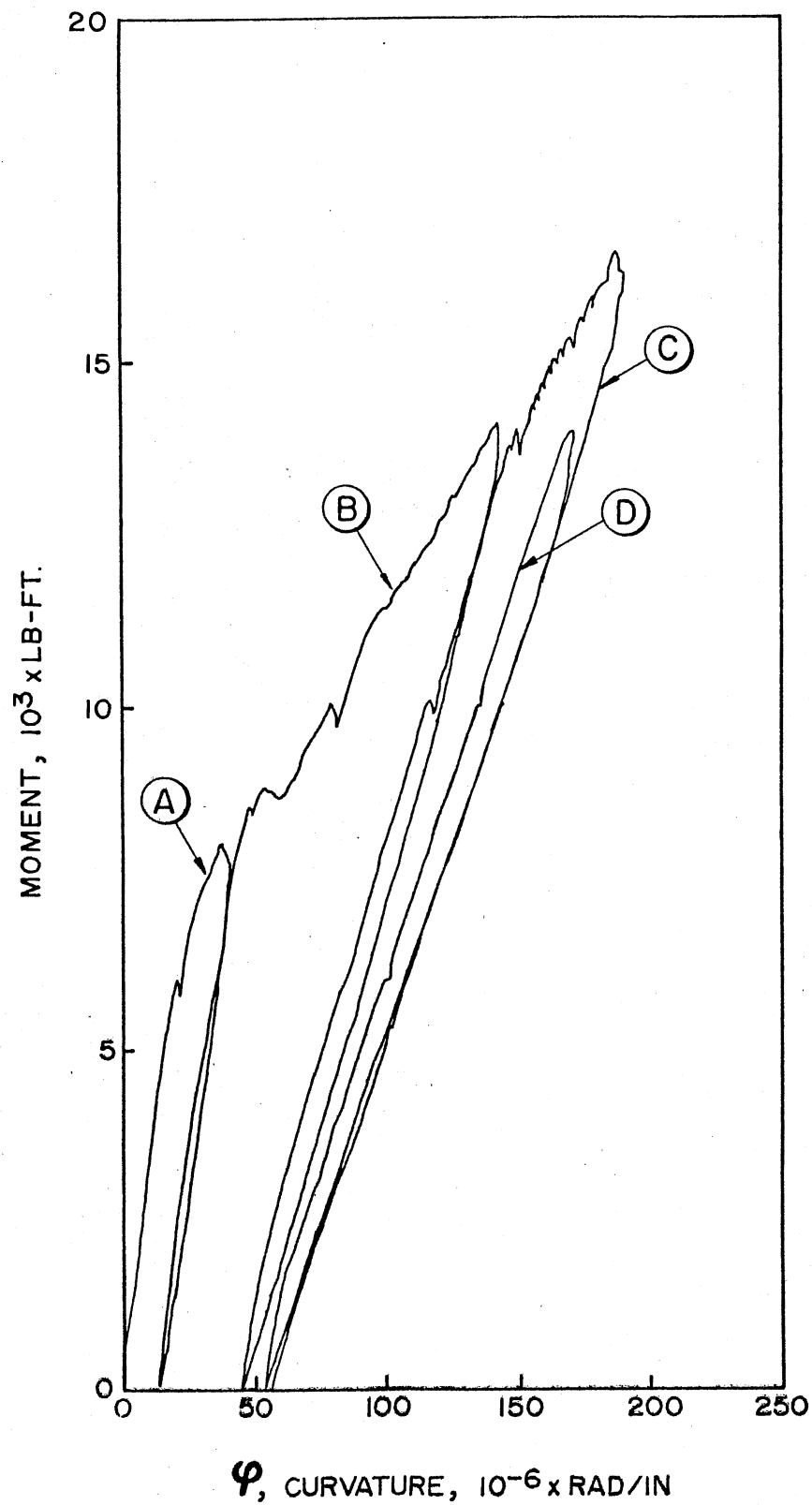
Figure 13. Typical Moment-Curvature Plot
From Preliminary Static
Load Tests

Although the $(EI)_a$ for beam 13 was lower than anticipated, comparisons between other beams were very satisfactory.

Strains measured at the center station were used to calculate the curvature, ϕ_s, at the maximum load of each loading cycle. These were compared with the average curvatures measured by relative displacement, ϕ_D, as shown in Figure 14. Note that the curvatures calculated from strains tended to be less than those found by displacements. To check a typical peak load, a theoretical section modulus and neutral axis were used to calculate curvature and strains from the applied moment. Although agreement was found with the measured steel strains, the concrete strains were less than estimated. It follows that the smaller curvature values may have been due to low concrete strain readings.

4.2 Impulse Tests

The test beams and the support equipment were shipped to Eglin AFB, Florida, following the preliminary static load tests. The test fixture was installed in Test Site C-80A and 12 tests were conducted there between 17 May and 19 September, 1974. Mission-related data were documented by Reichstetter (29).

4.2.1 Test Facilities

4.2.1.1 Test Site. A plan view of the test site, Figure 15, shows a test arena located a quarter mile from a control bunker. The elevation in Figure 15 shows the arrangement of the major test components. Cables stretched between a pair of 30 ft guyed poles supported the charge above the center of the test fixture. The charge standoff distance was set with a winch attached to one pole. Instrumentation
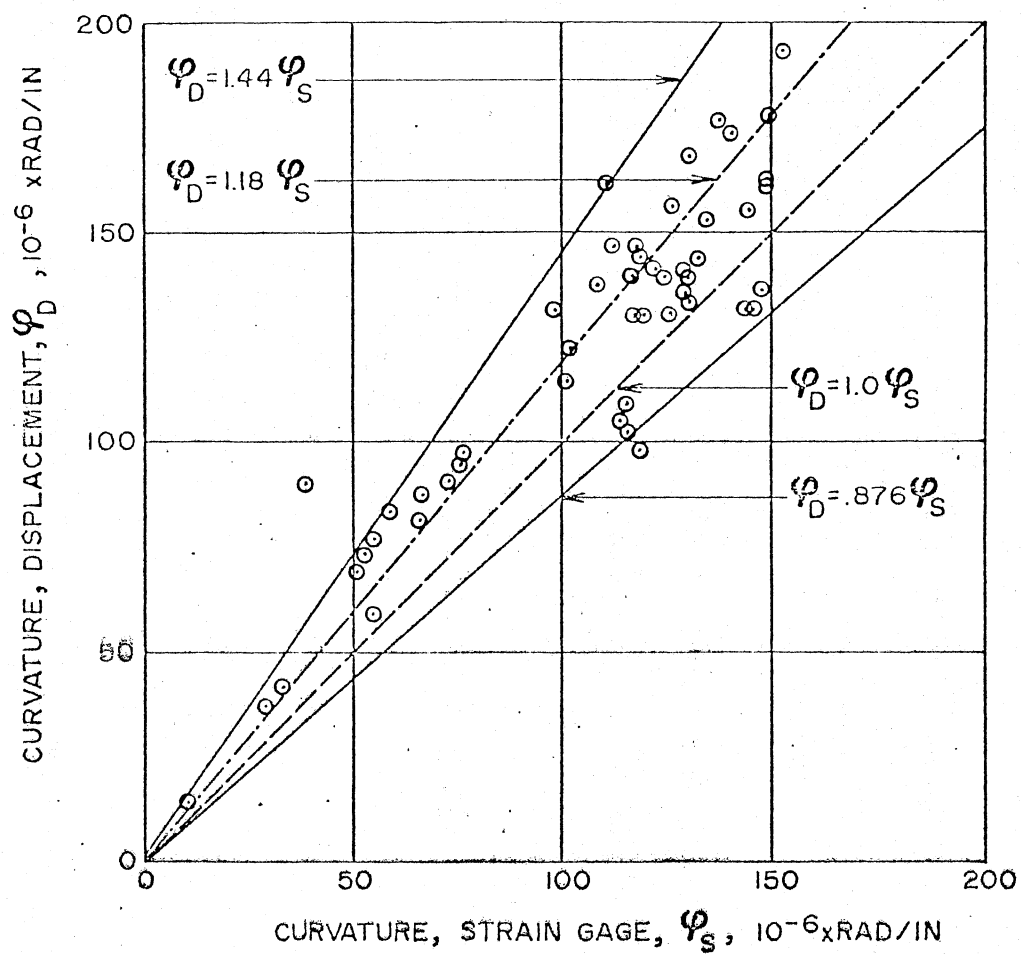
Figure 14.   Correlation Between Curvature
Measurements
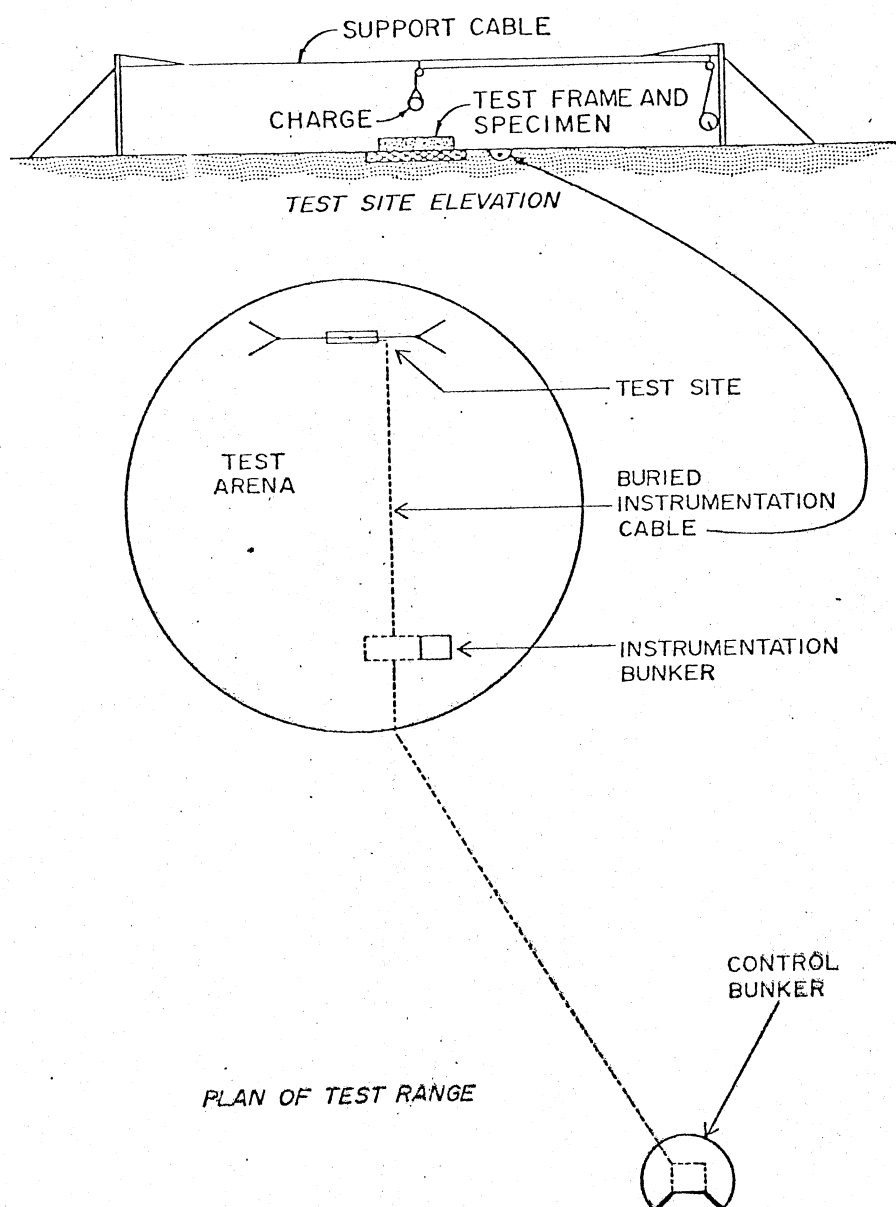
Figure 15.   Test Site Elevation and Range
C-80A Plan

lead-wires were buried in a shallow trench leading to an arena instrumentation bunker about 200 ft away. This bunker housed data acquisition equipment for the strain gage and load cell signals. The accelerometer and pressure transducer signals were transmitted to data acquisition equipment in the control bunker.

4.2.1.2 Data Acquisition. During a test, data were obtained from six load cells, eight strain gages, five accelerometers, and four pressure transducers. Table VII lists the manufacturer, model and specification of these instruments. The data were taken on the two sets of data acquisition equipment mentioned above. The pressure and accelerometer data were recorded on the VALTS Signal Conditioning and Recording system in the C-80A control bunker (30). The strain gage and load cell signals were recorded with similar equipment temporarily installed in the instrument bunker.

4.2.1.3 Explosive Charges. Twelve charges were procured by Eglin AFB, Florida for the test program. They were 18.75 in. diameter spheres of Pentolite weighing 214 lbs. Each charge was suspended from the overhead cable with a nylon harness, as shown in Figure 16. An M-6 detonator was placed in the center of each charge through a drilled hole. The charge was encircled by a "break-wire" to produce a time of detonation mark for telemetry time reference. This time was designated T$\emptyset$ in the reduced data shown in Appendix A.

4.2.1.4 Test Fixture. The test beams were installed in a massive instrumented test fixture which rested on a three-foot-thick foundation slab. As discussed in Chapter III, the test fixture was designed so that only the top surface of the test beam was loaded by the shock wave. The test fixture, shown in Figure 17, was constructed at the Oklahoma

TABLE VII

INSTRUMENTATION SCHEDULE

Instrument	Manufacturer and Model	Specification	Provided By
Accelerometers	ENDEVCO 2225	20,000 g	ADTC
Pressure Transducers	Kistler 202A1	5,000 psi	ADTC (Tests 1-5)
	PCB 102M24	5,000 psi	ADTC (Tests 6-12)
Strain Gages			
Concrete	BLH Electronics BLH A9-4	120 + 1.5 OHMS Gage Factor = 2.14	OSU
Steel	Budd Corporation C6-181B	120 + 0.2 OHMS Gage Factor = 2.09	OSU
Load Cells	BLH Electronics U1	10,000 lb	OSU
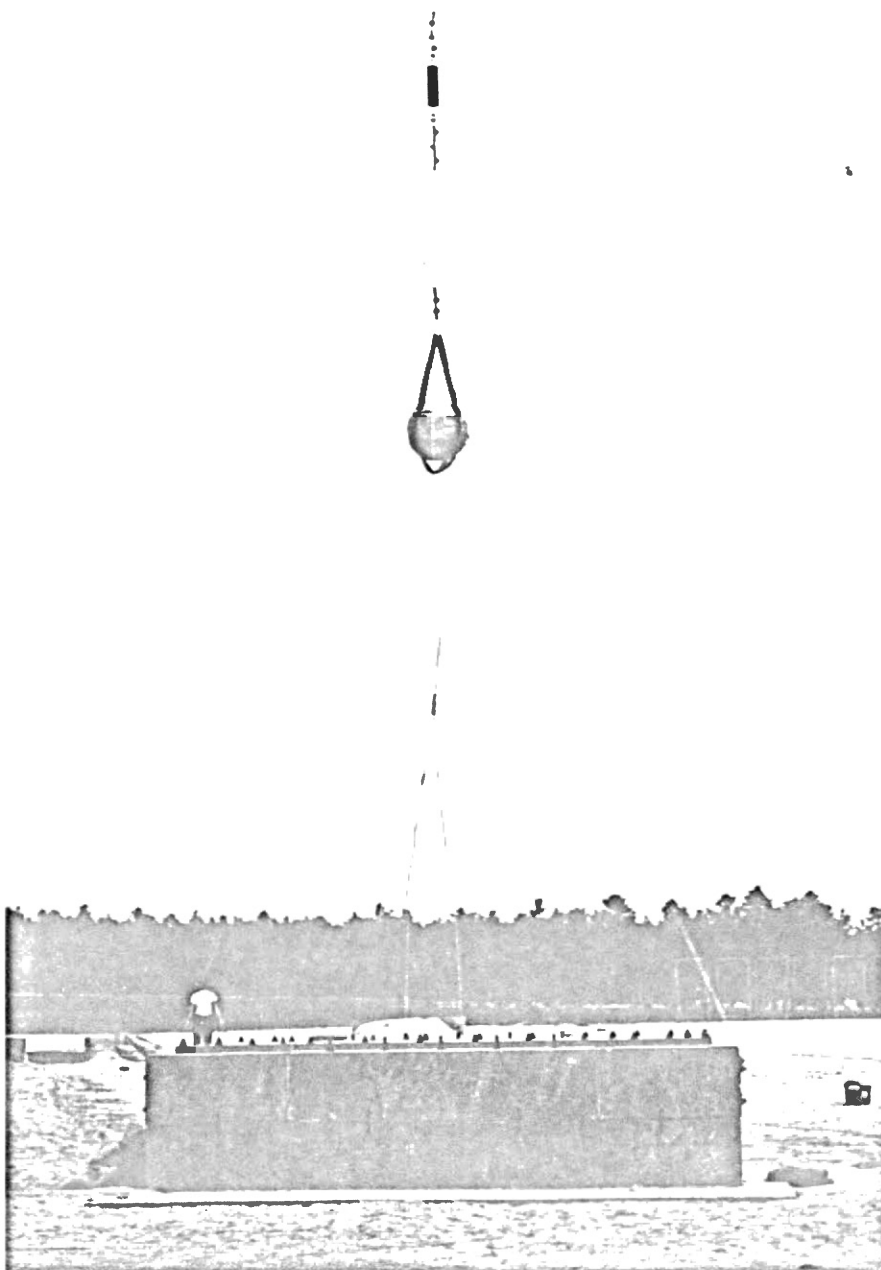
FIGURE 16.   Charge in Place Over Test Fixture Prior to Test.

BASE ASSEMBLY

SIDE RAIL

BEAM SUPPORT
MECHANISM

KEYWAY

END BLOCK
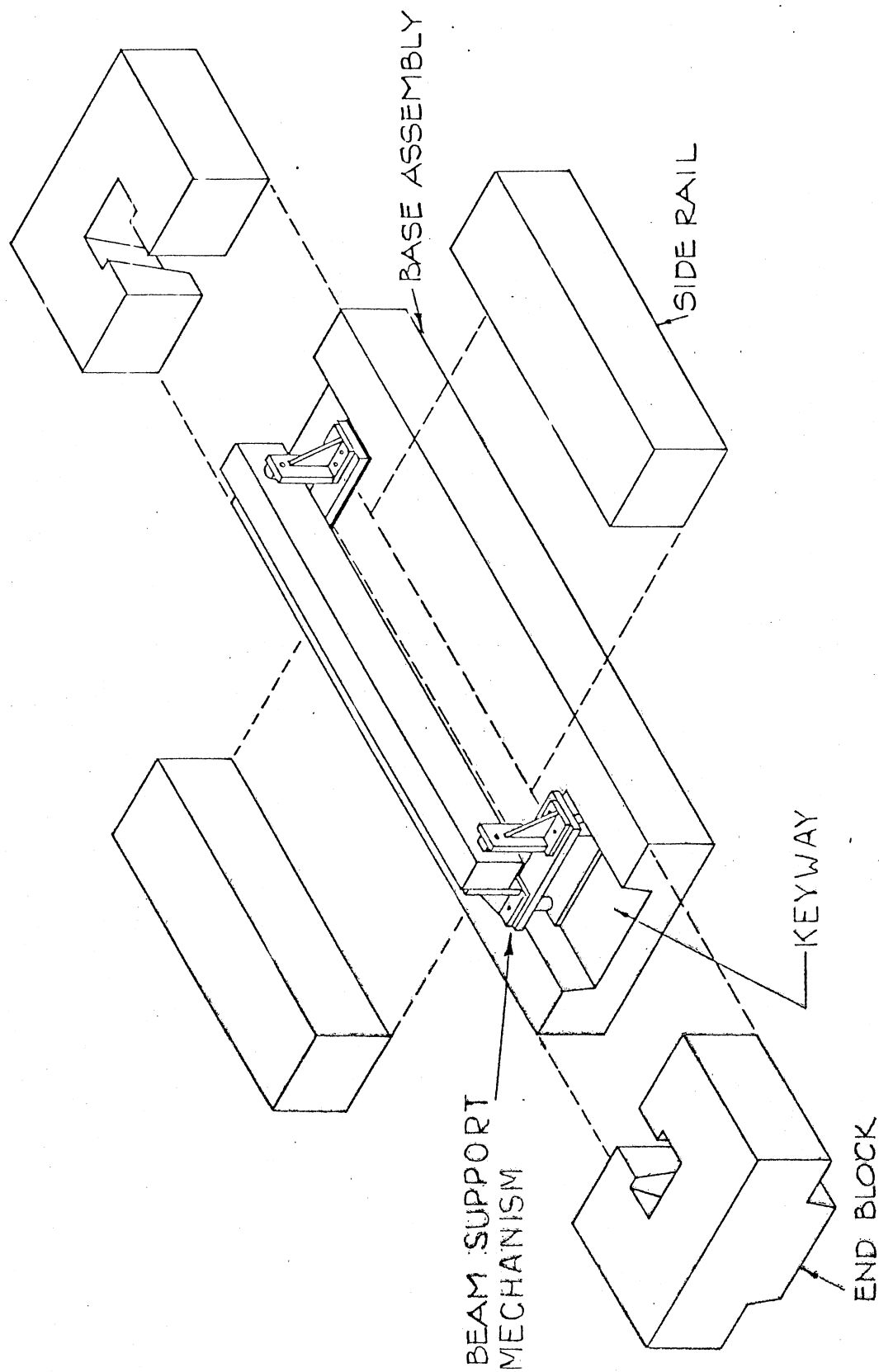
Figure 17. Test Fixture With Beam Installed on Support Mechanisms

State University Civil Engineering Laboratory in Stillwater, Oklahoma for the purpose of protecting the test beam, the instrumentation, and the beam support assembly. It featured a base slab with a key-way cast into each end. Three load cells were positioned in each key-way and a pair of beam support mechanisms were positioned over the load cells to comprise a beam support assembly. Each mechanism provided hinged supports and transmitted beam end reactions to the base slab through load cells. Four large cast concrete blocks were placed on the base slab to enclose the beam and its support assemblies. The end blocks and side-rails formed a 12 in. wide channel to enclose the beam. The four top blocks were fastened to each other and to the base slab by horizontal and vertical tie rods.

Two-inch-thick plates were placed on top of the fixture flush with the top surface of the beam to cover the space between the beam and the blocks, as shown in Figure 18. A small gap was left between the plate and the beam to prevent the plate from interfering with the beam motion. This space was covered with a light gage steel sheet to seal the inner cavity from blast pressure.

The top plate incorporated machined receptacles to hold the pressure transducer mounts, as shown in Figure 19. These mounts positioned the pressure transducers flush with the top surface of the plate. The transducer lead wires passed through conduits in the siderails and base slab to one key-way to shield them from blast effects.

Two mechanisms, Figure 20, were used to support the beam in the test fixture. They were required to provide simple supports for the beam ends, to allow the ends to displace axially without restraint, and to transmit the reaction loads to load cells and the base slab.
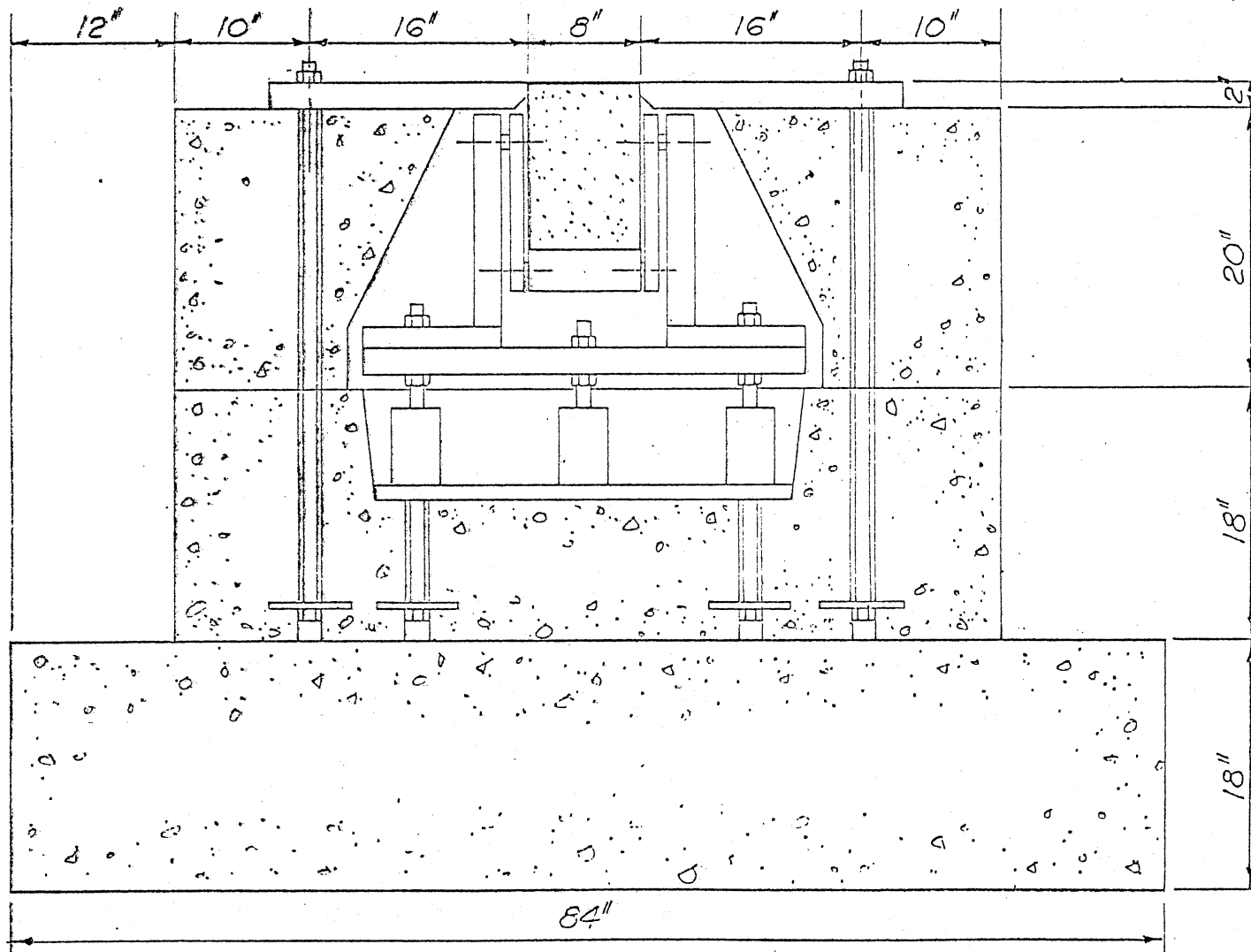
Figure 18. Cross Section Through End of Test Fixture With Top Plates, Beam Support Mechanism, and Load Cells in Place
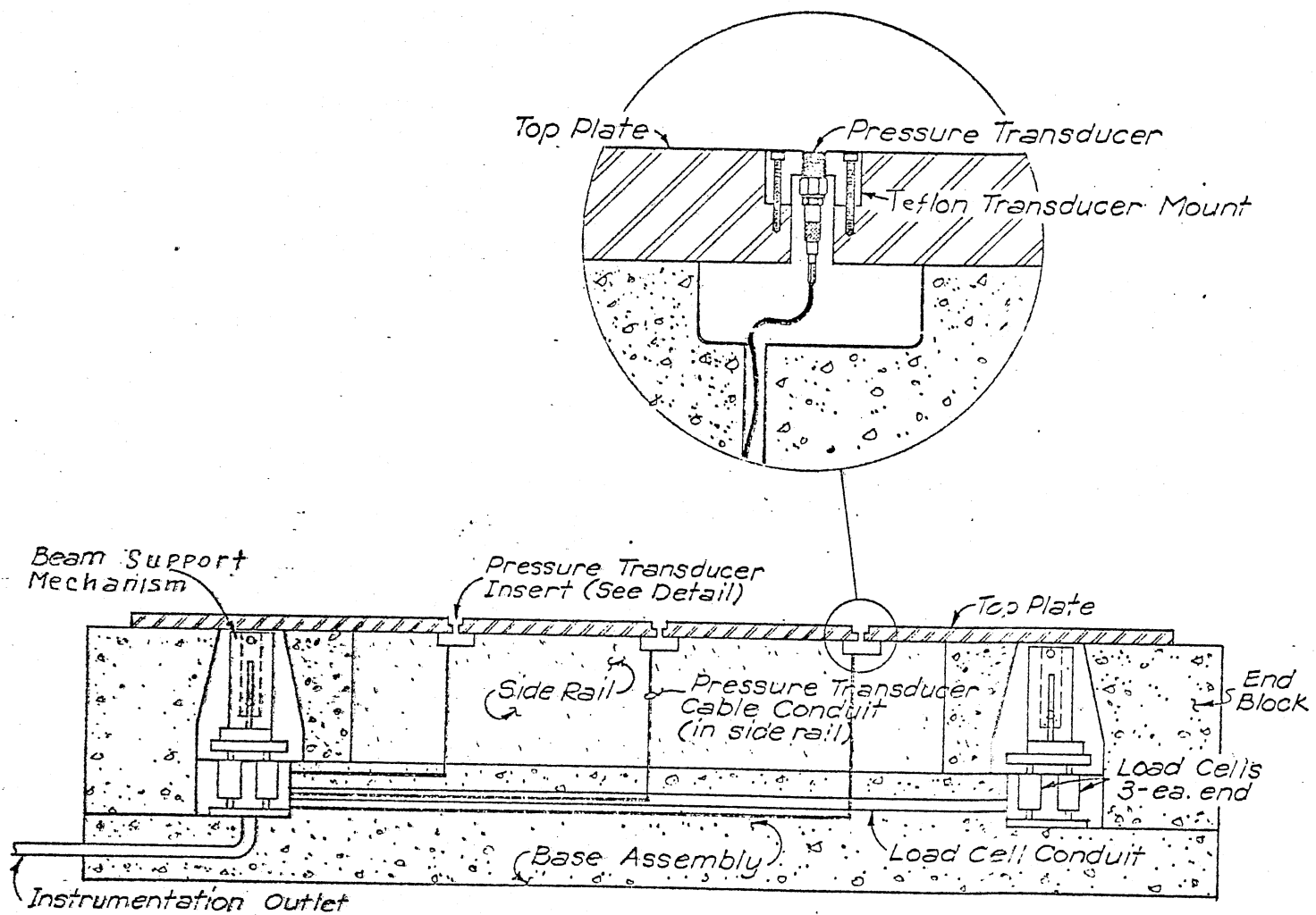
Figure 19. Test Fixture Cross Section
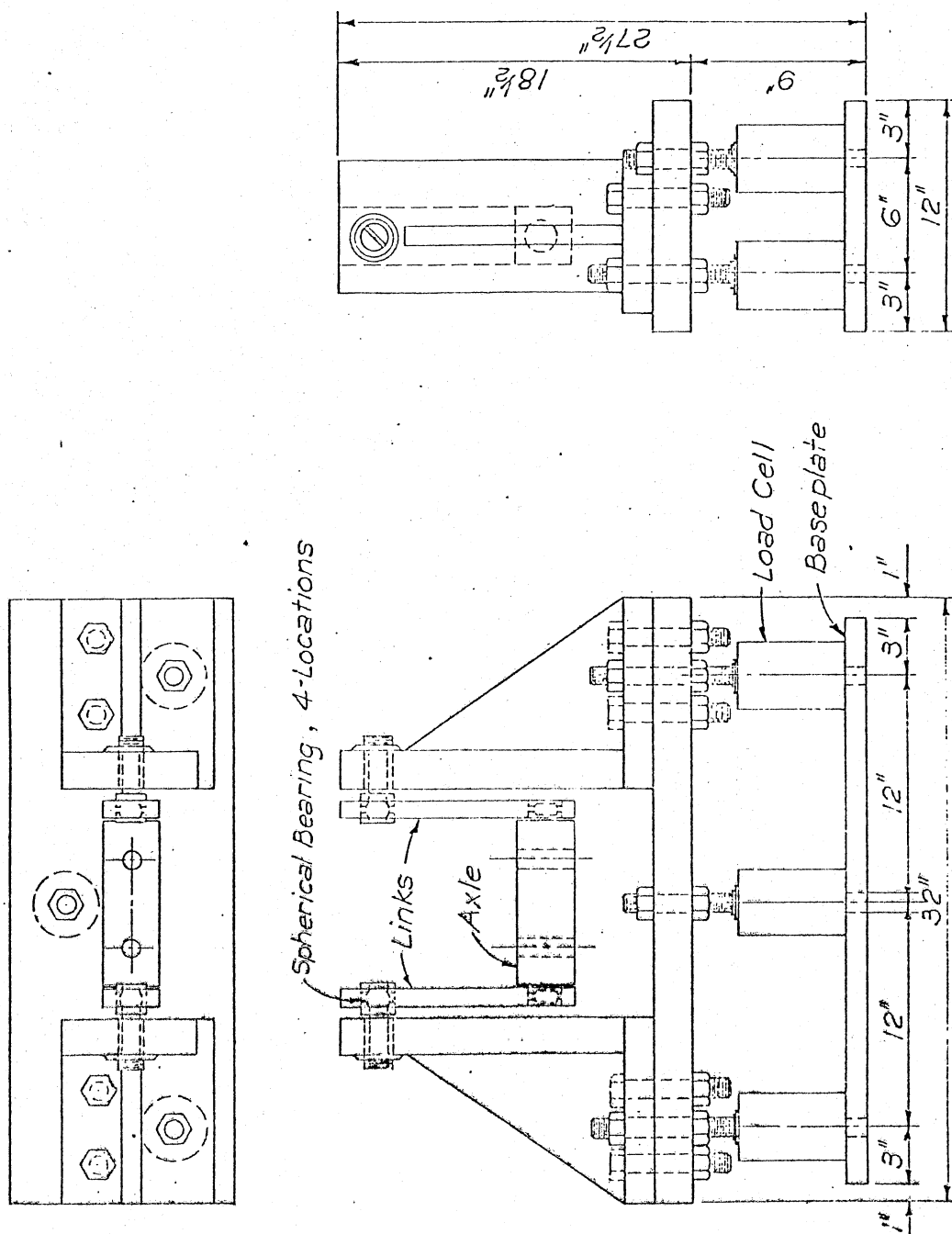
Figure 20. Beam Support Assembly

4.2.1.5 <u>Data Processing Facilities</u>. Following each test the data
were processed by the Eglin AFB Computer Sciences Laboratory. The data
were converted from the recorded analog signals to digital data at dis-
crete time increments. The pressure data were processed for a 15 ms
time interval. These data were converted to digital form in .0025 ms
time increments and were then integrated with respect to time to obtain
the impulse per unit area, I, in psi-ms, as a function of time. The re-
maining data--strains, loads and accelerations--were digitized over a
time interval of 75 ms in .0125 ms time increments. These data were
listed and copied on magnetic tape and transmitted to Oklahoma State
University for analysis. Tape numbers and data files are tabulated in
Appendix A.

4.2.2 <u>Test Procedures</u>

Each test was conducted in three stages: (1) installation and
hardware check-out; (2) charge placement and impulse testing; and (3)
post-test examination of the beam. In the first stage, two static load
tests were performed after the installation in the frame. The beam was
loaded as in the laboratory to produce a constant moment in the center
section of the member. A 10,000 lb load was applied and strains in
steel, concrete and load cells were manually recorded. The strain
gages and load cells were connected to the signal conditioning and re-
cording equipment and the calibration repeated with the recording
equipment. A qualitative examination of the data was performed using
oscillograph strip-outs to verify instrumentation and data acquisition
performance.

Air Force and range contractor explosive ordnance personnel pre-
pared the charge for placement, installed the detonator, and positioned
the charge at the required standoff distance over the test fixture. In
each test the charge was placed directly over the center of the test
beam. The charge was secured against wind drift with lines connecting
its harness to the test fixture. Final safety and instrumentation
checks were performed and the test was conducted.

Following the explosion the test specimen was examined for the
effects of the blast and photographed before removal from the test fix-
ture. Qualitative measurements of the beam center displacement were
made to estimate the permanent deformation. The specimen was then
removed from the test fixture and set aside. The damaged area in the
center of the beam was examined and photographed and larger flexural
cracks and their approximate widths at the level of the reinforcement
steel were noted.

4.2.3 Test Plan

Since there were no precedents for this type of test, it was anti-
cipated that several tests would be required to prove out test proce-
dures, hardware instrumentation, and data handling procedures. The
test plan was predicated on using several tests to identify and correct
problems with hardware. Following the preliminary tests a dual program
of testing was to be conducted. First, nominal beams were to be sub-
jected to the widest practicable range of impulses followed by tests of
modified beams at selected impulses.

The preliminary tests revealed important features which required
modification. Following the first test, the support mechanism

axle pins were found to be bent and a second set of axles was fabricated using high strength steel. Calibration levels were adjusted upward in anticipation of larger strains, pressures, and loads. The peak accelerations were many times those estimated and the high calibration levels required to accommodate these peak accelerations caused the much smaller beam free vibration accelerations to be the same order of magnitude as the instrumentation line noise errors. This posed the problem of separating the error signals from the accelerations measured during beam free vibration. On the fifth test a thin gasket was placed underneath a quarter-point accelerometer and the calibration on that channel was changed from 10,000 g's to 1000 g's. The calibration level change was meant to improve the signal-to-noise characteristics during beam free vibration. As a result the peak measured accelerations decreased significantly and the free vibration signal became more distinct. However, a zero shift could not be eliminated from the accelerometer data. Modified axles were installed before the third test and accelerometers were placed on each axle to monitor motion of the support mechanism.

After the first four tests the pressure transducers were replaced to provide more reliable pressure-time data. The test configuration was further modified by burying the test fixture so that the top surface of the beam, the test frame, and the ground level formed a plane. This was done to eliminate pressure relief which may have been present due to the vertical faces of the long narrow test fixture.

The beams of the fifth and sixth tests exhibited distress along their top edges near the center half of the span due to contact with the top cover steel. Although the steel plate had been initially placed a minimum of 0.2 in. away from the beam, contact was apparent.

A pair of 4 x 6 in. posts were placed at the bottom of the cavity between the two siderails to eliminate this interference.

Prior to test 7 one load cell did not satisfy an electrical check. A replacement load cell could not be obtained and it was left in place to continue its mechanical function. No data were taken from it during the last six tests. A log of all tests is given in Table VIII. Included are the test dates, the beam numbers, and post-test measurements.

4.2.4 Post-Test Observations

The beams suffered little damage in the first two tests. A vertical crack ran through the beams to their top surface as shown in Figure 21. These cracks were clean, straight tensile fractures on the top surface and were presumed to have resulted from beam rebound and subsequent curvature reversal which placed the top surface in tension. Cracking of the center section was characteristic of all test beams. Longitudinal hairline cracks were noted on the sides of these two beams about 1/2 in. below the top surface for 3 to 4 in. on either side of the centerline. These cracks appeared to be the beginning of shear failure, or spalling, of the top layer. In later tests, with smaller charge standoff distances, the top layer, 1/2 to 3/4 in. thick, exhibited shear failure for distances of 6 to 8 in. on either side of the centerline. In Figure 22 this process appeared to be in its initial stages. The outlined areas on the top surfcce appeared to be ready to separate from the beam. For still smaller standoff distances the concrete was crushed in a wedge-shaped zone about 2 in. wide and 1/2 to 3/4 in. deep as shown in Figure 23. For the smallest standoff idstances, the crushed zone was about 4 in. wide and 1 to 1½ in. deep.

TABLE VIII

TEST PARAMETERS AND POST-TEST MEASUREMENTS

Test Number	Beam Number	Test Date (1974)	Charge Distance,[1] ft	Age at Test, days	Estimated Permanent Center Displacement, in.	Maximum Crack Width,[2] in.	Sum of Crack Widths,[3] in.
1	15	17 May	16.00	310	0.45	--	--
2	16	29 May	15.25	317	0.34	--	--
3	12	19 June	12.75	358	0.72	0.135	--
4	4	21 June	12.25	308	0.04	--	--
5	10	21 Aug.	11.75	434	0.88	0.147	0.221
6	8	23 Aug.	11.75	378	0.80	0.168	0.272
7	7	10 Sept.	11.25	397	0.72	0.101	0.229
8	2	12 Sept.	11.25	393	1.02	0.203	0.352
9	5	13 Sept.	11.25	389	0.31	0.076	0.076
10	9	16 Sept.	10.75	398	0.99	0.171	0.329
11	3	18 Sept.	10.25	398	0.78	0.120	0.260
12	11	19 Sept.	11.25	457	0.90	0.155	0.246

[1] Measured from center of charge to top surface of beam.

[2] Average of width of largest crack on each side of beam, at level of reinforcing steel.

[3] Average of sum of measurable crack widths on each side of beam, at level of reinforcing steel.
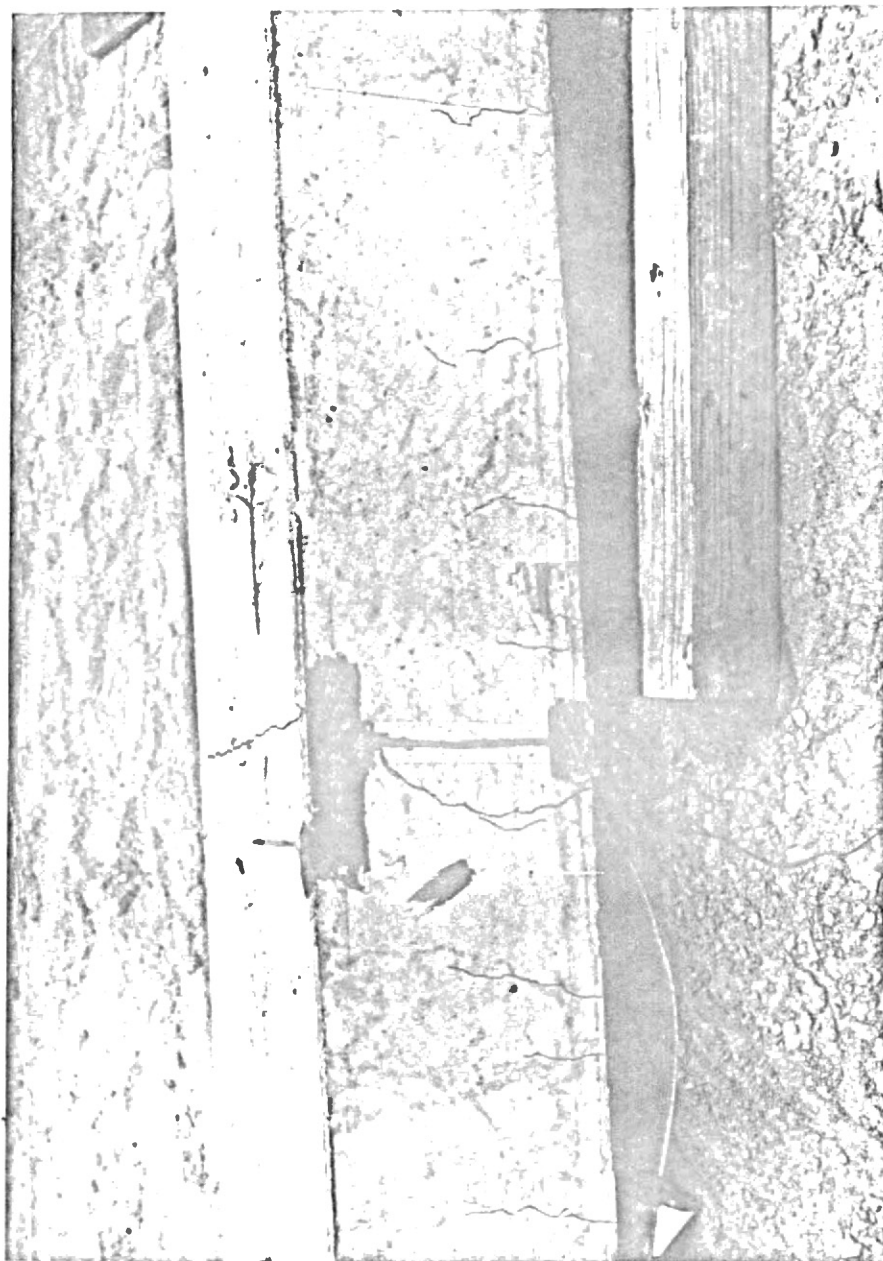
Figure 21.   Center Section of Beam After Test No. 1
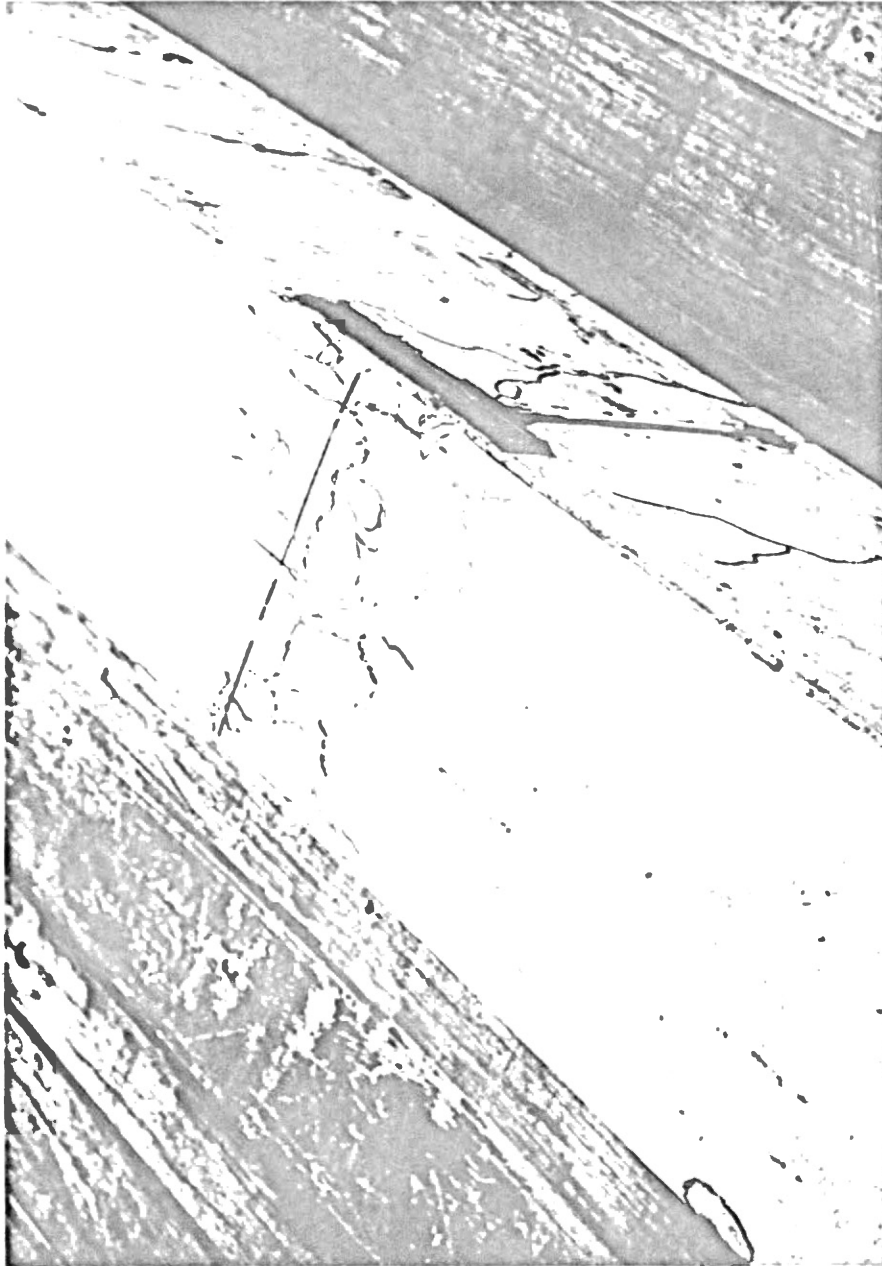
Figure 22. Center Section of Beam 12 After Test No. 3
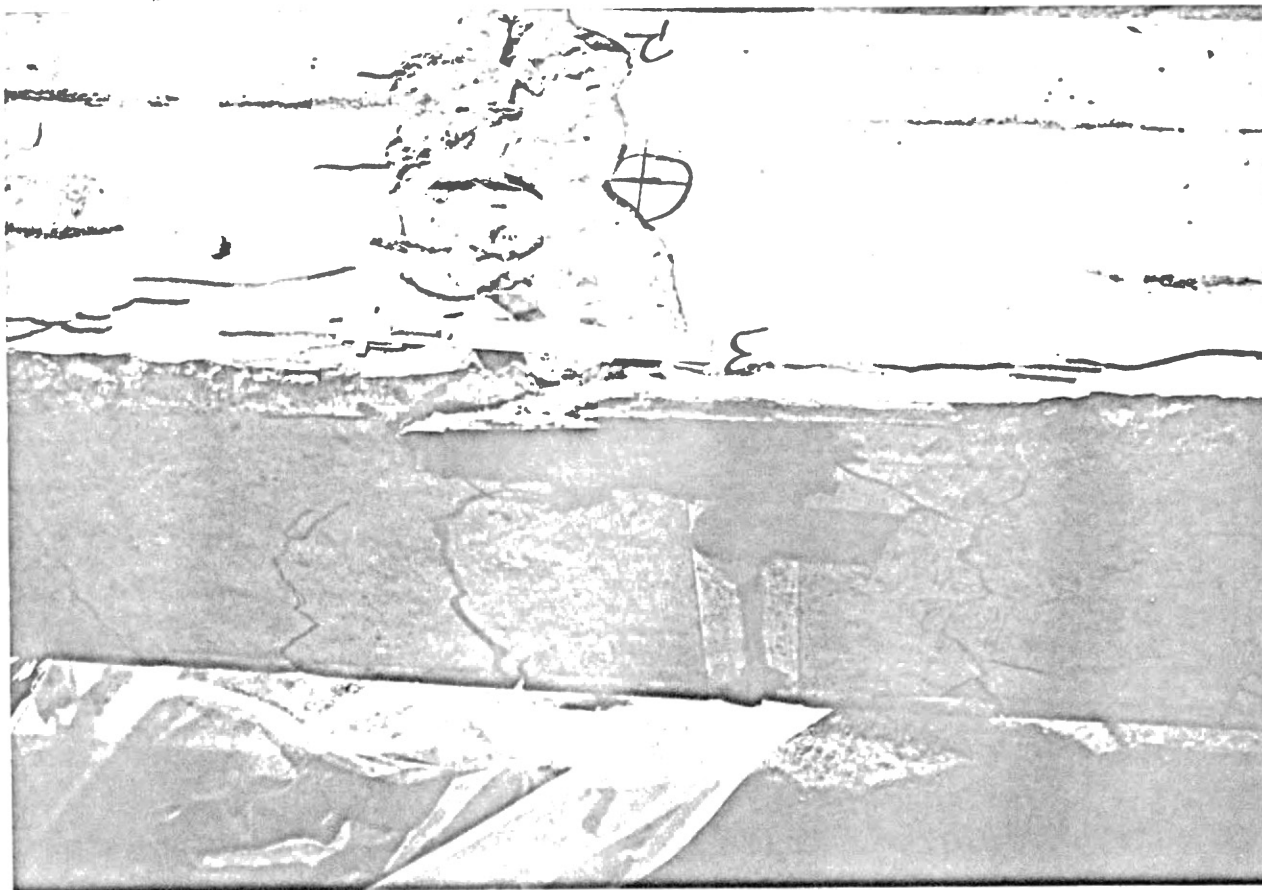
Figure 23. Beam 9 Center Section After Test 10 With Shallow
Wedge-Shaped Crushing Zone

This type of behavior did not occur in the high strength concrete beams, as can be seen in Figure 24. These two beams showed no crushing and had only a longitudinal hairline crack 1/2 in. below the top surface. In contrast with the nominal strength beams tested with the same standoff distance, the high strength concrete appeared to be quite durable and damage resistant.

The most severely damaged beam was the high strength steel beam in the seventh test. Figure 25 shows this beam immediately after testing and prior to removal from the test fixture. Figure 26 shows the same beam after removal from the test fixture. Furthermore, the beams with No. 9 bars experienced greater top surface crushing than nominal beams with similar charge standoff distances.

The crack widths at the level of the reinforcing steel were measured after the beams were removed from the fixture. Figure 27 is typical of the appearance of the cracking in the center section. The crack spacing was on the order of 6 to 8 in. The maximum crack width occurred in the center section and the crack widths decreased with distance from the center. The smallest measurable cracks were between 12 and 18 in. from the center. Beams 8 and 9, in which the shear stirrups had been omitted, did not exhibit shear distress.

Both beams with No. 9 bars had prominent longitudinal splitting cracks at the level of the reinforcing steel, as shown in Figure 28. For beam 4 these cracks extended 12 to 18 in. on either side of the centerline. Such splitting is associated with bond failure in static tests. It must be noted that these two beams did not exhibit ductile behavior during the post-test static loading, but instead exhibited massive failure in the concrete soon after the yield occurred.
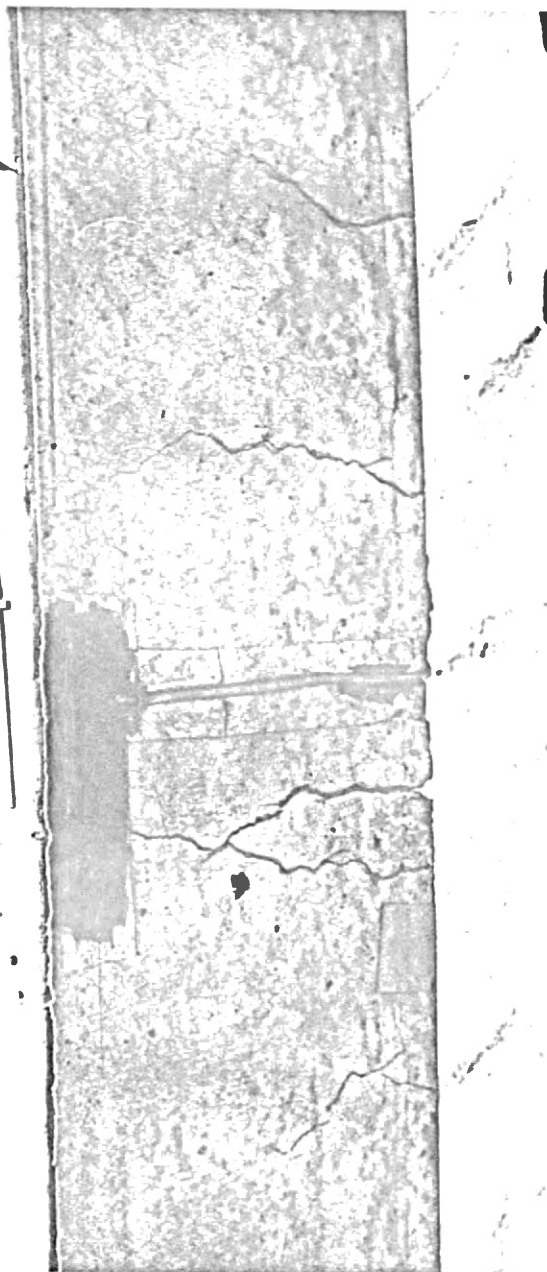
Figure 24. Center Section of Beam No. 3 After Test 1Γ
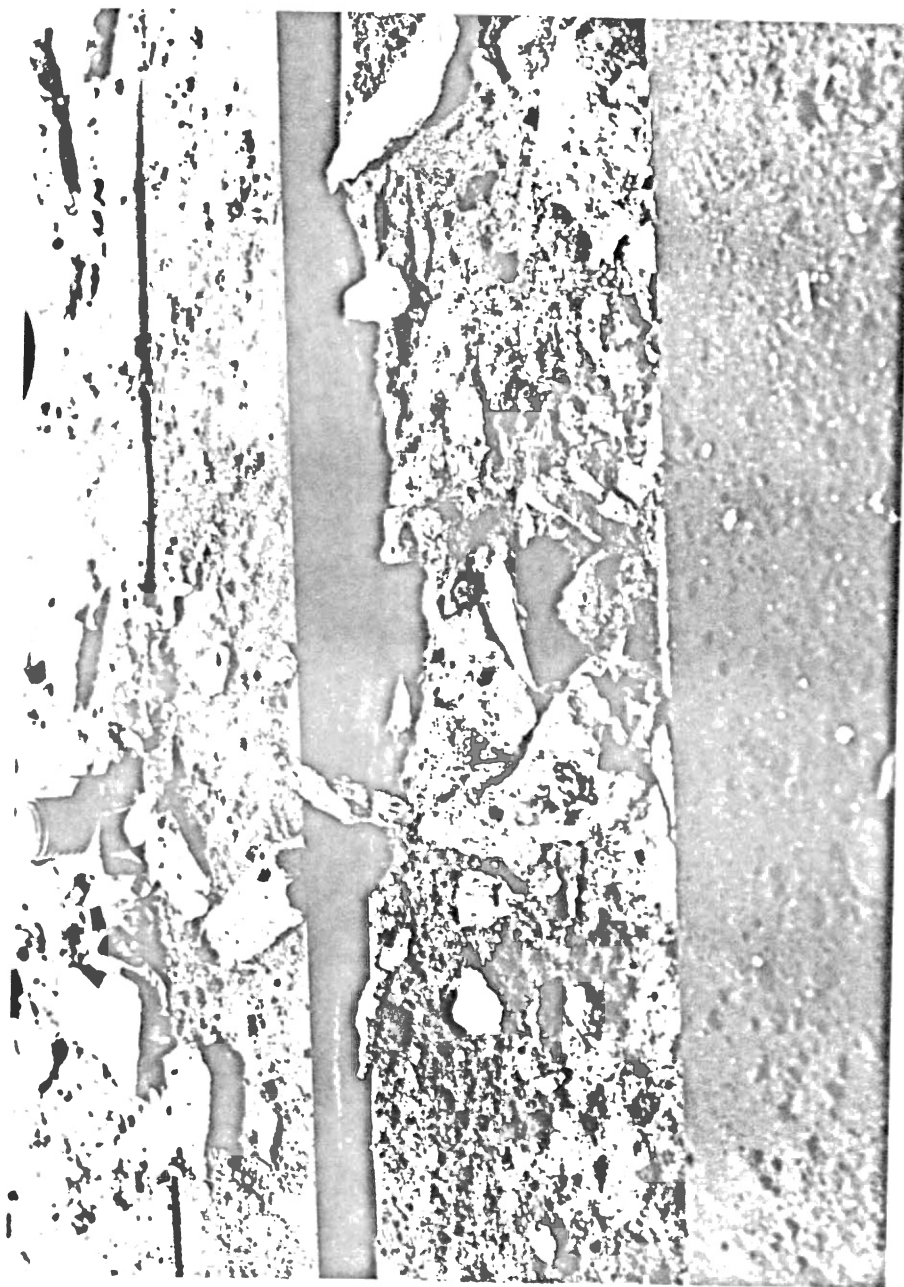
Figure 25. Center Section of Beam 7 After Test 7
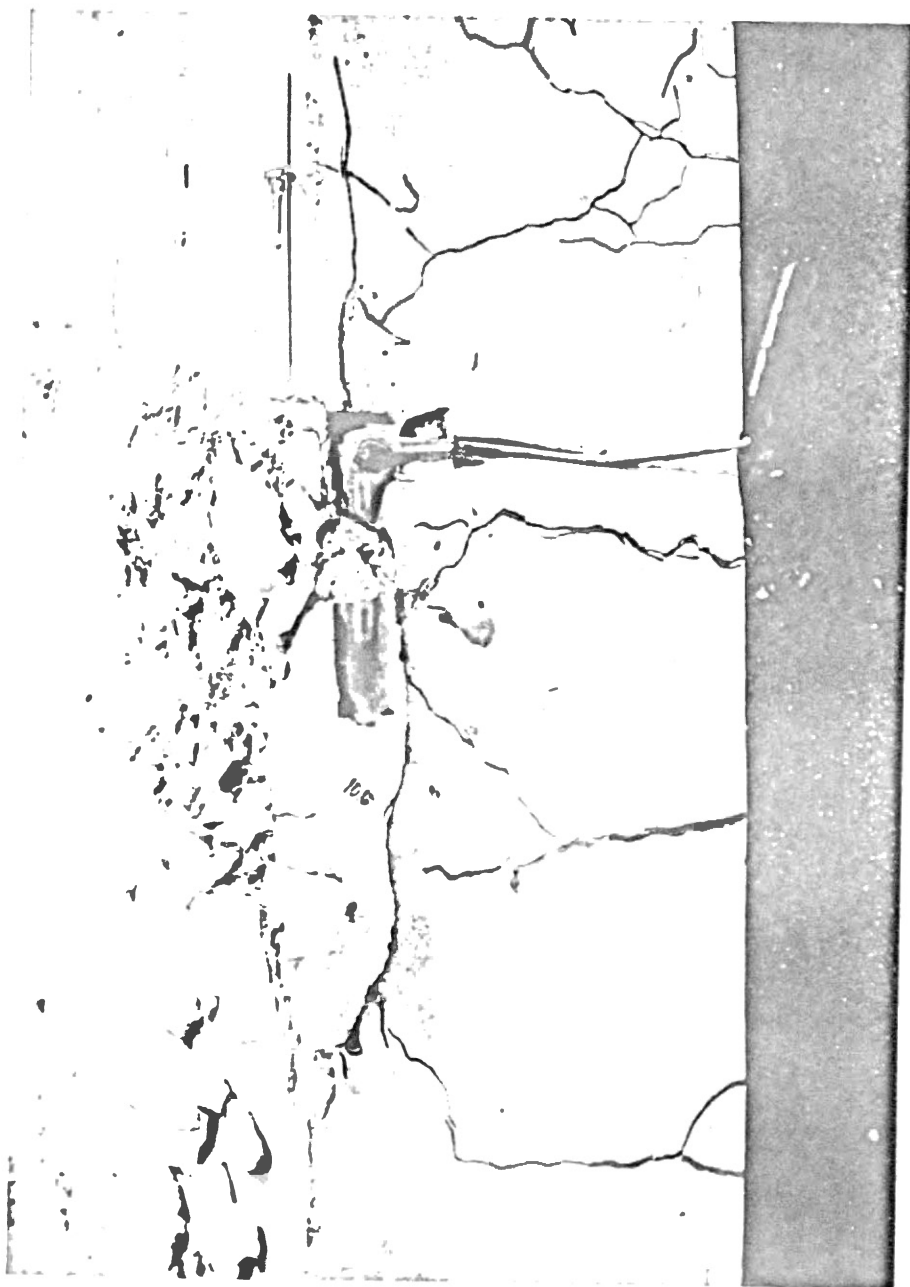
Figure 26.   Side View of Beam 7 After Test 7
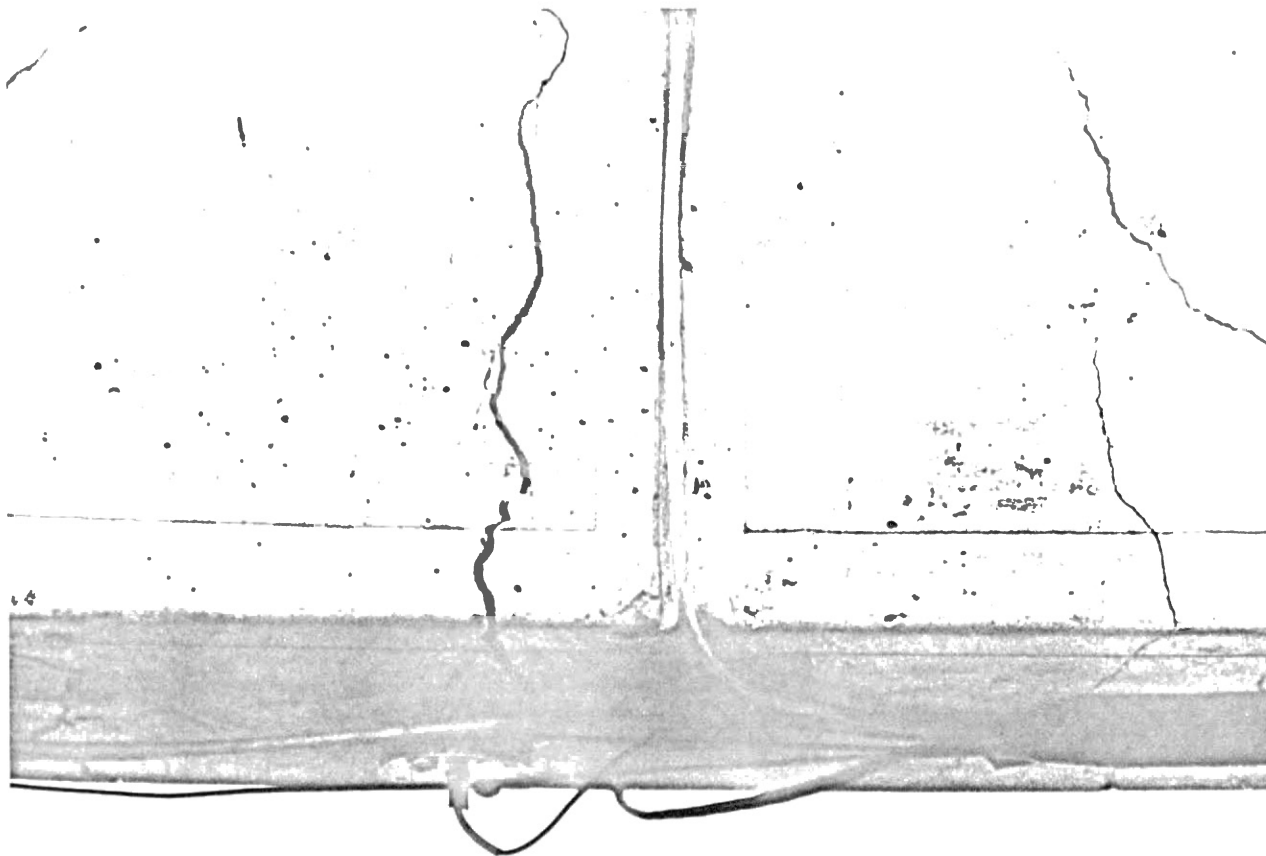
Figure 27. Side and Bottom of Beam No. 3 After Test 11, Showing
Width of Crack

Figure 28. Side View of Beam 4 After Test 4

4.3 Damage Assessment Tests

Although the impulse loadings caused significant crushing and spalling of the top surface and permanent displacement of the beam center, visual inspections could not define the extent of the damage. To quantify the damage and to relate it to delivered impulse, the beams were returned to Oklahoma State University, Stillwater, Oklahoma, for further testing.

The test configuration for the final load tests was identical to the preliminary static tests. Loads were applied as shown in Figure 12 and both loads and displacements were recorded on an X-Y recorder. The test procedure was to load a beam progressively to (1) yield of the steel, (2) ultimate moment, and (3) failure. Yielding was defined as the load at which the load-displacement plot ceased to be linear. The ultimate moment, M_u', was the largest measured moment and may or may not have coincided with failure. Failure was defined as a sudden, large loss of load due to the separation of a significant zone of concrete on the top surface of the beam. Additional loading was imposed and progressive failure occurred until the capacity of the beam was reduced to about 50% of the ultimate load. Typical data from final static tests are shown in Figure 29. The response of an undamaged nominal beam (beam 13) and a typical impulse damaged beam (beam 11) are shown for comparison. Variations between the static behavior of the damaged and undamaged beams are attributed to the impulse loading.

Load, strain, and deflection data were recorded at regular intervals during these tests. Small, sharp reductions of load noted in the load-deflection curves of Figure 29 occurred during the manual recording
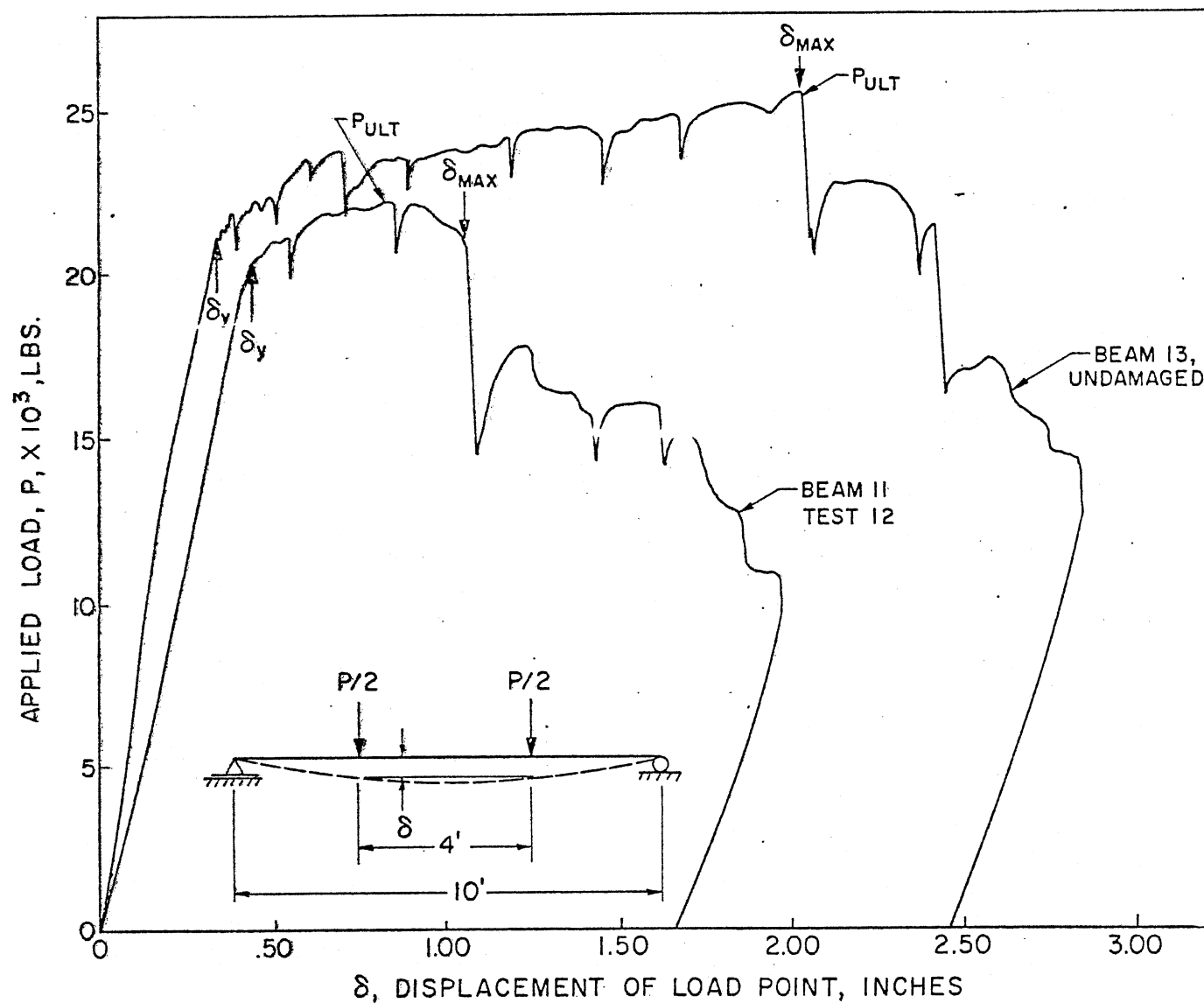
Figure 29. Comparison of Load-Displacement Curves of Impulse Damaged Beam and Undamaged Beam

of data and occasionally coincided with small failures in the compression zone of the beam. When the beam was reloaded, following the recording of data, the loads tended to follow the path which had been defined before halting the test.

The parameters necessary to evaluate the effects of impulse load are shown in Figure 29. For beam 13 the deflection at the end of the linear portion, δ_y, defines the initial yielding of the steel. For the damaged beams, δ_y is the deflection necessary to reload the beam to the maximum deformation attained during the impulse test. Deflection δ_{max} is the deflection related to beam failure as defined above and coincided with a large drop in load capacity and a significant loss of concrete in the compression zone. Finally, the ultimate load, which is related to the maximum moment on the cross section, is recorded. These data, recorded in Table IX by beam and test number, are used in Chapter IX to assess the effect of the impulse load on the damage sustained by the beams.

Two quantities which may be related to damage are the ductility ratio μ, δ_{max}/δ_y, and W_p, the work dissipated during plastic displacement. The static ductility ratio relates the ability of the beams to undergo plastic deformation. Note that the undamaged beam (beam 13) has a static ductility ratio of 6.30 whereas nominal beams subjected to impulse loading exhibited much smaller values. The work, W_p, was obtained by integrating the area under the load-deflection curve between δ_y and δ_{max}. The ability of the beam to undergo plastic deformation was significantly altered by the impulse load, as seen in Table IX. On the other hand, a significant change is not noted in the ultimate moment of the nominal beams.

TABLE IX

SUMMARY OF RESULTS OF STATIC STRENGTH
TESTS OF DAMAGED BEAMS

Test Number	Beam Number	Ultimate Moment, Kip-ft M_u'	Work Performed on Beam, Plastic Range W_p, Kip-in.	Displacement of Load Point at Yield, δ_y, in.	Displacement of Load Point at Failure, δ_{max}, in.	Ratio of Failure to Yield Displacement $\mu = \delta_{max}/\delta_y$
1	15	35.7	25.8	.40	1.53	3.81
2	16	38.2	27.9	.41	1.90	4.63
3	12	35.4	17.2	.57	1.12	1.97
4	4	70.3	2.8	.58	.64	1.10
5	10	30.0	16.7	.60	1.30	2.17
6	8	35.8	25.2	.56	.97	1.73
7	7	34.9	12.3	.60	1.08	1.80
8	2	35.8	18.9	.55	1.32	2.40
9	5	54.5	1.4	.54	.58	1.08
10	9	33.8	12.4	.55	1.03	1.87
11	3	39.5	25.4	.42	1.49	3.55
12	11	33.4	13.5	.52	1.05	2.02
--	13	38.5	40.8	.37	2.33	6.30

CHAPTER V

PRESSURE MEASUREMENTS

The pressure to which the test specimens were subjected was measured by pressure transducers attached to the test frame at three points. These data were integrated to determine the impulse of the blast wave and both pressure and impulse were compared with predicted values from Goodman (1). Although measures were taken to isolate the transducers from the frame vibration, the initial transducer was not well suited to the blast environment and was replaced after test 5. Results from the final 7 tests indicate greater reliability for the pressure measurement.

5.1 Discussion of Pressure Data

The pressure data were processed by standard data reduction techniques of the Eglin AFB Computer Sciences Laboratory. The positive pressure was integrated to determine the blast impulse and these results are summarized in Table X. Pressure-time signals from the fourth test are shown in Figure 30. In addition to an apparent zero shift, one should also note the oscillation present in the measurements. Although the zero shift for test 4 was negative, for other tests positive shifts were found. A Kistler transducer was replaced by a PCB transducer for test 5. The signal from the new transducer did not exhibit the oscillations or baseline shift and PCB transducers were used in the remaining tests (Table VII).

TABLE X

TEST IMPULSES AND PEAK PRESSURES

Test	Stand-off, ft	PF1 (Quarter) Impulse, psi-ms I'	I	P_0, psi	PF2 (Center) Impulse, psi-ms I'	I	P_0, psi	PF3 (Quarter) Impulse, psi-ms I'	I	P_0, psi	PF4 (Cavity) Impulse, psi-ms Tabulated	1.25ms	P_0, psi	Avg. I' psi-ms	Avg. I psi-ms
1	16.00	397	342	683	402	351	660	435	309	672	--	--	--	411	334
2	15.25	335	325	1259	324	309	1167	498	389	1416	--	--	--	386	341
3	12.75	555	365	1843	228*	172*	1413	--*	32*	--	--	--	--	555	365
4	12.25	260*	260*	1130	187*	187*	1202	336	334	1614	7.3	0	25	336	334
5	11.75	190*	191*	1227	284*	284*	1854	354	311	1166	63	3	22	354	311
6	11.75	445	405	1803	1008*	502	1796	530	410	1668	88	21	53	487	441
7	11.25										--	--	--	--	
8	11.25	600	380	1453	131*	131*	1700	588	470	1447	29	2	18	594	425
9	11.25	467	445	1344	138*	132*	1418	418	413	941	49	6	19	442	429
10	10.75	529	422	2148	578	395	1983	784	390	3259	102	8	86	630	402
11	10.25	480	350	1132	621	431	1342	--*	414	2205	200	14	135	550	398
12	11.25	407	351	1872	442	370	1807	414	364	1675	112	11	91	421	362

*Omitted from average.

I' = impulse at 15ms.

I = impulse at 1.25ms after shock wave arrival.

Average impulses are for top transducers.

The cavity pressure (Figure 30) generally did not exceed 20 psi. Although the top seal was not penetrated on test 4, it was on other tests and peak internal pressures on the order of 80 to 120 psi were recorded.

5.2 Calculated Impulse

The pressure-time data were numerically integrated at the time of data reduction to calculate the impulse of the explosion. The calculated impulse for each pressure transducer is recorded along with the peak pressure on the data plots of Appendix A. The numerical method integrated only positive pressures over the total time span (15 ms) of the plot. Consequently, a positive shift of the transducer zero was integrated, and caused, in several tests, significant errors in the calculated impulse. This impulse is recorded as I' in Table X.

To develop more reliable impulse data, pressure-time curves were reviewed and it was determined that the duration of the positive pressure for all tests was approximately 1.25 ms. The construction shown on PF3 of Figure 30 illustrates the evaluation of the positive pressure duration, t_d. The pressure data were then reviewed and the change in calculated impulse over a 1.25 ms period after the shock wave impingement on the beam was selected as the impulse. This value is recorded as I in Table X.

5.3 Correlation with Predicted Values

Peak pressures and calculated impulse are shown in Figures 31 and 32 as a function of standoff distance. Also shown on these figures are Goodman's predicted values (1) for both pressure and impulse.

Although scatter is noted in the data, the measured pressure shows reasonable agreement with predicted values. On the other hand, the
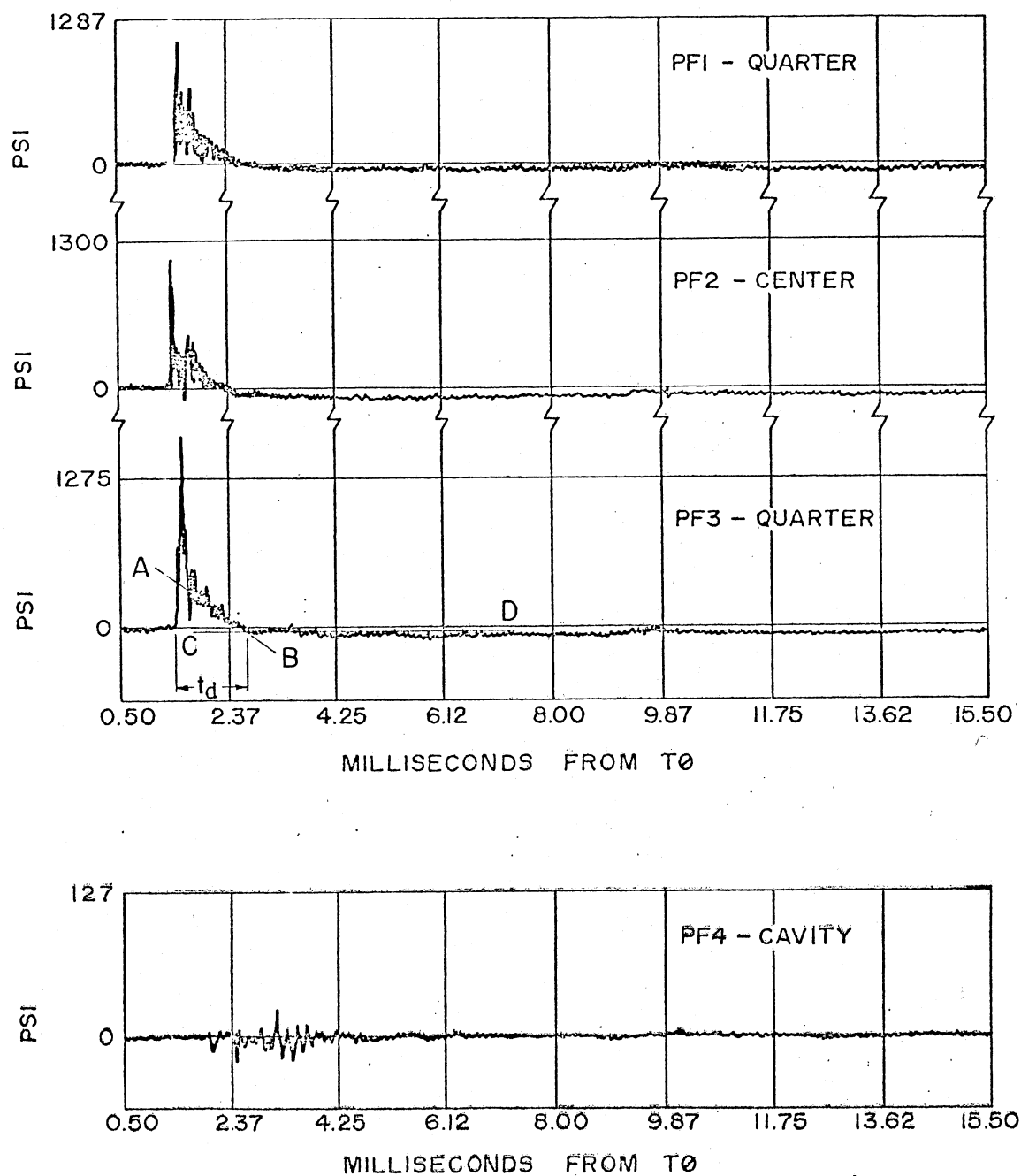
Figure 30. Plots of Typical Pressure Data and Illustration of Method to Estimate t_d, From Test 4
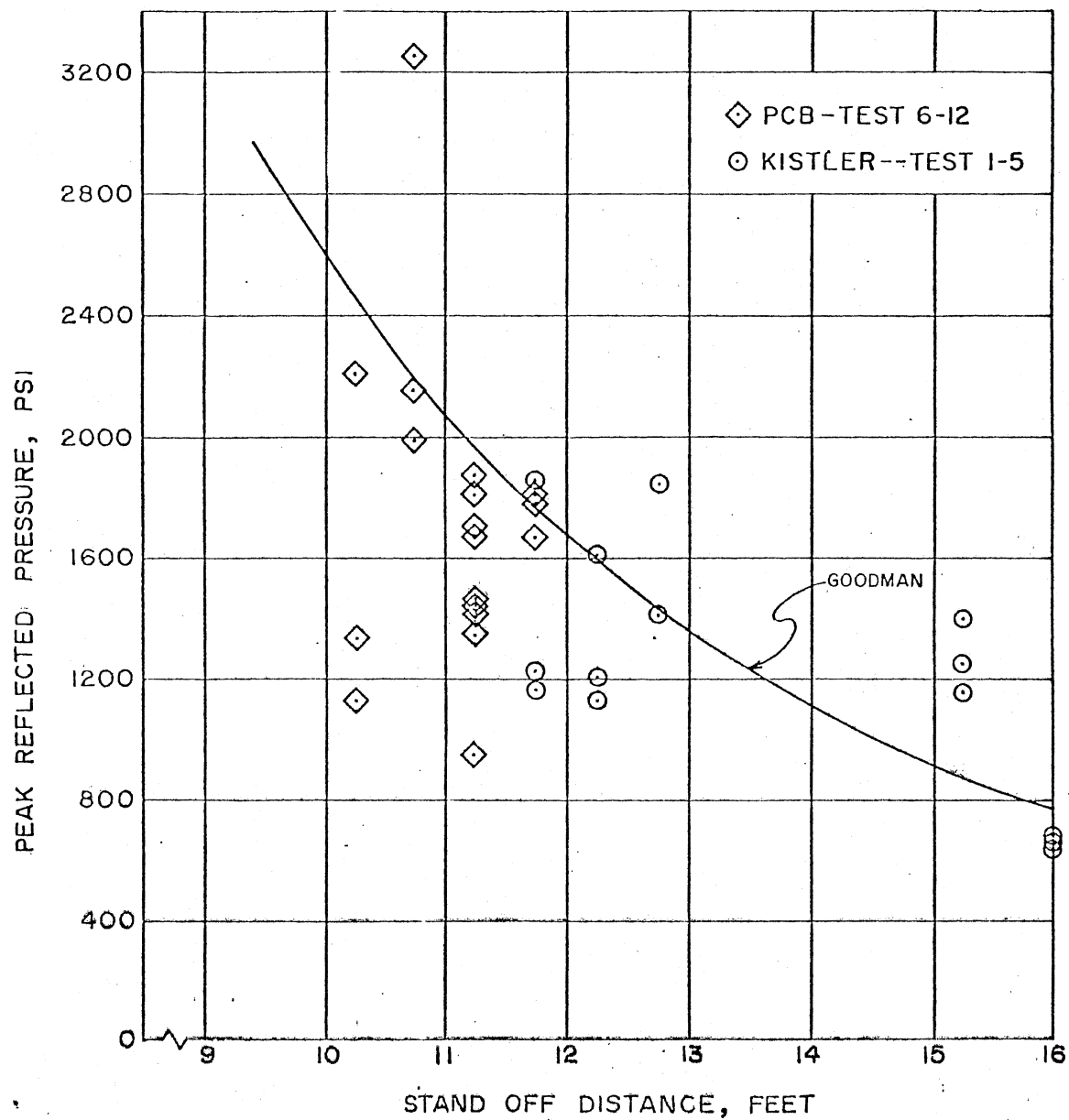
Figure 31. Comparison of Peak Reflected Pressure With
Predictions From Goodman (1)
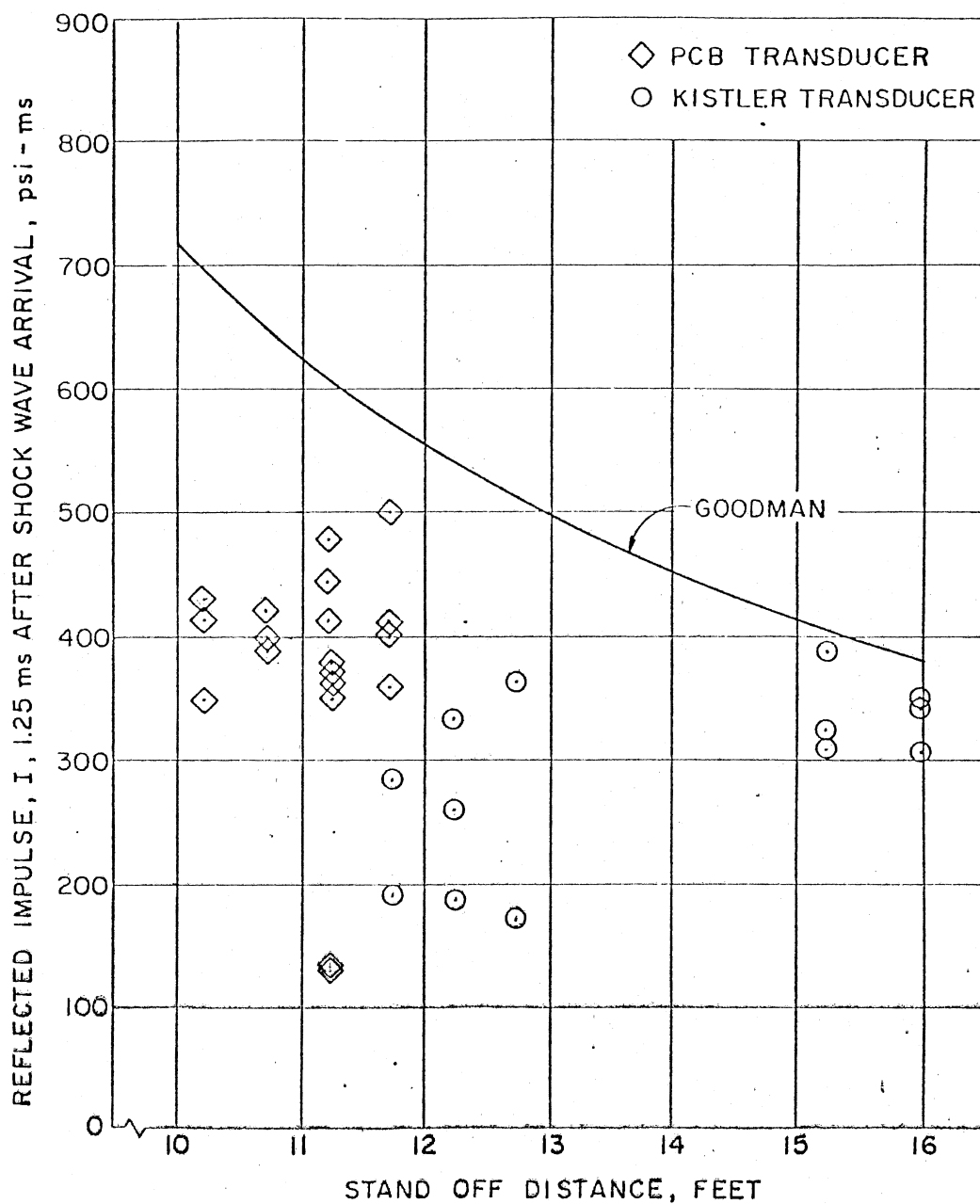
Figure 32. Comparison of Primary Reflected Impulse With Predictions From Goodman (1)

calculated impulse is always less than predicted. These results may not

be significant due to the response of the transducer to shock loading.

the measured pressure may overestimate the actual pressure due to the

very short rise time of the blast wave. Furthermore, the time at which

the zero shift occurs is not well defined. Therefore, these data should

be accepted as qualitative, and not precise values of pressure and im-

pulse. In future chapters the charge standoff distance, which was mea-

sured to within 1/4 inch, will be used to represent pressure and impulse

characteristics of the chemical explosion.

CHAPTER VI

ACCELERATION MEASUREMENT

To measure the time dependent lateral deflection of the test beams, several methods were studied and included mechanical, optical, and electrical devices. Accelerometers were selected because of the low cost of measurements, as compared with photographic methods, and presumed greater reliability when compared with possible mechanical methods. However, the shock loading produced accelerations which were an order of magnitude greater than anticipated. Furthermore, the accelerometers experienced a shift in the zero base line because of the very short rise time of the acceleration. The shift of the base line, coupled with the very high initial accelerations seriously limited the value of these data. To illustrate analysis techniques for accelerometer data, the test showing the best agreement with predicted results was selected. However, data from the majority of the tests were not suitable for the refined analysis discussed in this chapter. The reader is directed to Appendix A for the quality of these data.

6.1 Discussion of Data

Typical accelerometer response data are shown in Figure 33. Since the data were plotted utilizing the pressure data reduction program of the Eglin AFB Computer Sciences Laboratory, the negative accelerations are truncated (see Appendix A). However, the negative acceleration is

PROJECT AFATWG02 MSN 5037 17 MAY 74 STA AI SHOT I
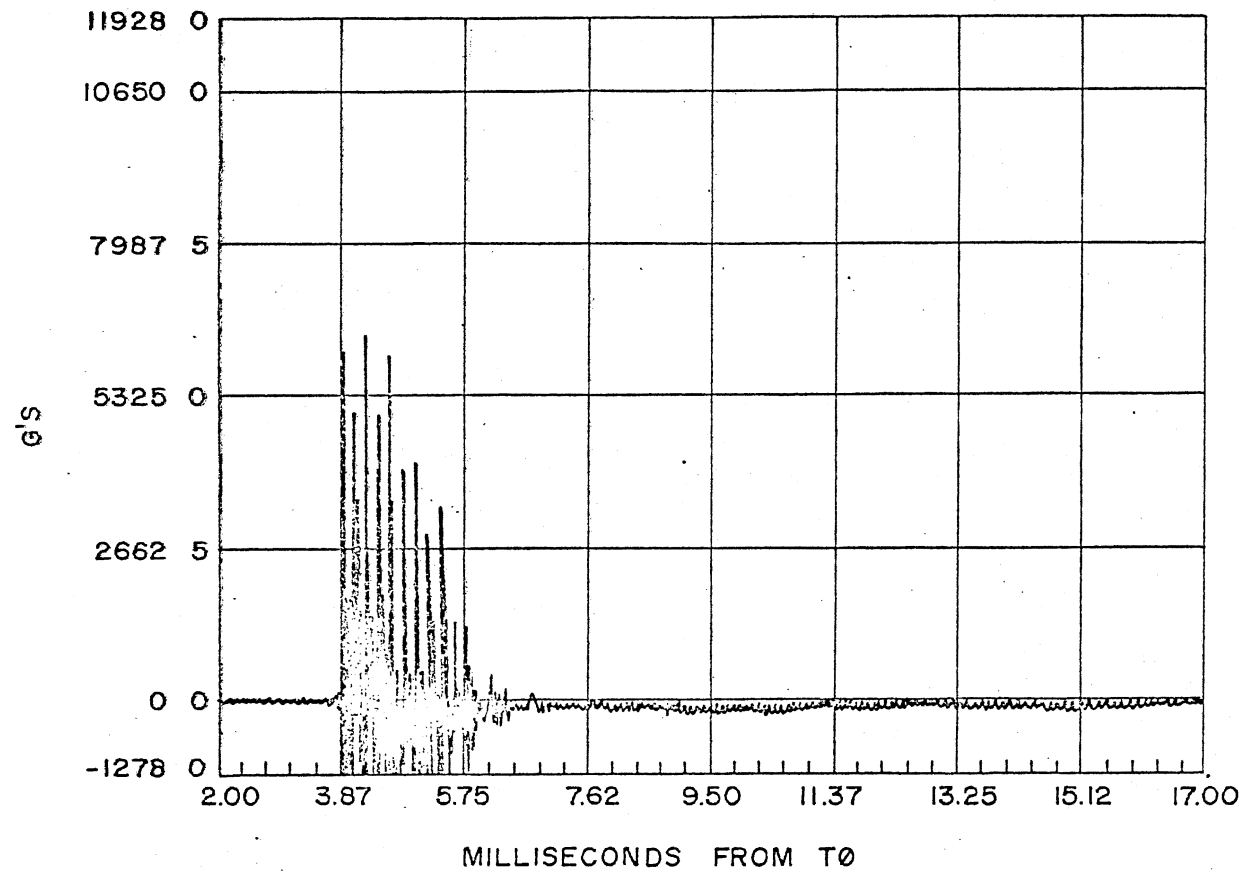
Figure 33. Plot of Typical Acceleration Record for
a Quarter Station, Test 1

recorded on tape and same order of magnitude as the positive acceleration. Figure 33 is a reproduction of data from Figure 71, Appendix A. Care was taken to preserve the character of the data: initial high acceleration and consequent high vibrations due to the shock wave; a smaller "secon dary" vibration noted approximately 5.75 ms from T$\emptyset$; and finally a negative offset of the zero reference of the transducer

The very short rise time of the shock loading produces stress waves which travel from top surface to the lower surface, and back until damped or the beam changes geometry. It was estimated that the acceleration of a unit length of the beam due to a suddenly applied pressure of 1360 psi (corresponding to an impulse of 500 psi-ms from Goodman) would be approximately 1280 g. Since the accelerometer measured accelerations due to both the lateral translation and the stress wave, a calibration level of 10,000 g was selected for initial tests.

However, the accelerations due to free vibration of the reinforced concrete beam is a function of mass and strain energy stored in the member. For a deflection of 2 inches, the member would experience approximately 150 g acceleration which is an order of magnitude less than the initial acceleration.

The displacement of the member is found by the integration of the acceleration record. Accelerations were integrated to determine velocities and velocities to displacements with assumed initial conditions of zero velocity and displacement. However, a characteristic of all accelerometer data is the shift in the instrument zero, illustrated in Figure 33. For most records, the zero shift is of the order of 50 g, or approximately one-third of the maximum free vibration acceleration.

The suitability of these data for the calculation of beam deflections is very questionable when one compares the level of the initial acceleration and the shift of the instrument zero with the predicted acceleration caused by strain energy stored in the member. Measures were taken to reduce the initial shock accelerations, and thereby improve the quality of the data. Following test 4, gasket material was placed between the accelerometer and the housing to reduce the level of the initial shock accelerations and a calibration level of 1000 g was specified for the final eight tests. Although the shock accelerations were significantly reduced, the shift of the instrument zero was not eliminated. To account for the effect of the zero shift, special numerical methods were adopted to integrate the data.

6.2 Data Analysis

6.2.1 Method for Numerical Integration

An integration procedure was developed to minimize the effects of the zero shift in the signal. It was assumed that the error, created by the shock loading, was a constant, A_e, for the remainder of the test. It was further assumed that: (1) each accelerometer data point, $A(t)$, was composed of a "true" and an "error" component,

$$A(t) = A_T(t) + A_e; \tag{6.1}$$

(2) that the true velocities, $V_T(t)$, near the end of the data run were very small relative to the initial velocities at t_d; and (3) that during a final interval Δt, the change in true velocity ΔV_T due to the true accelerations was small or zero.

Constants of integration were determined by the integration of the accelerometer data over the final time interval, Δt, and setting this

result to zero. From this calculation, A_e was determined. Several

values for Δt were studied and a value of 15 ms was used for all tests.

With A_e determined, the data were integrated numerically from the final

data point to the time of the arrival of the shock wave to estimate the

initial beam velocity. The member displacements were determined by the

integration of the resulting velocity curves.

6.2.2 Results of Data Analysis, Test No. 11

Beam velocities and deflections were determined for all tests.

However, the results were unreliable, and at best, questionable. The

results for test 11, better than average, illustrate the correlation

between observed and calculated deflections. Figures 34 through 48

illustrate the variation of acceleration, velocity, and displacement

with time for beam and axle stations. In these figures, acceleration,

velocity and displacement are positive when directed away from the

explosive charge, or toward the ground.

The change in velocity of the beam is a measure of the impulse

imparted to the member by the blast pressure loading. From impulse-

momentum relationships,

$$V = \frac{Ib}{m} \tag{6.2}$$

where

   V = velocity of the rigid body at the end of the impulse;

   I = impulse in psi-ms;

   b = width of the beam; and

   m = mass per unit length.

To predict the beam initial velocity, properties of the explosive load-

ing were taken from Goodman (1). For test 11, the estimated impulse was
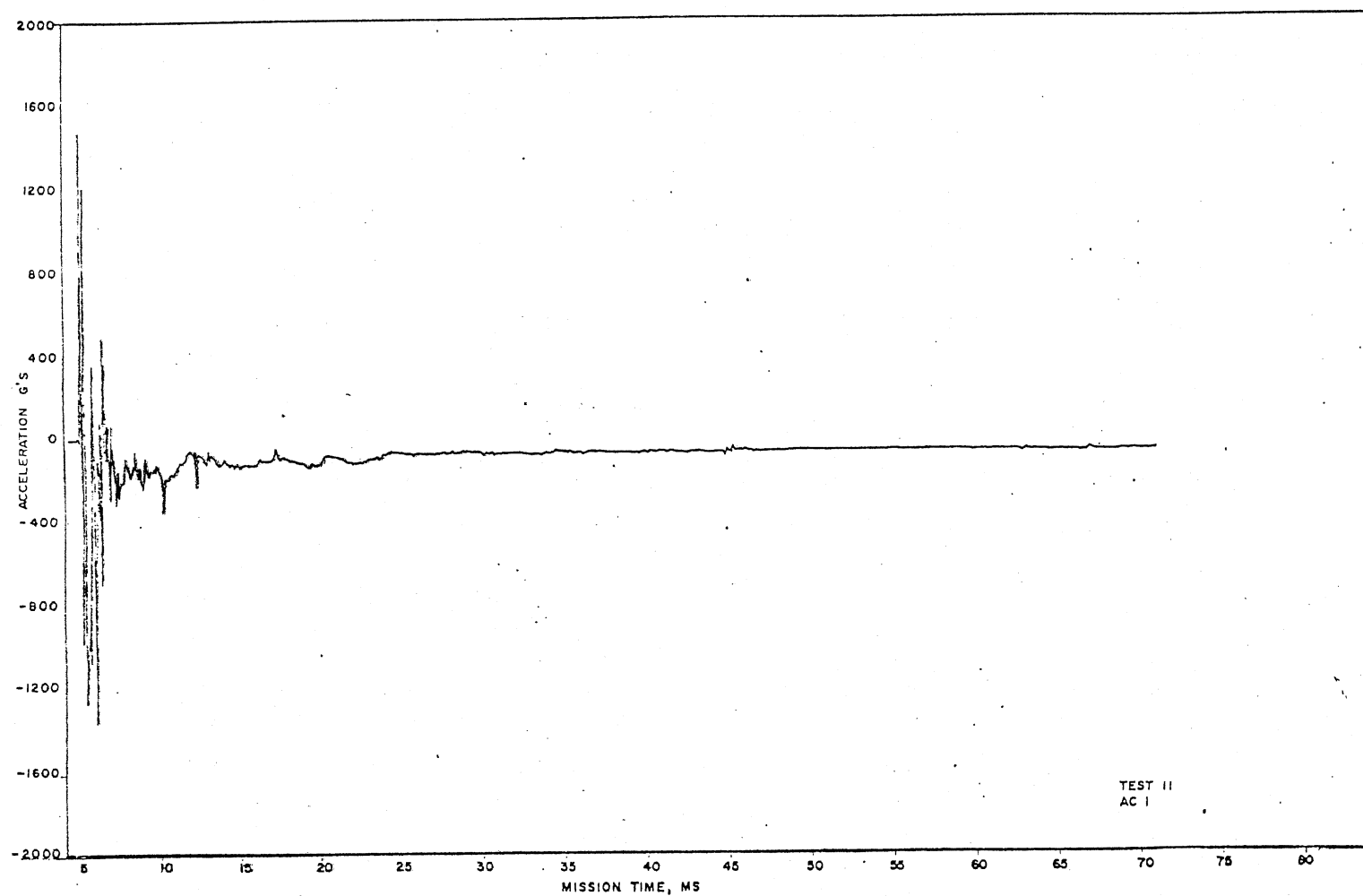
Figure 34. Quarter Point Accelerometer-AC 1, Test 11
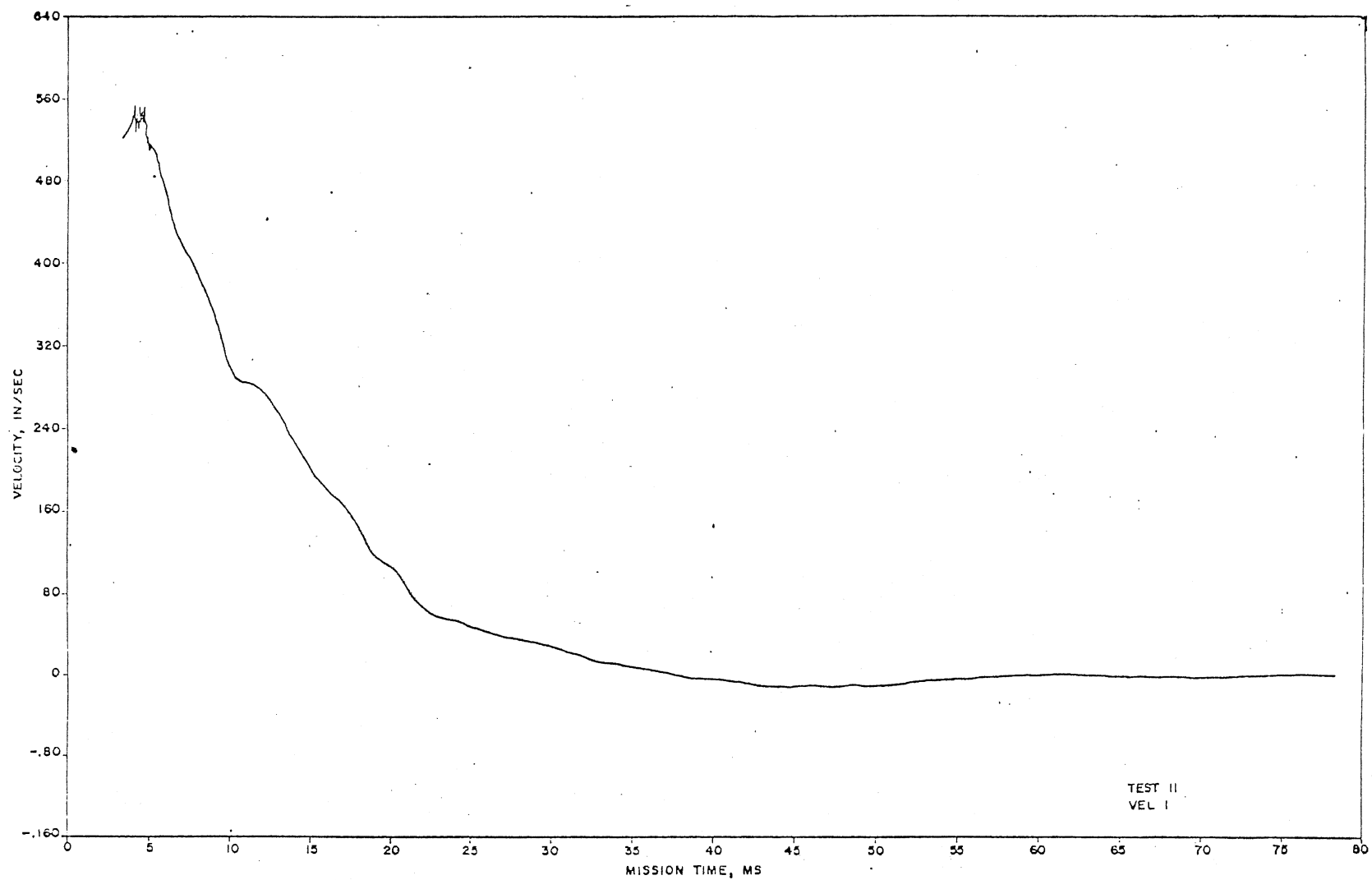
Figure 35. Calculated Quarter Point Velocity From AC-1, Test 11
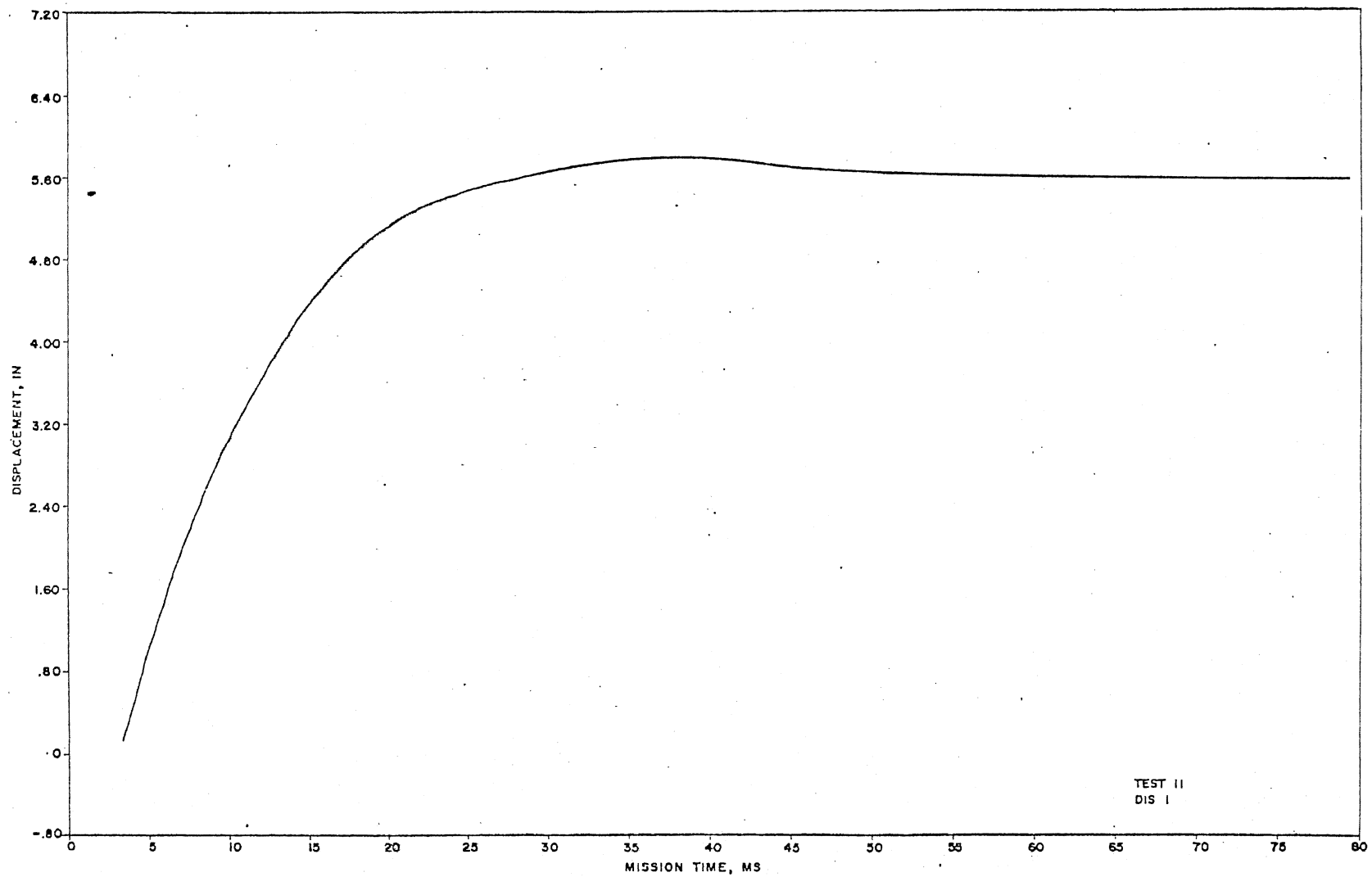
Figure 36. Calculated Quarter Point Displacement From AC-1
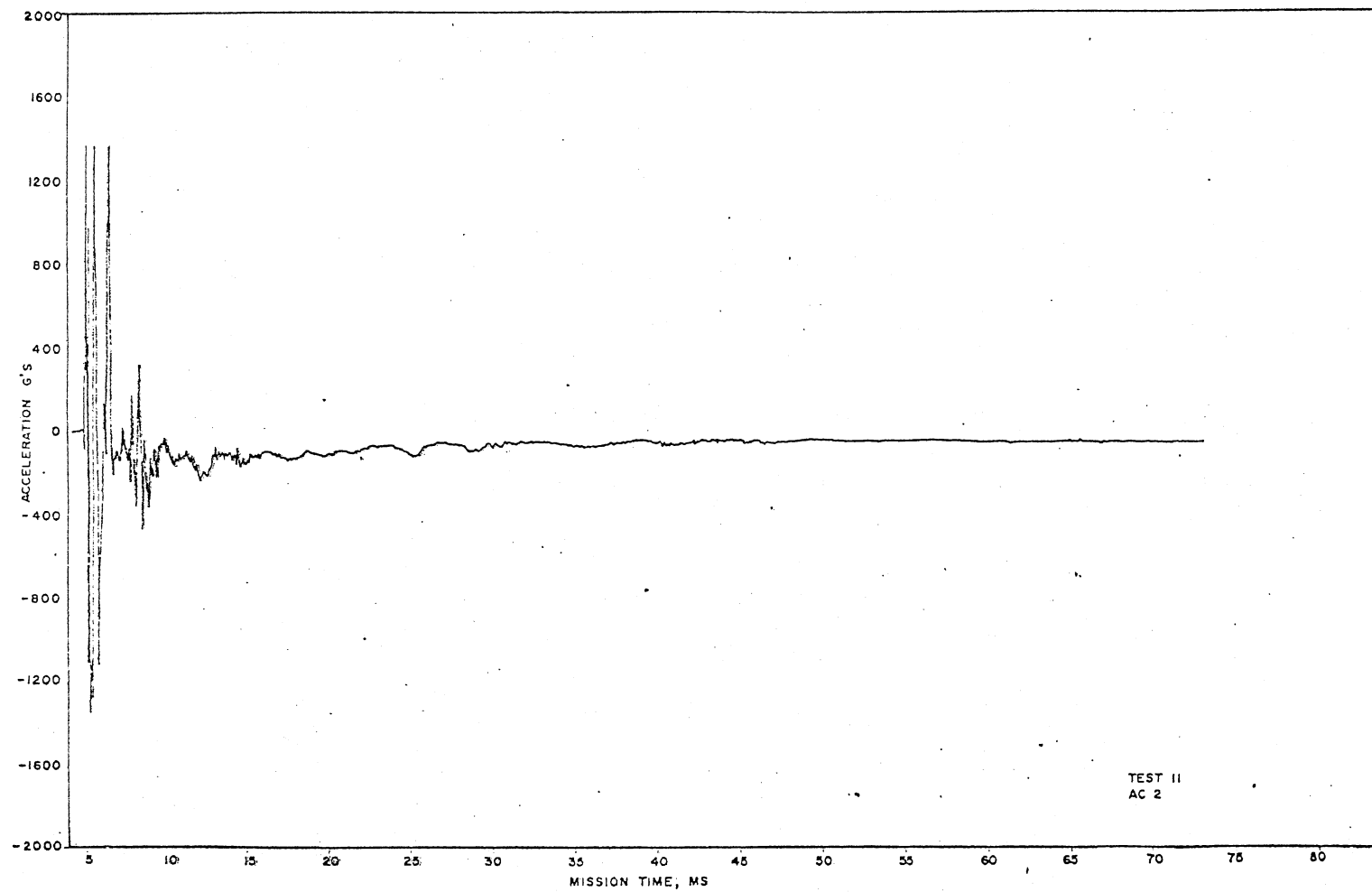
Figure 37. Center Accelerometer AC-2, Test 11
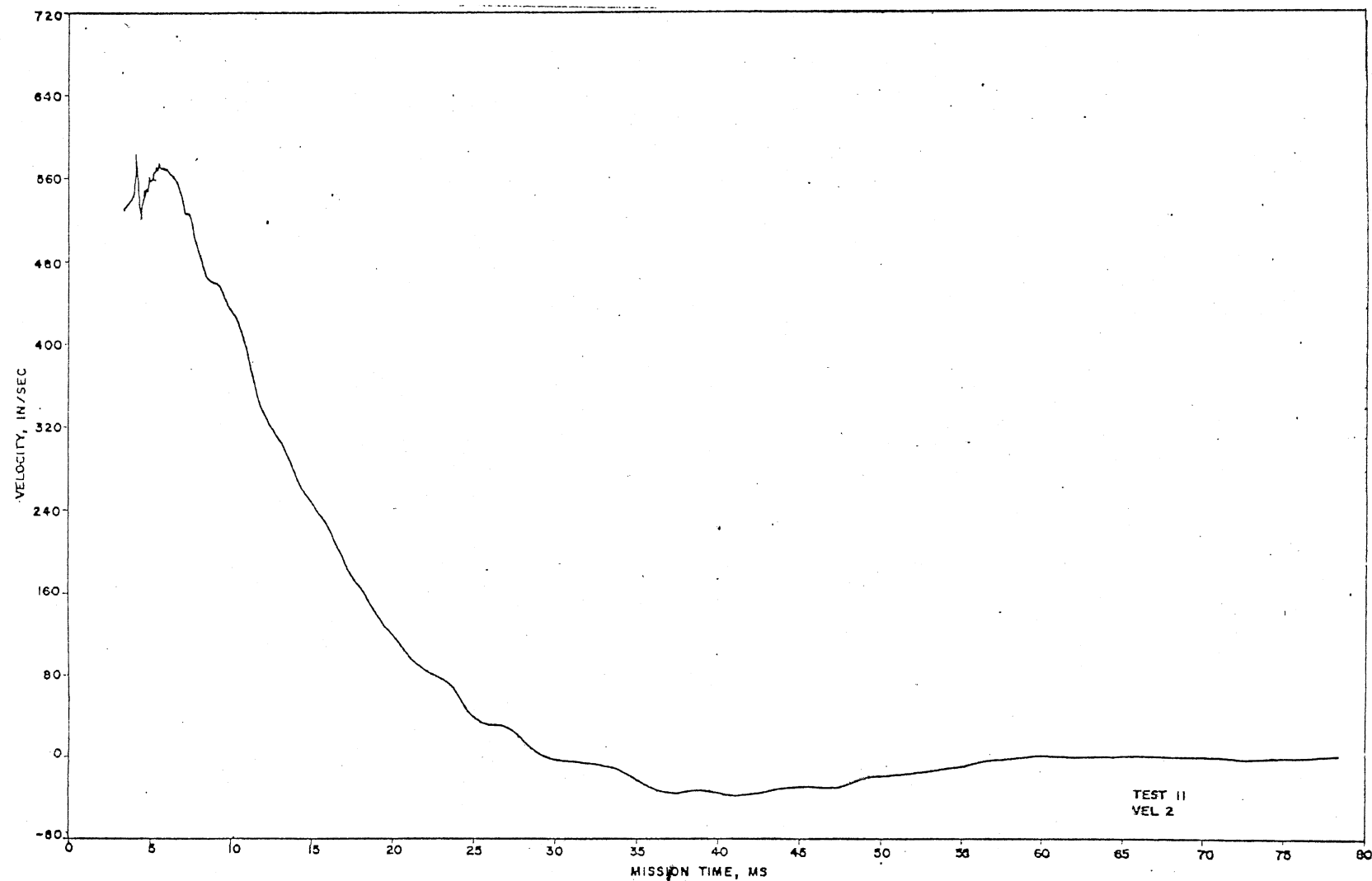
Figure 38.   Calculated Center Velocity From AC-2, Test 11
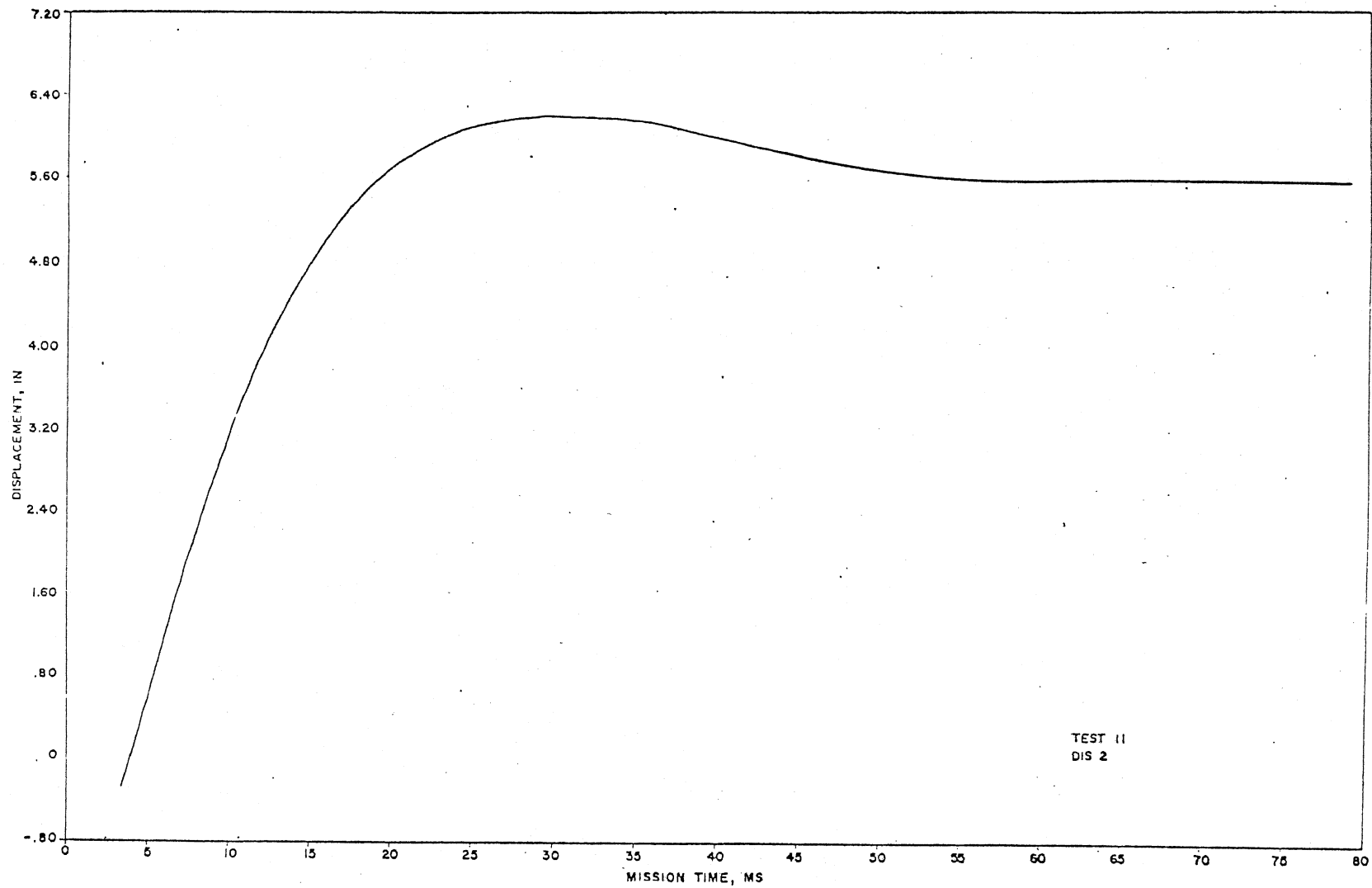
Figure 39. Calculated Center Displacement From AC-2, Test 11
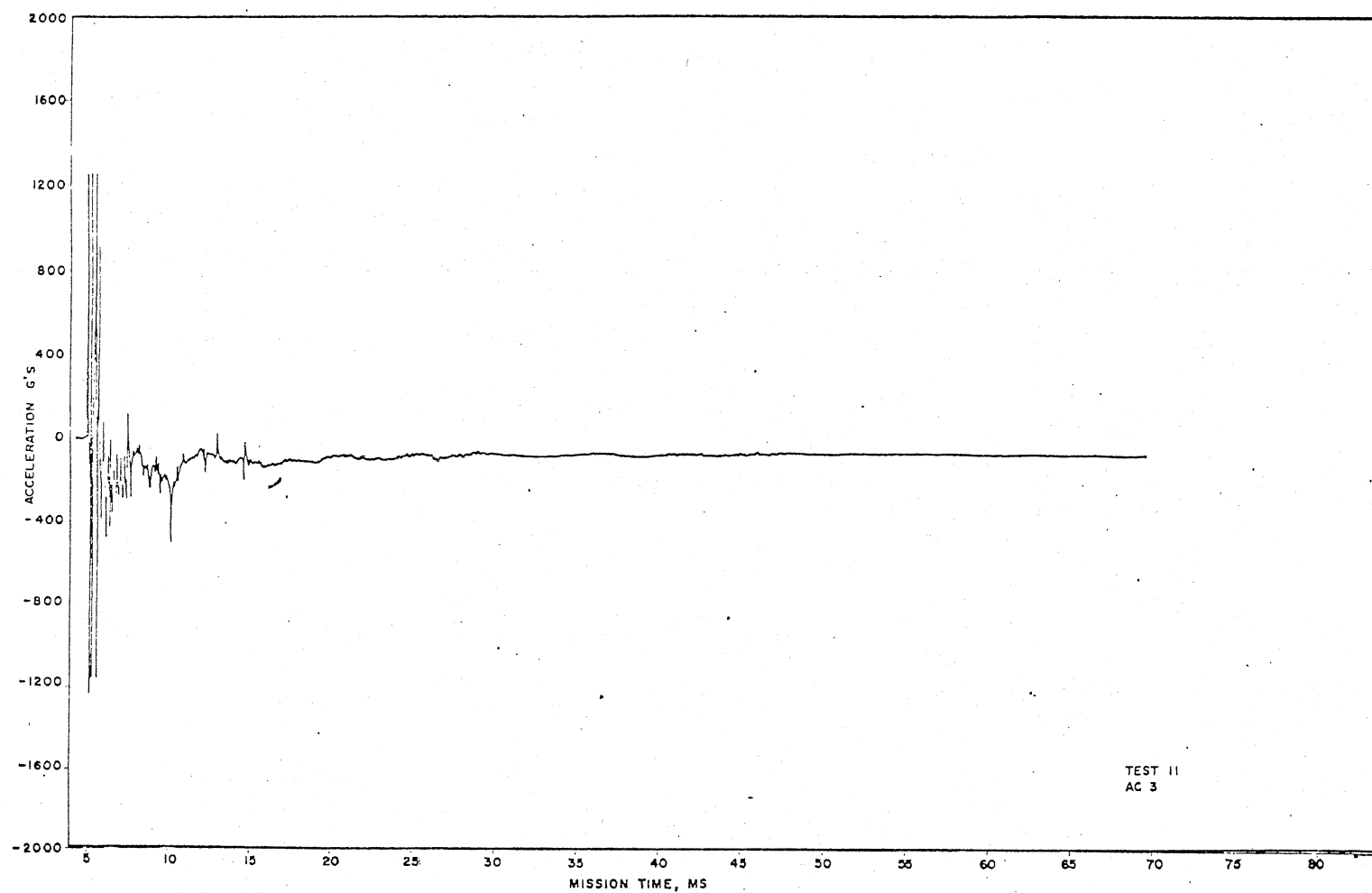
Figure 40. Quarter Point Accelerometer AC-3, Test 11
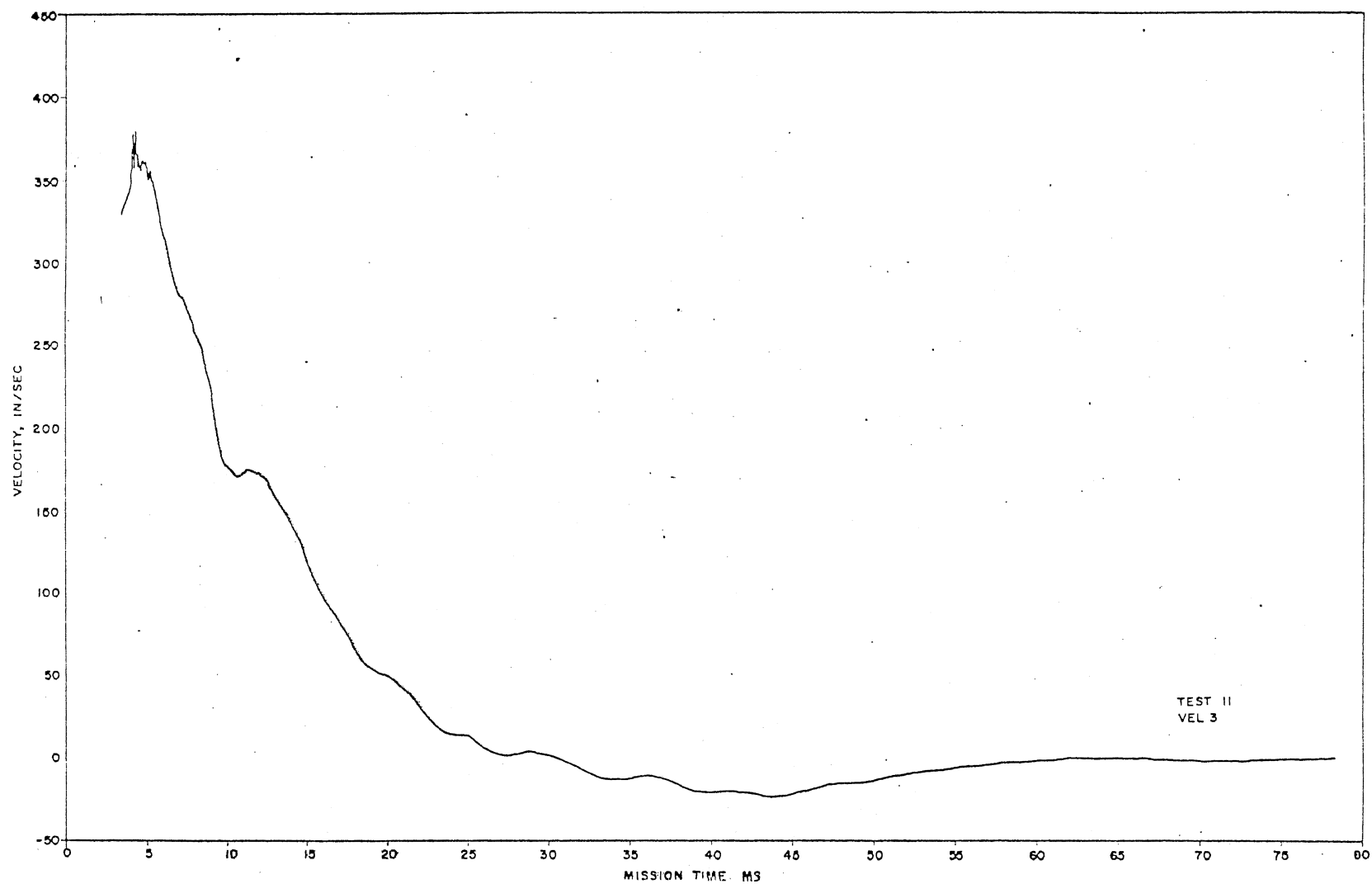
Figure 41. Calculated Quarter Point Velocity From AC-3, Test 11
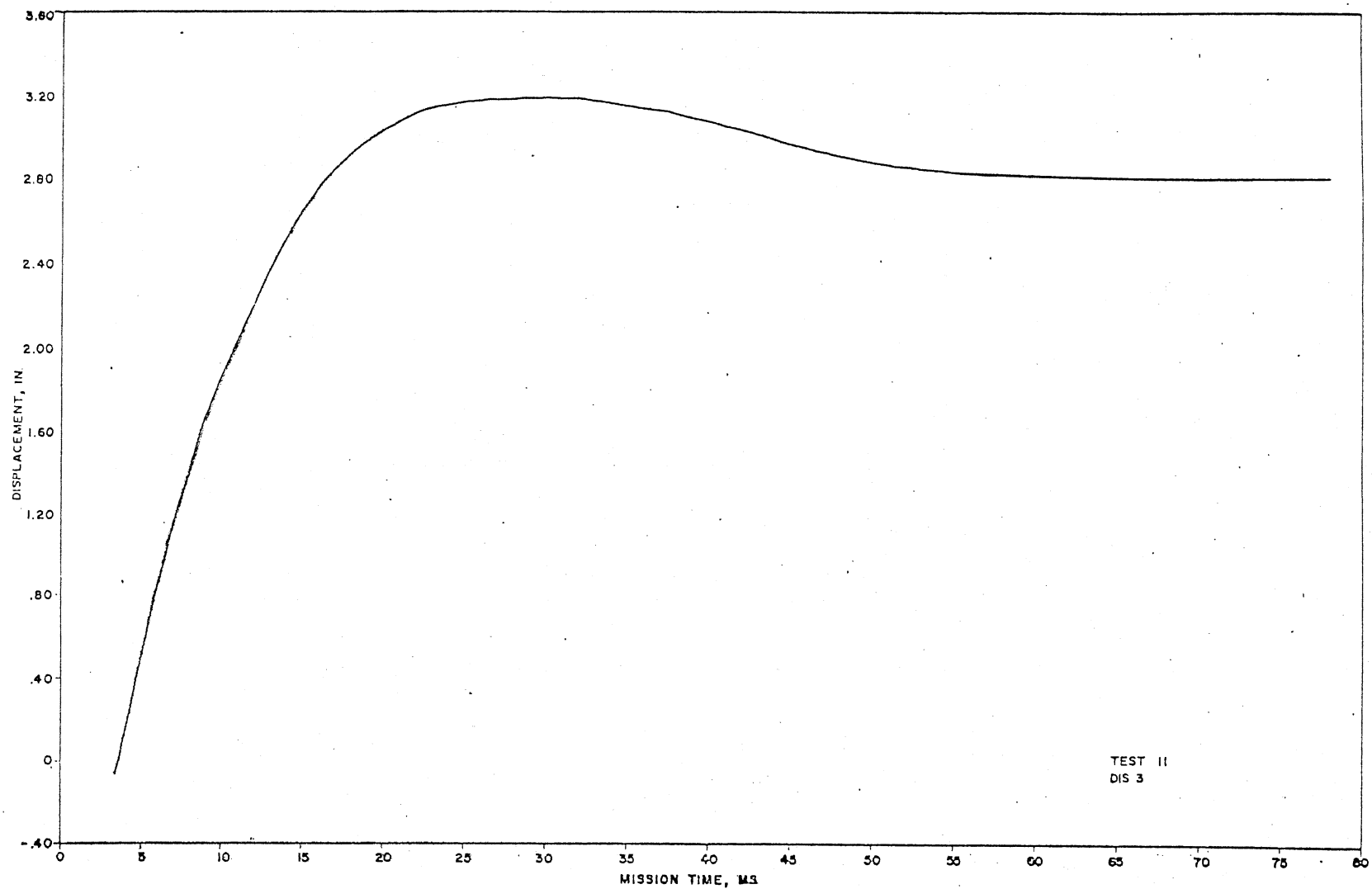
Figure 42. Calculated Quarter Point Displacement From AC-3, Test 11
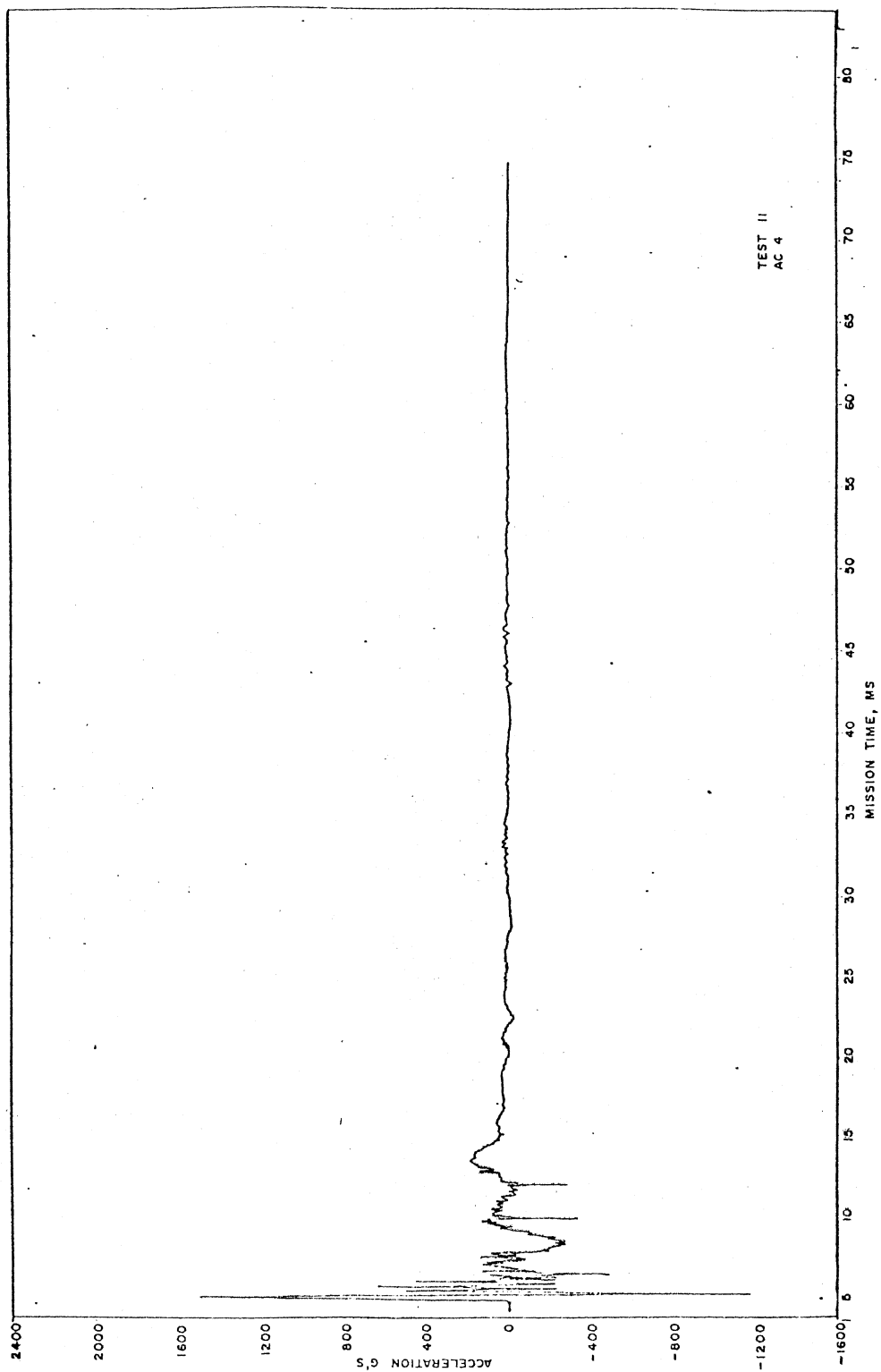
Figure 43. Axle 1 AC-4, Test 11
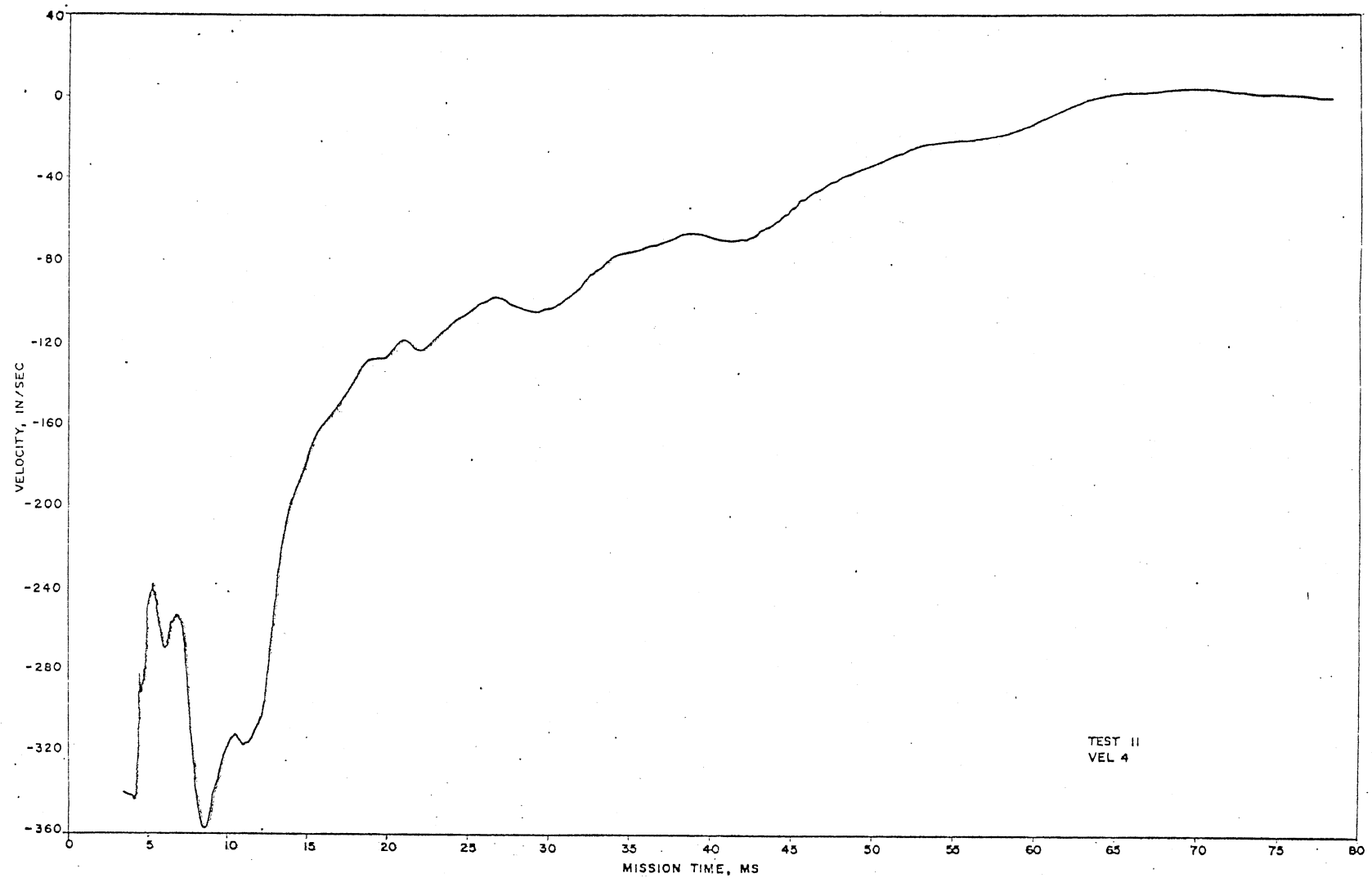
Figure 44. Calculated Axle Velocity From AC-4, Test 11
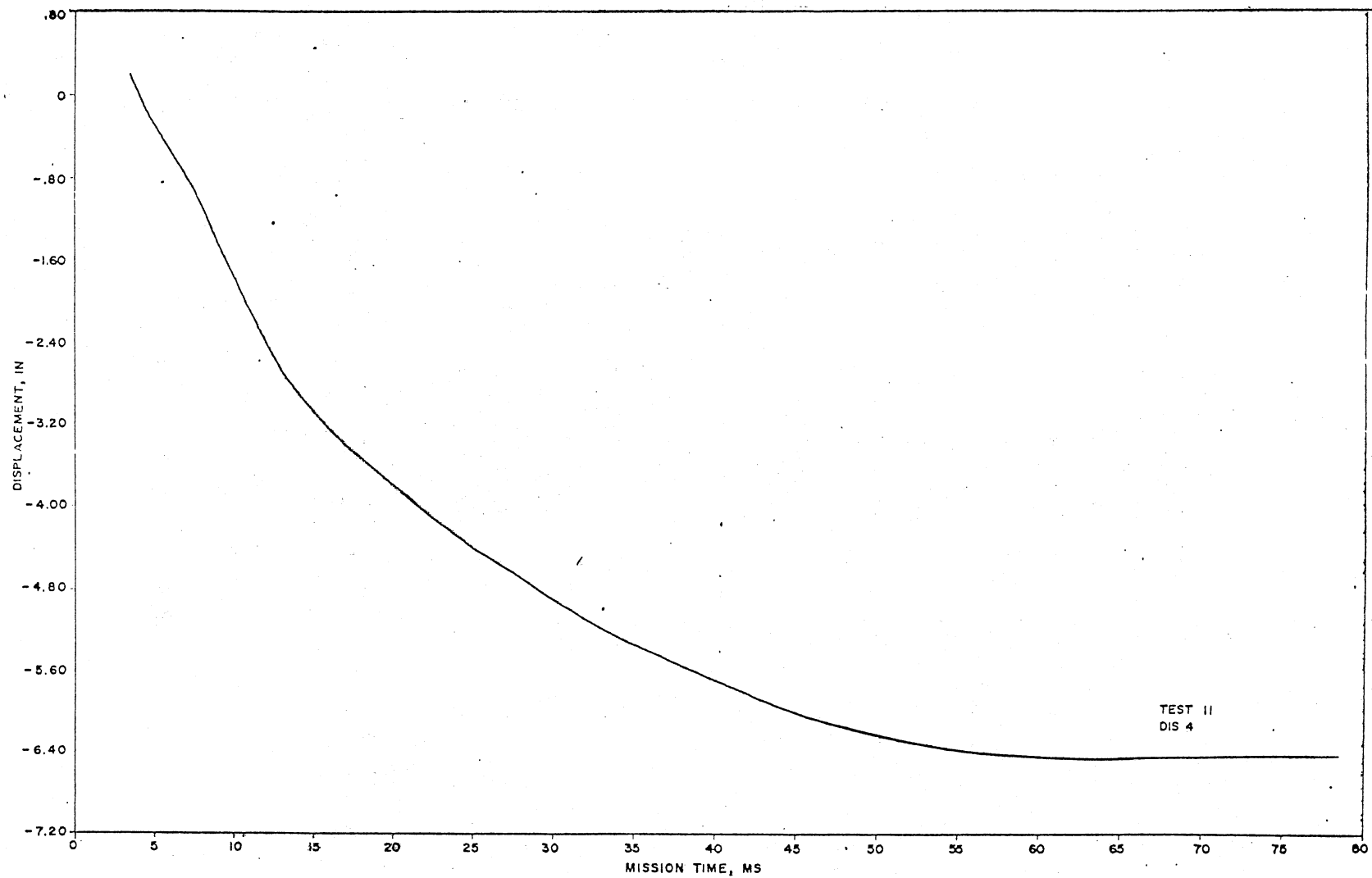
Figure 45. Calculated Axle Displacement From AC-4, Test 11
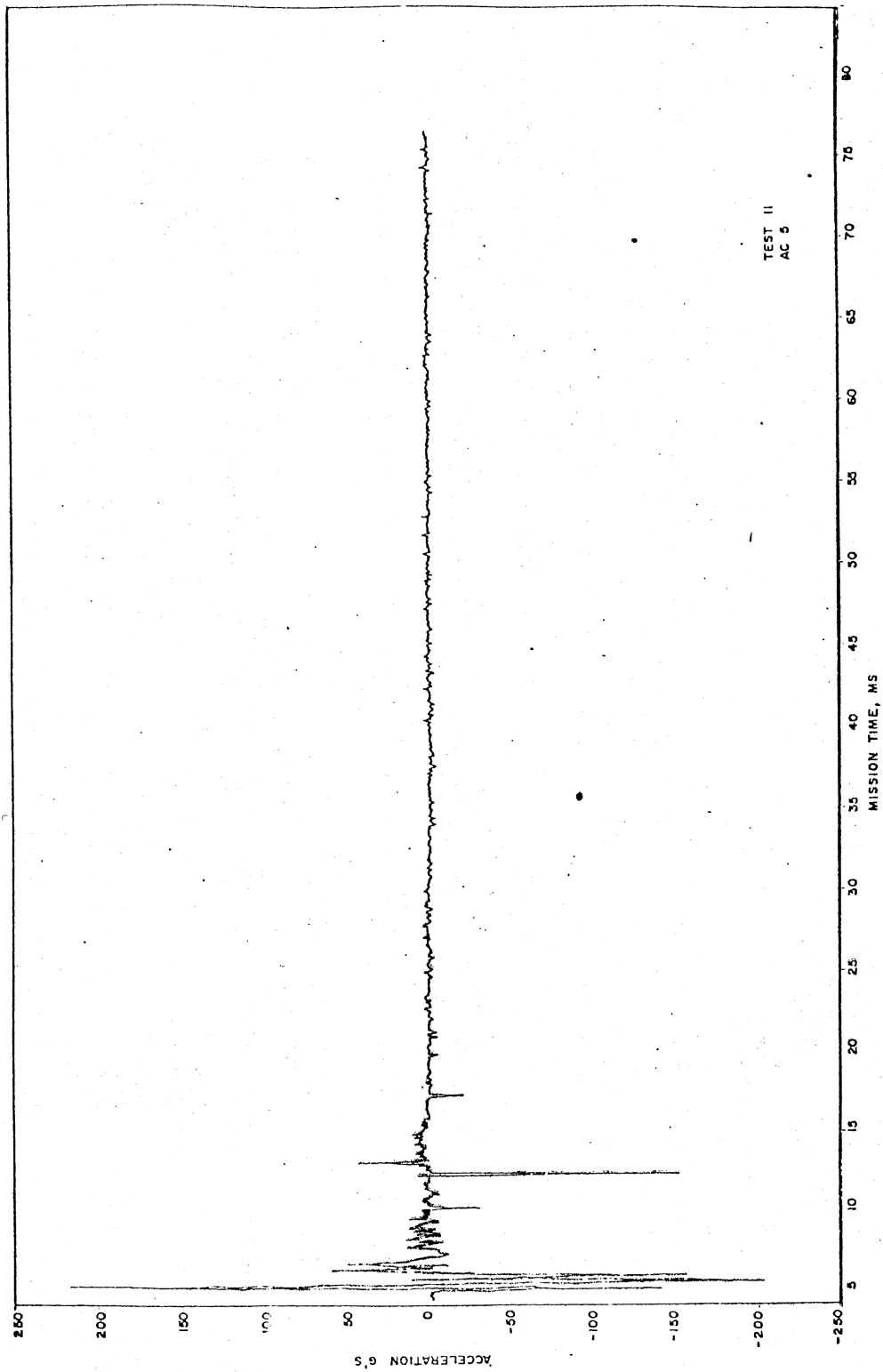
Figure 46. Axle 2 AC-5, Test 11
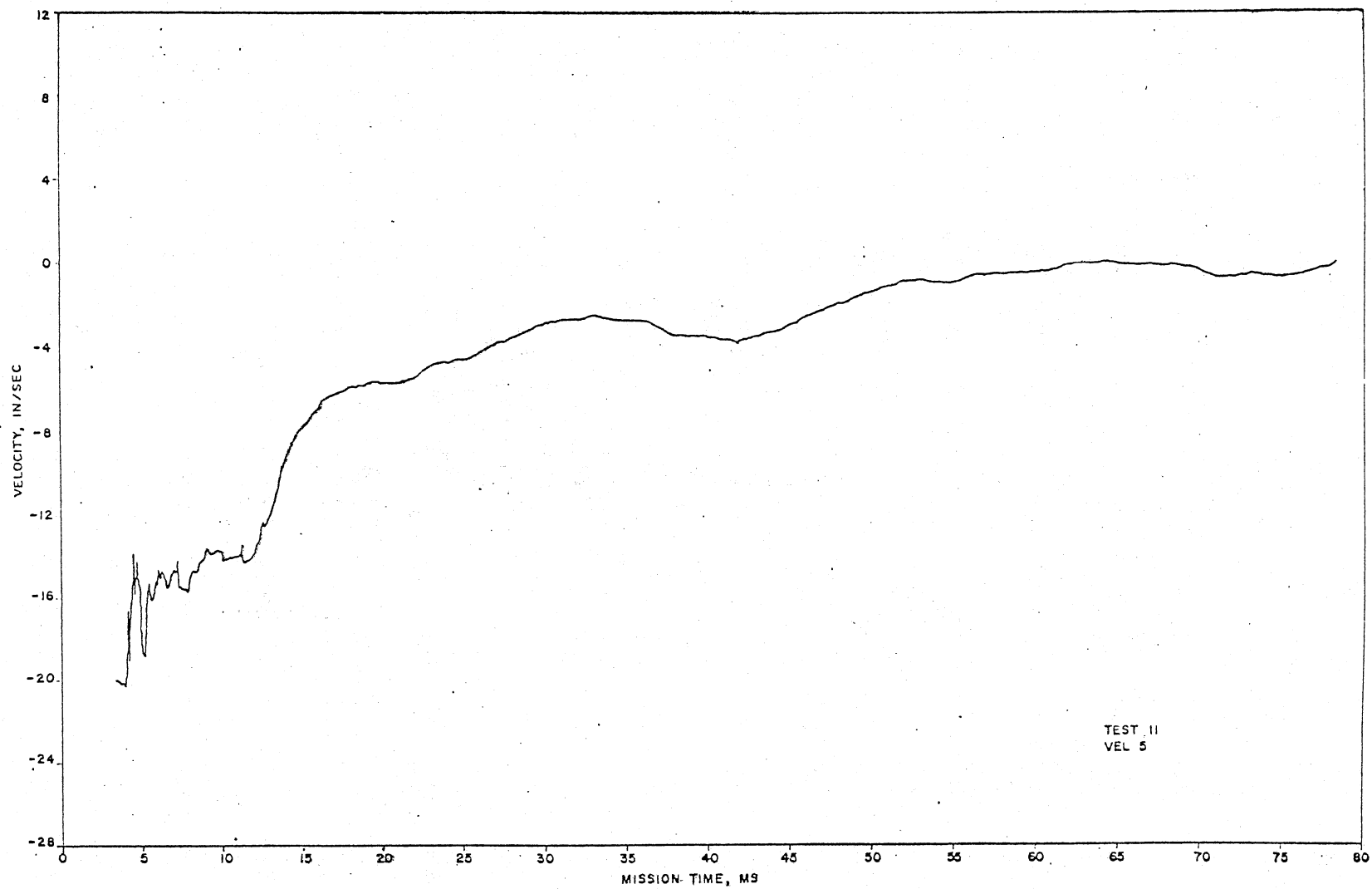
Figure 47. Calculated Axle Velocity From AC-5, Test 11
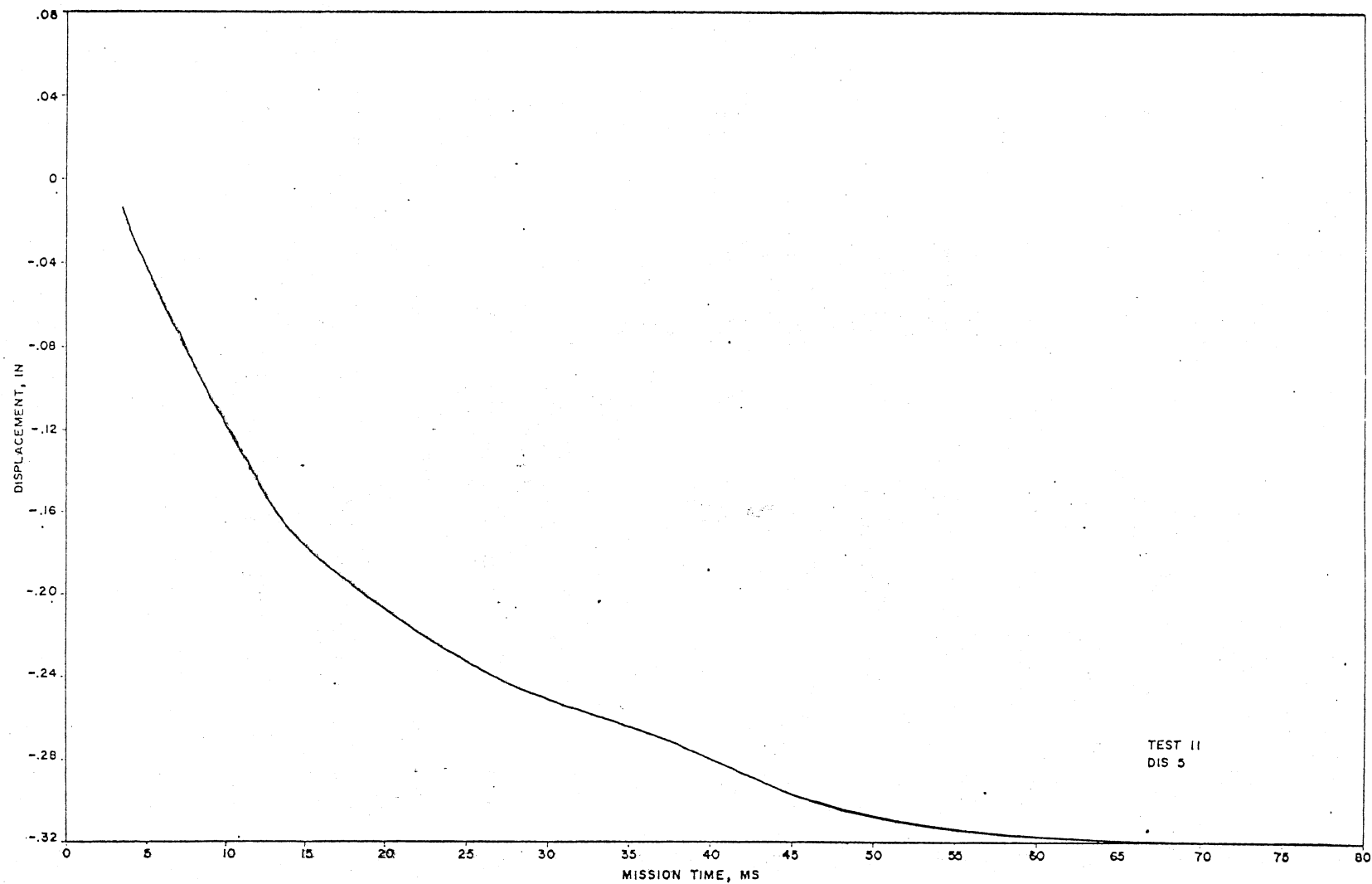
Figure 48.   Calculated Axle Displacement From AC-5, Test 11

690 psi-ms (Figure 32) which would yield an initial velocity of 250 in./sec. The calculated initial velocities of the member at the end of the pressure pulse (Figures 35, 38 and 41) are given in Table XI.

Although there appears to be a reasonable correlation between predicted and measured initial velocity, attention is called to Figures 44 and 47, the velocity of the support axles. Note that the axles appear to have an initial upward velocity. This is more typical of the quality of the data.

The integration of the velocity to determine displacement is shown in Figures 36, 39, and 42 for the beam stations and Figures 45 and 48 for axle measurements. These results are also summarized in Table XI, along with predicted maximum displacement. The predicted maximum displacement was calculated by the addition of the estimated maximum elastic displacement to the measured plastic deformation. It was assumed that permanent deformation measured after the test was the maximum plastic deformation. Furthermore, it was assumed that the beam end support mechanism remained rigid during beam motion.

Again, one notes reasonable agreement between measured and calculated deformation. On the other hand, calculated deflections of an axle indicate an upward motion greater than the deflection of the beam. This was more representative of the quality of calculated beam deflections.

6.3 Summary

Of the data which was obtained from the test, the accelerometer data were the least reliable. Although the example presented in this report shows reasonable agreement between calculated and anticipated velocity

TABLE XI

SUMMARY OF CALCULATED DISPLACEMENTS AND VELOCITIES FROM TEST 11

Accelerometer Station	Displacement, in.		Velocity at Approx. End of Pulse, in./sec[1]
	Maximum Calculated	Maximum Estimated	
A_1 (Quarter)	3.87	.78	471
A_2 (Center)	3.95	1.33	568
A_3 (Quarter)	2.08	.78	315
A_4 (Axle)	-5.83	--	-268
A_5 (Axle)	- .26	--	- 14.8

[1]Pulse duration, t_d, assumed to be 1.25 ms.

and deflection, results from other tests do not agree within an order of magnitude.

The accelerometer installation was not suitable for measurements of the shock phenomenon. Furthermore, the accelerometer was sensitive to the very short rise time associated with the shock loads, causing a shift of the instrument zero which approached the level of acceleration to be measured.

CHAPTER VII

REACTION MEASUREMENTS

End reactions were measured by load cells installed between the
test fixture and the beam support mechanism (Chapter IV). Typical data
from a single load cell, as well as end reactions, are presented in
this chapter. Analysis of these data provided reasonable agreement with
predicted end reactions determined by a computer simulation of an im-
pulse loaded beam. Although the measured reactions exceeded predicted
reactions by approximately 50%, the difference was due to vibration of
the support mechanism. Simple spring-mass models were developed to in-
vestigate frequencies related to the load reaction mechanism and soil
supported test fixture. Finally, data from a simple field test indi-
cated a response within the frequency range calculated from spring-mass
models. The studies indicate that vibration characteristics noted in
the load cell response were due to dynamic interaction of the beam with
the support mechanism and test fixture.

7.1 Discussion of Data

Preliminary estimates of beam reactions were based on the assump-
tions of a uniform member connected by hinges to rigid supports. Due
to the assumption of support rigidity, the reaction force was predicted
to increase to a maximum limiting value, to remain essentially constant
until the maximum center displacement occurred, then reduce to zero.

However, the vibration of the load reaction mechanism produced measured reactions which exceeded the beam end forces.

Although the load cells provided reliable end reaction data throughout the test program, several minor problems were noted. Before test 7, a load cell (No. 4) was found to be damaged and reaction measurements for the final six tests were unavailable for one end of the beam. The load cell was found to be defective following a severe electrical storm. A second load cell (No. 3) was subjected to sufficient overloading in test 11 to produce permanent strains which indicated a residual load of 7000 lbs. However, laboratory tests revealed the load cell had retained the original linear relationship between strain and load, and it was used in test 12.

Load cell data from test 3 are shown in Figure 49. Negative forces are related to compression in the load cells and indicate an upward force on the load reaction mechanism. The measured reactions exceeded 12,400 lbs upward and were less than 2000 lbs downward. Also shown in these data are two frequencies which will be important for later discussions. The first is the vibration having a period of approximately 4 ms. The second has a longer natural period and approaches 40 ms.

End reactions, the sum of loads measured by load cells 1, 2 and 3, are presented for tests 11 and 10 in Figures 50 and 51. Data for test 11 are presented to complement acceleration and strain data, given in Chapters VI and VIII. Test 10 is compared with test 11 to illustrate the 7000 lb residual load shown in Figure 50.

While Figures 50 and 51 describe the reaction history over the total data period, a significant response is limited to less than 30 ms following impulse loading. This time period is accentuated in

PROJECT 9134WOO2 MISSION 3052 19 JUNE 1974 LOAD CELL 1 TEST 3

MILLISECONDS FROM TØ
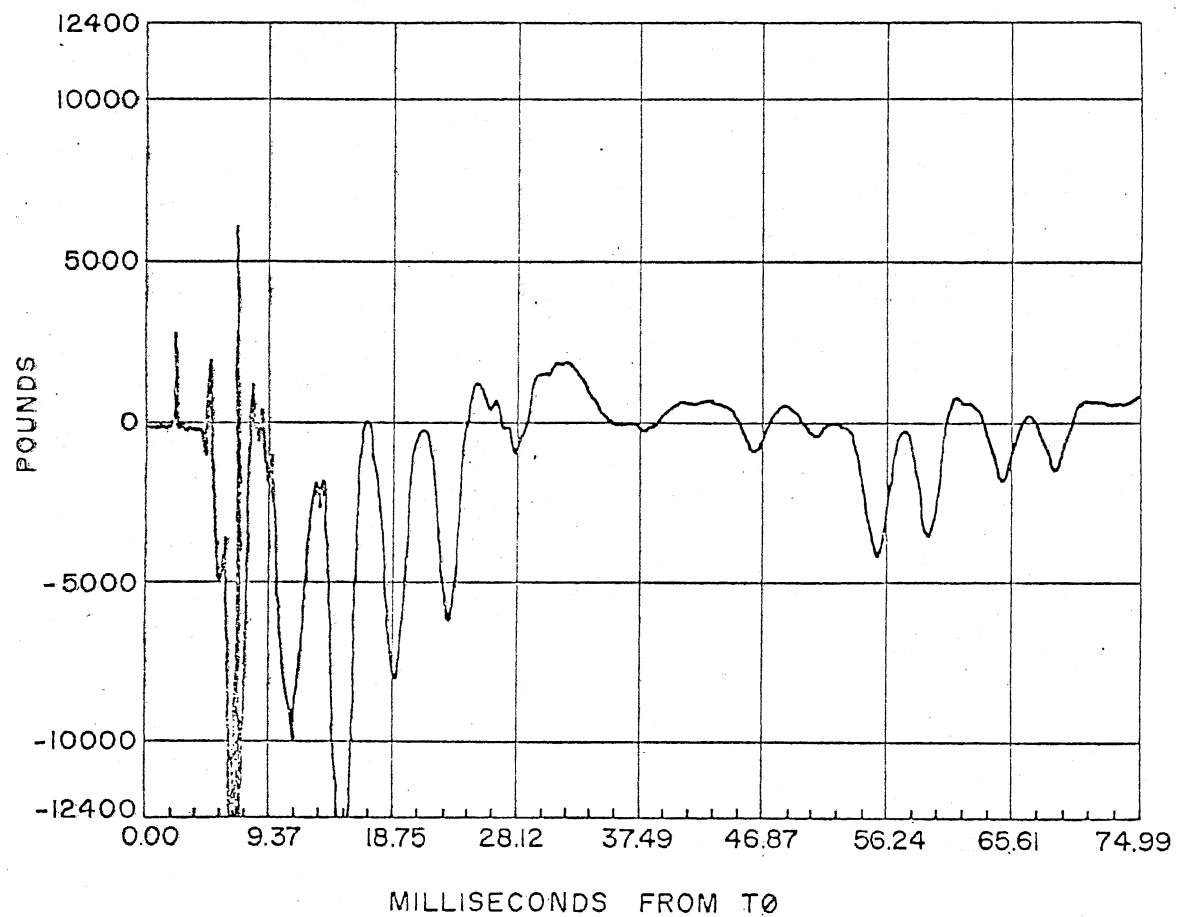
Figure 49. Typical Load Cell Data From Test 3
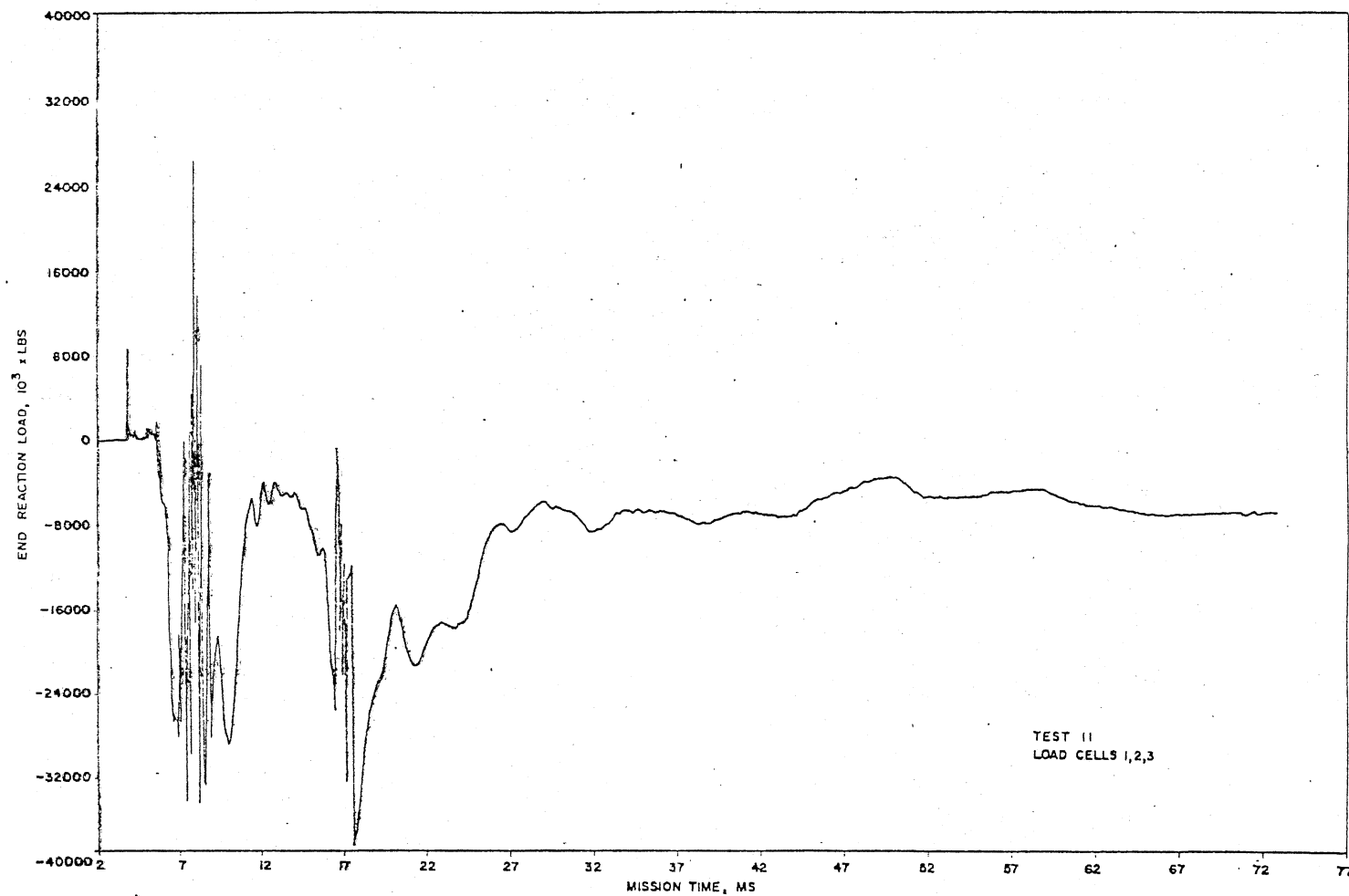
Figure 50. End Reaction Load From Beam 3, Test 11
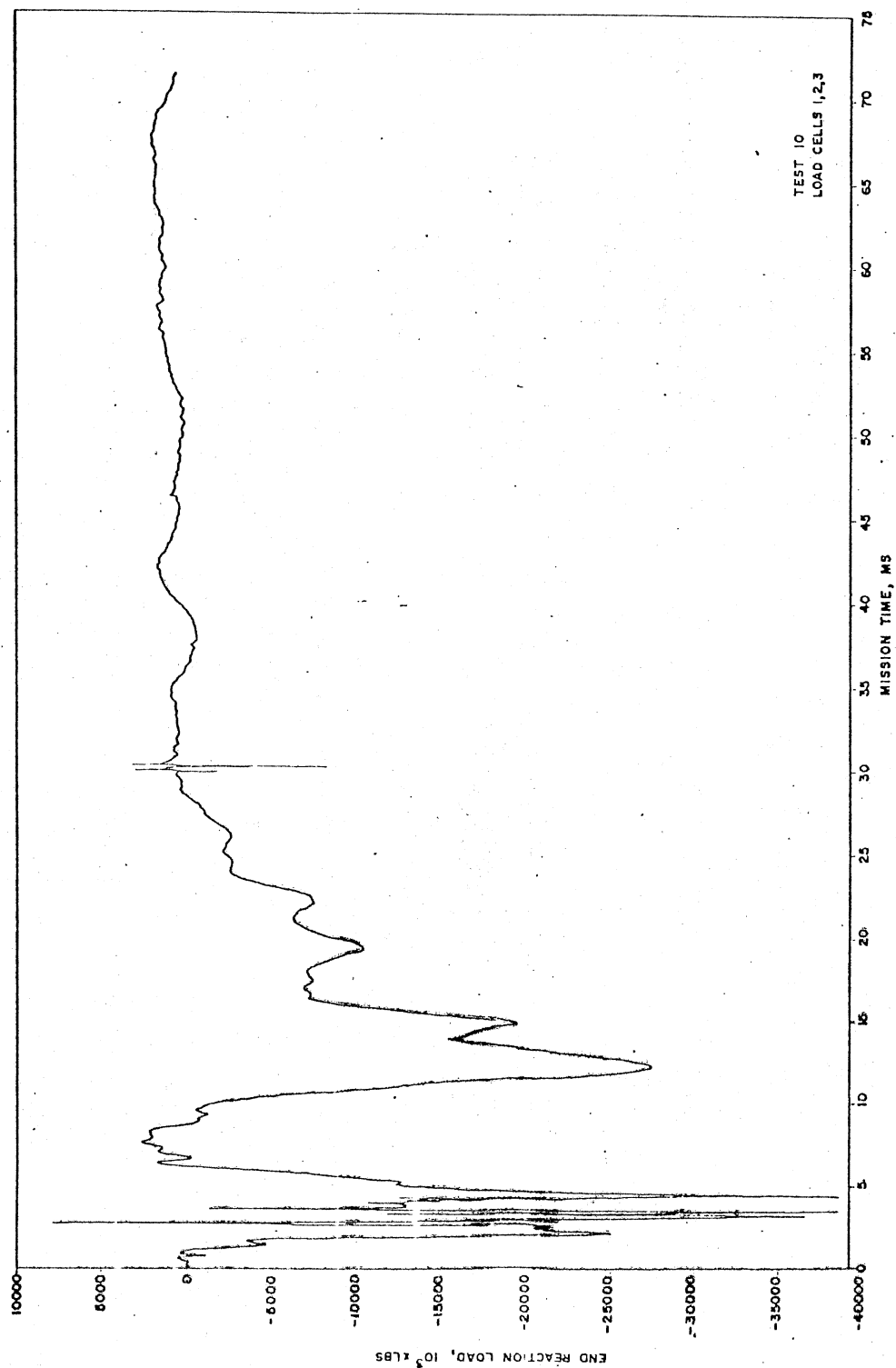
Figure 51. End Reaction Load From Beam 9, Test 10

Figures 52, 53 and 54 which give results of tests 10, 11 and 12. The repeatability of test data, indicated by Figures 52 and 53, was typical of reaction calculations. Tests 10 and 12 were performed on nominal beams with charge standoff distances of 10.75 and 11.25 ft, respectively. It should be recalled that load cell 3 was damaged during test 11. However, satisfactory load cell performance is seen in test 12. Furthermore, when tests 10 and 12 are compared with test 11, Figure 54, it may be noted that the damage occurred within 5 ms of the arrival of the shock wave. Reaction data of Figure 54 (test 11) indicates a negative force 7 ms after the arrival of the shock wave while Figures 52 and 53 (tests 10 and 12) show positive values. The difference between the measured reactions at this time is approximately 7000 lbs.

Finally, little difference was noted in the reaction data between tests. Both the magnitude of the reaction and the shape of the reaction time curves appeared to be independent of beam type and charge standoff distance.

7.2 Frequency Analysis of Test System

The vibration noted in the measured reactions cause amplification of beam end forces through the heavy support mechanisms. To identify the possible source of vibration, a study was performed utilizing simple spring-mass models. The models and equations of motion are given in Appendix C. The results of this study are presented in Table XII. Model I was a simply supported elastic beam which had a frequency of 179 rad/sec. Model II was an elastic beam supported on springs which represented the load reaction mechanism and load cells. The

TABLE XII

SUMMARY OF CALCULATED FREQUENCIES FROM
LUMPED MASS MODELS

Model Number	ω^1 rad/sec	T^2 ms/cycle	ω rad/sec	T ms/cycle	ω rad/sec	T ms/cycle
I			179	35		
II			174	36	1540	4.1
III	91	69	175	36	1542	4.1

$^1\omega$ = natural frequency.

^2T = period of motion.
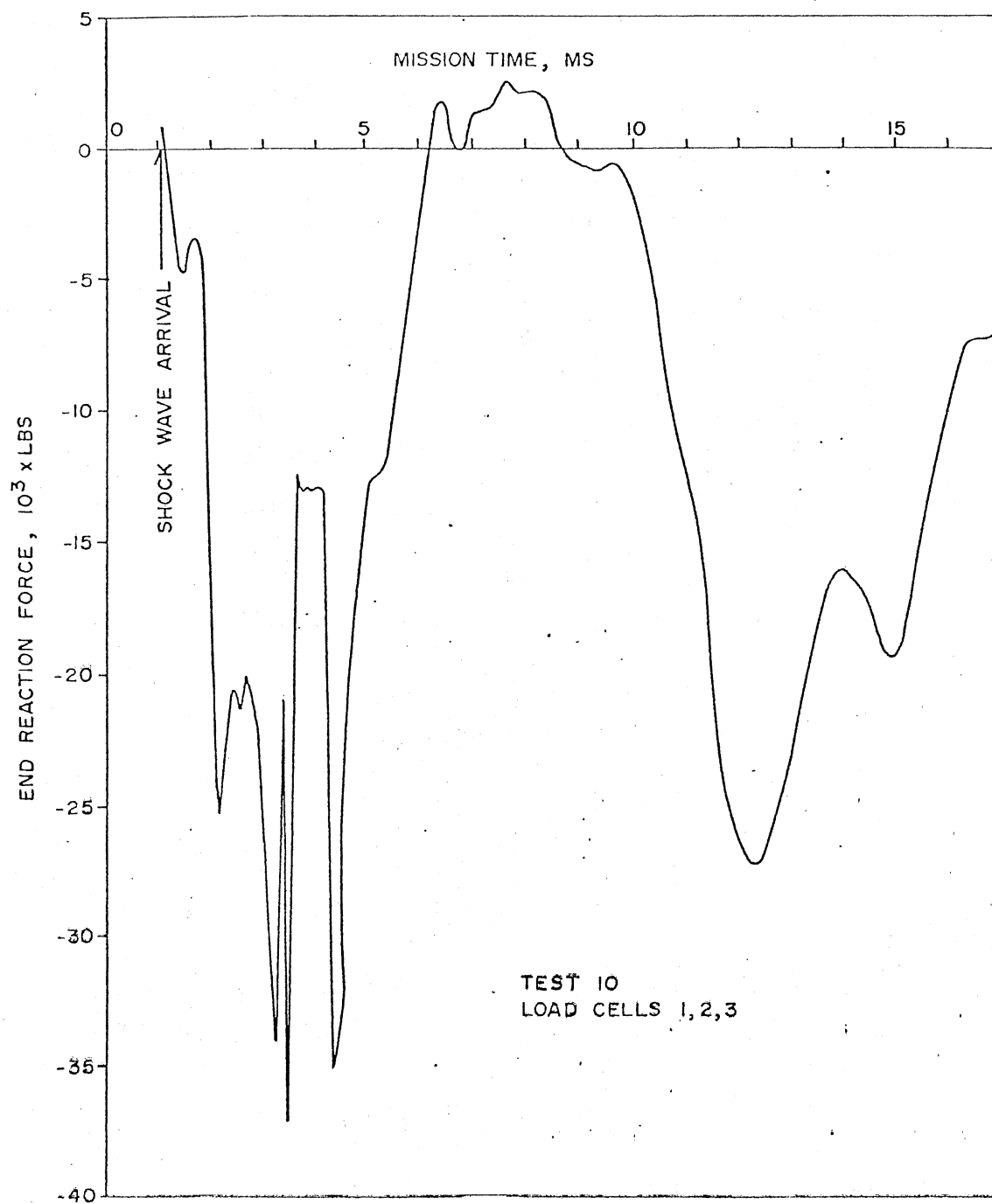
Figure 52. Measured End Reaction Force of Beam
9, Test 10 (Nominal)
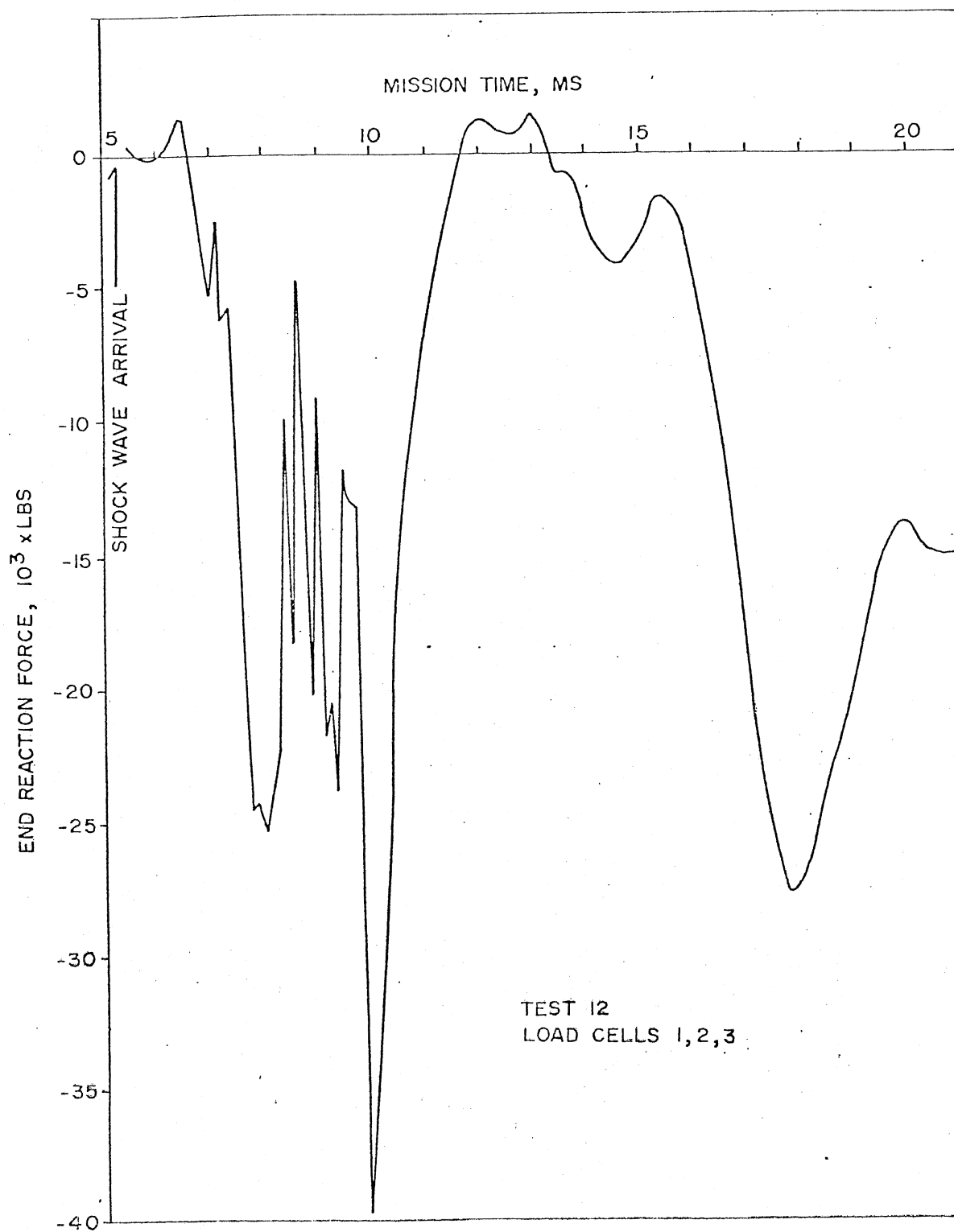
Figure 53.   Measured End Reaction Force of Beam 11,
Test 12 (Nominal)
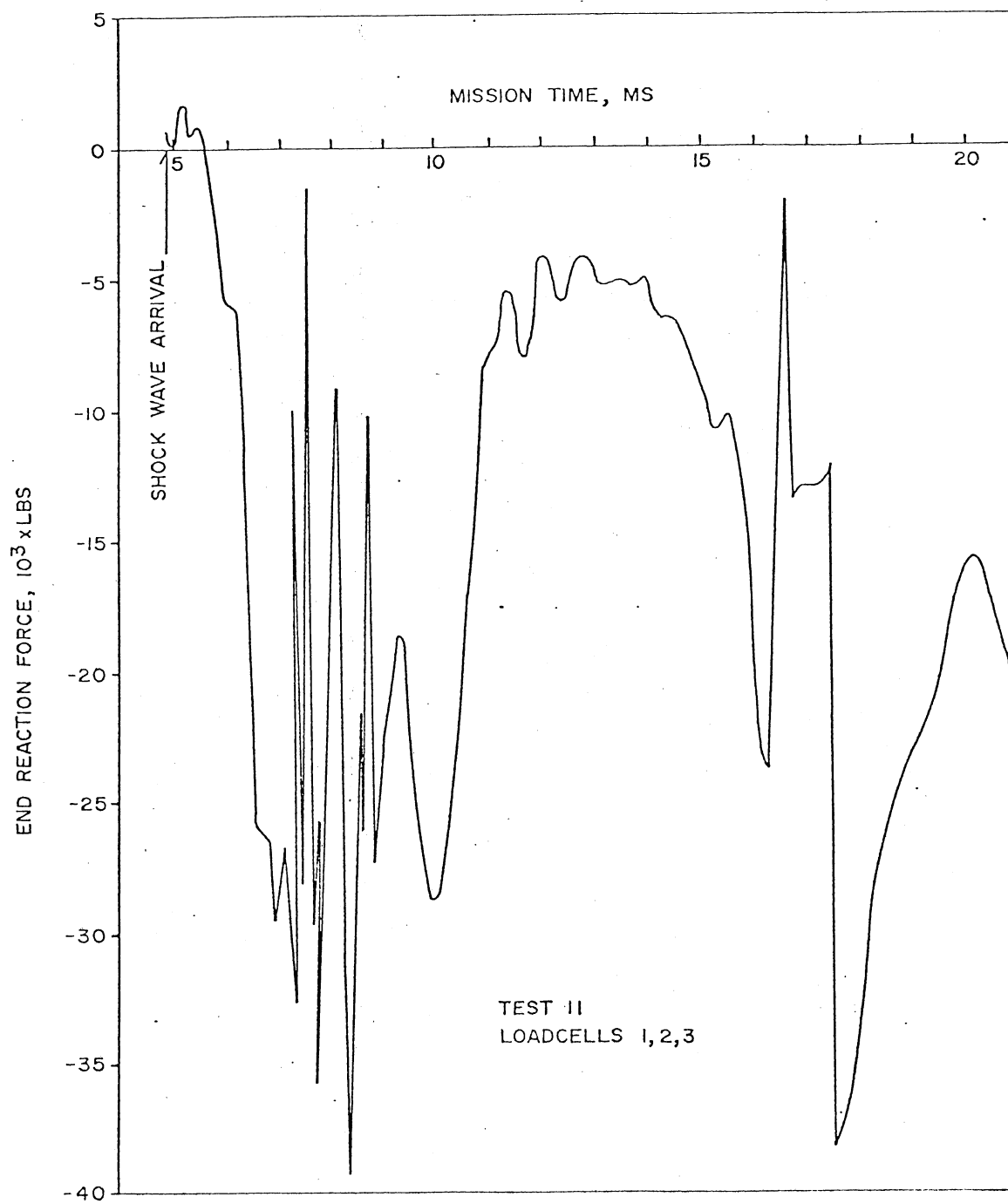
Figure 54. Measured End Reaction Force of Beam 3, Test 11
(High Strength Concrete)

frequency related to the vibration of the support mechanism was approximately 1540 rad/sec, for a period of 4.1 ms. Finally, Model III includes both the mass of the test fixture as well as an equivalent soil spring. The frequency related to the vibration of the test fixture was found to be less than the fundamental frequency of the beam and would, therefore, have little influence on the response. However, a frequency similar to that calculated for the support mechanism is found in the reaction data (Figures 49 through 54).

A limited vibration study of the support mechanism was performed. The beam was struck at a support and the reaction recorded as shown in Figure 55. The period of vibration is from 3 to 6 ms, which includes the calculated period related to an elastic support mechanism. One should also note the measured reaction. Although the force of the impact was large, it did not reach 2000 lbs, which indicates the transmissibility of the system.

7.3 Calculated Reactions--IMPBC

In this section the measured results will be compared with results from digital computer program IMPBC (2). Since details of the program do not permit the description of flexible supports, the oscillation noted in the experimental data cannot be reproduced. However, suitable agreement is noted between measured and calculated reactions.

The nonlinear response of the impulse loaded beam was predicted by IMPBC. The material properties used for the calculations are presented and discussed in Appendix B. Studies were performed for both the nominal beam of test 1) and the high strength concrete beam of test 11. These results are shown in Figures 56 and 57 as functions of applied
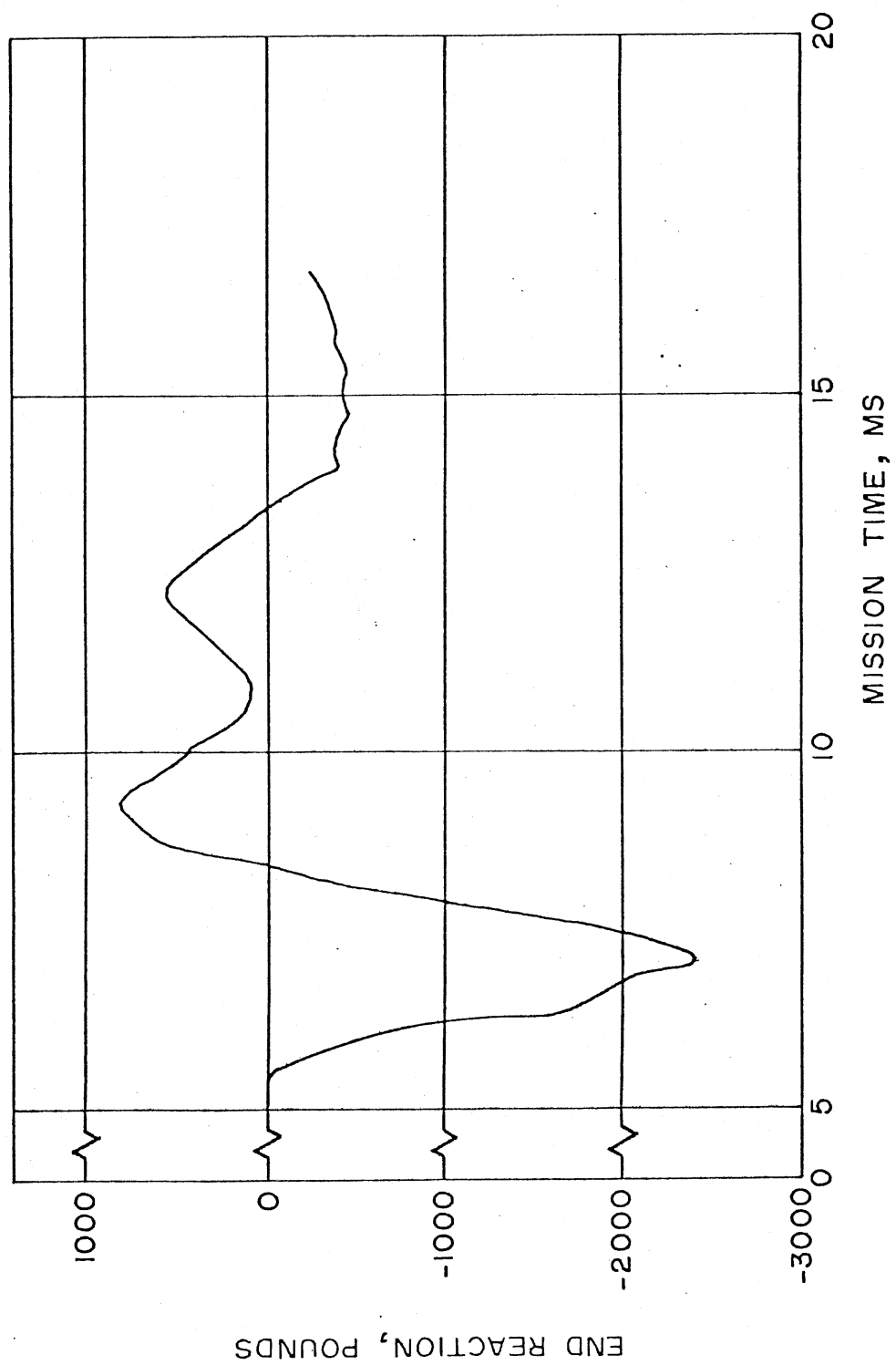
Figure 55. End Support Response for Hammer Blow at Axle Station
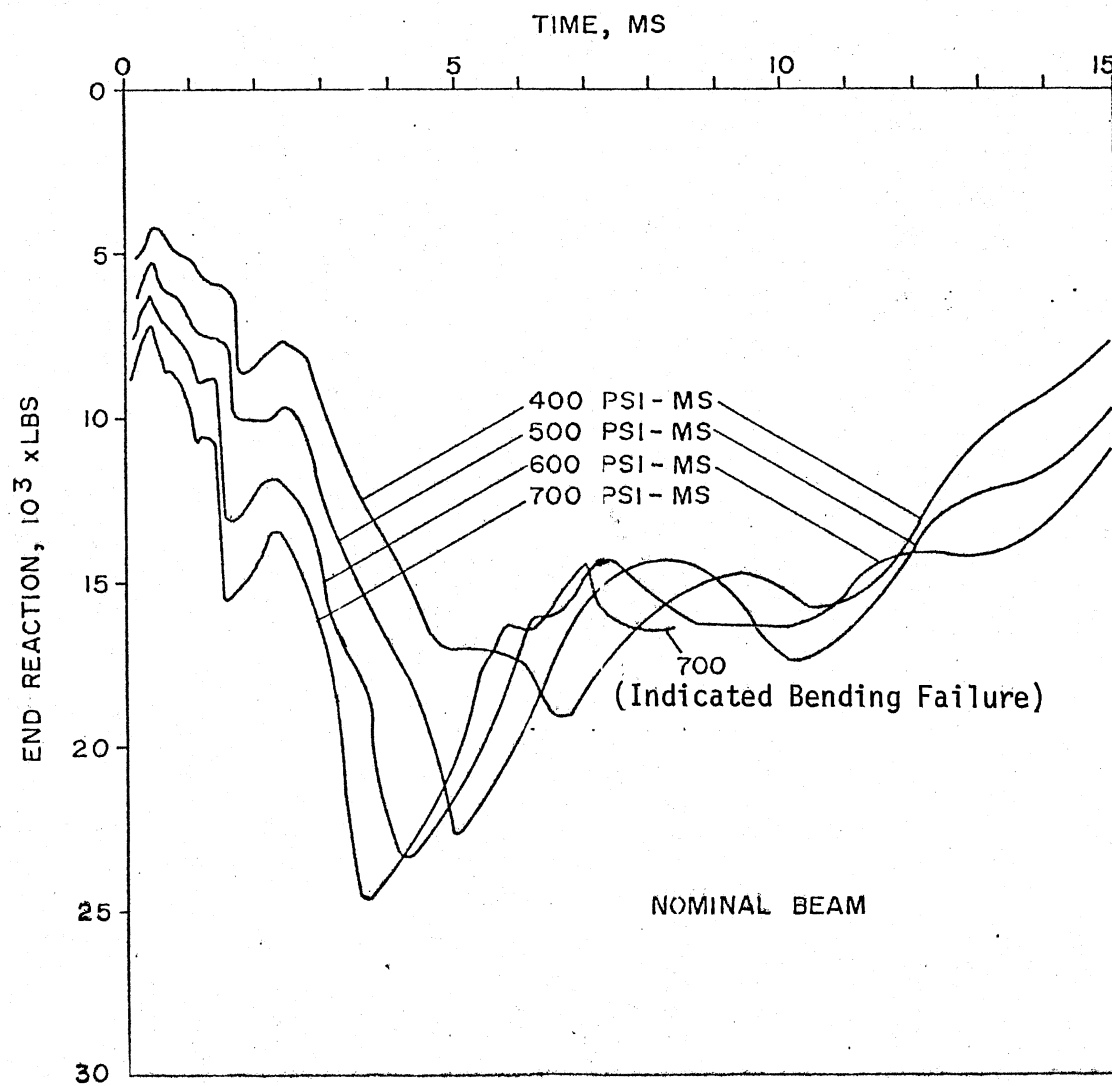
Figure 56. IMPBC Simulated End Reaction, Force for Nominal Beam
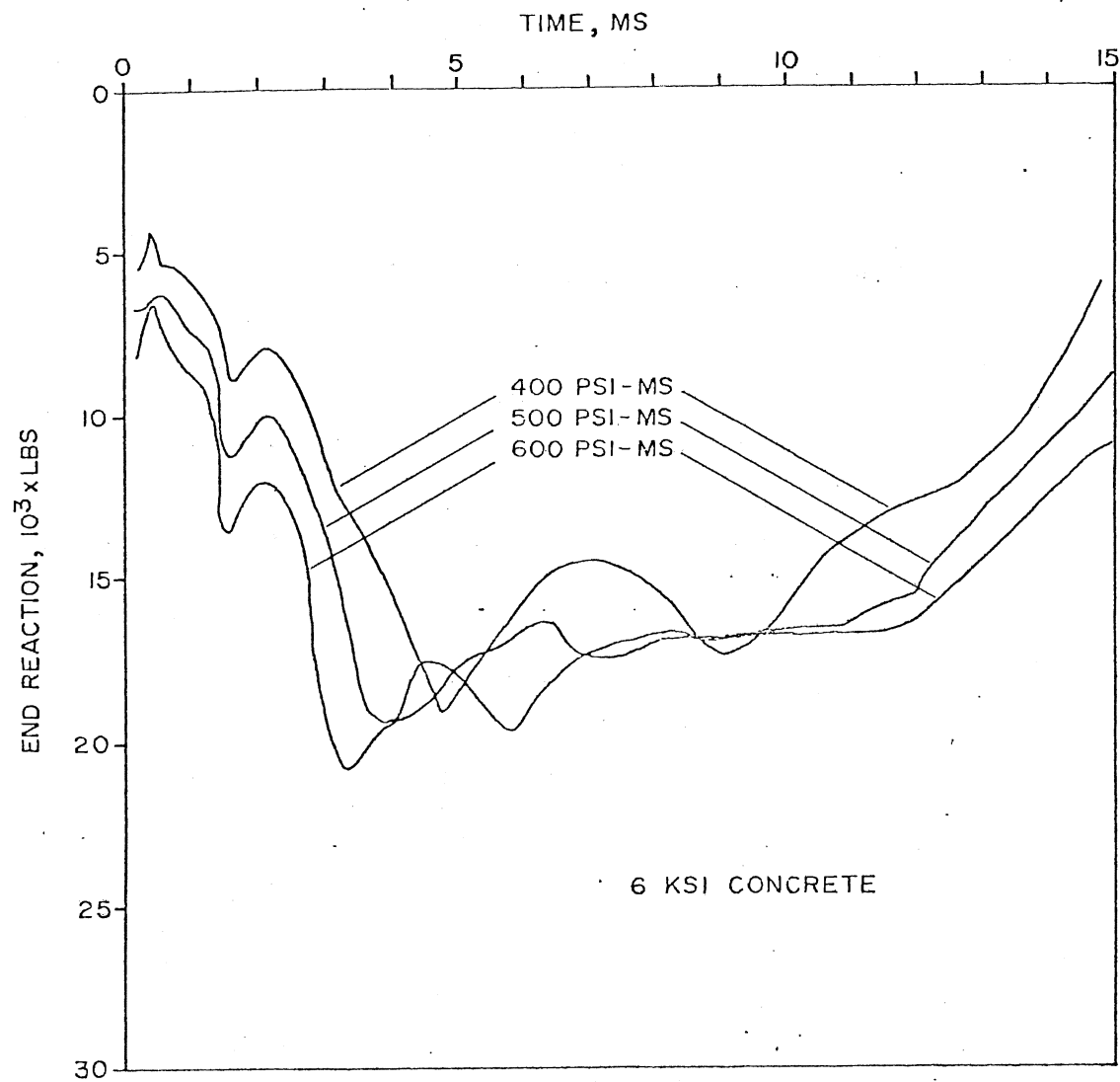
Figure 57. IMPBC Simulated End Reaction for 6 KSI
Concrete Beam

impulse. Note that for an impulse of 700 psi-ms failure was indicated for the nominal beam. The response of the high strength concrete beam, shown in Figure 57, is similar to that of the nominal beam, a characteristic of the experimental data. Furthermore, the calculated results indicate small changes in response for large changes inthe applied impulse. A 50% increase in the applied impulse produces a 10% increase in the measured reaction. Similar conclusions are available from measured data.

7.4 Summary

The load cells provided a reliable system for measurement of reaction forces due to the beam and support mechanism. Although vibration of the support system could not be modeled by IMPBC, the reactions obtained from the numerical study compare favorably with measured reactions when one examines the transmissibility of the test system: measured reactions are greater due to the mass and flexibility of the support mechanism. The frequency of the support mechanism was predicted by the model as well as measured experimentally. Excellent agreement was noted between these values. Finally, it is proposed that the digital computer program be studied for possible modification to include support flexibility.

CHAPTER VIII

BEAM STRAIN MEASUREMENT

Strain gages were placed at the mid-point and two quarter points
along the beams to monitor strains of the concrete and reinforcing
steel during the impulse test. Typical strain data from the third test
are shown to illustrate characteristics of the data. The method for
the calculation of curvatures from measured strains is presented along
with data from Test 11 to illustrate the curvature characteristics.
Excellent agreement was found between curvatures from tests 10, 11, and
12 and with those calculated from the IMPBC simulations.

8.1 Strain Data Characteristics

One pair of quarter point and center strain gages are presented in
Figures 58 and 59 to illustrate typical test data. These figures are
reproductions of computer plots produced by the Computer Sciences Labora-
tory of Eglin AFB, Florida. The identification of data channels is pre-
sented in Figure 69, Appendix A. Positive strain values in these
figures denote compressive strain. The steel gage data channels were
calibrated to 7500 μ in/in., several times the expected yield strain,
while the concrete gage data channels were calibrated to 3000 μ in/in.,
the order of the magnitude of the static crushing strain. Since the
concrete gages were located between the elastic neutral axis and the
top surface, the measured concrete strains were approximately 50 percent
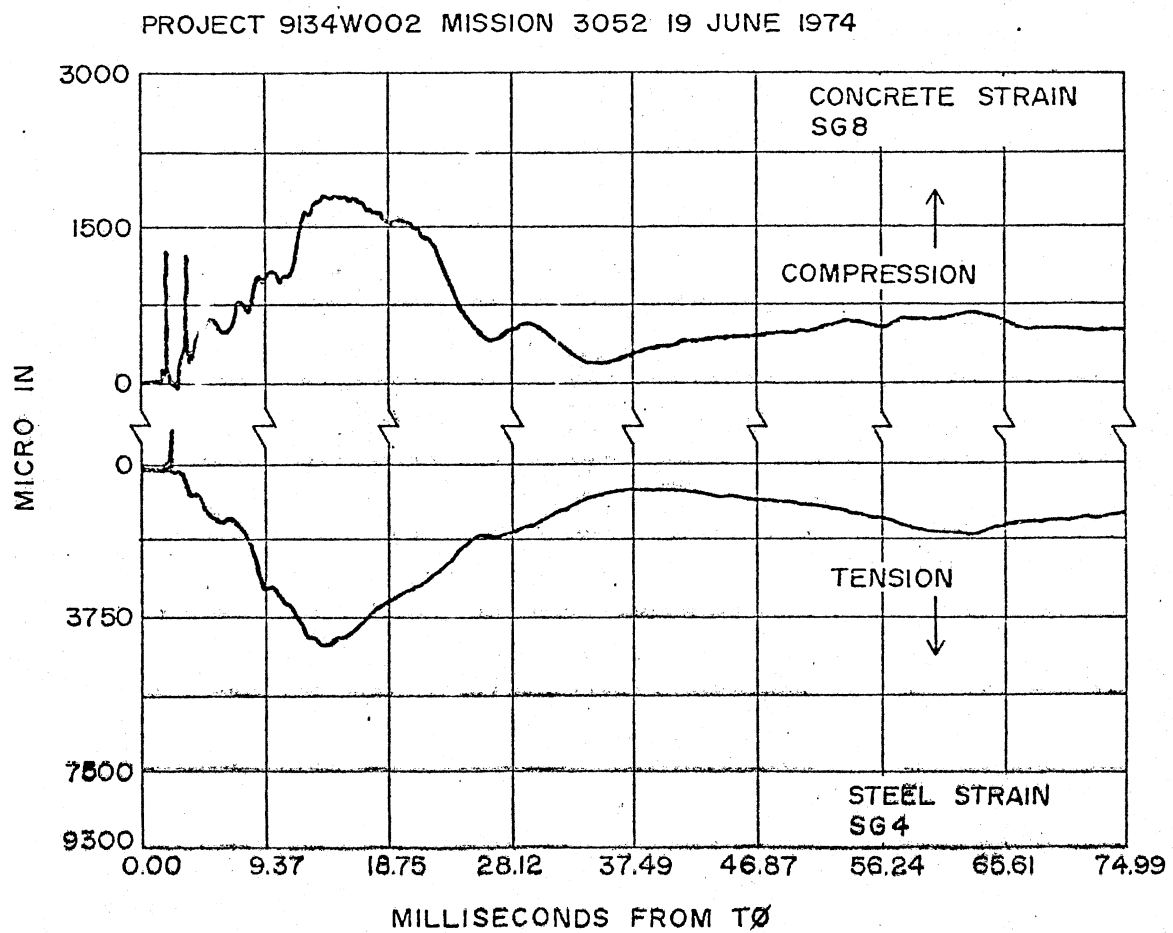
Figure 58. Typical Quarter Station Strain Data, Test 3
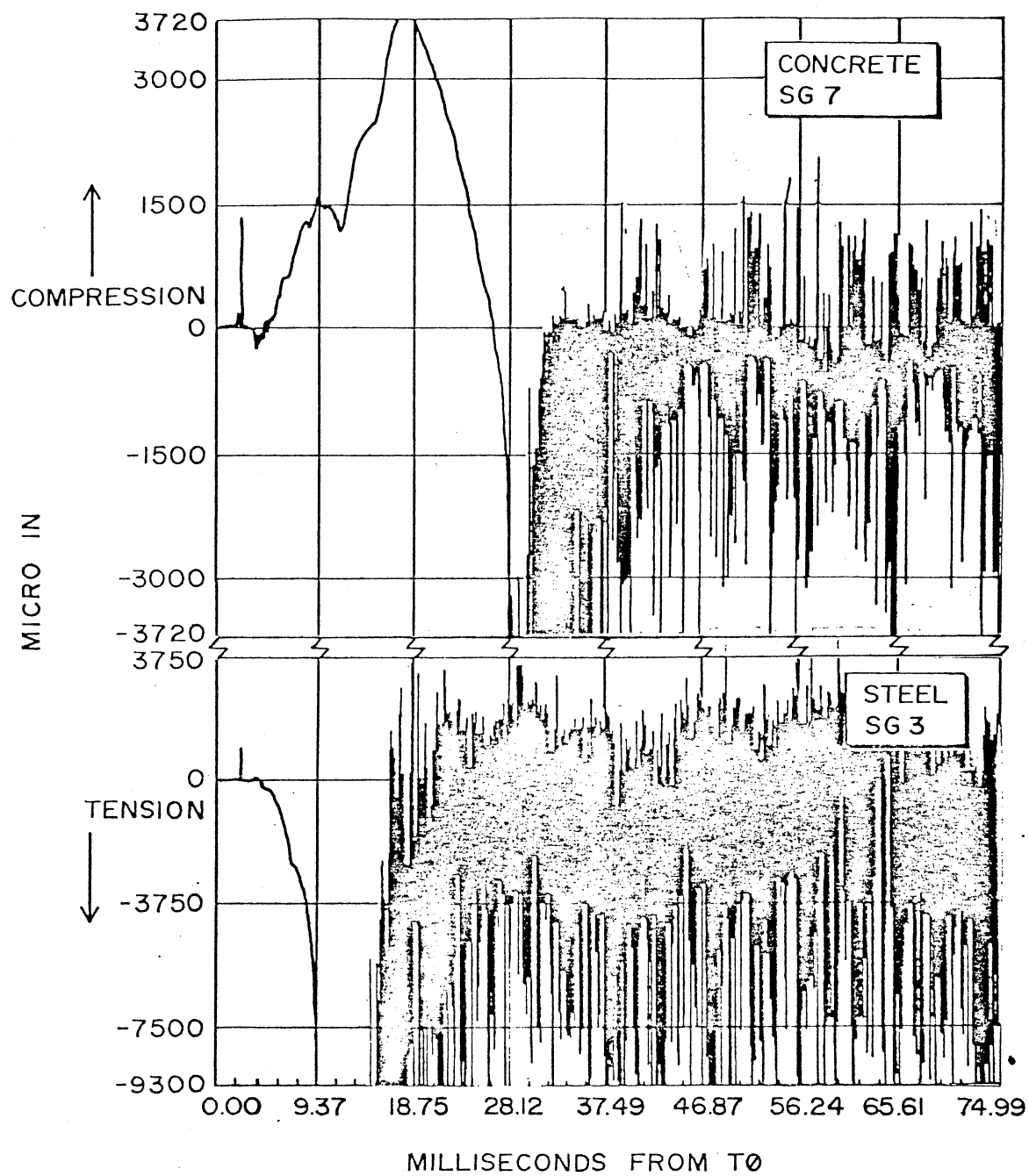
Figure 59. Typical Center Station Strain Data, Test 3

of the top surface strain, provided simple beam theory is applicable. Throughout the test series, continuous data records were available from the quarter point strain gages.

The center gages, on the other hand, performed as shown in Figure 59. Inspection following the tests showed the center concrete gages to be broken in tension, presumably the result of beam rebound from the maximum displacement, or spalled off as the result of compression failure. The broken circuits were evident from the very high frequency, large amplitude signals which covered the latter part of the plots, as shown in Figure 59. Post-test continuity checks of steel gages indicated open circuits, although visual confirmation was not possible. The failure may have been due to gage distress or broken lead wires.

8.2 Measured Beam Curvature

The strain gage data provided a measure of both the steel and concrete response to the impulse load. However, to determine the flexural response it was necessary to estimate beam curvature at the mid- and quarter points by assuming planes remain plane. From the measured strain values one may calculate curvature by:

$$\phi = \frac{(\varepsilon_c - \varepsilon_s)}{X_G} \tag{8.1}$$

where

ϕ = curvature, rad/in.;

ε_c = concrete strain, in/in., compressive strains positive;

ε_s = steel strain, in/in.;

X_G = vertical distance between steel gage and concrete gage, in., where X_G = 9.8 in. for No. 6 bars, and X_G = 9.6 for No. 9 bars.

Calculated curvatures are shown for test 11 in Figure 60. The calculated quarter point curvature, ϕ_1, was the average of the two quarter point curvatures. Likewise, the center curvature, ϕ_2, is calculated from the average steel and concrete strains at the center station. However, strain gage signals which were missing or appeared to malfunction were omitted from the calculations.

The curvature shown in Figure 60 is typical of the observed flexural response. First, curvatures were indicated prior to shock wave arrival, the results of the electrical interference. Second, the average rate of change of the center curvature for the first three milliseconds after shock wave arrival was greater than that of the quarter point curvatures. Third, the quarter curvature reached and oscillated about a constant value with small amplitude for about 12 ms. Fourth, a discontinuity is noted in the center curvature at 500 μ rad/in., after which the curvature rate increased substantially. This is approximately the yield curvature predicted for the high strength concrete beam by the IMPBC simulations, as shown in Figure 83, Appendix B.

8.3 Correlation With Calculated IMPBC Curvature

Curvatures for a nominal beam from tests 10 and 12 are compared with IMPBC results in Figure 61. Results for the high strength concrete beam of test 11 are shown in Figure 62. The computer simulations were run with three impulse loads, 400, 500 and 600 psi-ms to encompass the estimated test impulses. Although values predicted by Goodman (1)
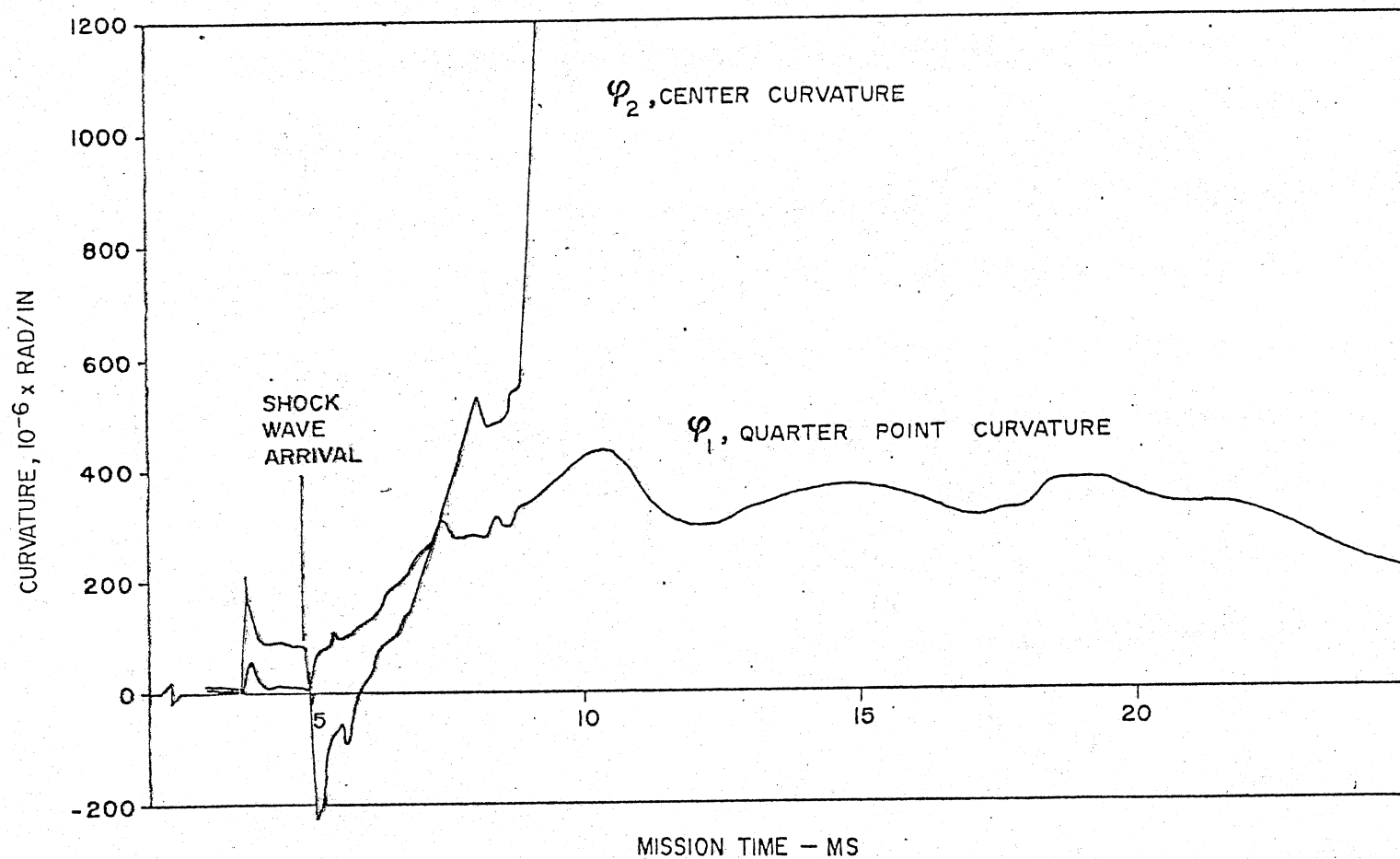
Figure 60. Curvatures Calculated From Center and Quarter Point
Strain Data, Beam 3, Test 11
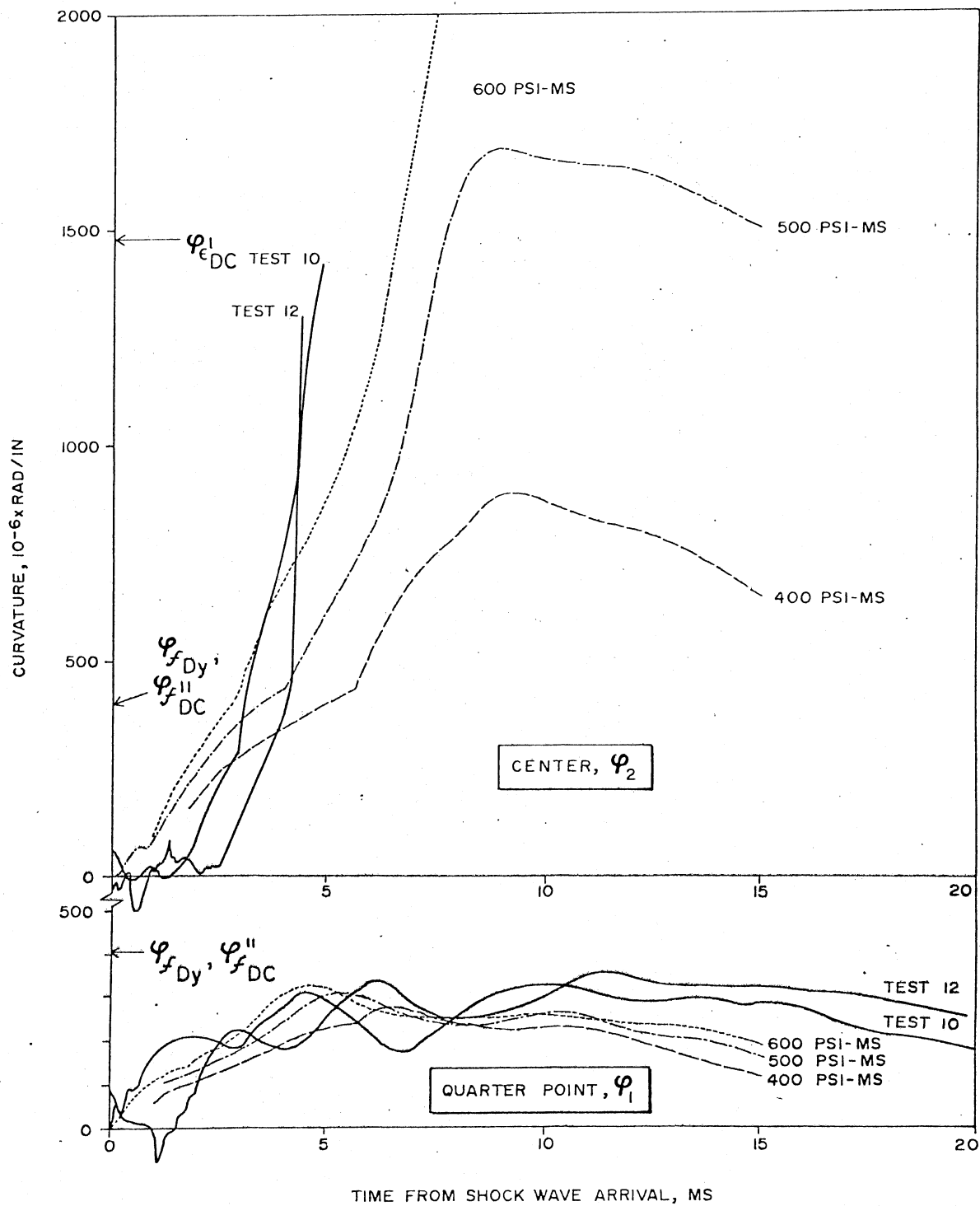
Figure 61.   Comparison of Impulse Test With IMPBC
Calculated Curvature, Nominal Beams
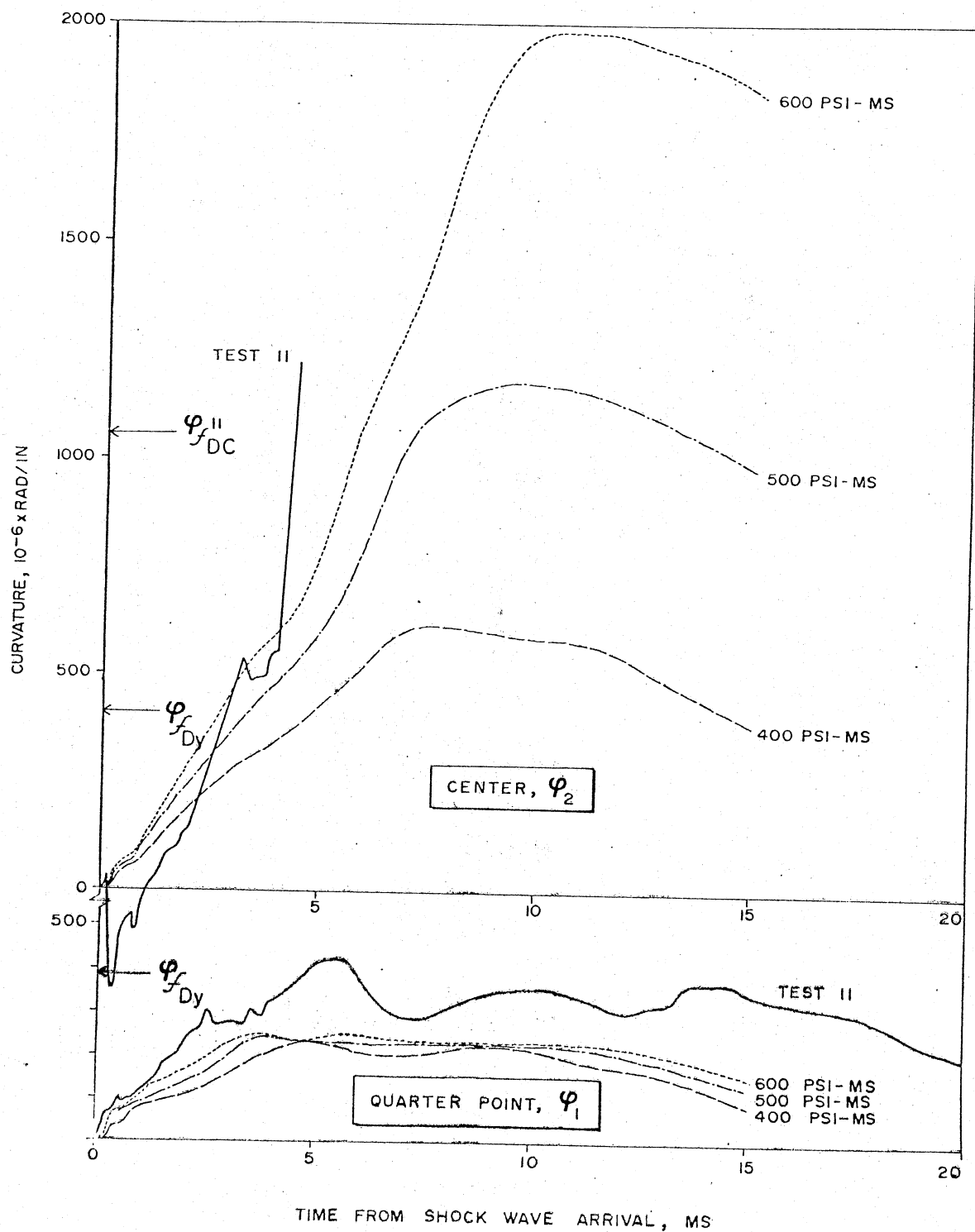
Figure 62. Comparison of Impulse Test With IMPBC
Calculated Curvature, High Strength
Concrete Beam

were 648 and 610 psi-ms for tests 10 and 12, respectively (Figure 30),
measured values were lower. It is probable that the actual impulse is
between the two values. Curvatures which correspond to selected points
on the idealized material stress-strain curves are identified in the
figures. These curvatures designate transition points on the curve of
moment variation with curvature, as shown in Figure 83, Appendix B.
These points are: (1) $\phi_{f_{Dy}}$, corresponding to the steel strain at yield
and the transition of the member from elastic to plastic behavior; (2)
$\phi_{f''_{DC}}$, corresponding to the maximum concrete stress, a discontinuity in
the idealized concrete stress-strain curve where the maximum concrete
stress remains constant; and (3) $\phi_{\epsilon'_{DC}}$, corresponding to the estimated
failure strain of the concrete.

Excellent agreement is noted between test and simulation curvatures.
Although the test initial curvature rate of change, or slope, appeared
to be greater than the simulated curvature, both test and calculated
center curvature values indicate a change in slope near the estimated
value for yield, $\phi_{f_{Dy}}$. The similarity of the curves shown in Figures
61 and 62 tends to substantiate the yield phenomenon assumed for the
construction of the moment-curvature variation, as well as add confi-
dence to measured strain values.

8.4 Summary

The performance of the center steel and concrete strain gages were
not influenced by the support vibration noted in reaction measurements.
Due to the stiffness of the support mechanism and load cells, small
displacements cause large indicated loads. However, the end displace-
ments were estimated to be orders of magnitude less than the beam center

displacement. Although the center point gages were generally destroyed very soon after shock wave arrival, until failure the gages were reliable and gave reasonable data. The quarter point gages provided a continuous record throughout the test.

Excellent agreement was noted between measured end results calculated by computer program IMPBC. Measured data substantiated the simulated response. Although failure was not observed for any of the test members, IMPBC indicated the failure of the nominal beams would occur at an impulse between 600 and 700 psi-ms.

CHAPTER IX

BEAM DAMAGE ASSESSMENT

The visual inspection which followed the blast tests provided a
qualitative assessment of blast damage. For several tests, the damage
appeared slight to nonexistent. Therefore, it was necessary to develop
a more precise evaluation of the damage caused by the impulse loading.
The beams were shipped to the Oklahoma State University, Stillwater for
final inspection and tests. The beams were loaded statically to failure
and results of these tests were presented in Chapter IV. In this chapter
a method, similar to one presented by Biggs (3), is proposed and evalu-
ated for predicting damage caused by impulse loads. Although the study
is limited to nominal beams, it is proposed that the method may be ex-
tended to the other beams of this test as well as other members, such as
plate and slab structures.

9.1 Final Static Test Results

The data from the final static tests are summarized in Table IX. In
this chapter the properties of the damaged beams are presented as a func-
tion of charge standoff distance and include residual plastic work capac-
ity, residual ductility, and the ratio of measured to theoretical ulti-
mate moment. These data are shown in Figures 63, 64, and 65.

Although scatter is apparent in the data for residual plastic work,
shown in Figure 63, several trends are apparent. First, the beams with
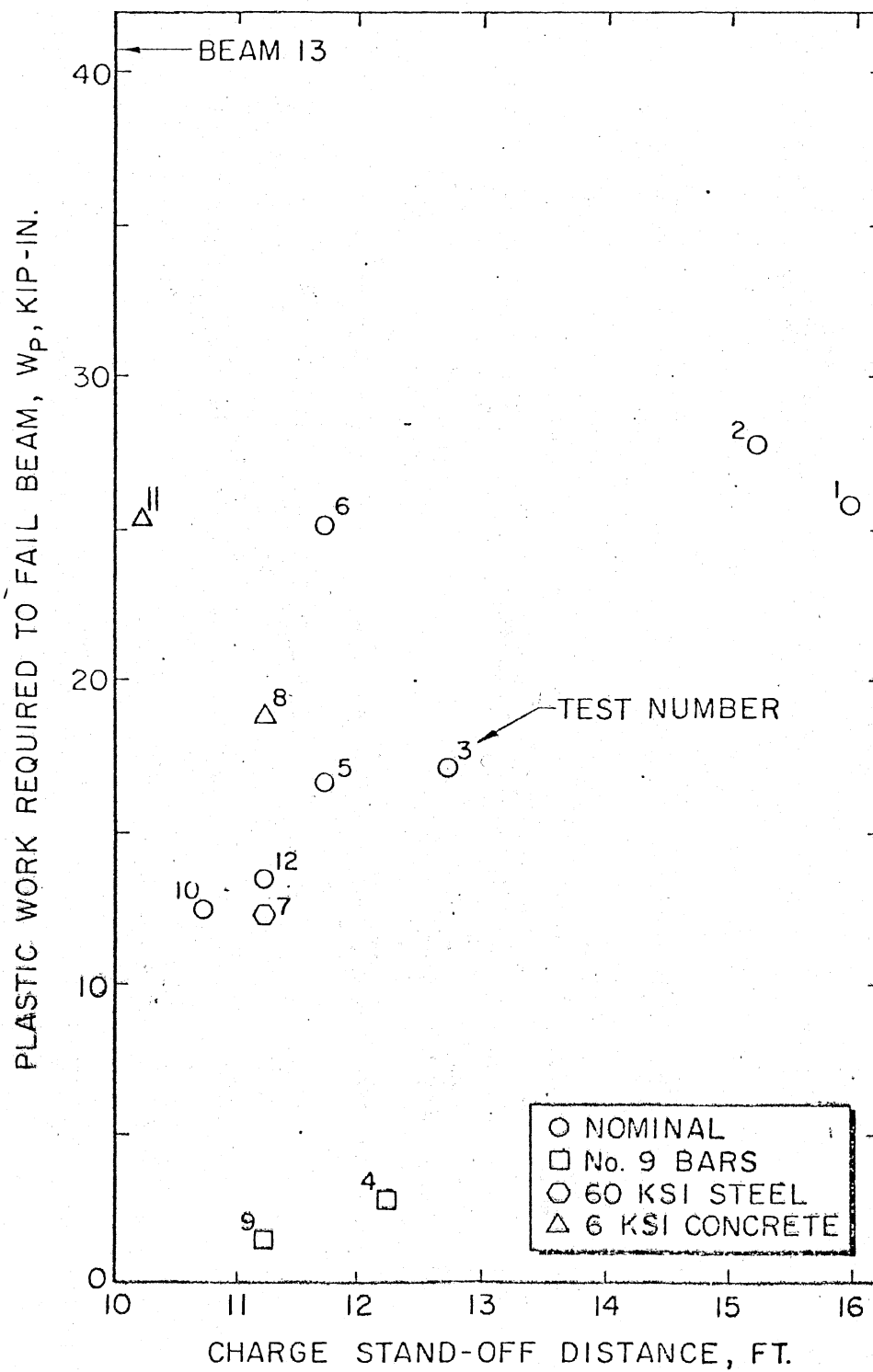
Figure 63. Variation of Residual Plastic Work
With Charge Standoff Distance
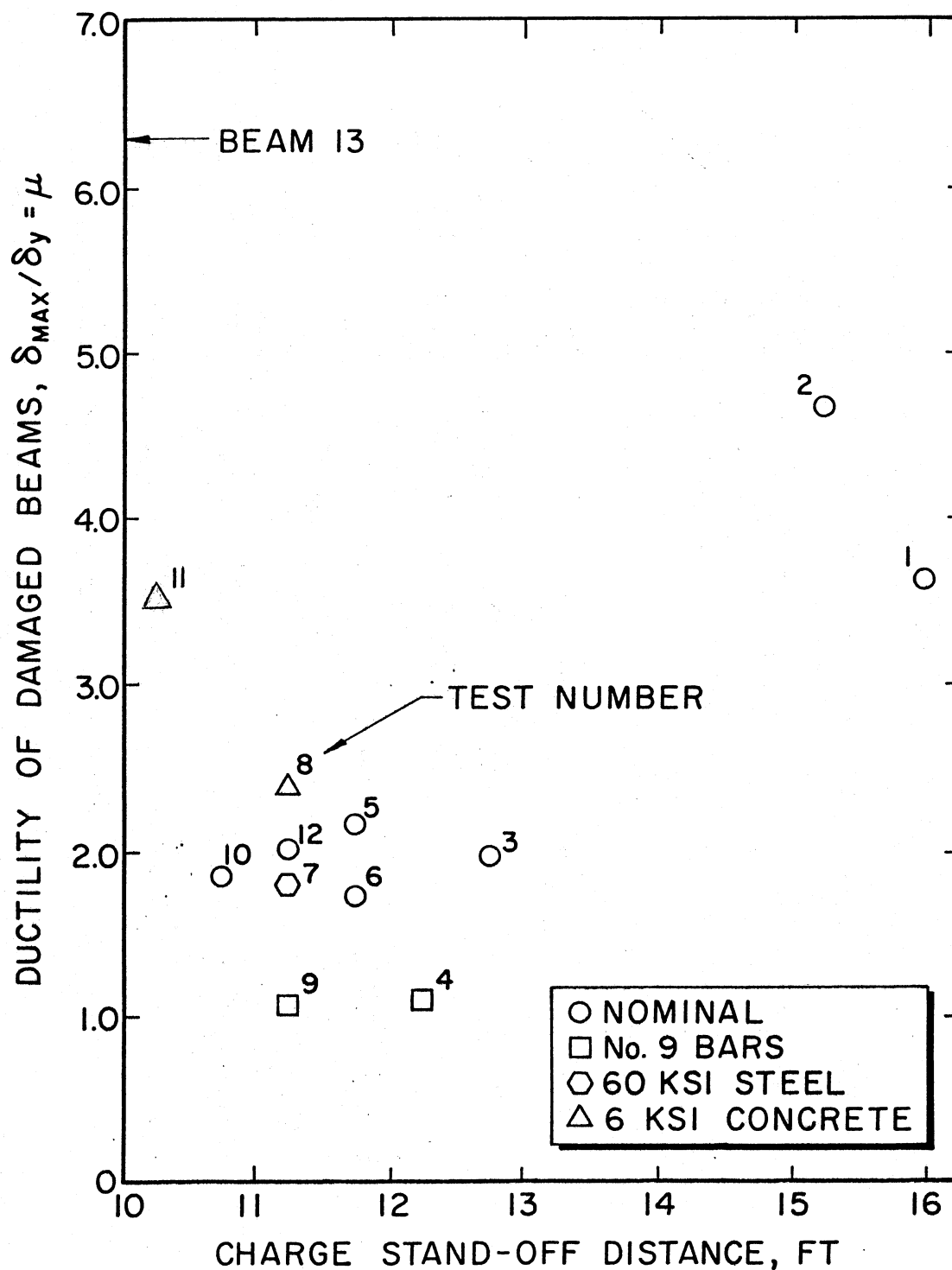
Figure 64.   Variation of Ductility With Charge
Standoff Distance
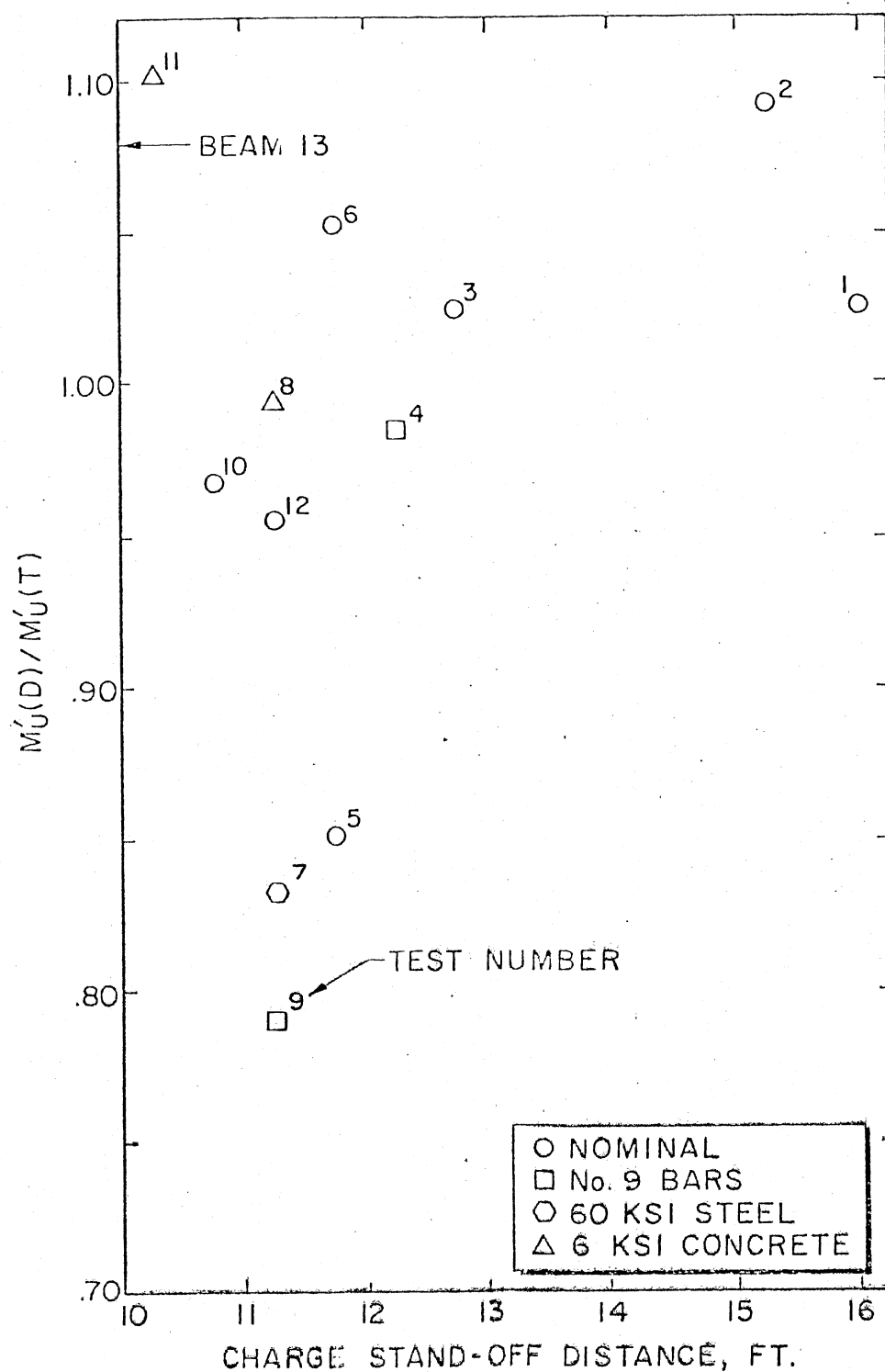
Figure 65. Variation of Measured to Theoretical
Ultimate Moment Ratio With Change
of Standoff Distance

increased reinforcing steel, the high strength beams, exhibit little residual work capacity. Second is the relation between charge standoff distance and residual work capacity: as the charge standoff distance decreases, residual plastic work is decreased. Finally, the high strength concrete beams exhibited the largest residual work capacity, although they had been subjected to the greatest impulses.

In Figure 64, residual ductility is compared with charge standoff distance. The correlation noted for residual work capacity applies equally to ductility. The high strength beams (No. 9 bars) exhibit little ductility, while the high strength concrete beams show the greatest ductility.

Finally, measured and theoretical moments are compared in Figure 65. It is interesting to note that the change in the maximum moment with impulse is less significant than the change noted in residual plastic work. Furthermore, the measured ultimate moment of the undamaged nominal beam, beam 13, compares very favorably with the theoretical ultimate moment. It was assumed that similar agreement would be present had undamaged beams of the other beam types been available for static tests.

Figures 63, 64, and 65 show effects of impulse loads on the reinforced concrete beams. The standoff distance of the Pentolite charge was assumed to be a measure of the level of impulse delivered to the beam. The reduction of residual plastic work may be interpreted as a measure of damage caused by the blast loading. Although only limited data are available for high strength concrete and high steel ratio beams, a trend is apparent for these members.

The static response of damaged and undamaged nominal beams is compared in Figure 29. Except for the reduced ductility of the damaged

beams, the two curves exhibit similar characteristics. Little difference is noted in either the ultimate moment or the initial slope of the curves. In this section the damage due to the blast loading will be studied. Differences between the static tests will be related to damage produced by the kinetic energy imparted to the beam during the impulse loading.

In Figure 66 the residual plastic work of damaged beams are compared with the toal work capacity of an undamaged member. Except for test 6, excellent agreement is noted between standoff distance and the plastic work ratio. These data, along with the characteristics noted in Figure 29, will be the basis for the damage criterion developed in the next section.

9.2 Impulse Damage Phenomenon

The effect of the high intensity impulse loading is to transform energy from the blast pressure wave to kinetic energy in the beam. Since the duration of the positive pressure is less than 2 ms, it may be assumed that the transfer is instantaneous, imparting to the beam a lateral velocity which is consistent with the support constraints. Since the pressure wave impacts the beam center, then moves toward the supports, it is reasonable to assume a sinusoidal velocity variation. The kinetic energy related to the initial velocity must be dissipated by plastic deformation of the beam or stored in the beam as elastic strain energy. The static plastic work, or toughness, will be used to determine the capacity of the beam to dissapate kinetic energy. However, the moment due to static loading should approximate the shape of the dynamic bending moment. In the laboratory, this was accomplished by a trapezoidal moment
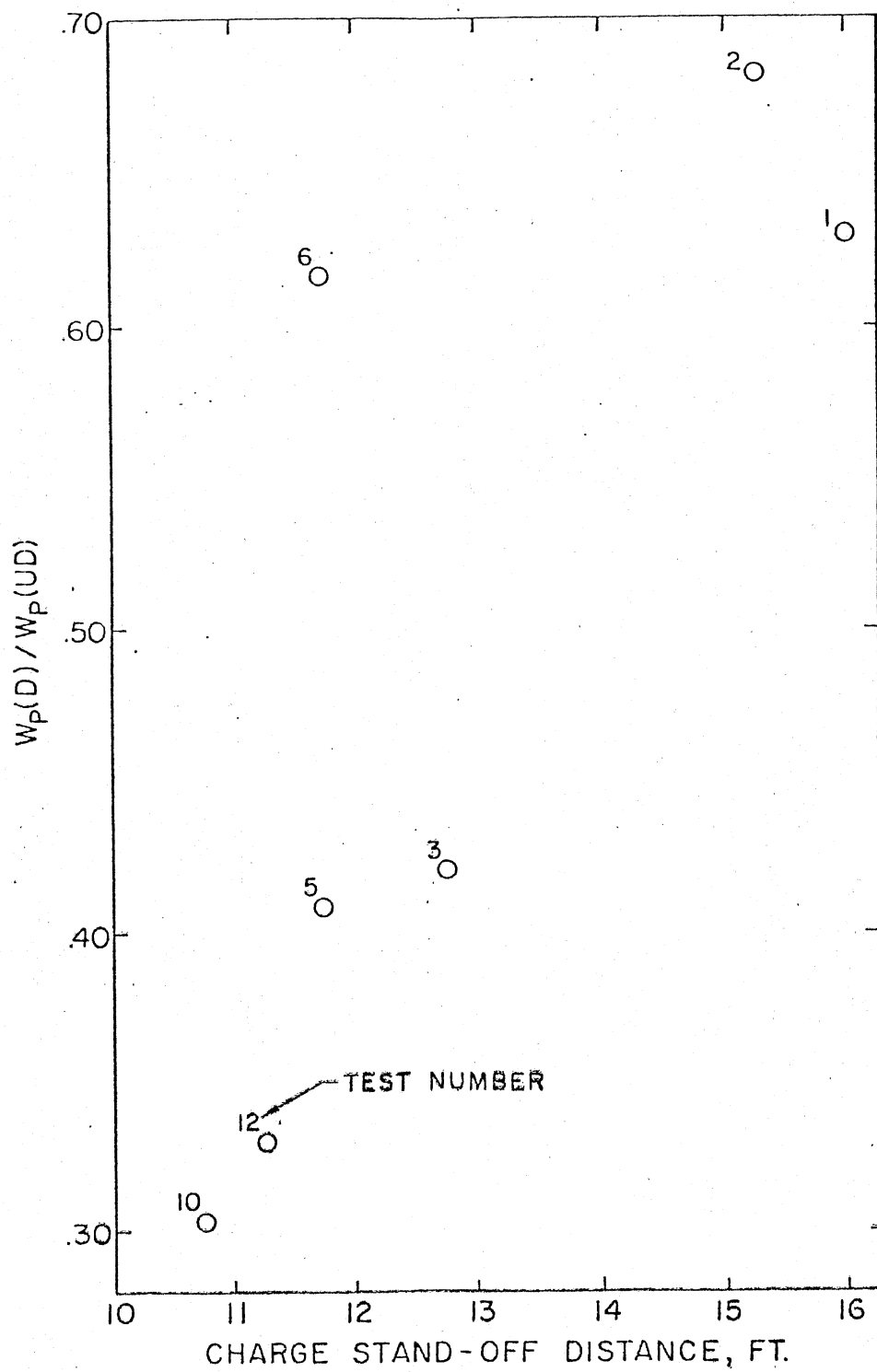
Figure 66. Variation of Residual Plastic Work
Ratio for Nominal Beams

distribution where the center 48 in. of the beam was subjected to constant moment. The work related to this loading was recorded and will be used to estimate beam impulse capacity.

9.3 Prediction of Impulse Damage

A correlation between residual plastic work and applied impulse is shown in Figure 66 for nominal beams. As the charge standoff distance is decreased, the residual plastic work decreases. The work was determined from the laboratory resistance-displacement curves, shown in Figure 29. However, these data may be arranged as shown in Figure 67. Instead of a common initial point, failure is selected as the point common to both damaged and undamaged beam resistance-deflection curves. The basis for the proposed method for damage analysis is given by this figure. The reinforced concrete member has a predictable capacity for plastic work. If a portion of this capacity is expended, the remaining capacity can be determined by a static test. The reduction in work capacity may then be related to kinetic energy which had been dissipated.

Thus, the primary assumption of this technique is that the kinetic energy imparted to the beam by the impulse loading is transformed partially into elastic strain energy stored in the beam and energy dissipated by plastic deformation. It is further assumed that the beam initial velocity distribution is sinusodial with a maximum center velocity V_{max}.

$$V_{max} = \frac{Ib}{m} \qquad (9.1)$$

where

I = impulse, psi-ms;
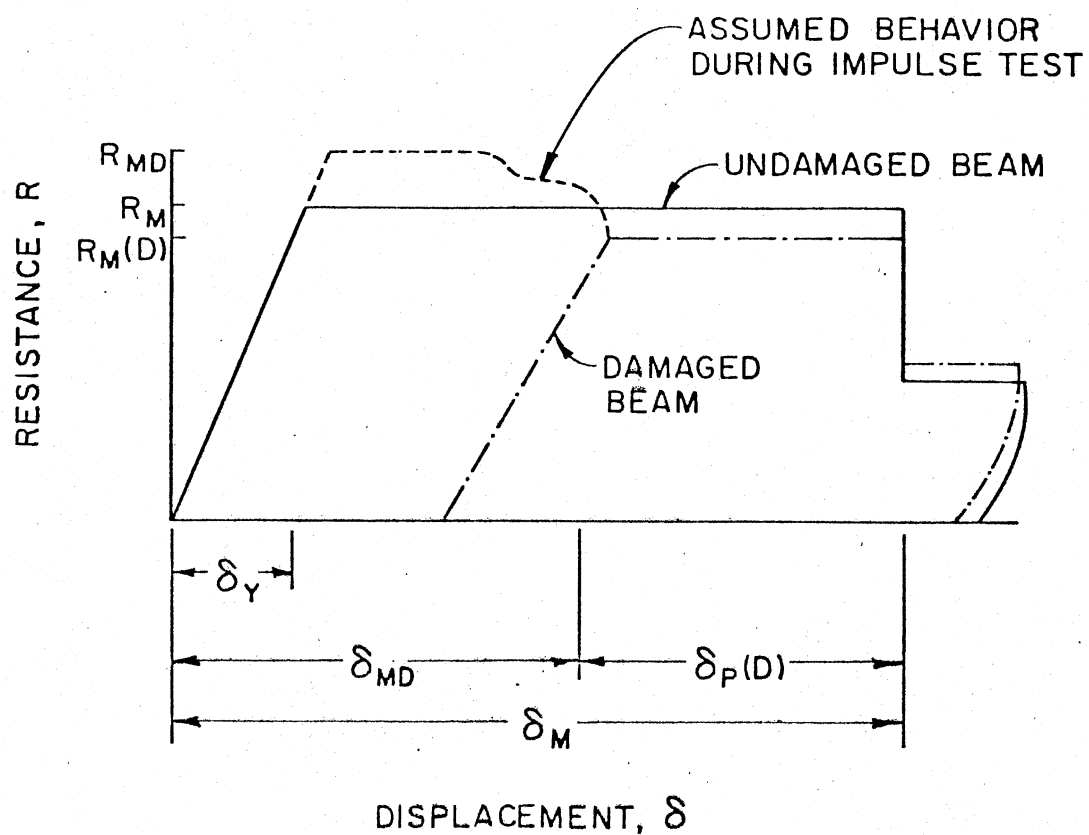
Figure 67. Idealized Resistance-Displacement Curves
for Damaged and Undamaged Beams

b = beam width, in.;

m = beam mass per length, $lb\text{-}sec^2/in^2$.

The total kinetic energy of the beam is given by:

$$KE = \frac{I^2 b^2 L}{4m} \tag{9.2}$$

where L is the length of the member.

It is assumed that the kinetic energy required to produce failure must be greater than or equal to the total static work capacity of an undamaged beam. For the beam of Figure 67 the total work capacity is taken as the area under the curve to δ_m, where a substantial drop in load capacity occurs:

$$W = R_m \delta_y \left(\mu - \frac{1}{2}\right) \tag{9.3}$$

where μ is ductility, the ratio of the maximum deflection δ_m to the elastic deflection δ_y. The total work may also be related to the total plastic work capacity, $W_p(UD)$:

$$W = W_p(UD) \frac{(\mu - 1/2)}{(\mu - 1)} \tag{9.4}$$

Equating kinetic energy (Equation (9.2)) and maximum work capacity (Equation (9.4)), the minimum impulse required to fail an undamaged beam is,

$$I = \left[\frac{4m}{b^2 L} \frac{W_p(UD)(\mu - 1/2)}{(\mu - 1)}\right]^{1/2} \tag{9.5}$$

This is also the value of impulse predicted by Biggs (3).

If a resistance-deflection curve is available for an undamaged member, it will be possible to estimate the impulse to which a beam was subjected from resistance-deflection curve of the damaged beam. The residual plastic work, $W_p(D)$, is found from the damaged beam curve

of Figure 67 and is related to the capacity of the member to dissipate kinetic energy. This may be represented mathematically as

$$KE + W_p(D) \geqq W \tag{9.6}$$

where KE is the kinetic energy of the impulse loading. Substituting for W and KE (Equations (9.2) and (9.4)),

$$I \geqq \frac{2}{b} \left(\frac{m}{L}\right)^{1/2} \left[\frac{W_p (UD)(\mu - 1/2)}{(\mu - 1)} - W_p(D)\right]^{1/2} \tag{9.7}$$

where I is an estimate of the minimum impulse to which the beam was subjected.

For the test data of Table IX, it is possible to predict the minimum impulse to which the nominal beams were subjected by Equation (9.7). The results are shown in Table XIII, along with the predicted impulse of Goodman (1). From data obtained from the undamaged beam, it is estimated that an impulse of at least 708 psi-ms would be required to produce failure. It should be noted that there is agreement between this estimate and the calculated results of digital computer program IMPBC.

9.4 Summary

Post-test visual inspection of the beams indicated moderate to slight damage. However, the final static tests indicated significant losses in plastic work capacity which were related to the dissipation of kinetic energy.

A method for predicting damaged based on work of Biggs (3) was proposed. Although reliable measured values of impulse were unavailable, excellent agreement was noted between impulse predicted by

TABLE XIII

ESTIMATE OF TEST IMPULSE FROM RESIDUAL
PLASTIC WORK AND GOODMAN (1)

Test No.	Minimum Kinetic Energy Imparted to Beam, kip-in., Eq. (9.6)	Impulse I, psi-ms	
		Eq. (9.7)	Goodman[1]
1	18.9	460	375
2	16.8	434	410
3	27.5	555	520
5	28.0	560	560
6	19.5	468	560
10	32.3	602	650
12	31.2	595	620
Beam 13	44.6[2]	708	--

[1]From Figure 32.

[2]Maximum work available for kinetic energy.

Goodman and Equation (9.7). It is reasonable to assume that the method presented in this report may be extended to other concrete structures.

CHAPTER X

SUMMARY AND RECOMMENDATIONS

These tests provided both qualitative and quantitative data of the blast-response phenomenon for reinforced concrete beams. The major results are summarized and recommendations are proposed for additional studies.

Three general conclusions of this study are:

1. The impulse tests provided valuable information concerning the coupling of the blast pressure wave with the beam, although the threshold impulse for beam failure was not defined.

2. The technique of statically testing the impulse-damaged beams was a valuable method for obtaining quantitative assessment of beam damage.

3. The high strength concrete beams, of the types tested, exhibited the most resistance to damage on the basis of both qualitative and quantitative observations. On the other hand, the beams with high steel ratios were the least resistant to impulse loading.

10.1 Test Evaluation

10.1.1 Test Equipment

The test beams were suitable for the test program. Although the beams were not model sized, they were not too large to handle in the

field or in the laboratory. The test fixture performed well during the blast tests. It sustained little damage and would be available for future test programs. However, the support mechanism and reaction measurement devices should be modified to provide more reliable measurement of beam end forces. The present design did not isolate beam end forces from those caused by the motion of the support mechanism.

The bare spherical Pentolite charge suspended above the test specimen was effective in providing the required impulse loads. However, the measured impulses found by integrating the pressure-time data were generally less than those predicted by Goodman.

10.1.2 Instrumentation

The load cells and strain gages provided reliable data throughout the test program. The concrete and steel strain gages performed well, even though certain gages failed as beam damage accumulated. The load cell data were also reliable. However, in future tests, low mass, rigid transducers should be considered for reaction force measurements.

Although pressure data were improved by changing pressure transducers, additional work is required to investigate the response of transducers to the very short duration, high pressure loading produced in these tests. The PCB transducers appeared to give consistent results, but the accuracy of these measurements should be studied.

The accelerometer installation utilized for these test did not prove to be suitable. A zero shift, which was of the order of magnitude of the data, was produced by large shock transients. High speed photography as well as mechanical scratch gages should be considered for deflection measurment in future tests.

10.1.3 Damage Assessment

An important development of this work was the assessment of damage from a comparison of static resistance-deflection characteristics of damaged and undamaged beams. The variations noted in these curves were attributed to the impulse loading. It was found that: (1) for the range of standoff distances studied, there was not a large reduction in the ultimate moment capacity of the damaged beams; (2) there appeared to be substantial reductions in the ductility of the damaged beams; and (3) of the parameters studied, the residual plastic work, which includes items 1 and 2, exhibited the greatest change with the standoff distance.

The beam damage assessment method was used to predict test impulse. The impulse predicted by the damage criterion for the nominal beams compared favorably with Goodman (1). Similar evaluations could have been made if undamaged samples of the other beam types had been available.

10.1.4 Comparison of Test Data With IMPBC Analysis

Results of program IMPBC were compared with experimental reactions and curvatures. Excellent agreement was noted between calculated and measured curvatures. Comparison of reactions must be qualified because of the vibration of the support mechanism. Measured reactions are a combination of beam end forces and support mechanism inertial forces. However, the IMPBC results are similar to the measured data when one considers the effect of the change of impulse on the change in reaction. Finally, the agreement between IMPBC and Biggs (3) for failure impulse should be noted.

It is concluded that the program becomes a versatile and valuable analytical tool for investigating the impulse-response characteristics of reinforced concrete beams. However, it is also recommended that the digital computer program be extended to include:

1. A criterion to represent loss of material from the top layers of concrete in the highest moment region, and account for the changed cross section by revising the moment-curvature curves at the affected nodes.

2. Automatic evaluation of strain rate effects within the program.

3. Damage assessment criterion developed in this work.

10.1.5 Beam Performance

Beam damage was evaluated on the basis of visual observations and static load tests to failure. On the basis of visual observations, the high strength steel beam appeared to sustain the most damage; however, the static tests showed the large steel area beams to have the least residual energy capacity. The high strength concrete beams appeared to have the greatest blast resistance on the basis of both visual observation and residual static capacity.

10.2 Recommendations for Additional Studies

Limited studies should be performed to evaluate the damage criterion presented in this report for other structural members. The program should include static testing of undamaged members, to predict failure impulse, followed by blast tests. It is further recommended that the existing test fixture be utilized for these tests.

The members which should be investigated are:

1. Tee and double-tee beams, with attention to web shear failure and shear transfer from flange to web in high moment regions;

2. Composite beams, with attention to shear transfer from the concrete to the steel portion of the member;

3. Prismatic beams with compression reinforcement.

4. Prestressed concrete beams, both post- and pre-tensioned.

A SELECTED BIBLIOGRAPHY

(1) Goodman, H. J. "Compiled Free-Air Blast Data on Bare Spherical Pentolite." Aberdeen Proving Ground, Maryland: Ballistic Research Laboratories, Report No. 1092, July, 1956.

(2) Dawkins, W. P. "A Method of Analysis for Reinforced Concrete Beam-Columns Subjected to Impulse Loading." Report submitted to Oklahoma State University, March, 1971.

(3) Biggs, John M. Introduction to Structural Dynamics. New York: McGraw-Hill Book Co., Inc., 1964, pp. 199-224.

(4) Manjoine, M. J. "Influence of Rate of Strain and Temperature on Yield Stresses of Mild Steel." Transactions, Journal of Applied Mechanics, American Society of Mechanical Engineers, Vol. 66, No. 4 (December, 1944), pp. A.211-A.218.

(5) Norris, Charles H., et al. Structural Design for Dynamic Loads. New York: McGraw-Hill Book Co., Inc., 1959, p. 27.

(6) Allgood, J. R. and G. R. Swihart. Design of Flexural Members for Static and Blast Loading. ACI Monograph No. 5. Detroit: American Concrete Institute, 1970, pp. 23-25.

(7) Perrone, Nicholas. "On a Simplified Method for Solving Impulsively Loaded Structures of Rate-Sensitive Materials." Transactions, Journal of Applied Mechanics, American Society of Mechanical Engineers, Vol. 87 (September, 1965), pp. 489-492.

(8) Watstein, D. "Effect of Straining Rate on the Compressive Strength and Elastic Properties of Concrete." Proceedings, Journal of the American Concrete Institute, Vol. 49, No. 8 (April, 1953), pp. 729-744.

(9) Atchley, B. L. and H. L. Furr. "Strength and Energy Absorption Capabilities of Plain Concrete Under Dynamic and Static Loadings." Proceedings, Journal of the American Concrete Institute, Vol. 64, No. 11 (November, 1967), pp. 745-746.

(10) Keenan, William A. "Dynamic Shear Strength of Reinforced Concrete Beams--Part I." Port Hueneme, Calif.: Naval Civil Engineering Laboratory, Technical Report No. R-395 (AD627661), December, 1965.

(11) Fox, E. N. "Some Exploratory Tests on the Strength of Concrete Beams Under Pulse Loads." Mechanical Properties of Non-Metallic Brittle Materials. Ed. W. H. Walton. London: Butterworths Scientific Publications, 1958, pp. 283-299.

(12) Galloway, J. W. and K. D. Rathby. "Effects of Rate of Loading on Flexural Strength and Fatigue Performance of Concrete." Crowthorne, Berkshire: Transport and Road Research Laboratory, Report No. LR 547, 1973.

(13) Mylrea, T. E. "Effect of Impact on Reinforced Concrete Beams." Proceedings, Journal of the American Concrete Institute, Vol. 36, No. 6 (June, 1940), pp. 581-594.

(14) Kluge, R. W. "Impact Resistance of Reinforced Concrete Slabs." Proceedings, Journal of the American Concrete Institute, Vol. 39, No. 5 (April, 1943), pp. 397-412.

(15) Bate, S. C. C. "The Strength of Concrete Members Under Dynamic Loading." Proceedings of a Symposium on the Strength of Concrete Structures. London: Cement and Concrete Association, 1956, pp. 487-524.

(16) Simms, L. G. "Actual and Estimated Resistance of Some Reinforced-Concrete Units Failing in Bending." Journal of the Institution of Civil Engineers, Vol. 23, No. 4 (February, 1945), pp. 163-179.

(17) Hansen, Robert J. "Long Duration Impulsive Loading of Simple Beams." Journal of the Boston Society of Civil Engineers, Vol. 35, No. 3 (July, 1948), pp. 272-285.

(18) Penzien, J. and R. J. Hansen. "Static and Dynamic Elastic Behavior of Reinforced Concrete Beams." Proceedings, Journal of the American Concrete Institute, Vol. 50, No. 7 (March, 1954), pp. 545-568.

(19) Nordell, William J. "Hinging in Statically and Dynamically Loaded Reinforced Concrete Beams." Port Hueneme, Calif.: Naval Civil Engineering Laboratory, Technical Report No. R-489 (AD642108), October, 1966.

(20) Nordell, William J. "Plastic Hinge Formation in Reinforced Concrete Beams." Port Hueneme, Calif.: Naval Civil Engineering Laboratory, Technical Report R-371 (AD617246), June, 1965.

(21) Mavis, F. T. and E. A. Richards. "Impulsive Testing of Concrete Beams." Proceedings, Journal of the American Concrete Institute, Vol. 52, No. 1 (September, 1955), pp. 93-102.

(22) Mavis, F. T. and M. J. Greaves. "Destructive Impulse Loading of Reinforced Concrete Beams." Proceedings, Journal of the American Concrete Institute, Vol. 54, No. 3 (September, 1957), pp. 233-252.

(23) Balog, Louis et al. A discussion of "Destructive Impulse Loading of Reinforced Concrete Beams." Proceedings, Journal of the American Concrete Institute, Vol. 54, No. 9 (March, 1958), pp. 811-824.

(24) Shaw, W. A. and J. R. Allgood. "Blast Resistance of Reinforced Concrete Beams Influenced by Grade of Steel." Proceedings, Journal of the American Concrete Institute, Vol. 55, No. 10 (March, 1959), pp. 935-946.

(25) Mavis, F. T. and J. J. Stewart. "Further Tests of Dynamically Loaded Beams." Proceedings, Journal of the American Concrete Institute, Vol. 55, No. 11 (May, 1959), pp. 1215-1223.

(26) Wadlin, G. K. and J. J. Stewart. "Comparison of Prestressed Concrete Beams and Conventionally Reinforced Concrete Beams Under Impulsive Loading." Proceedings, Journal of the American Concrete Institute, Vol. 50, No. 4 (October, 1961), pp. 407-422.

(27) Hamilton, Wayne A. "Dynamic Response of Pretensioned Prestressed Concrete Beams." Proceedings, Journal of the American Concrete Institute, Vol. 65, No. 10 (October, 1968), pp. 851-855.

(28) Cowles, Bruce C. and Wayne A. Hamilton. "Repetitive Dynamic Loading on Pretensioned Prestressed Beams." Proceedings, Journal of the American Concrete Institute, Vol. 66, No. 9 (September, 1969), pp. 745-747.

(29) Reichstetter, F. G. "Blast Loaded Concrete Beam Test." Eglin Air Force Base, Florida: Armament Development and Test Center, Data Package 74-11, Project AFATWG02, November, 1974.

(30) Armament Development and Test Center. "Vulnerability and Lethality Testing System." Technical Report No. ADTC-TR-72-127. Eglin Air Force Base, December, 1972.

(31) Gupchup, Vijay N. and Indravandan K. Shah. "Static and Dynamic Behavior of Reinforced Concrete Arches." Boston: Massachusetts Institute of Technology, Civil Engineering Dept., Report No. R63-5, March, 1963.

(32) Wu, Tien Hsing. Soil Dynamics. Boston: Allyn and Bacon, 1971, pp. 168-169.

APPENDIX A

IMPULSE TEST DATA

As many as 23 channels of pressure, load, strain, and accelero-
meter data were recorded during the impulse tests. These data were
recorded as analog signals and later converted to discrete digital data.
The data are available in three forms: (1) computer printout listings;
(2) computer-generated plots; and (3) computer data tapes. The loca-
tion and channel notations of the various instruments are shown schema-
tically in Figure 68. The figure is a top view of the beam and its two
support mechanisms. It shows locations of: (1) the load cells; (2)
accelerometers on the bottom surface of the beam and beam support axles;
(3) steel strain gages on the reinforcing bars; (4) concrete strain
gages on the beam sides; and (5) pressure transducers at three locations
on the top surface of the test fixture and at one location within the
fixture cavity.

The mission times in the data lists are elapsed times, in milli-
seconds, measured from a reference time, T0, and are listed in Table
XIV by test and instrument group. It will be noted that for several
tests the given reference times for all instruments do not agree. For
those tests, all data analysis was referenced to the time given in
Table XIV.

The data listings and data tapes are on file at Oklahoma State
University, School of Civil Engineering. The data are stored on three

149

TABLE XIV

DATA PROCESSING REFERENCE TIME, $T\emptyset$ [3]

Test	Accelerometers (15 ms Record)	(75 ms Record)	Pressures (15 ms Record)	Strains (75 ms record)	Loads (75 ms Record)	Reference Time Selected for Data Analysis
1	894	--	894	886	--	886
2	647	647	647	--	--	647
3	647	647	645	645	645	645
4	363	363	363	364	364	363
5	39	39	39	39	39	39
6	74	75	75	72	72	72
7	--	--	--	932	932	932
8	934	934	934	930 [1]	930	930
9	481	480	481	478 [2]	478	478
10	933	933	933	933	933	933
11	694	693	694	690	690	690
12	804	804	804	800	800	800

[1] Strain gages SG2 and SG6 are referenced to 934 ms.

[2] Strain gages SG2 and SG6 are referenced to 481 ms.

[3] Time from word 11 of header record, in ms.

tapes with the Oklahoma State University Computer Center, serial Nos. T6528, T9090, and T6530 with 114, 180, and 10 files, respectively. The tapes are nine track, 1600 bpi in IBM 360 format. Each file represents data for an instrument for a single test and consists of:

(1) 1 header record (2A4, 14I5);

(2) 48 data records (125 (F6.3, F8.0));

(3) 1 end of file.

The header record contained 15 items, 1 alphanumeric word and 14 integer words, as follows:

Word	Item
1	Project number (which is AFATWG02)
2	Mission number
3	Day
4	Month
5	Year
6	Station
7	Test number
8	T0 time, hours
9	T0 time, minutes
10	T0 time, seconds
11	T0 time, milliseconds

Words 12 through 15 are not applicable.

The data records are arranged into two columns of 125 rows. The first column is the elapsed time from T0 in milliseconds and the second is the data, calibrated in the following units:

(1) Strain, μin./in.;

(2) Pressure, psi;

(3) Loads, lbs;

(4) Accelerations, g's (386 in./sec^2 per g unit).

The tape data files are indexed in Table XV on a test-by-test basis. The index number is a decimal number of the form a.bbb where a is the tape number and bbb is the file on the tape.

Finally, the plotted data are presented in Figures 69 through 79. These are copies of figures which were produced by the Eglin AFB Computer Sciences Laboratory.

TABLE XV

TAPE DATA FILE INDEX

Test	Mission Number	Strain Gage Data Files								Load Cell Data Files					
		SG1	SG2	SG3	SG4	SG5	SG6	SG7	SG8	LC1	LC2	LC3	LC4	LC5	LC6
1	5037	2.016	2.014	2.017	2.018	2.019	2.015	2.020	2.021	--	--	--	--	--	--
2	3703	1.011	--	1.012	1.013	1.014	--	1.015	1.016	1.017	1.018	1.019	1.020	1.021	1.022
3	3052	1.047	2.005	1.048	1.040	1.041	2.006	1.042	1.043	1.044	1.045	1.037	1.038	1.039	1.046
4	5047	3.001	2.003	3.002	3.003	3.004	2.004	3.005	3.006	1.062	1.063	1.064	1.065	1.066	1.067
5	3028	1.077	3.077	1.078	1.079	1.080	3.008	1.081	1.082	1.083	1.084	1.085	1.086	1.087	1.088
6	5023	1.129	3.009	1.130	1.131	1.132	3.010	1.133	1.134	1.135	1.136	1.137	1.138	1.139	1.140
7	2072	1.150	--	1.151	1.152	1.153	--	1.154	1.155	1.156	1.157	1.158	--	1.159	1.160
8	4703	1.115	1.113	1.098	1.116	1.114	1.117	1.024	1.118	1.119	1.120	1.121	--	1.122	1.123
9	5702	1.163	1.161	1.164	1.165	1.166	1.162	1.167	1.168	1.169	1.170	1.171	--	1.172	1.173
10	1705	2.087	2.080	2.088	2.089	2.090	2.081	2.091	2.092	2.093	2.094	2.095	--	2.096	2.086
11	3707	2.032	2.031	2.033	2.034	2.035	--	2.036	2.037	2.038	2.039	2.040	--	2.041	2.042
12	4701	2.043	2.063	2.044	2.045	2.046	2.064	2.047	2.048	2.049	2.050	2.051	--	2.052	2.053

Tape-file designation = a.bbb, where: a = tape number; a = 1 = tape T9090;
bbb = file number; a = 2 = tape T6528;
a = 3 = tape T6530.

TABLE XV (Continued)

Test	15 ms A1	A2	A3	A4	A5	75 ms A1	A2	A3	A4	A5
1	2.007	2.008	2.009	--	. ---	2.102	2.103	2.104	--	--
2	1.004	1.005	1.006	--	--	1.001	1.002	1.003	--	--
3	1.028	1.029	1.030	1.031	1.032	1.023	1.024	1.025	1.026	1.027
4	1.049	1.050	1.055	1.052	1.053	1.058	1.059	1.060	1.061	--
5	1.068	1.069	1.070	1.071	1.072	1.089	1.090	1.091	1.092	1.093
6	2.097	2.098	2.099	2.100	2.101	1.141	1.142	1.143	1.144	1.145
7	--	--	--	--	--	--	--	--	--	--
8	1.104	1.105	1.106	1.107	1.108	1.099	1.100	1.101	1.102	1.103
9	1.174	1.175	1.176	1.177	1.178	2.105	2.106	2.107	2.108	2.109
10	2.075	2.076	2.077	2.078	2.079	2.070	2.071	2.072	2.073	2.074
11	2.022	2.023	2.024	2.025	2.026	2.110	2.111	2.112	2.113	2.114
12	2.054	2.055	2.056	2.057	2.058	2.065	2.066	2.067	2.068	2.069

Note: Header spans "Accelerometer Data Files"

TABLE XV (Continued)

| | 15 Ms | | | | 75 Ms | | | |
Test	P1	P2	P3	P4	P1	P2	P3	P4
1	2.010	2.011	2.012	2.013				
2	1.007	1.008	1.009	1.010				
3	1.033	1.034	1.035	1.036				
4	1.054	1.055	1.056	1.057				
5	1.073	1.074	1.075	1.076	1.094	1.095	1.096	1.097
6	1.125	1.126	1.127	1.128	1.146	1.147	1.148	1.149
7	--	--	--	--	--	--	--	--
8	1.109	1.110	1.111	1.112				
9	1.179	1.180	2.001	2.002				
10	2.082	2.083	2.084	2.085				
11	2.027	2.028	2.029	2.030				
12	2.059	2.060	2.061	2.062				

Pressure Data Files
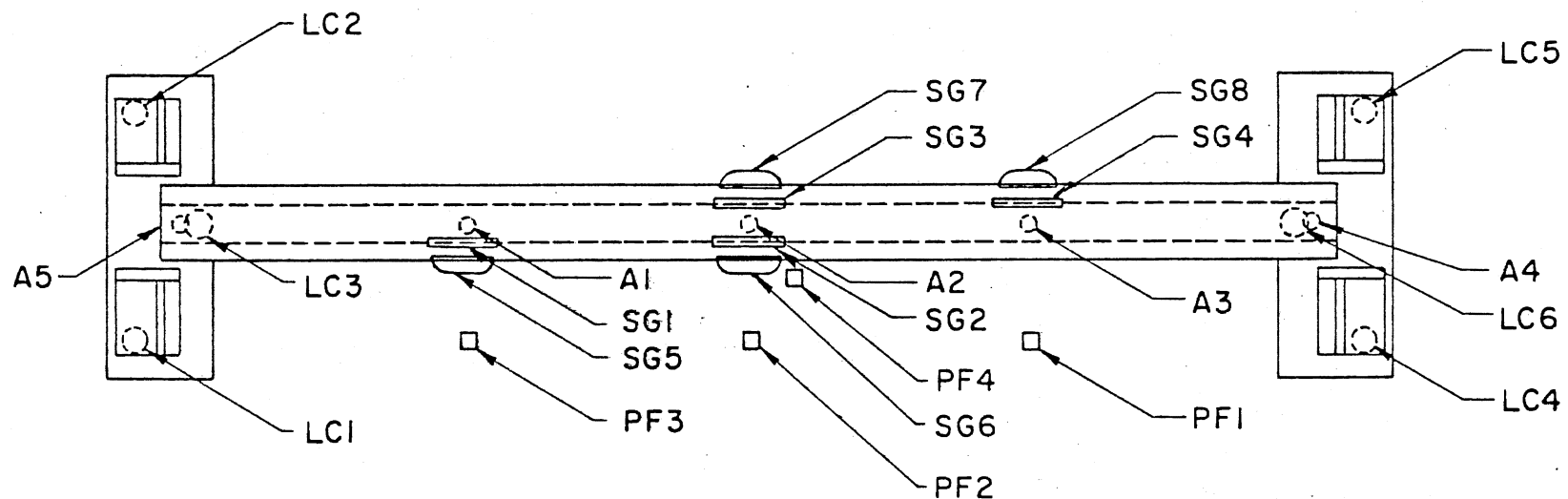
○ LOAD CELLS BENEATH BEAM SUPPORT MECHANISM, LCI-LC6

○ ACCELEROMETERS; AI, A2, A3 ON BEAM BOTTOM SURFACE; A4, A5 ON BEAM AXLES, A

▱ CONCRETE STRAIN GAGE; ON BEAM SIDE, SG5-SG8

▭ STEEL STRAIN GAGE; ON REINFORCING STEEL, SGI-SG4

□ PRESSURE TRANSDUCER; PFI-PF3 ON TOP STEEL COVER; PF4 IN TEST FIXTURE CAVITY

Figure 68. Schematic of Instrumentation Location and Data Channel Notation
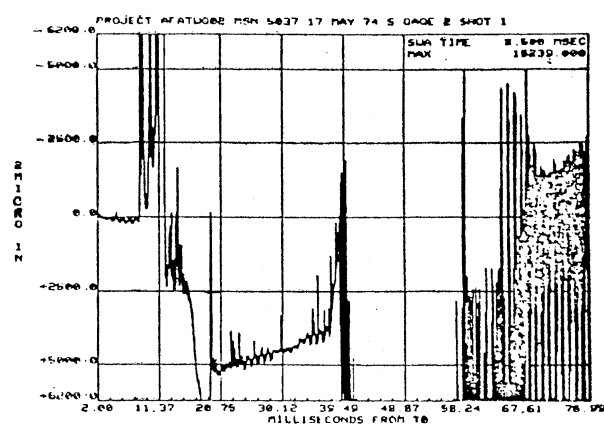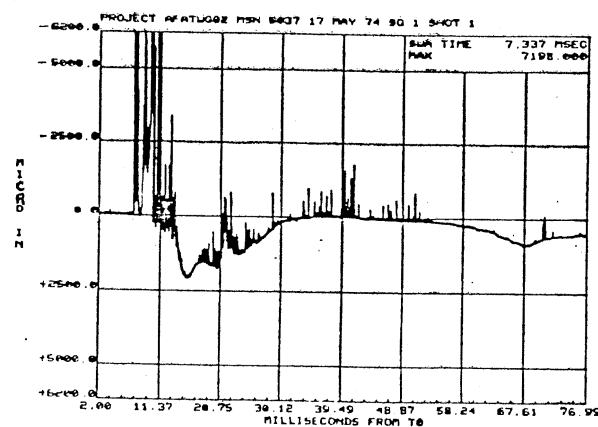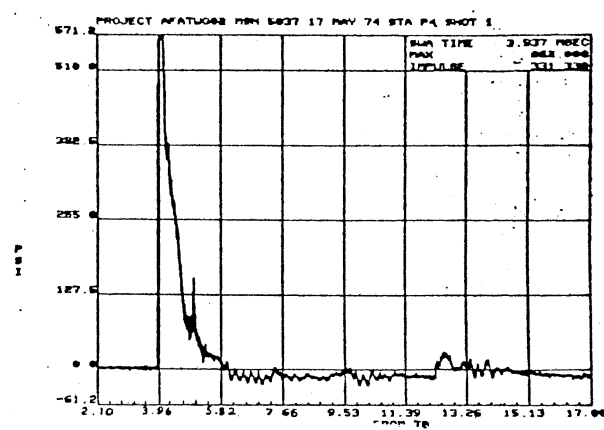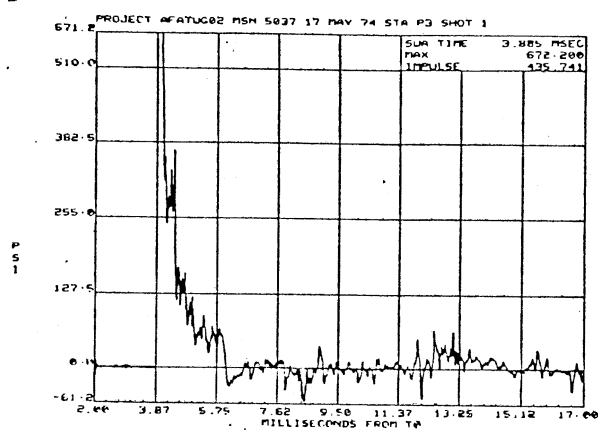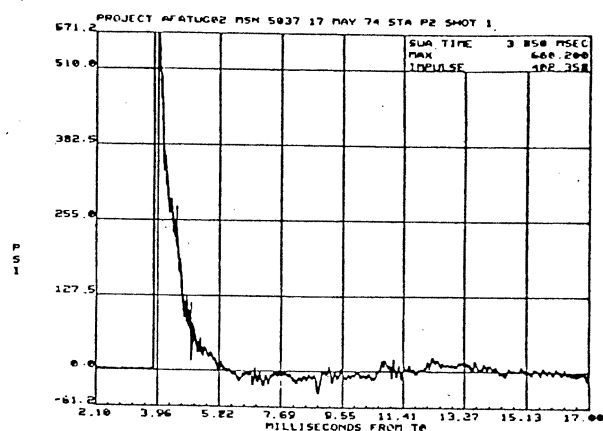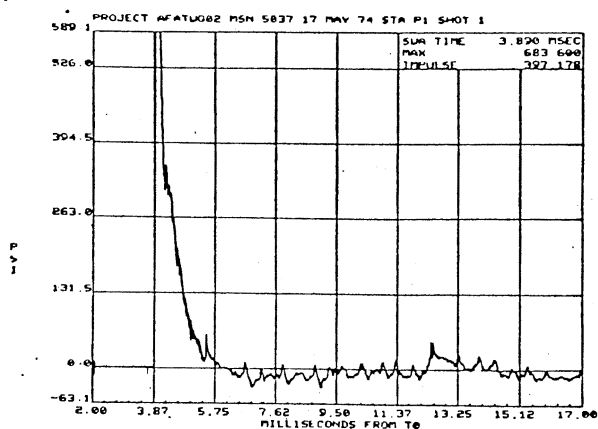
Figure 69. Data From Impulse Test 1, Beam 15, 17 May 1974
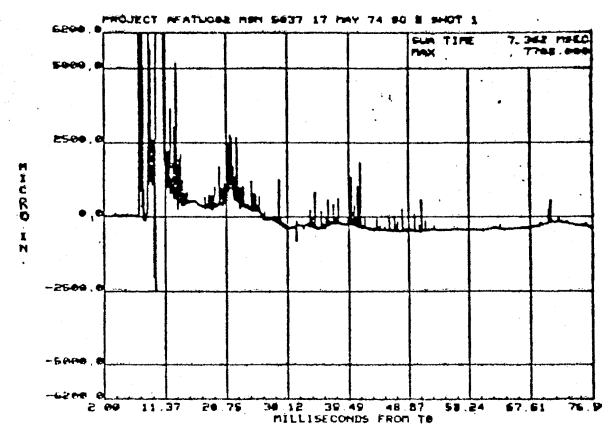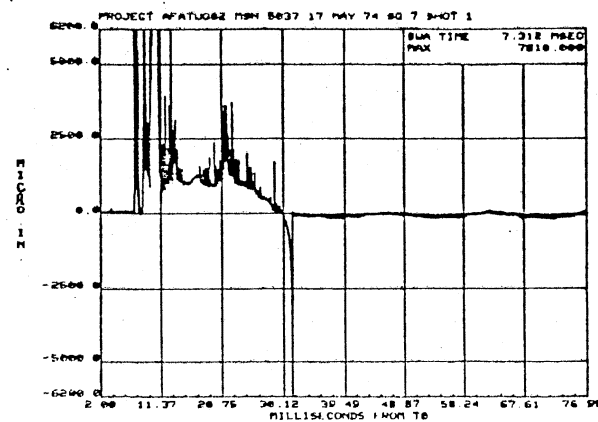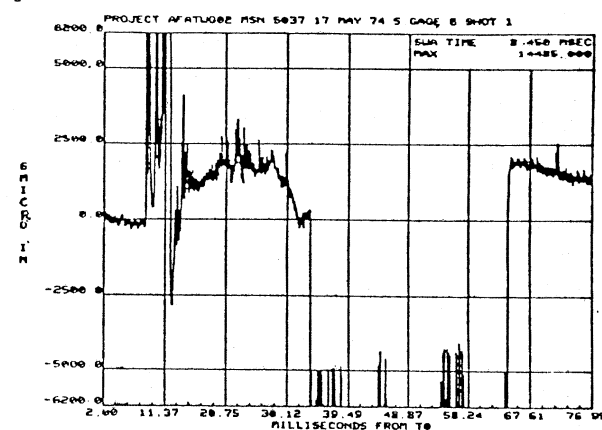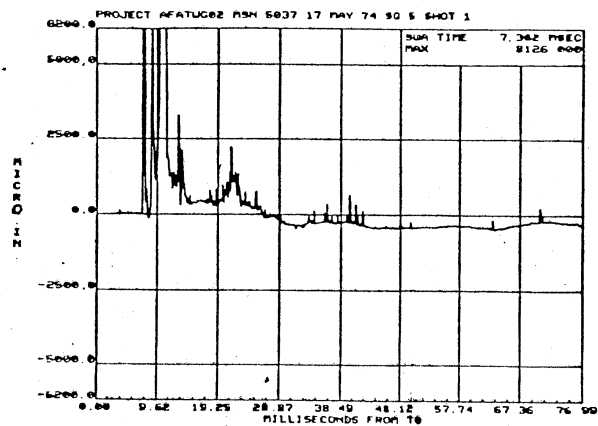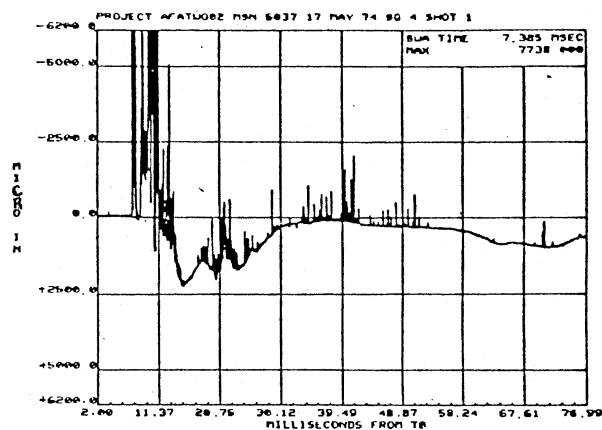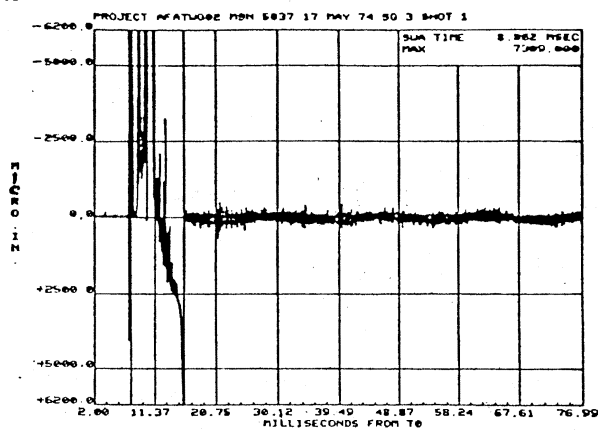
Figure 69. (Continued)
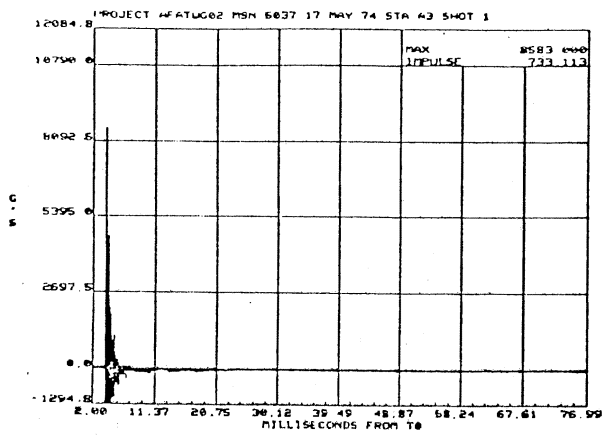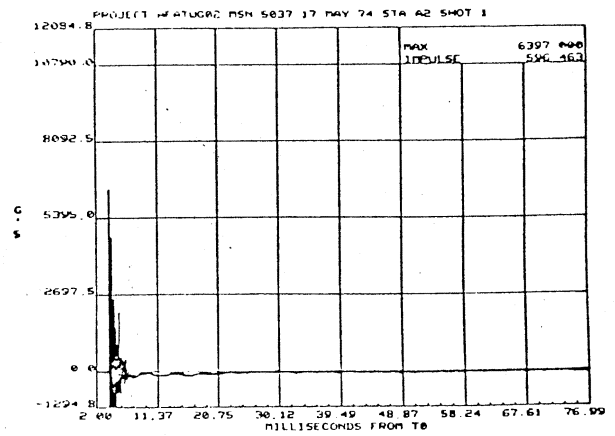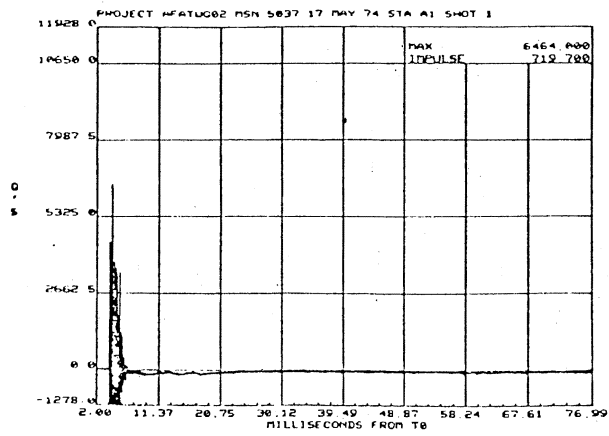
Figure 69. (Continued)
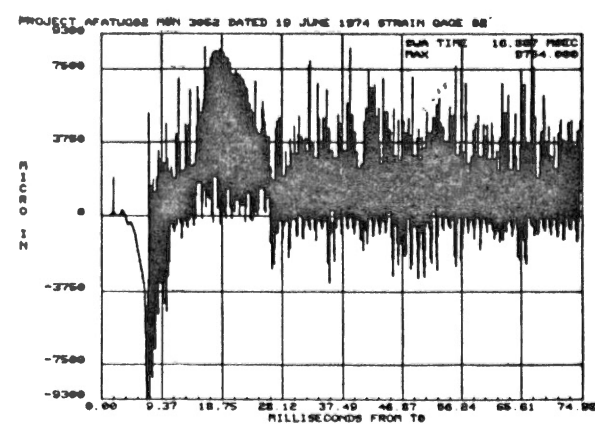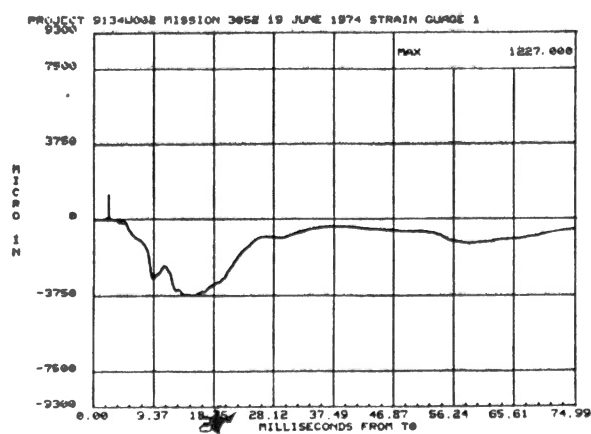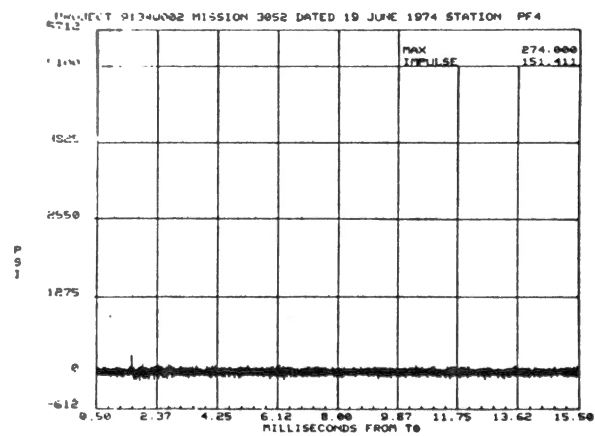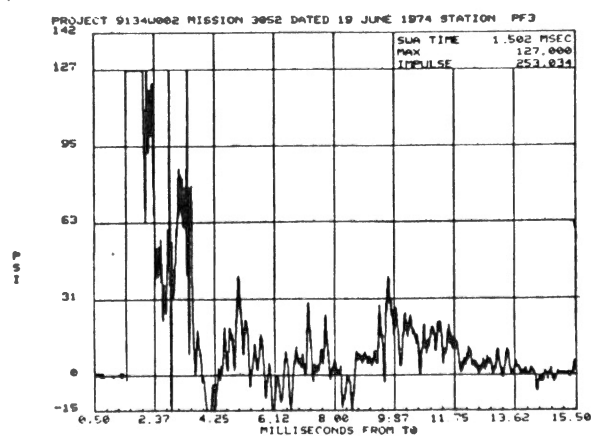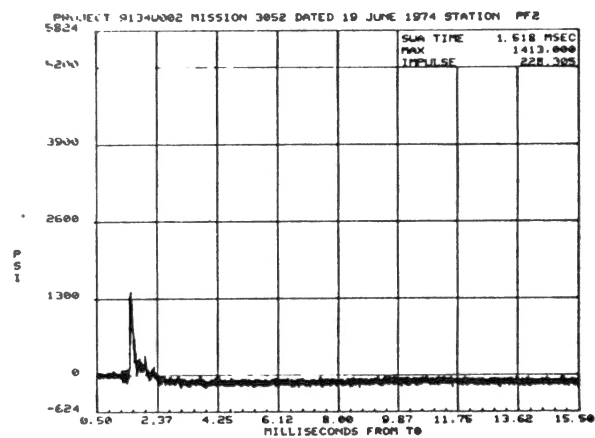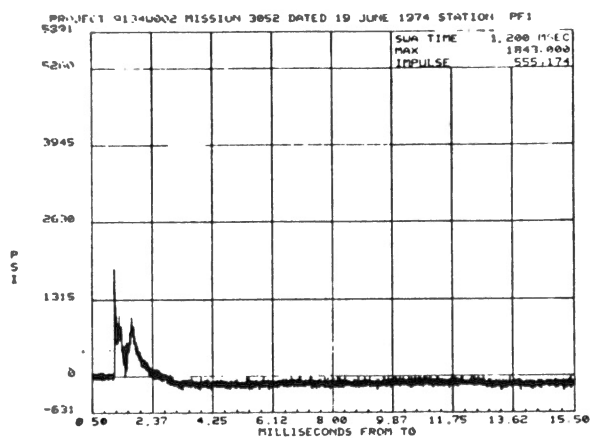
Figure 70. Data From Impulse Test 3, Beam 12, 19 June 1974
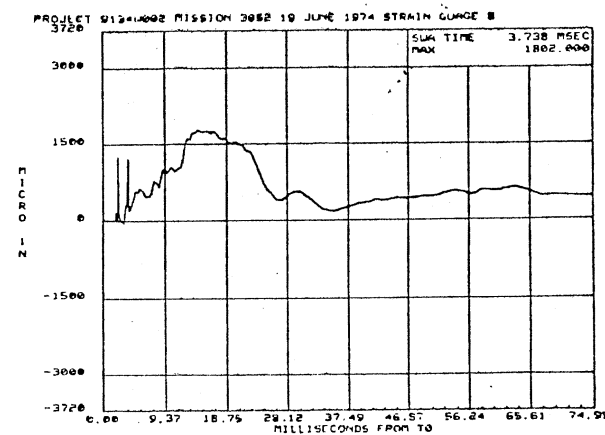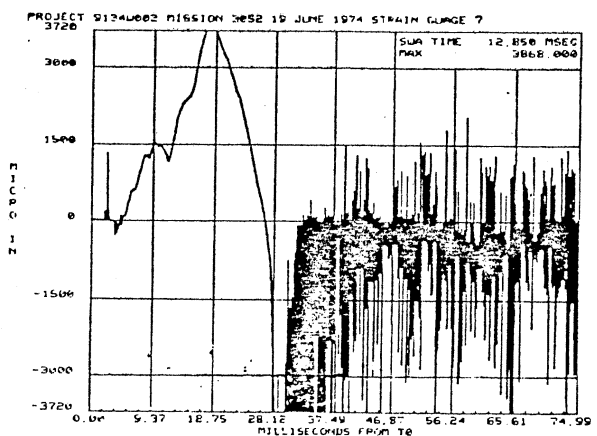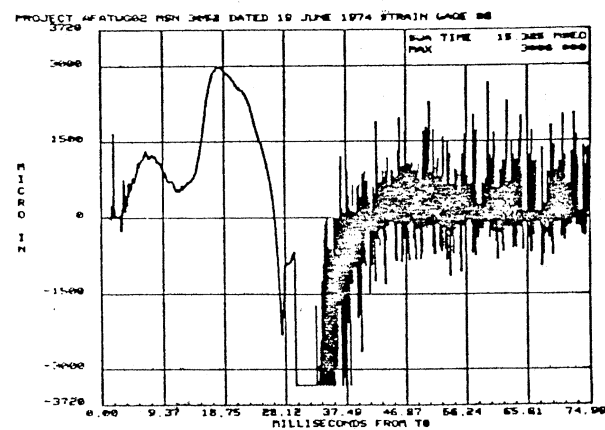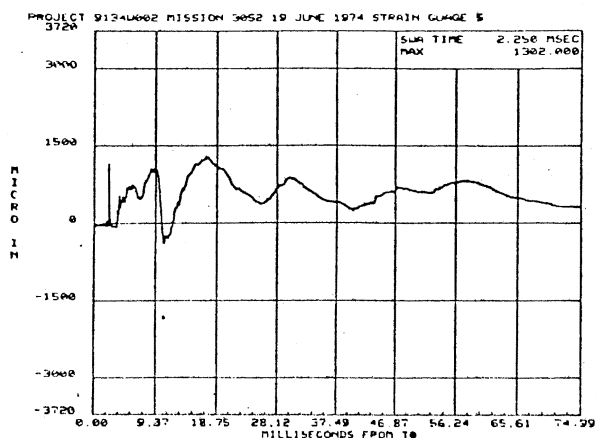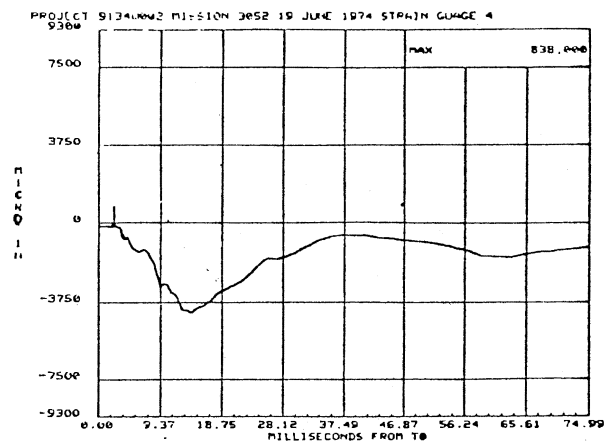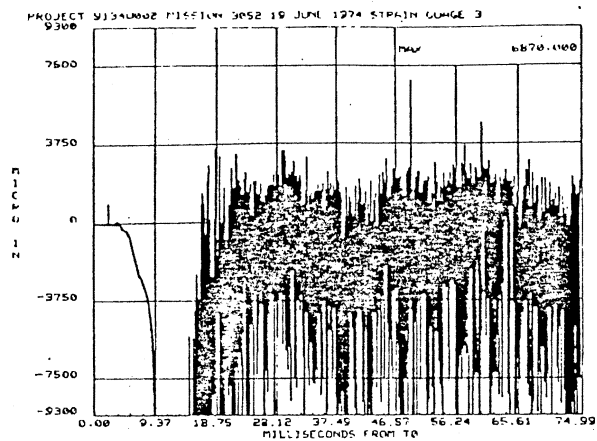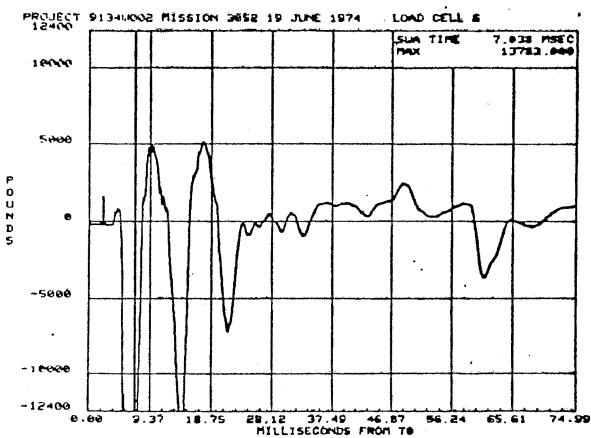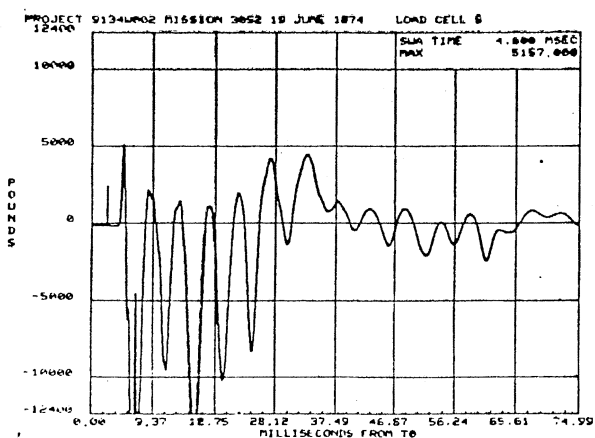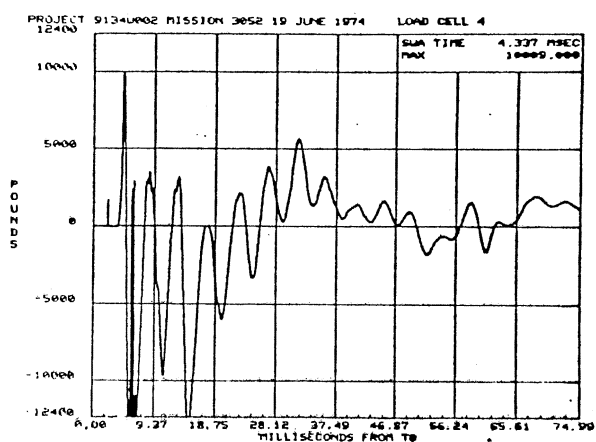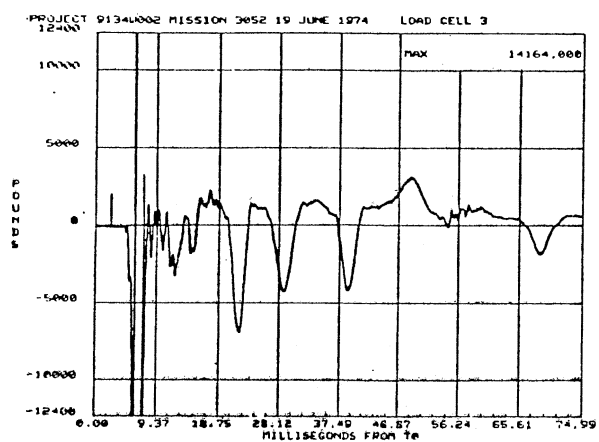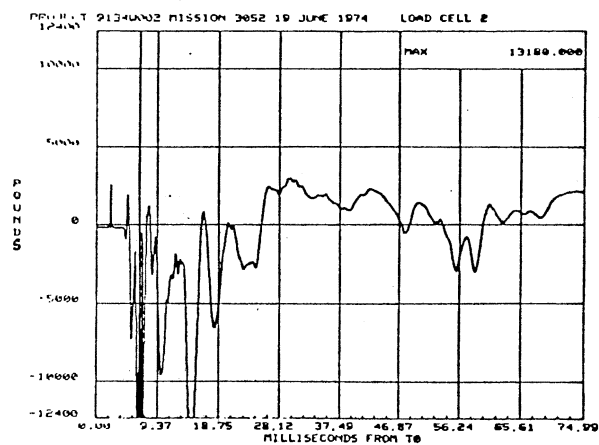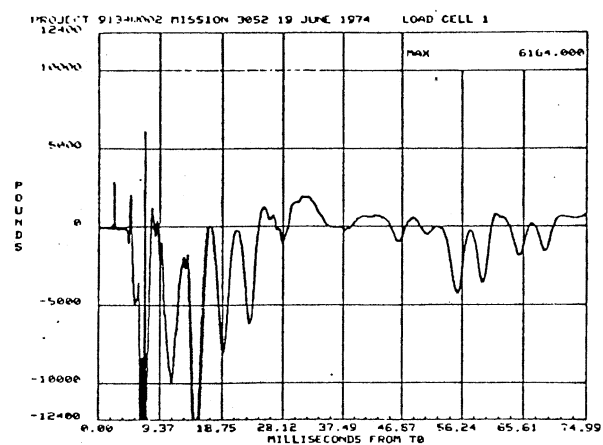
Figure 70. (Continued)

Figure 70. (Continued)

163
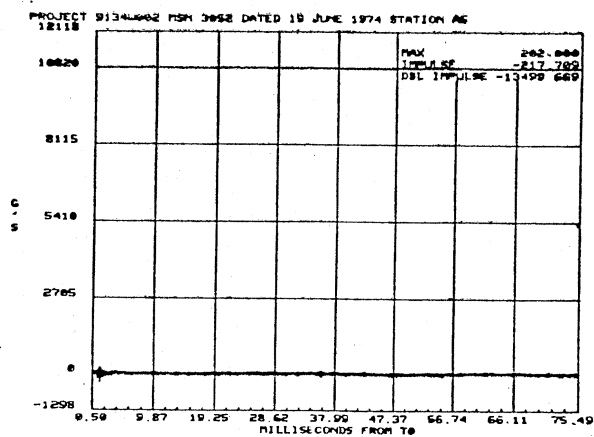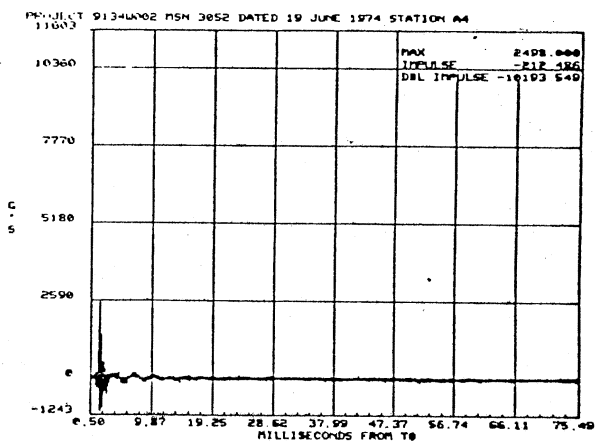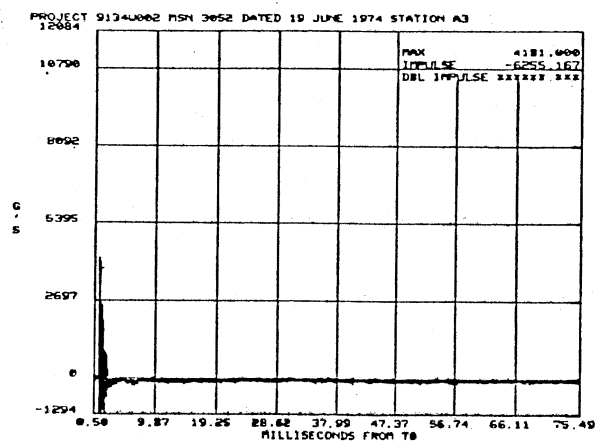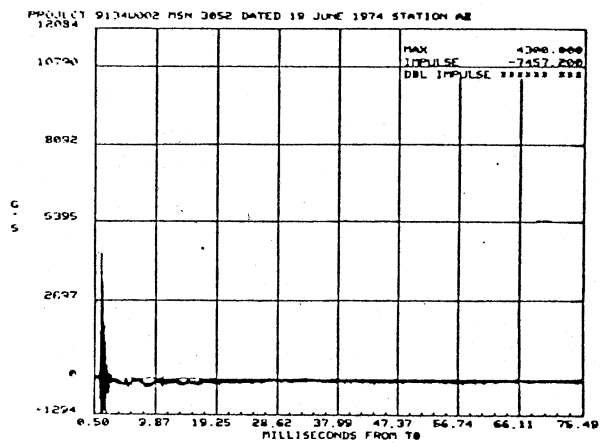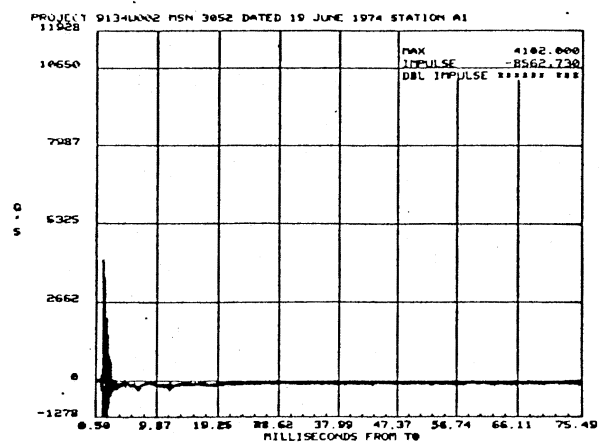
Figure 70. (Continued)
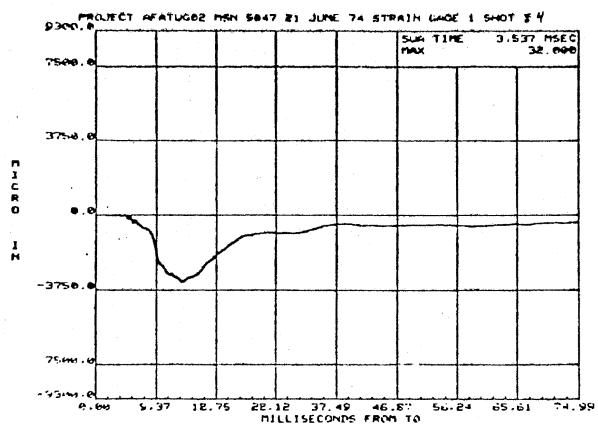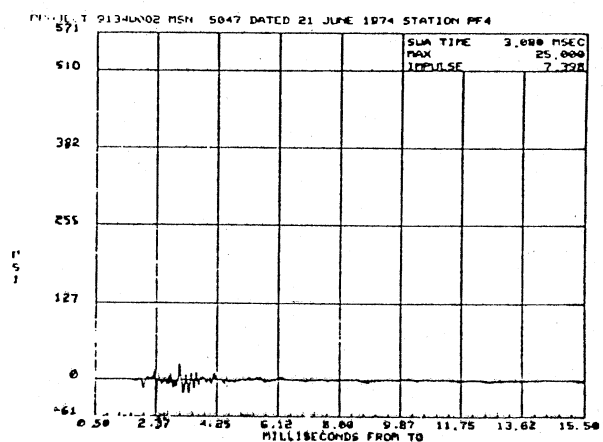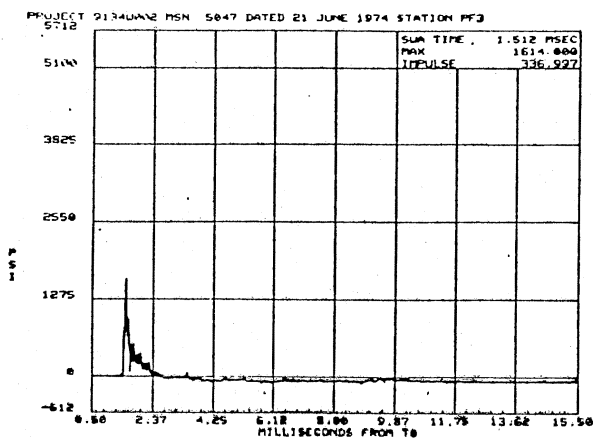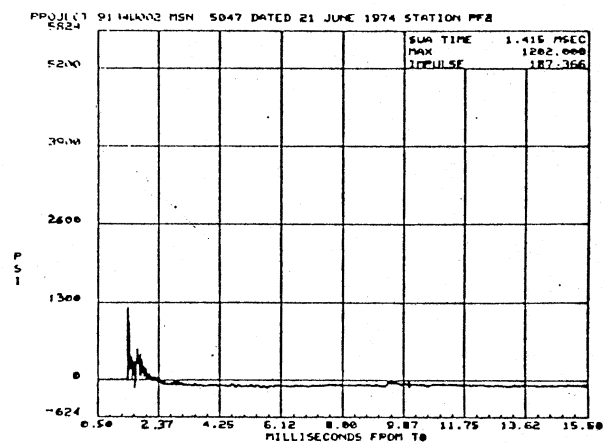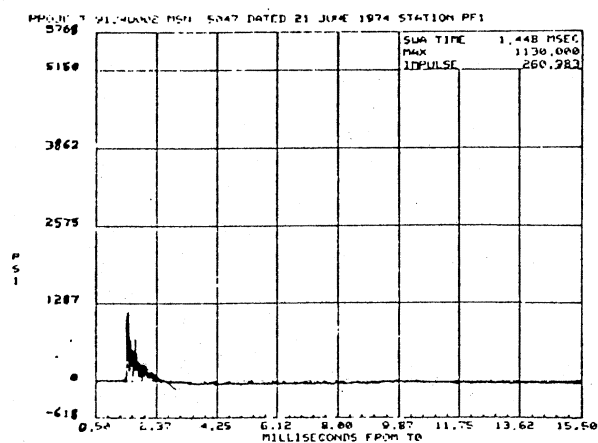
Figure 71. Data From Impulse Test 4, Beam 4, 21 June 1974
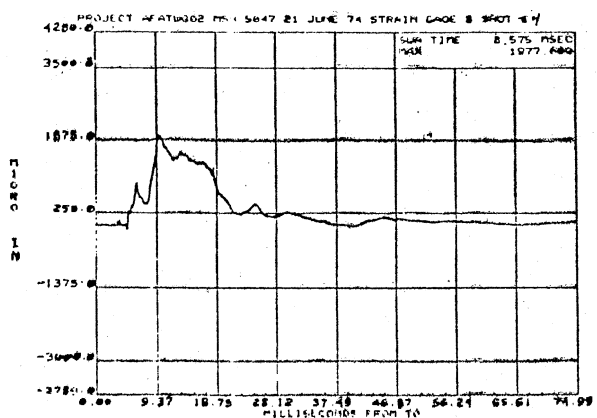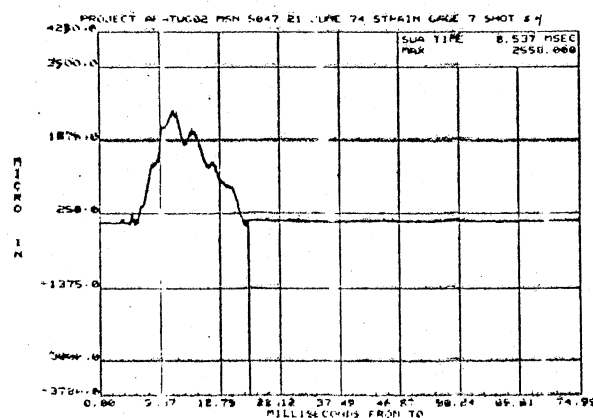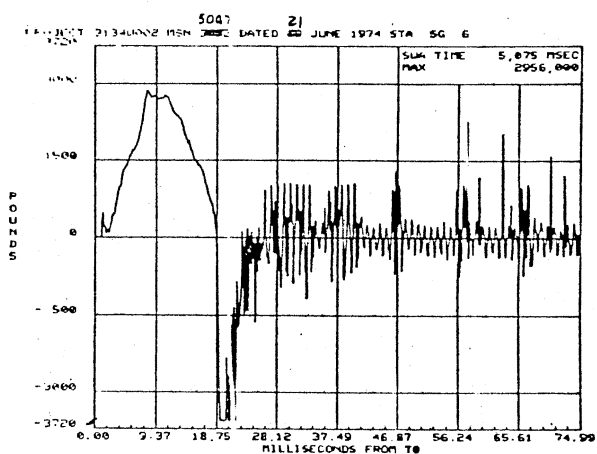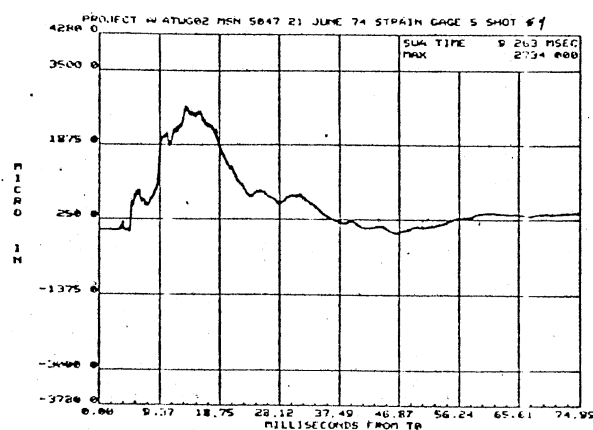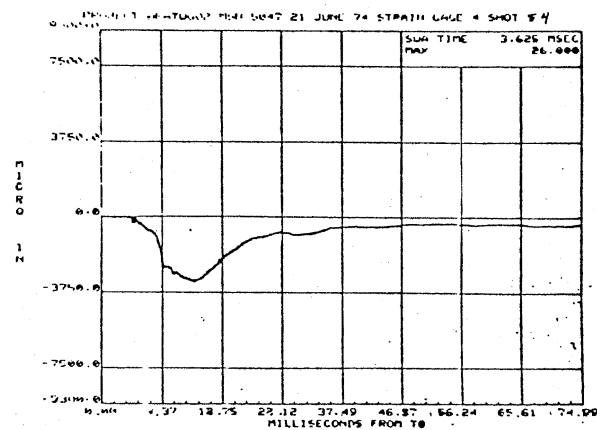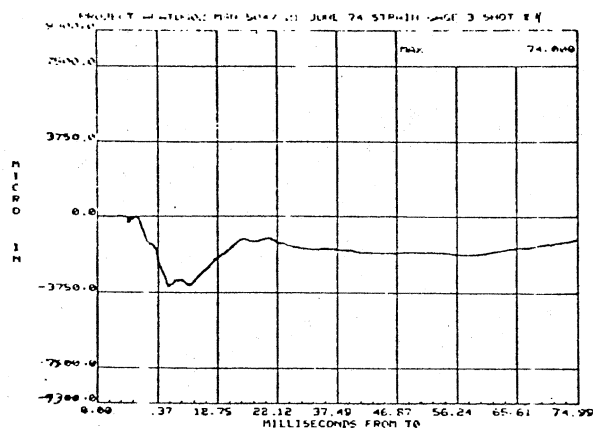
Figure 71. (Continued)
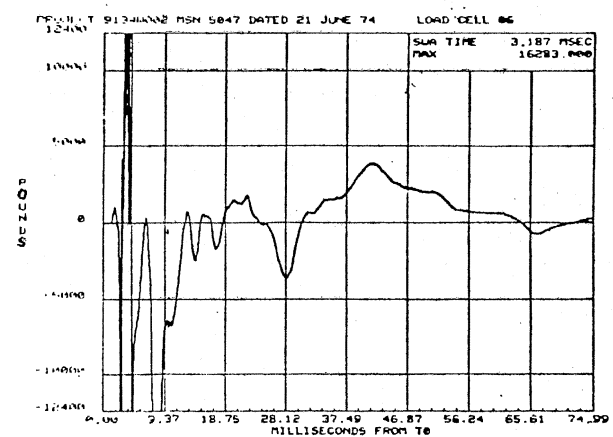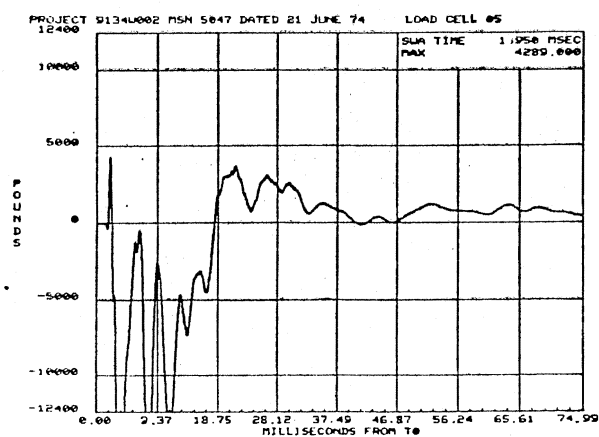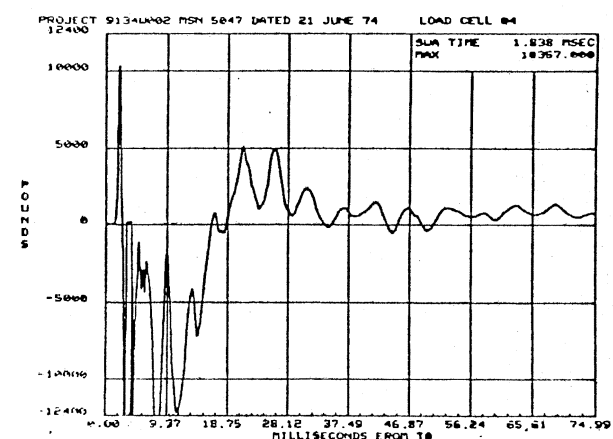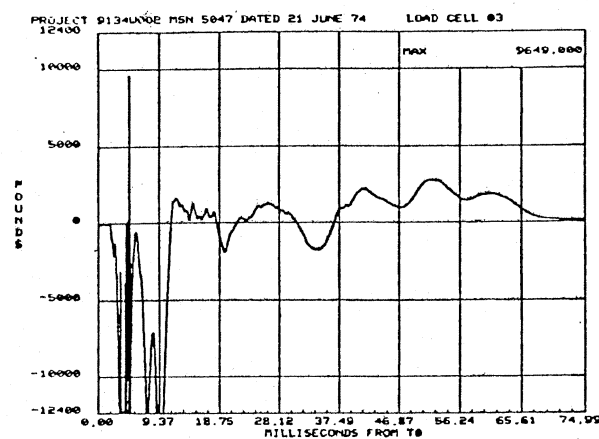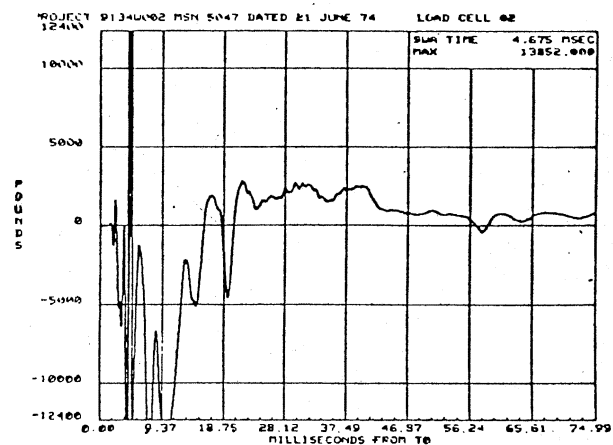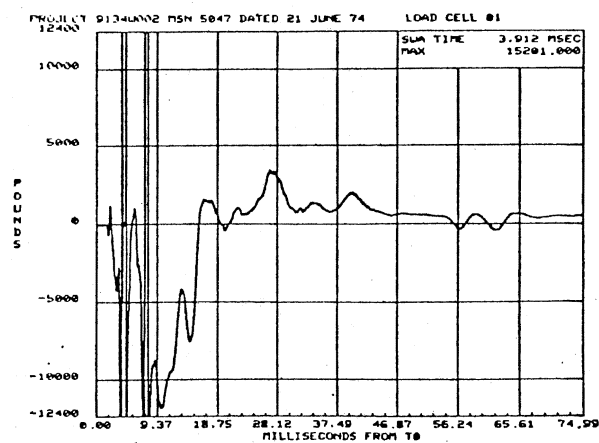
Figure 71. (Continued)
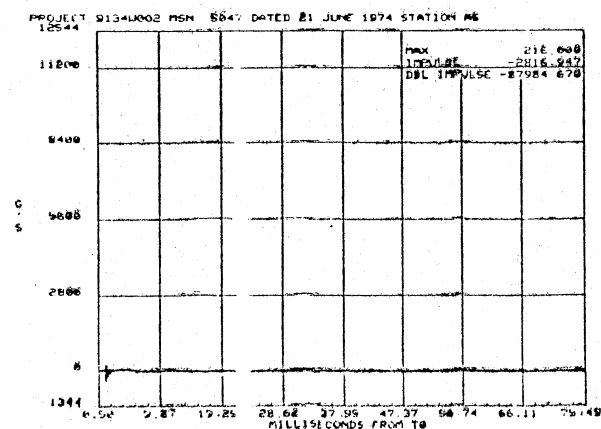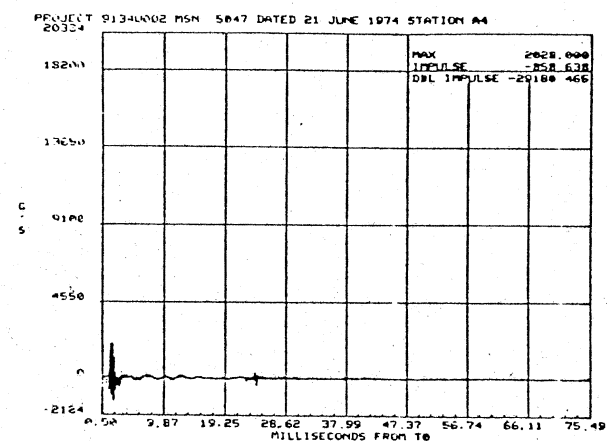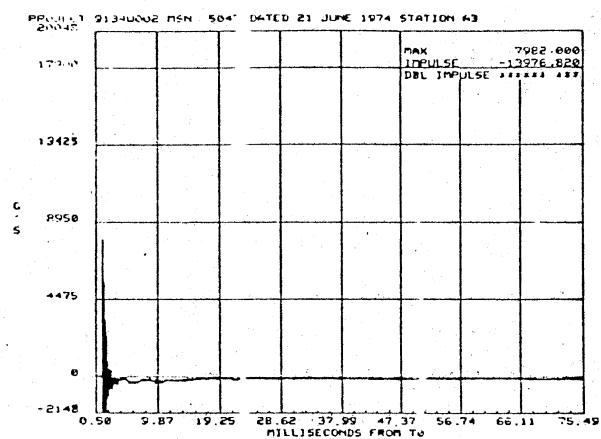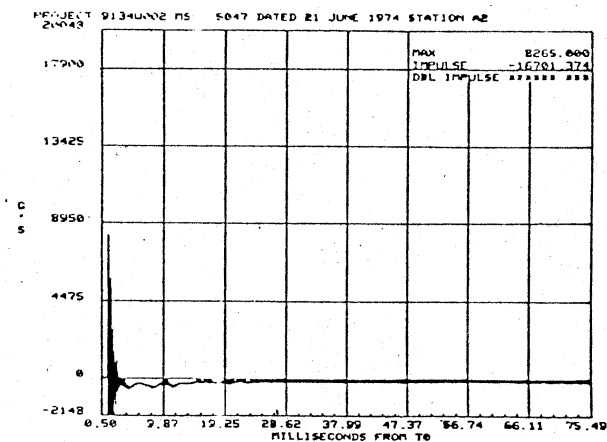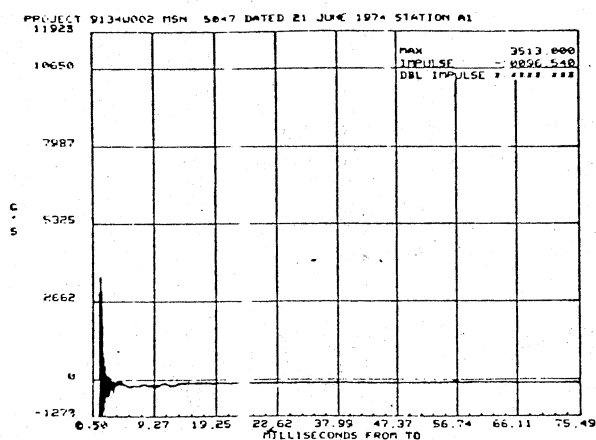
Figure 71. (Continued)
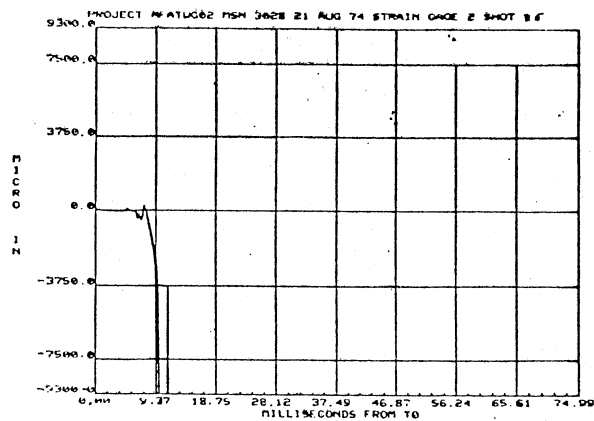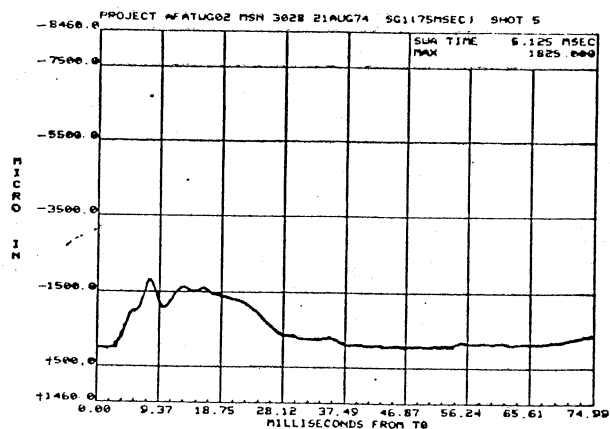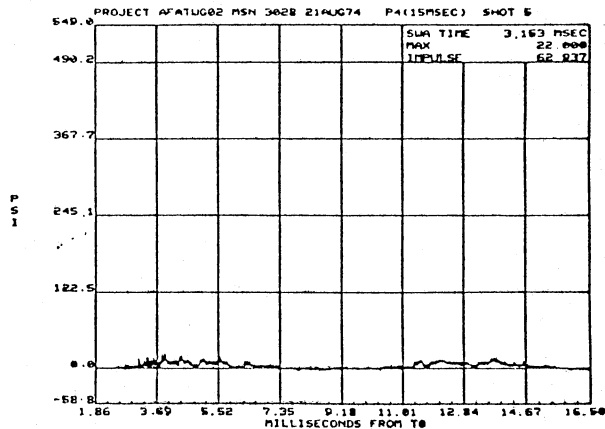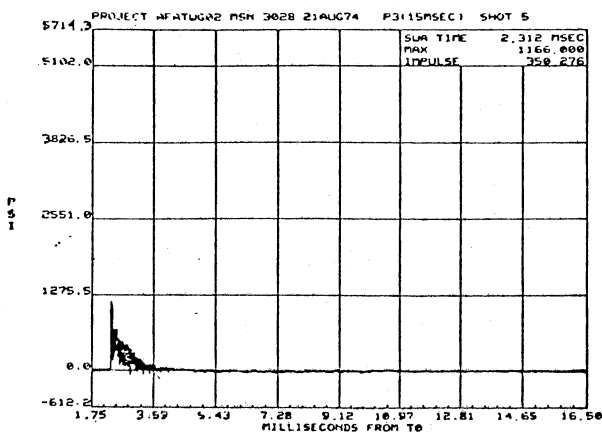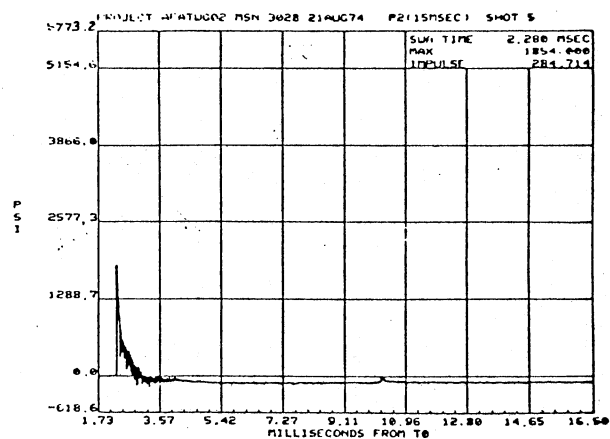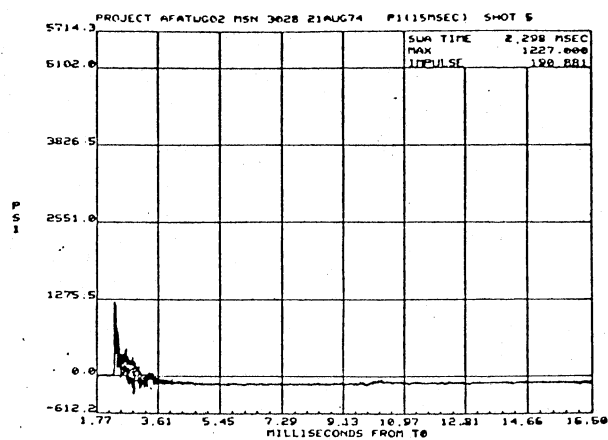
Figure 72. Data From Impulse Test 5, Beam 10, 21 August 1974
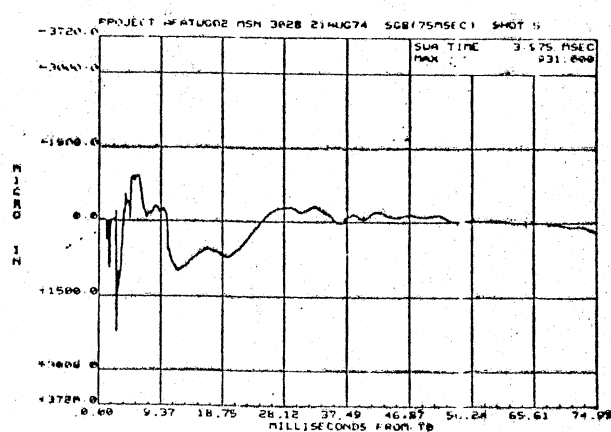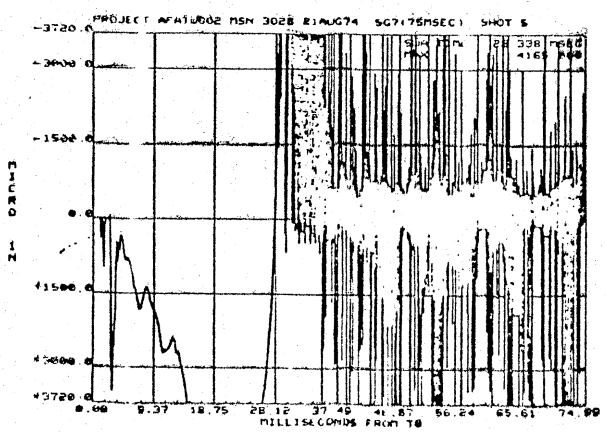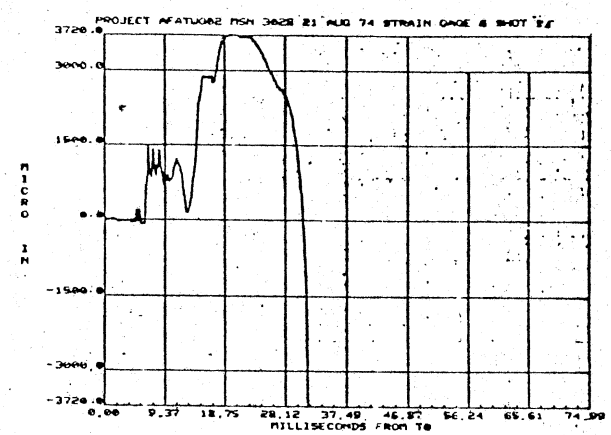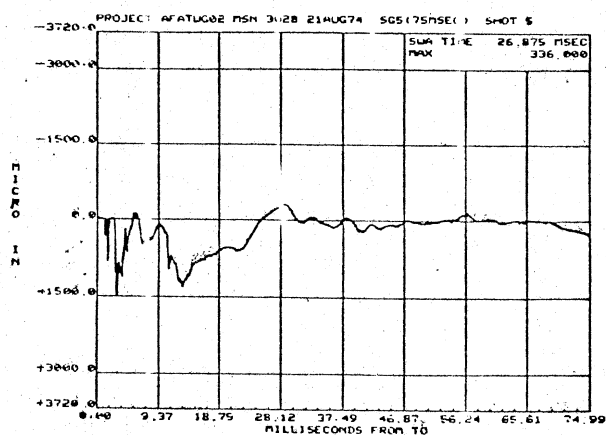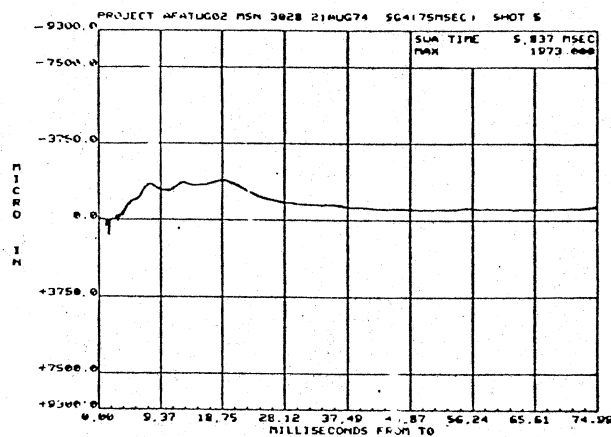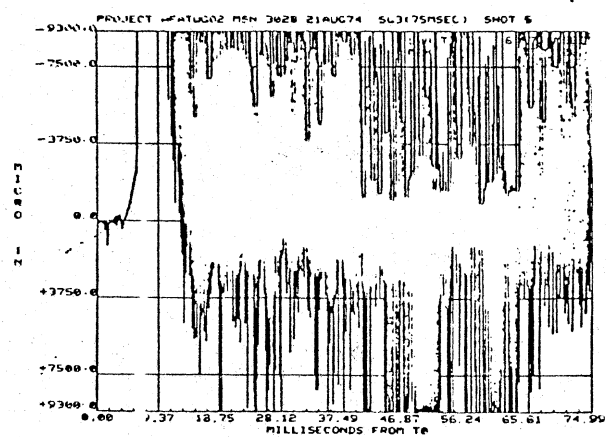
Figure 72. (Continued)
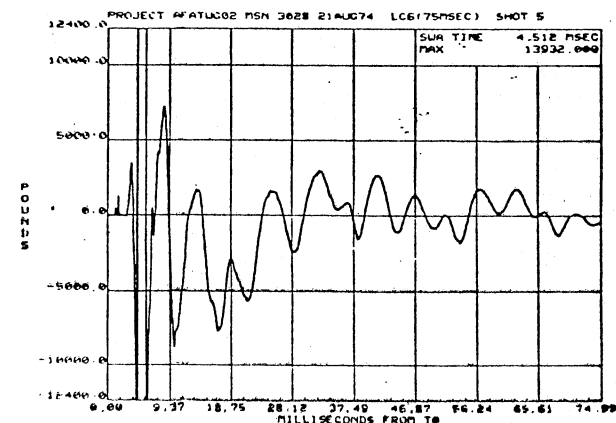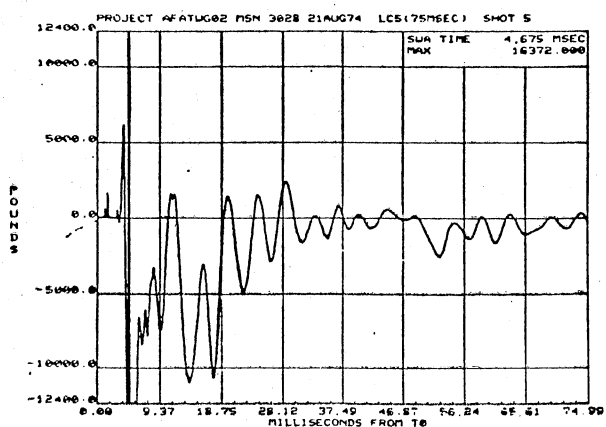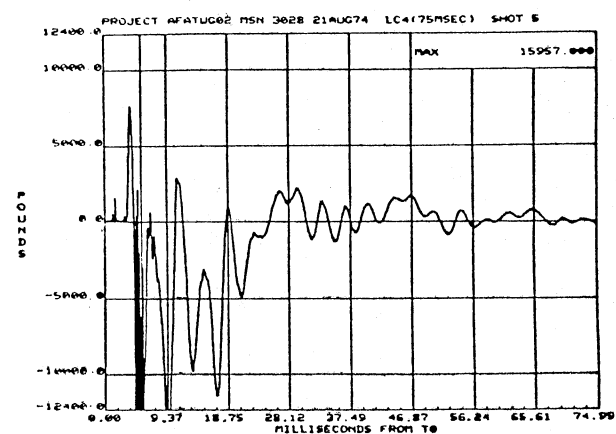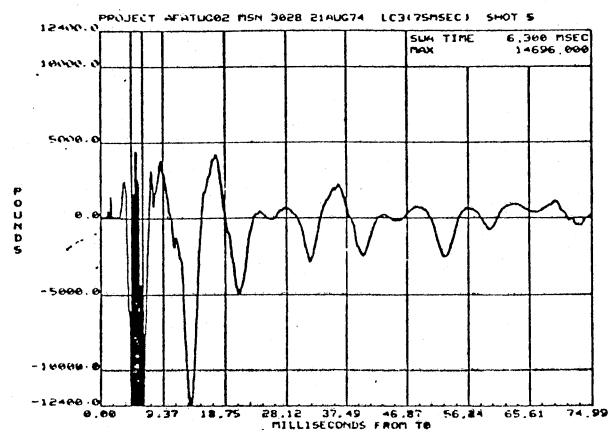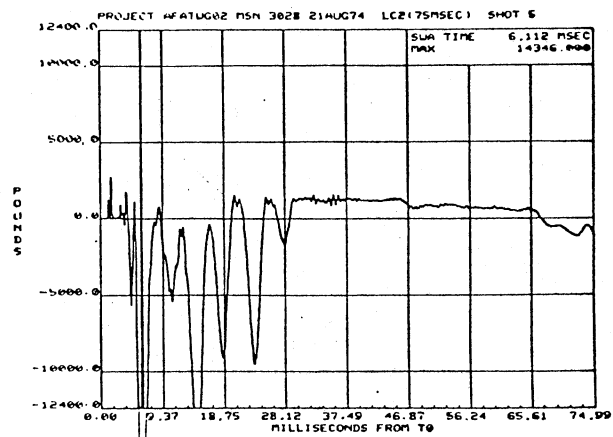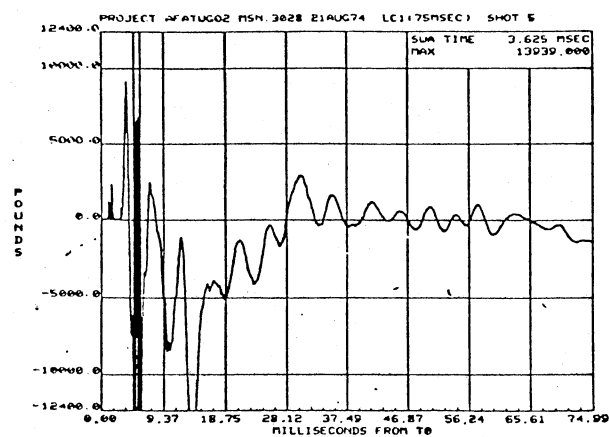
Figure 72. (Continued)
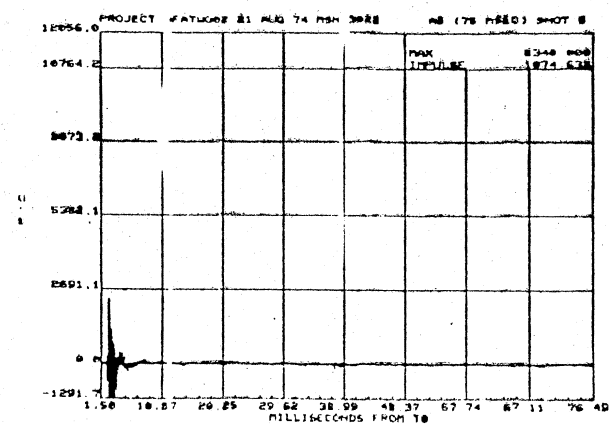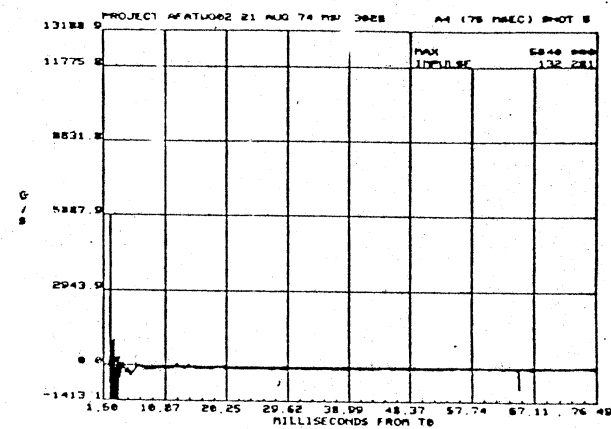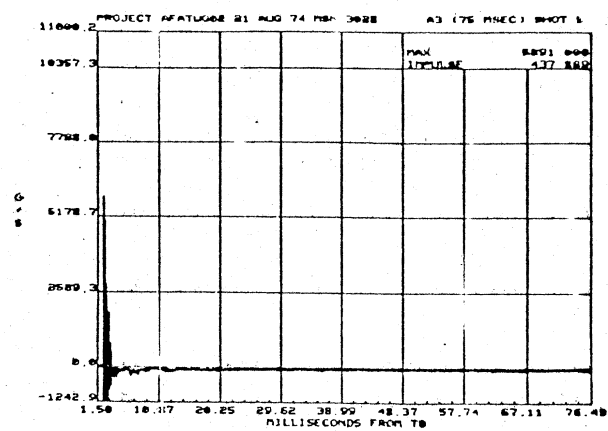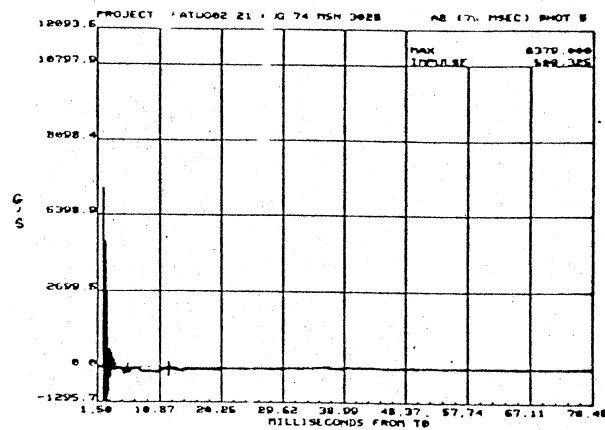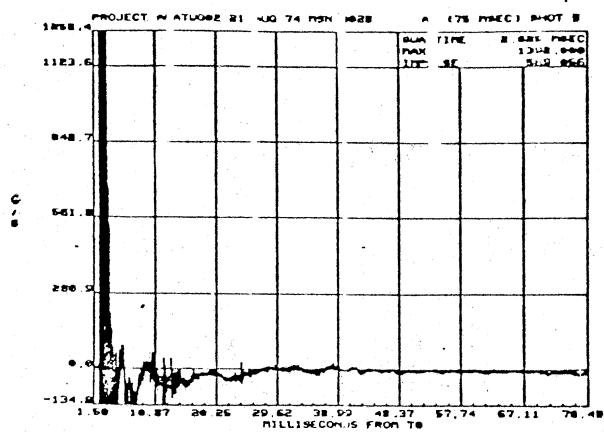
Figure 72. (Continued)
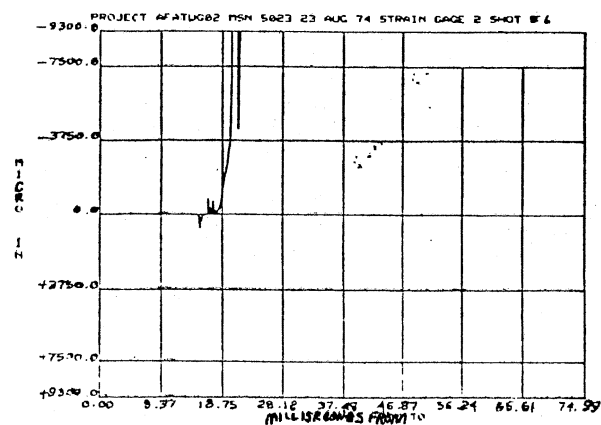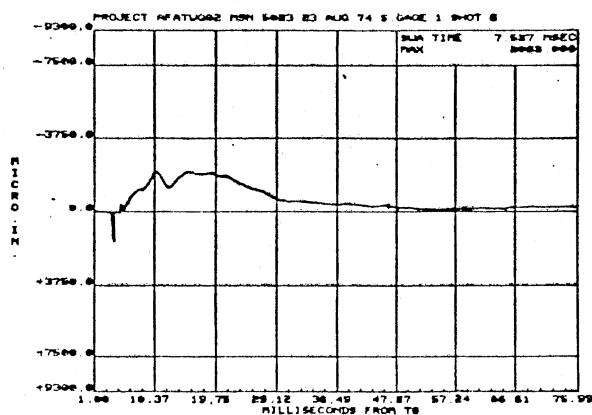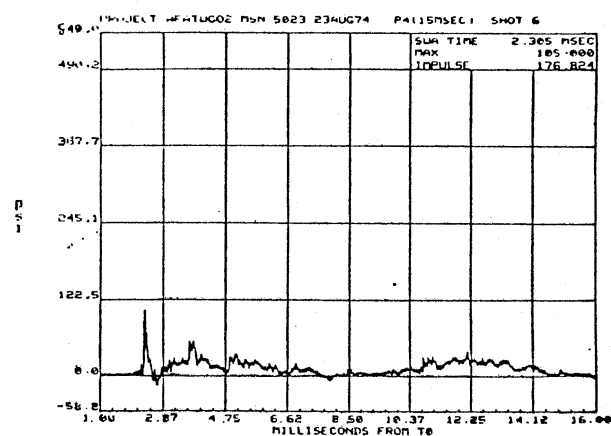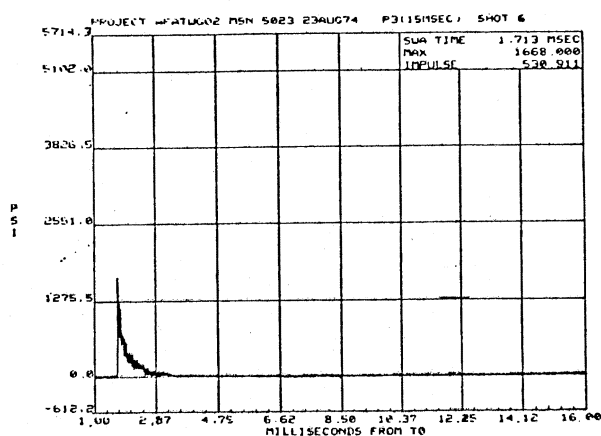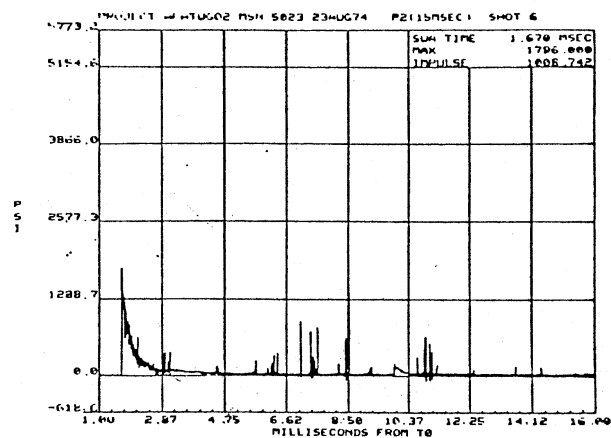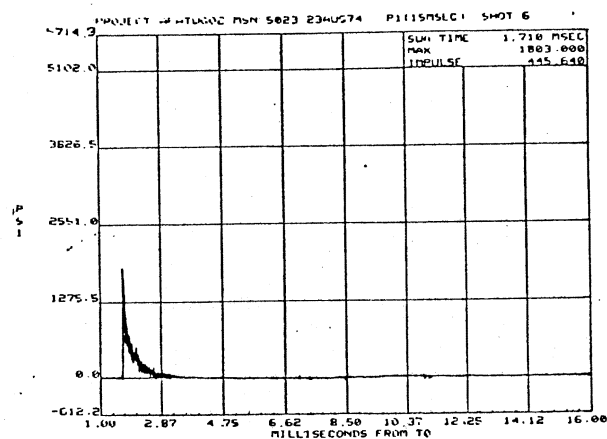
Figure 73.   Data From Impulse Test 6, Beam 8, 23 August 1974
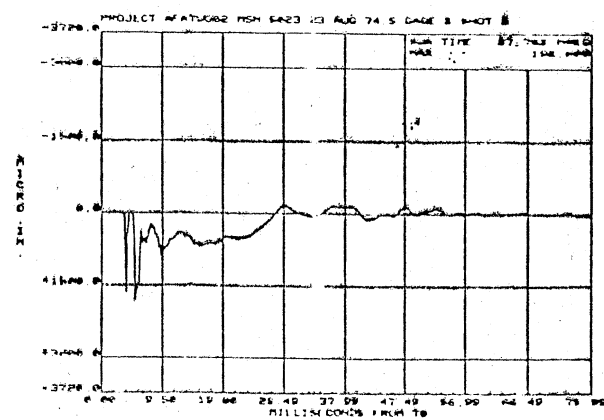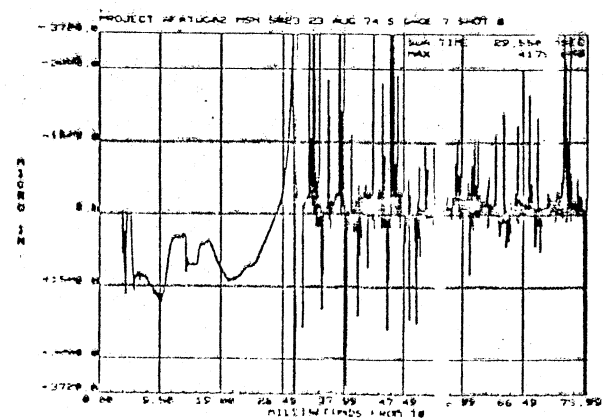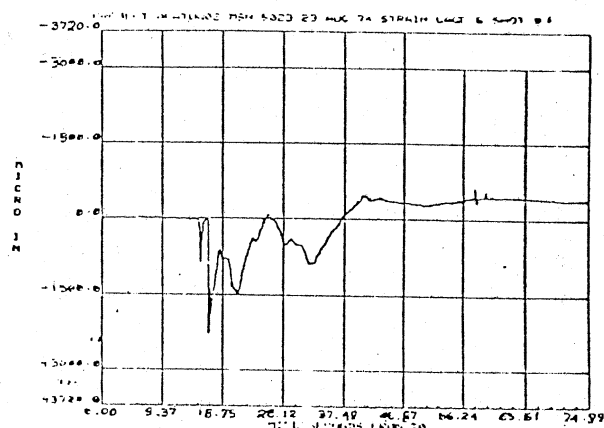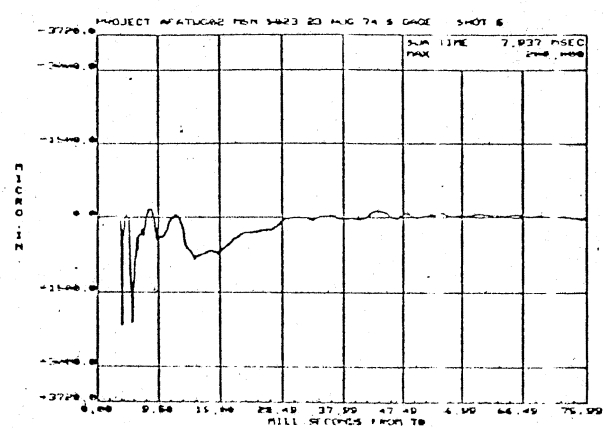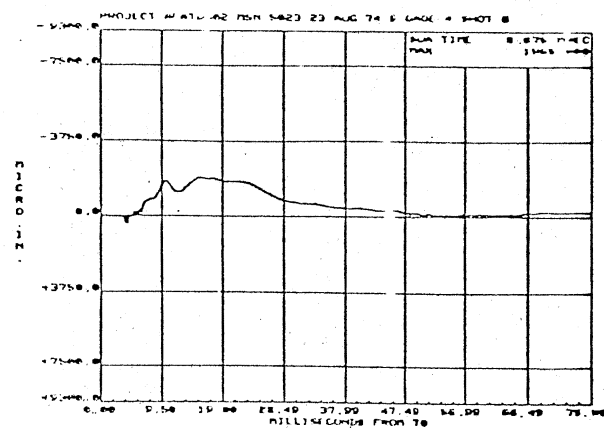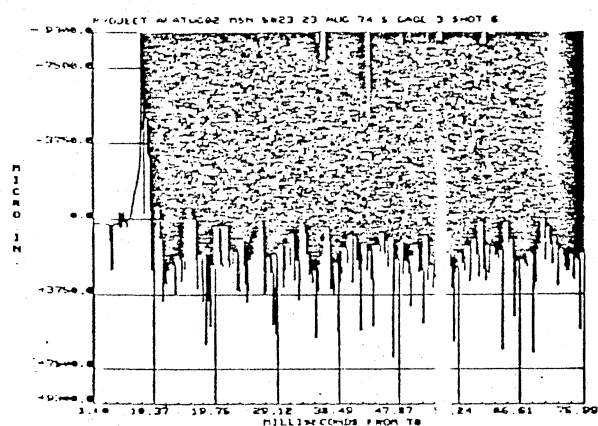
Figure 73. (Continued)
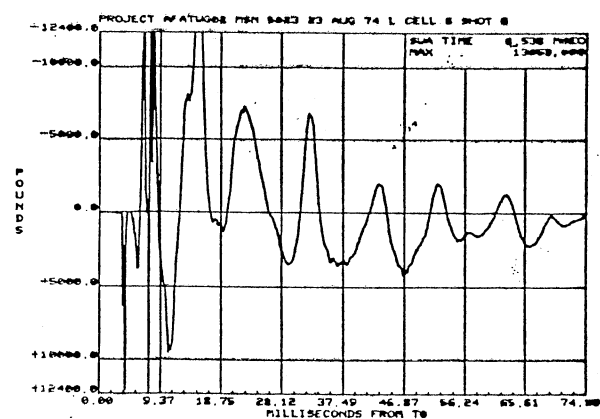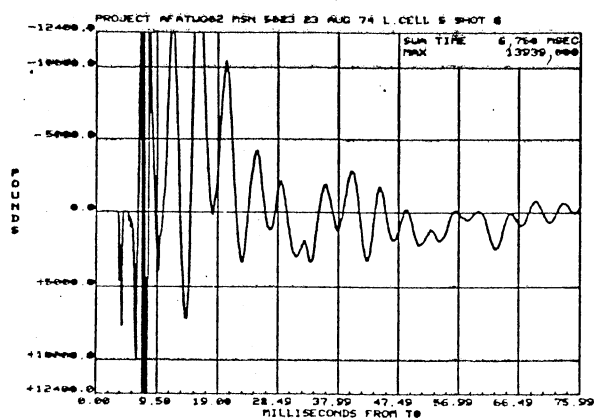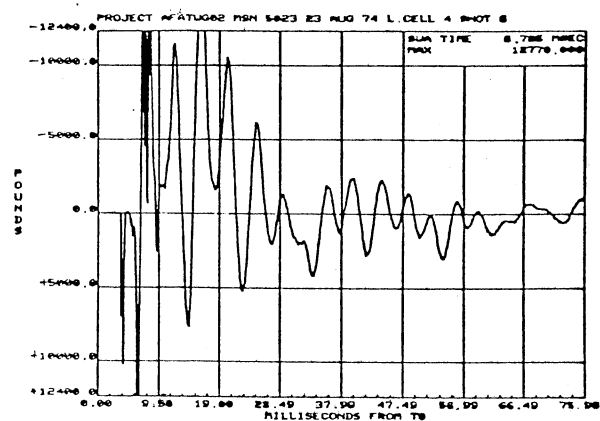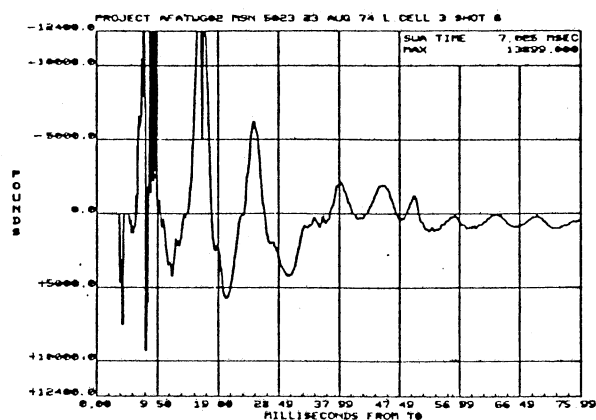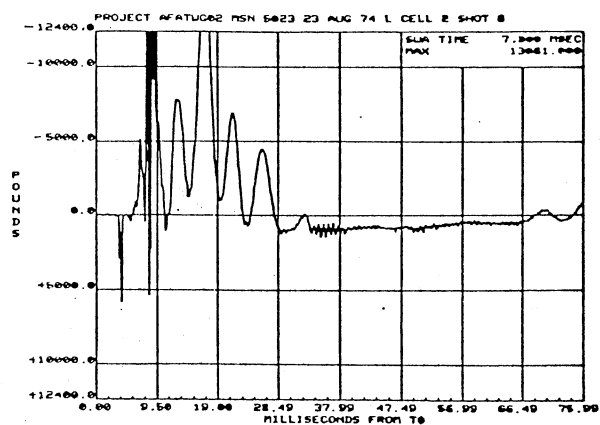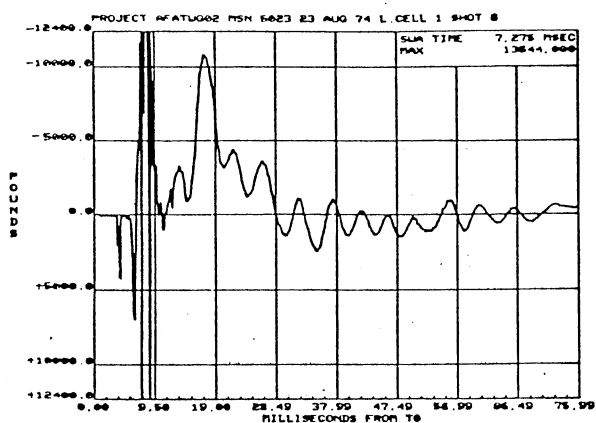
Figure 73. (Continued)
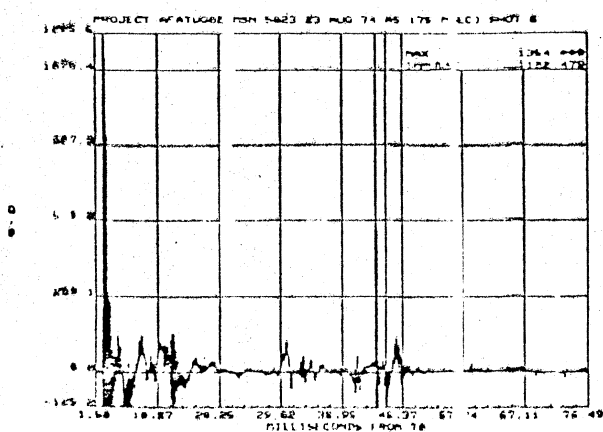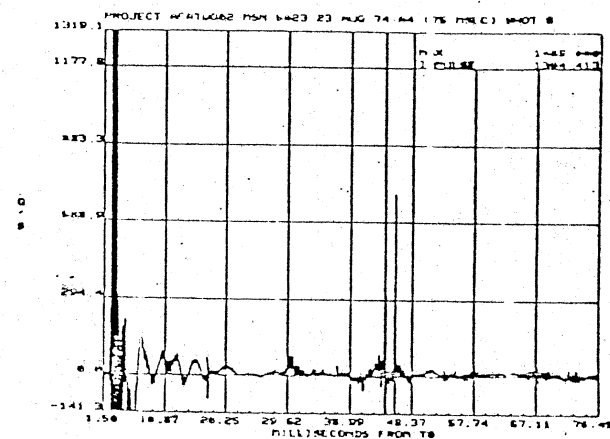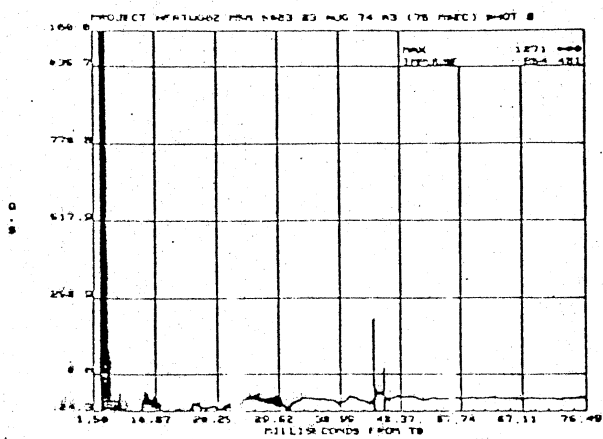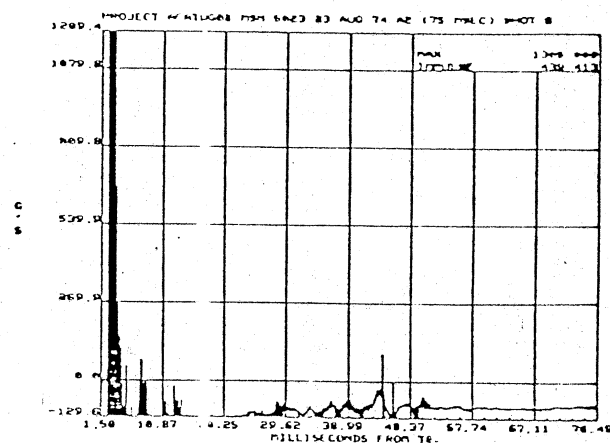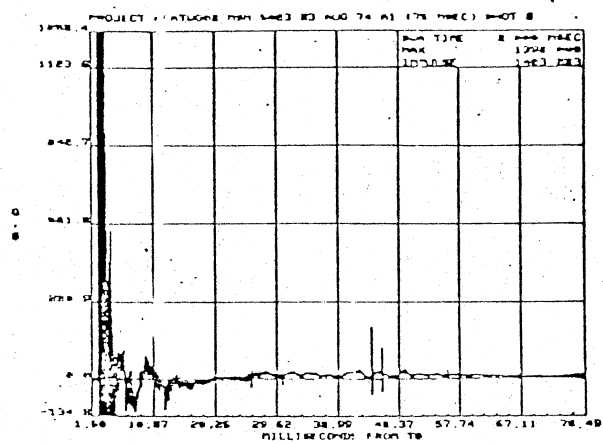
Figure 73. (Continued)
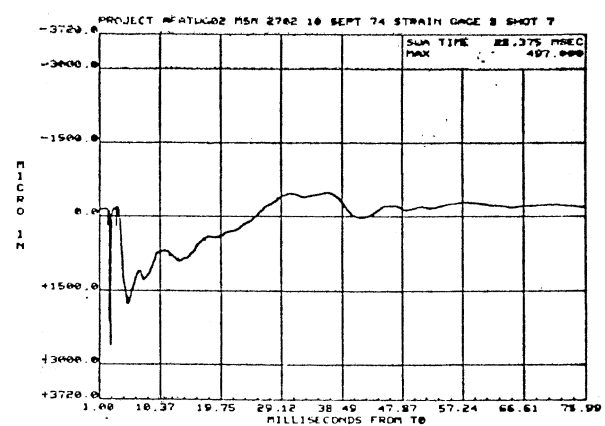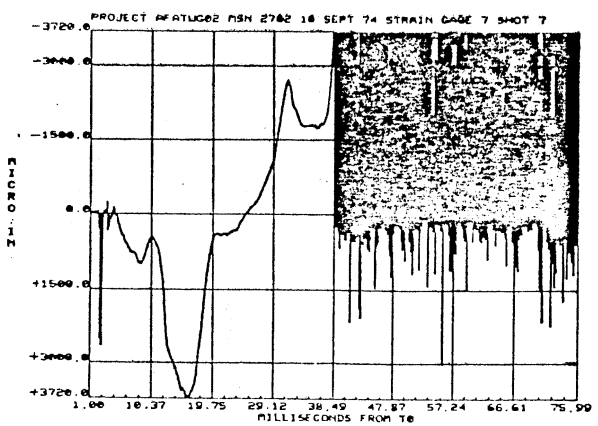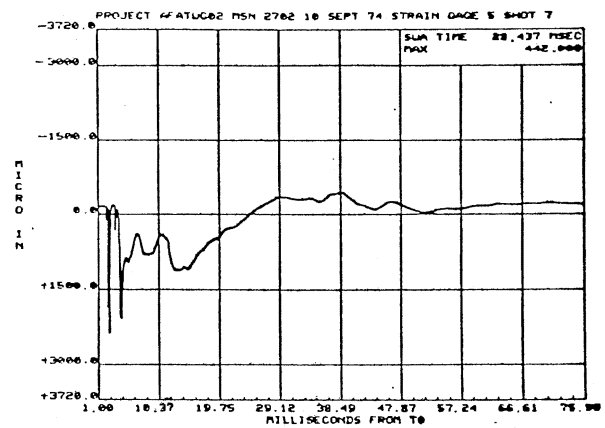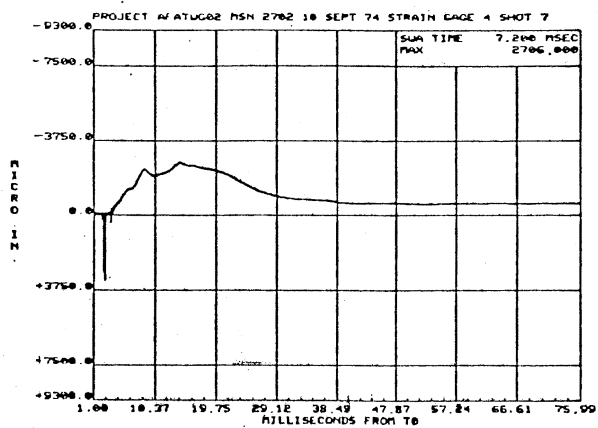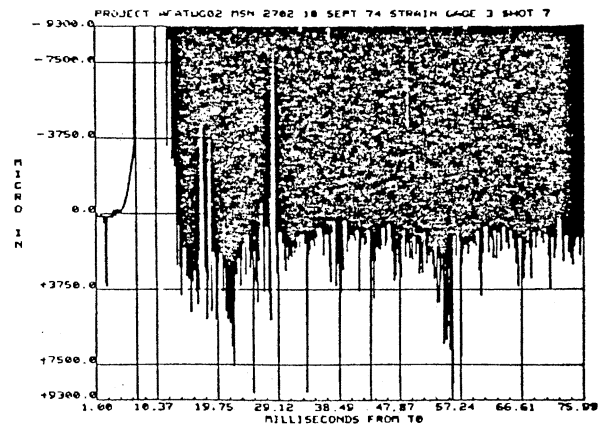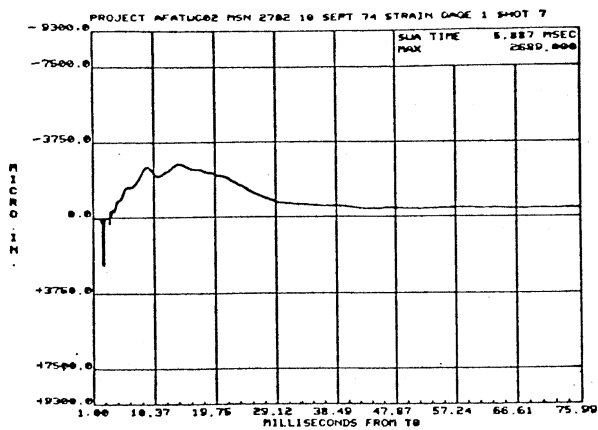
Figure 74.   Data From Impulse Test 7, Beam 3, 10 September 1974
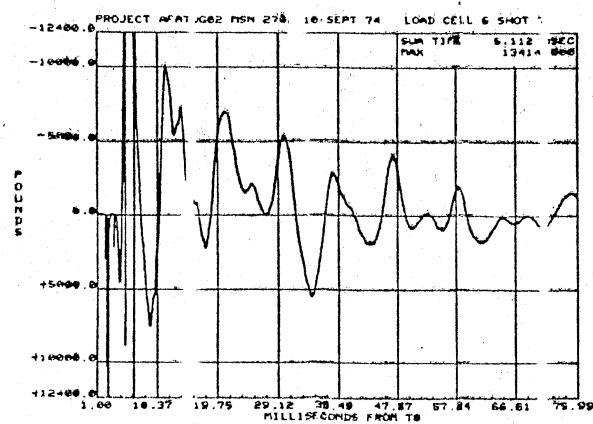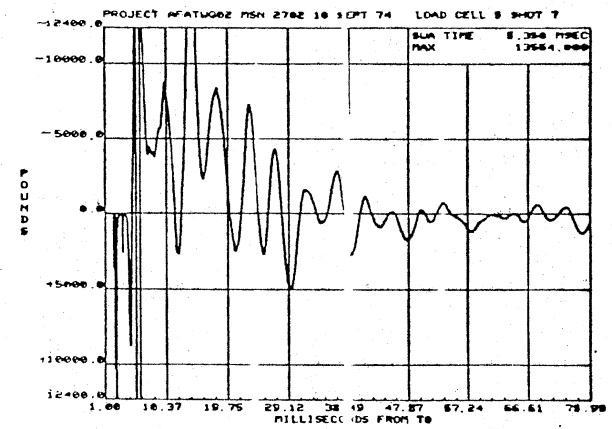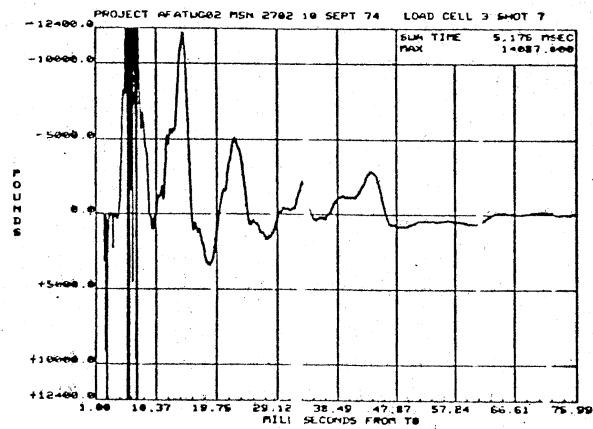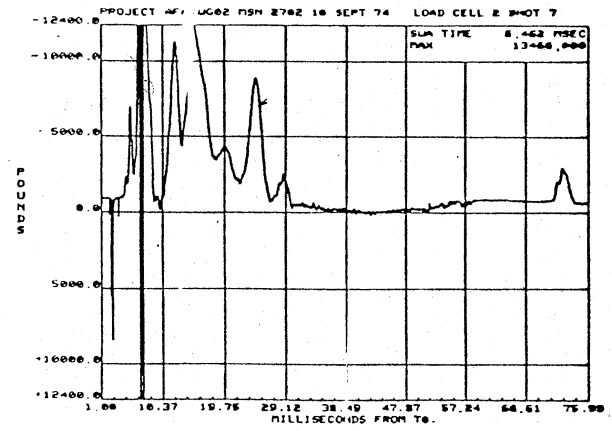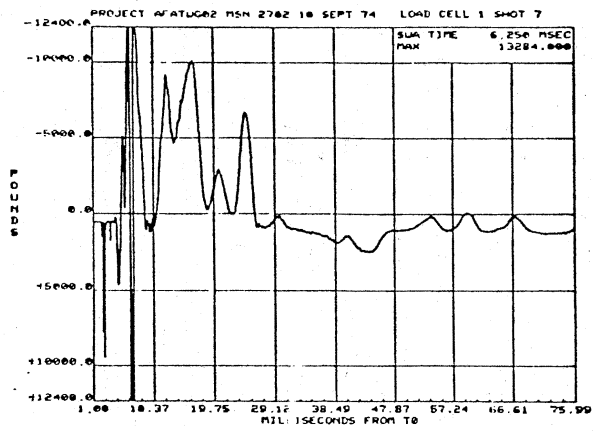
Figure 74. (Continued)
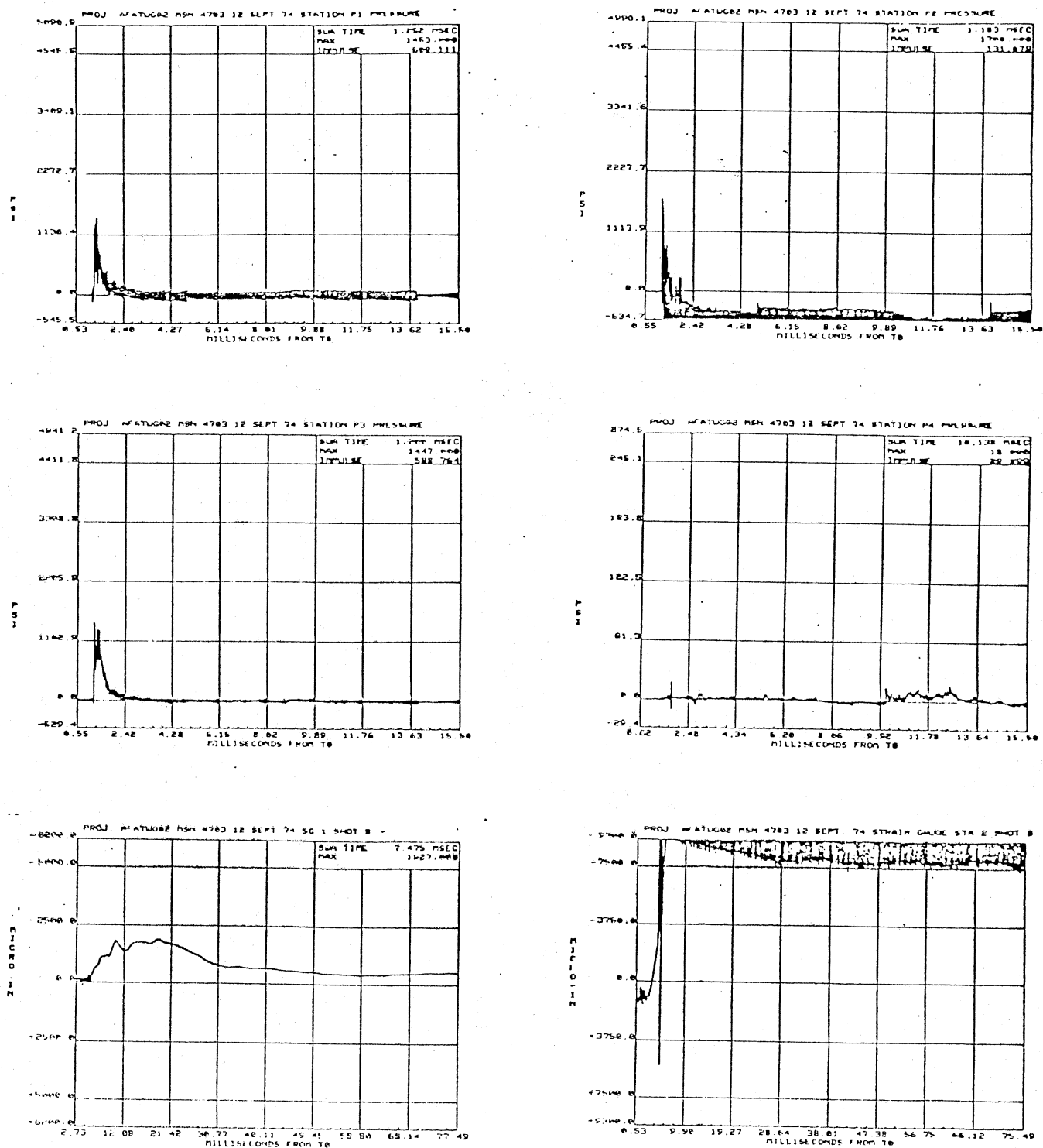
Figure 75 .   Data From Impulse Test 8, Beam 2, 12 September 1974
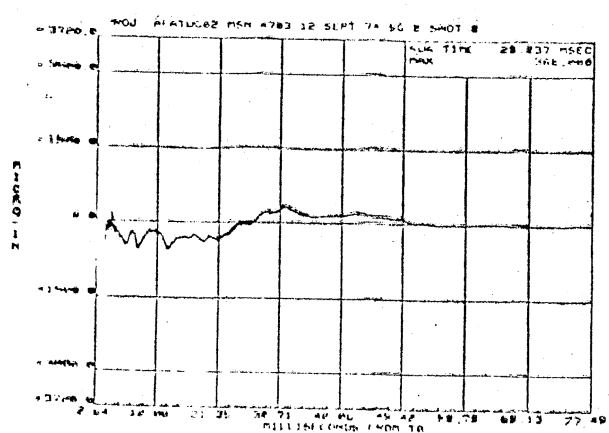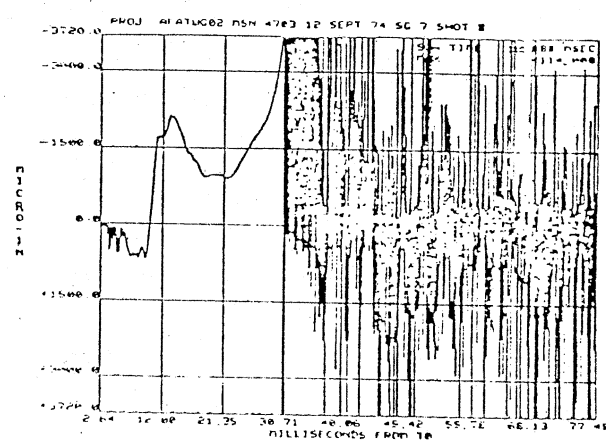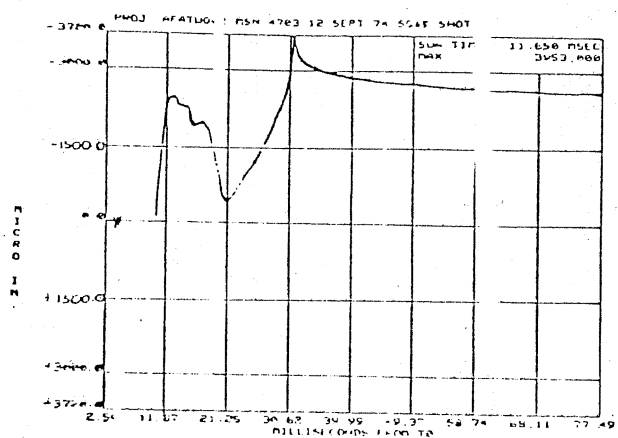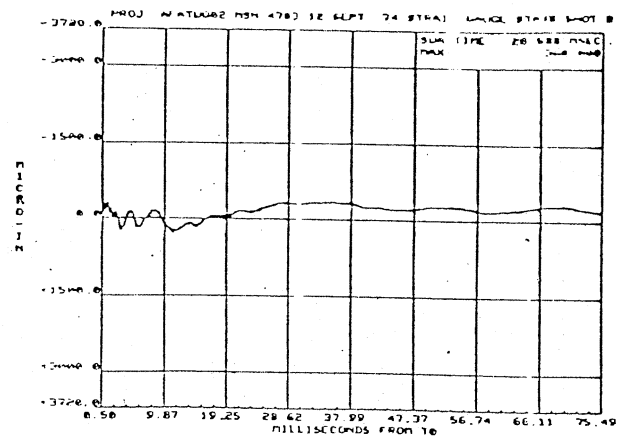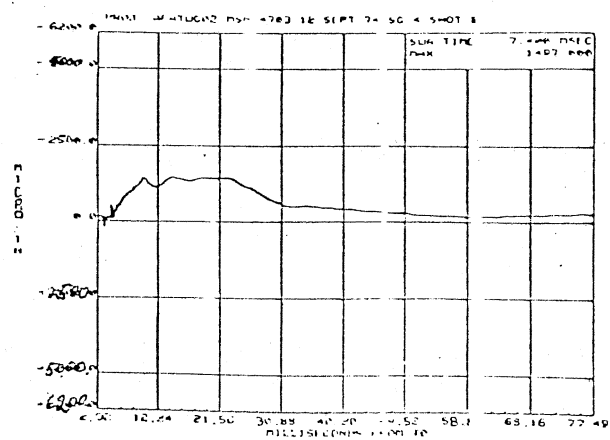
Figure 75. (Continued)
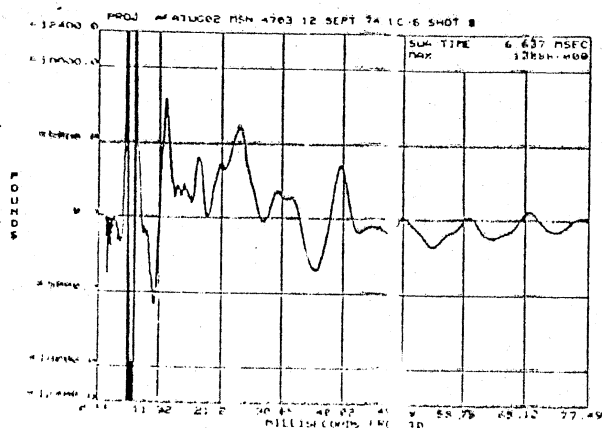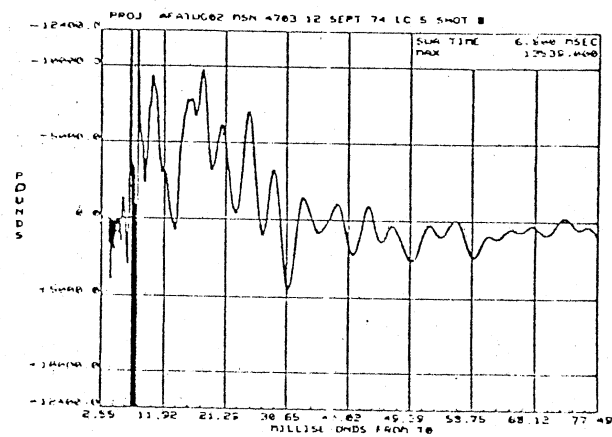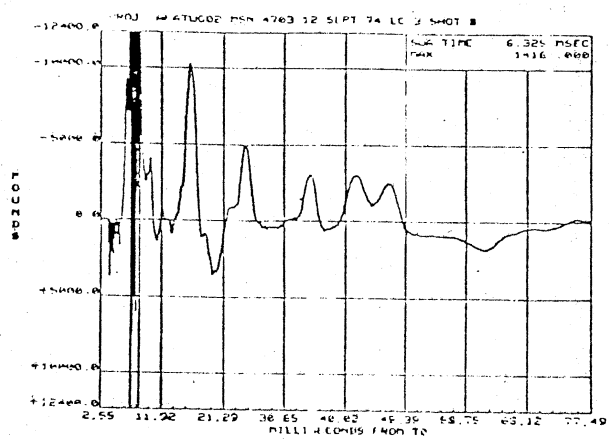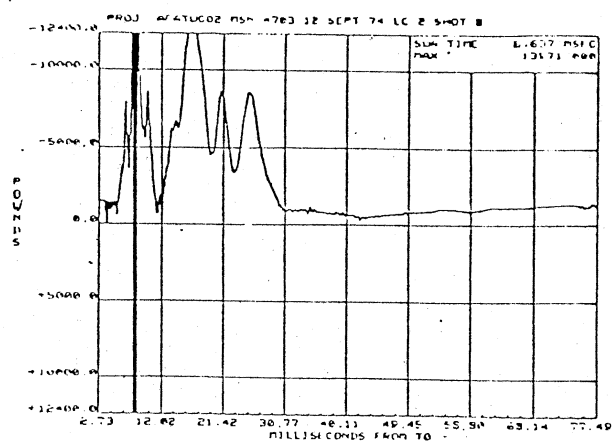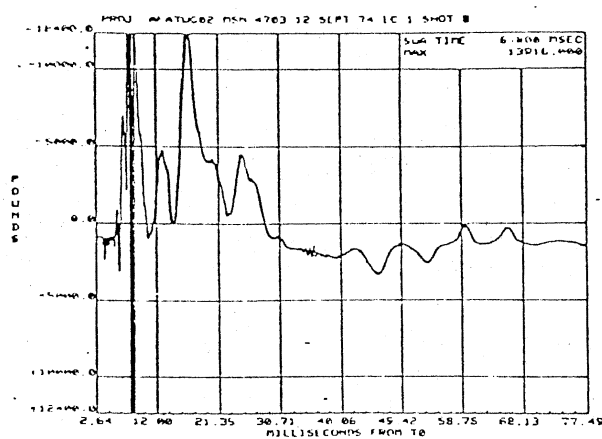
Figure 75. (Continued)
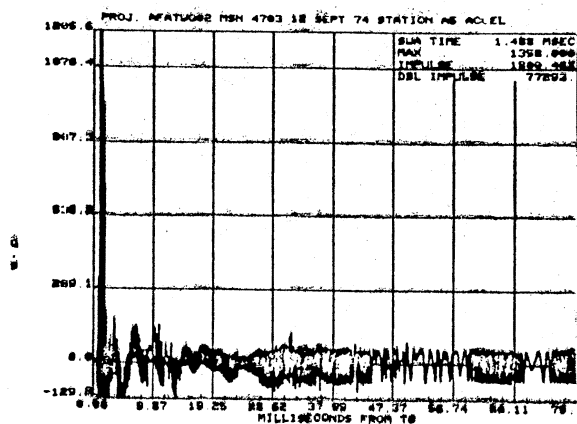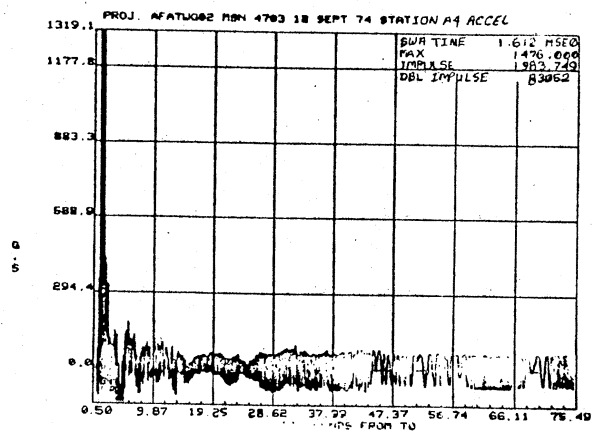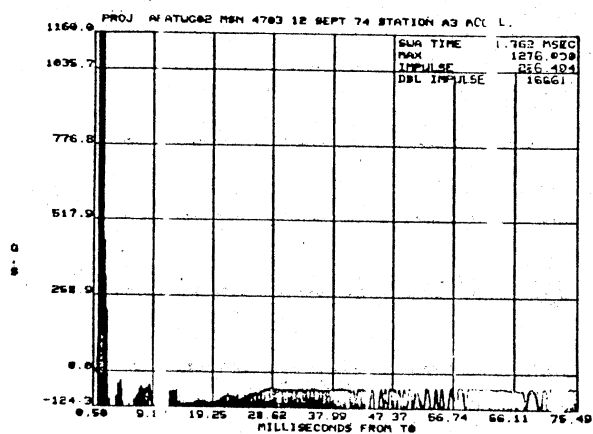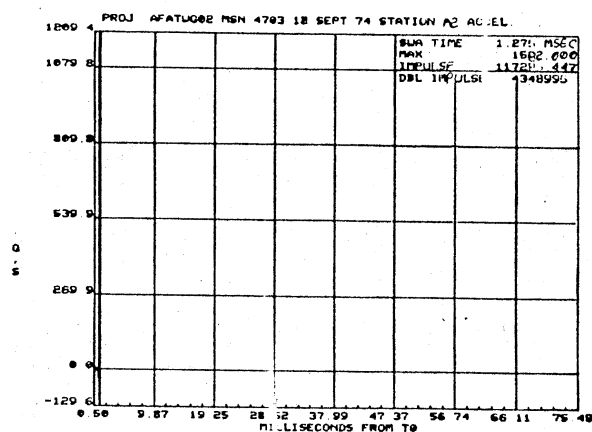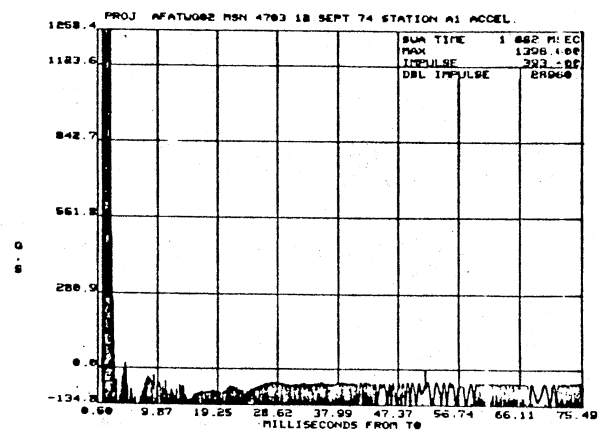
Figure 5. (Continued)
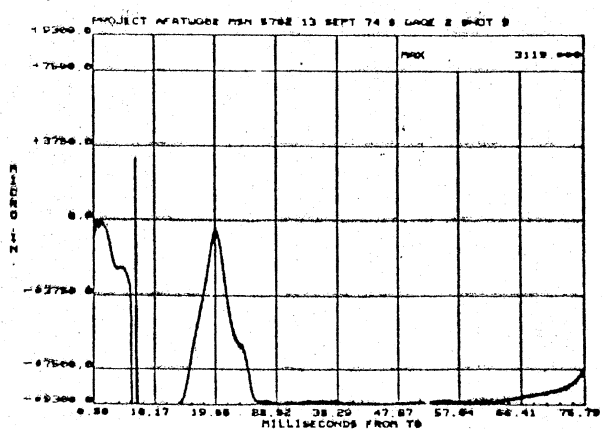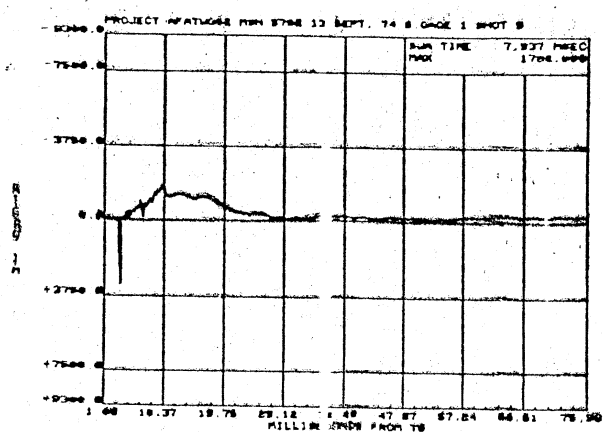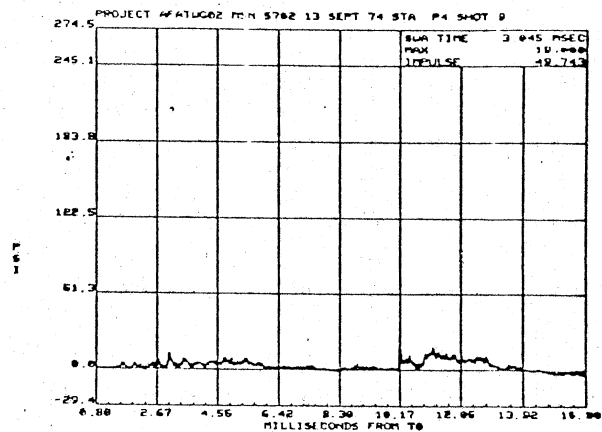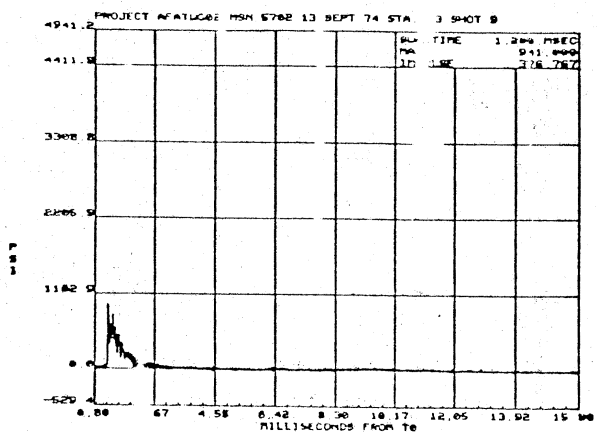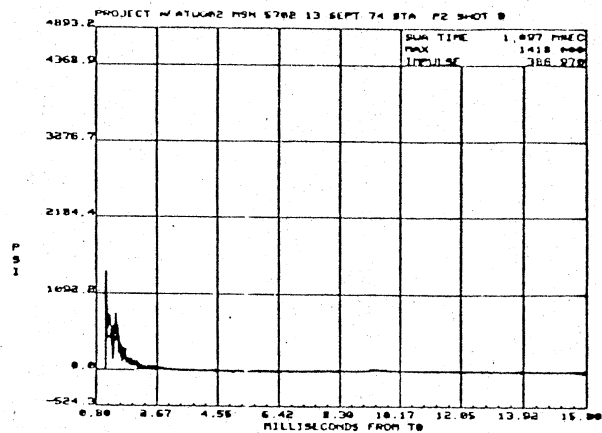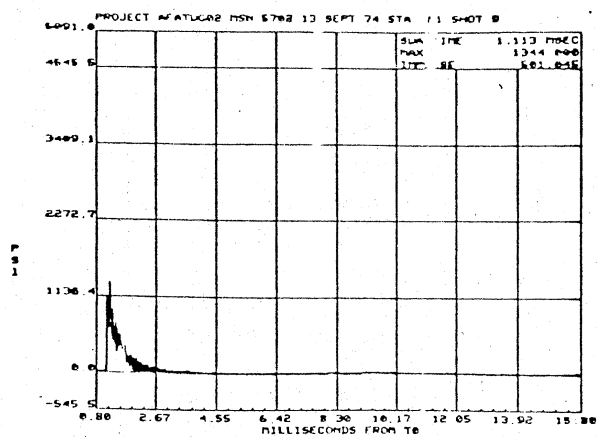
Figure 76. Data From Impulse Test 9, Beam 5, 13 September 1974
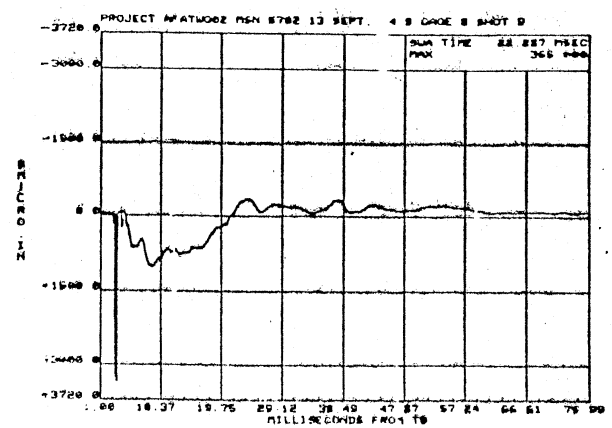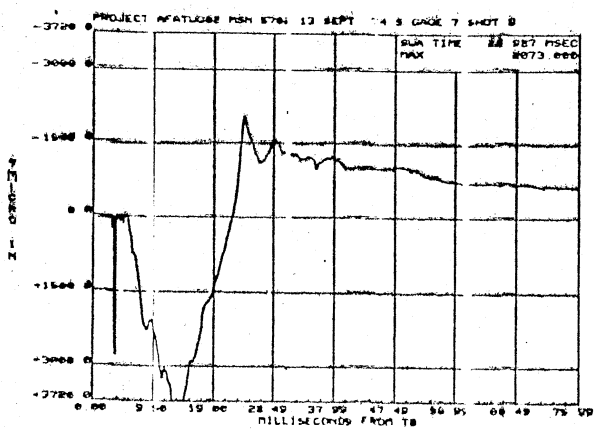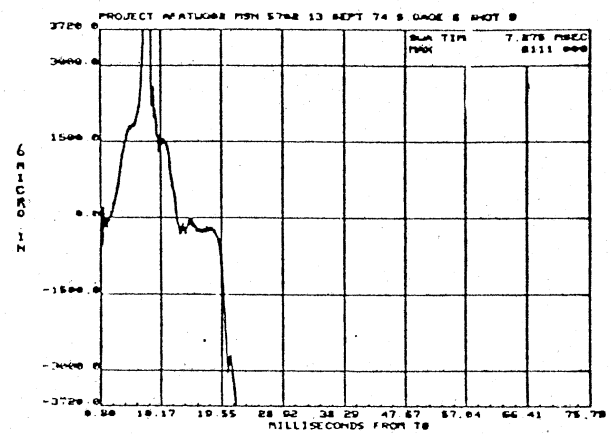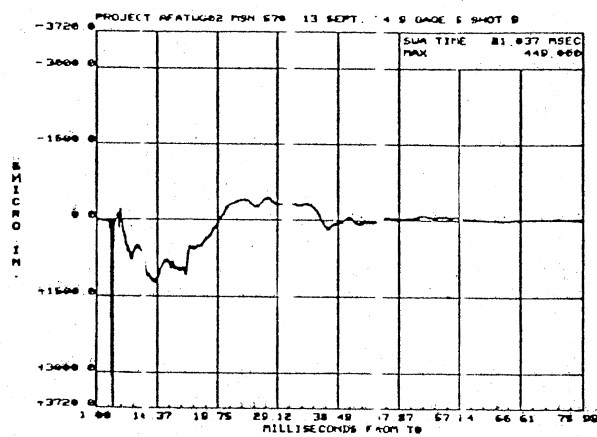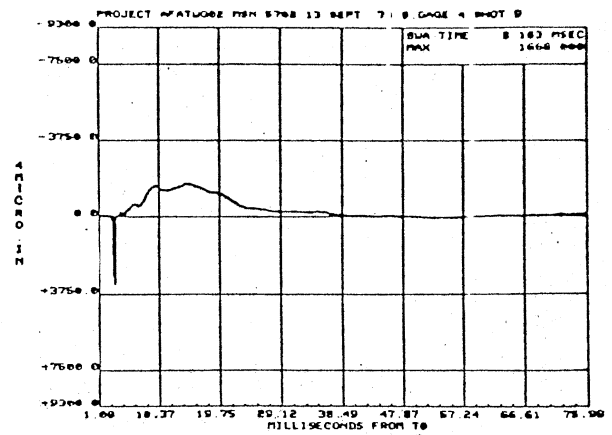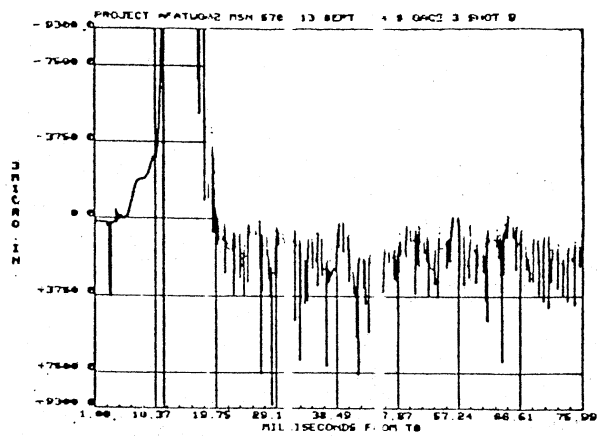
Figure 76. (Continued)
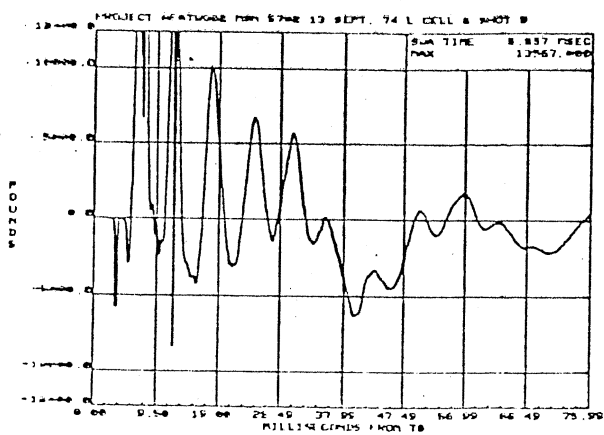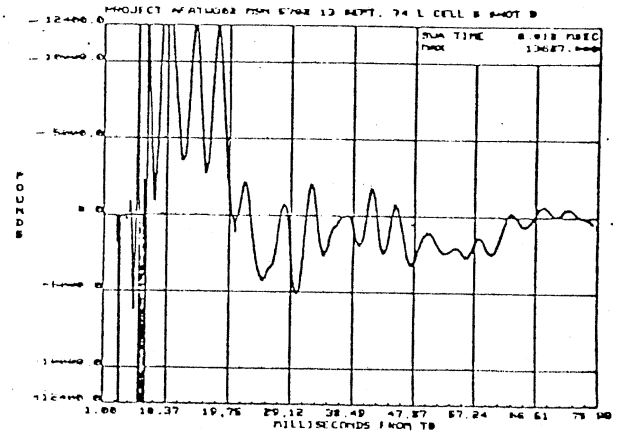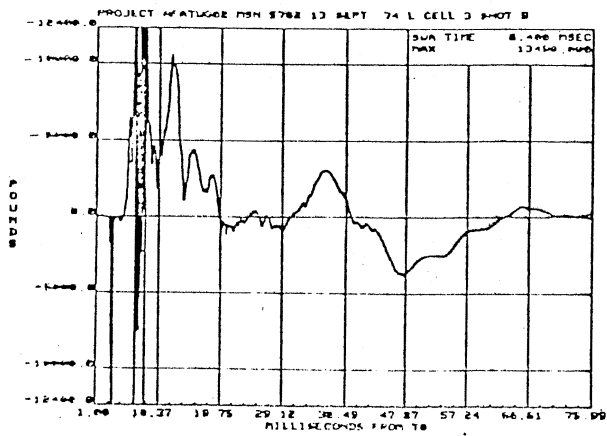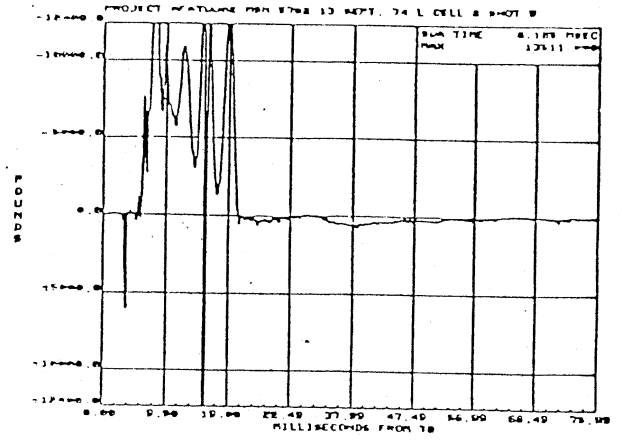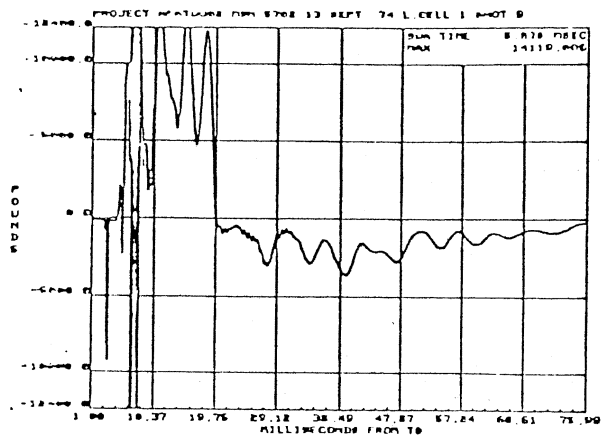
Figure 76. (Continued)
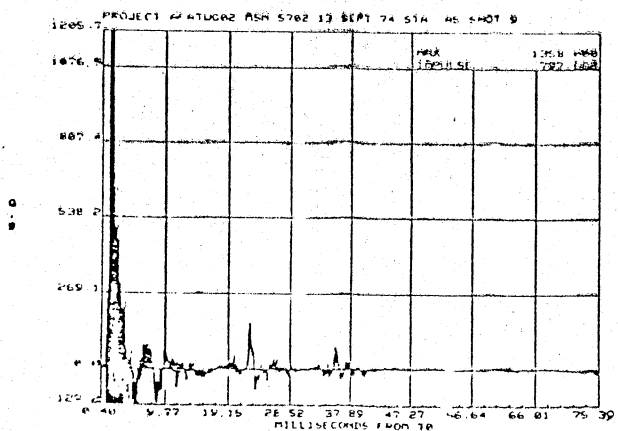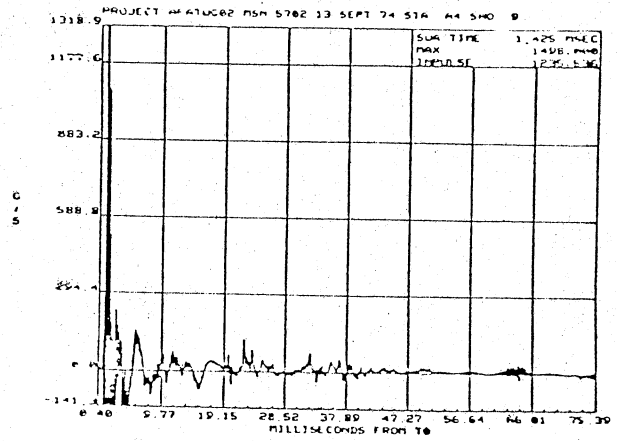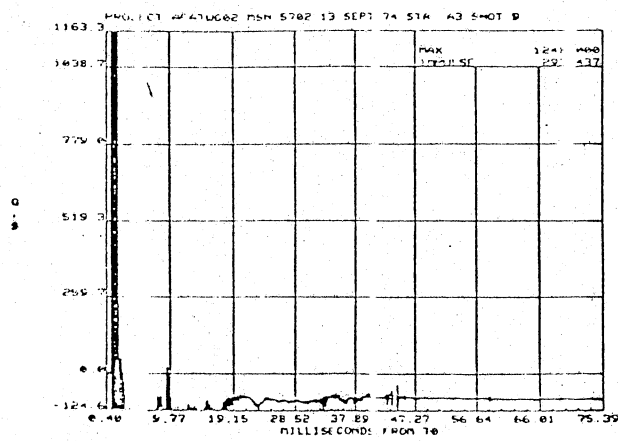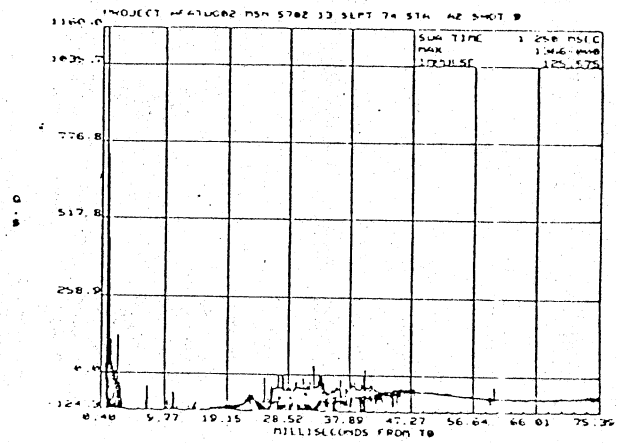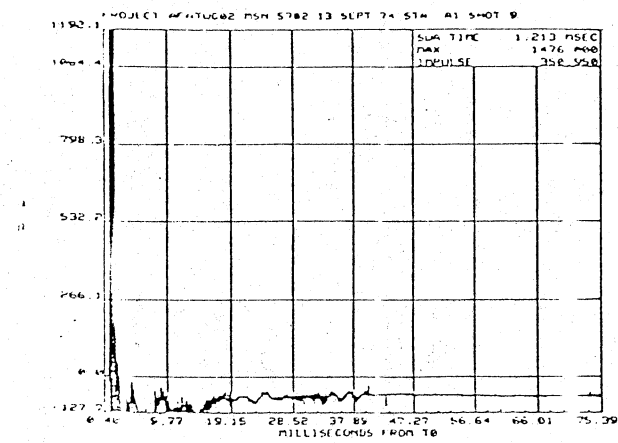
Figure 76. (Continued)
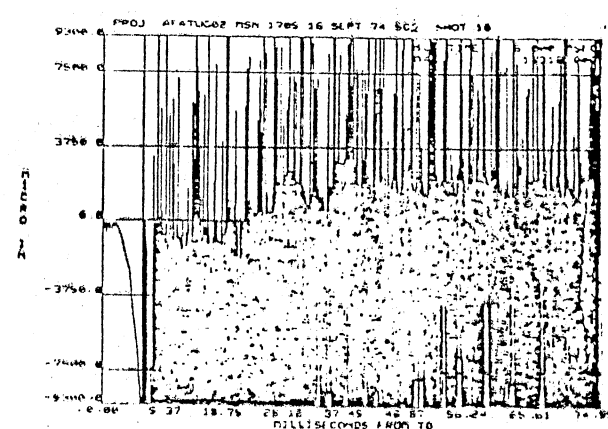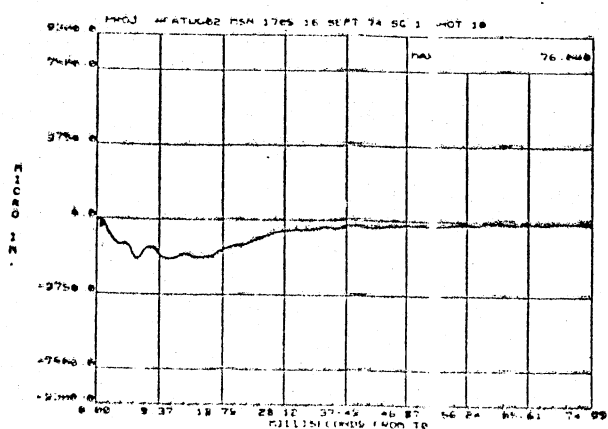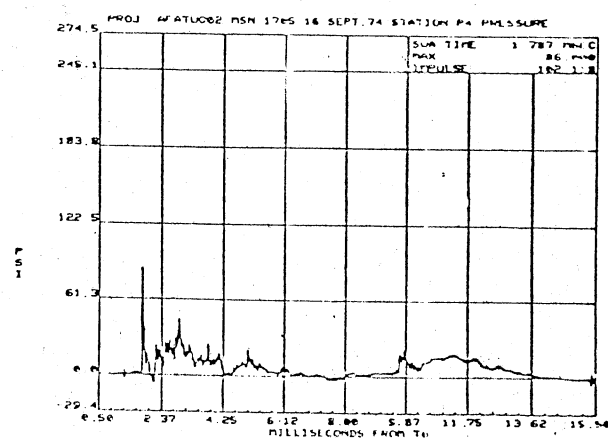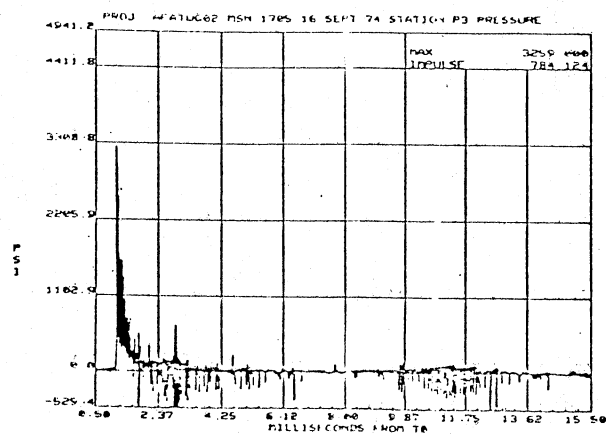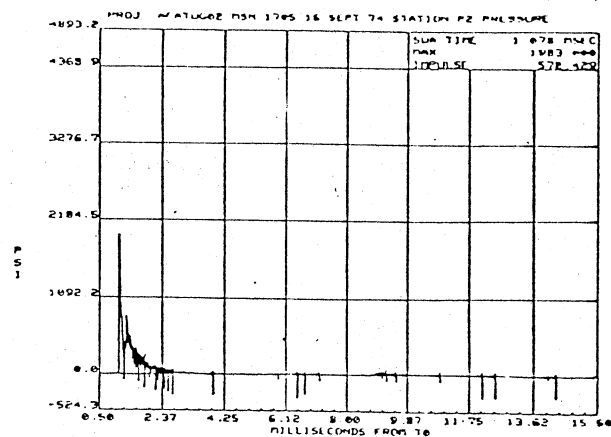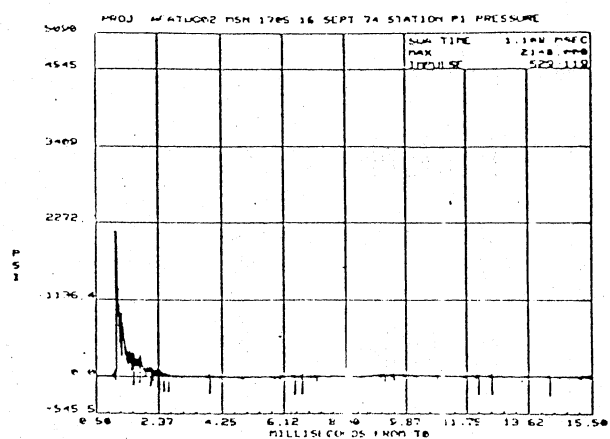
Figure 77. Data From Impulse Test 10, Beam 9, 16 September 1974
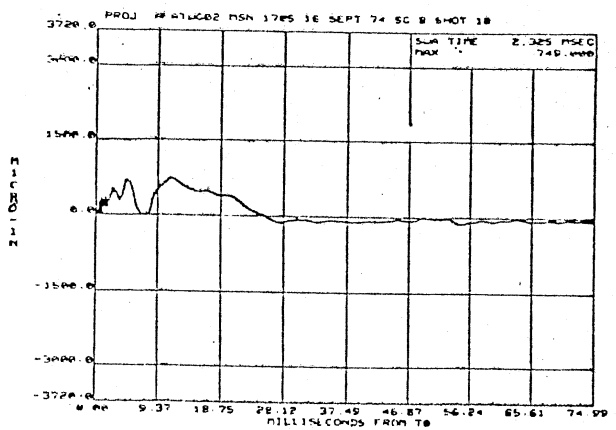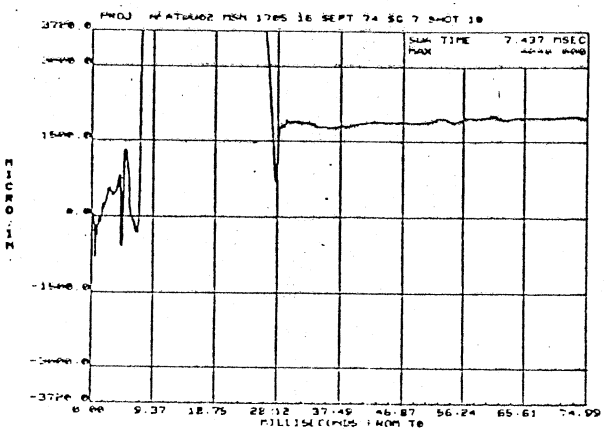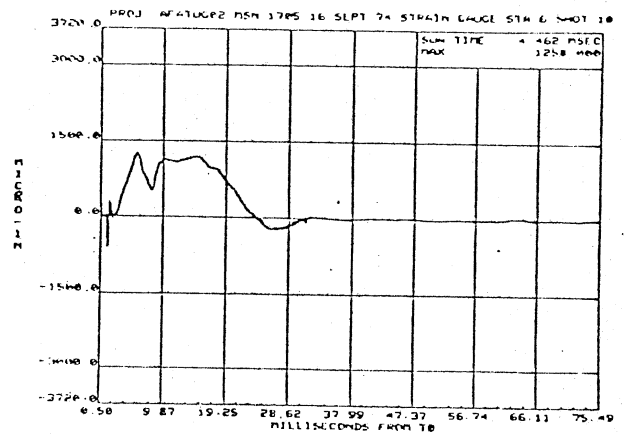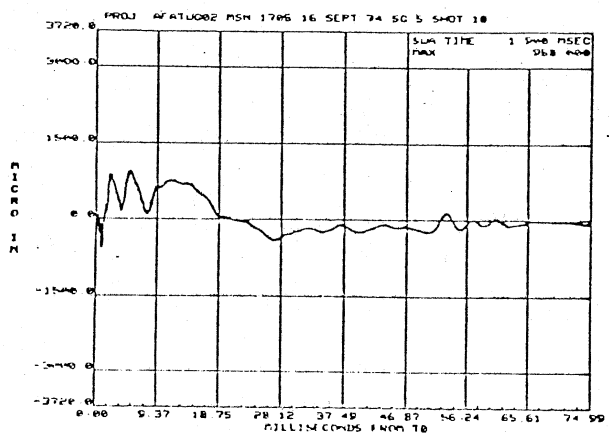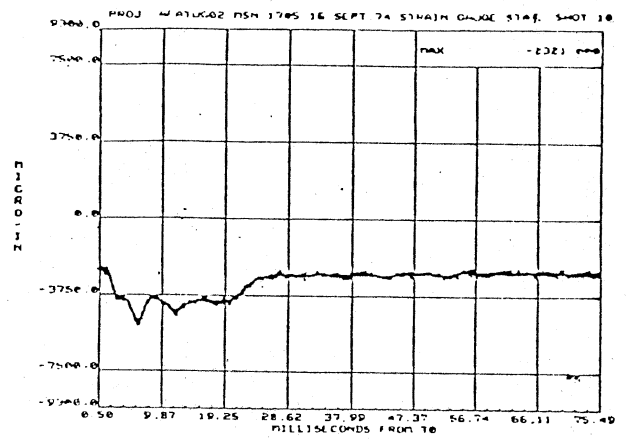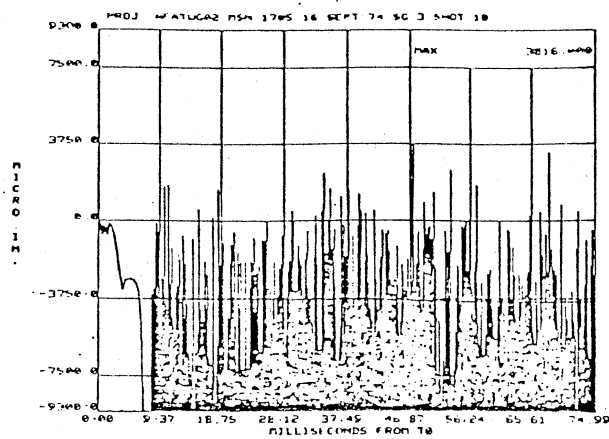
Figure 77. (Continued)
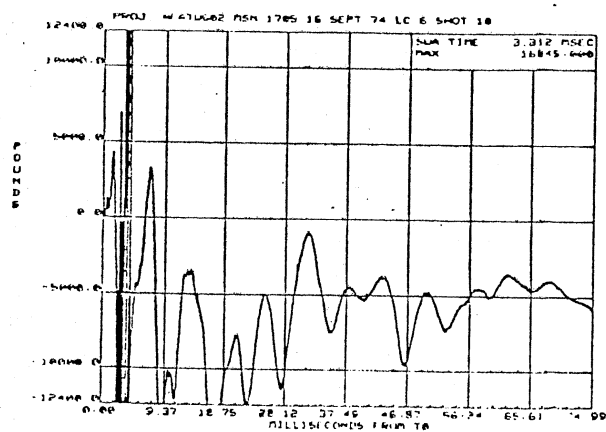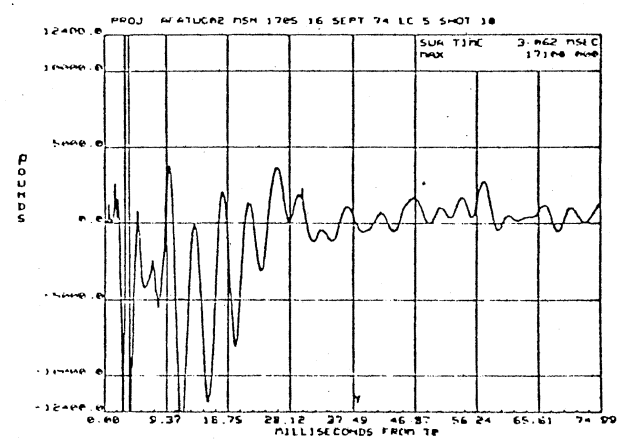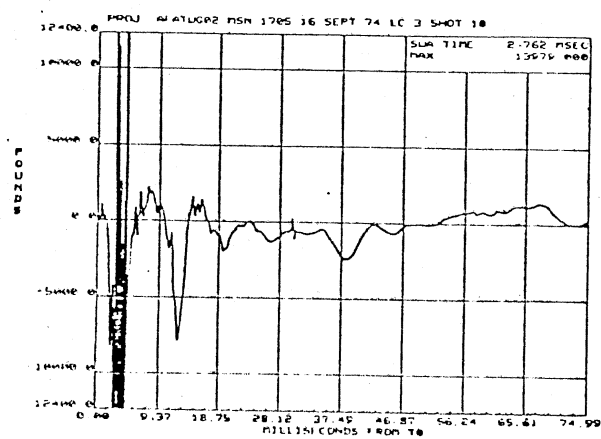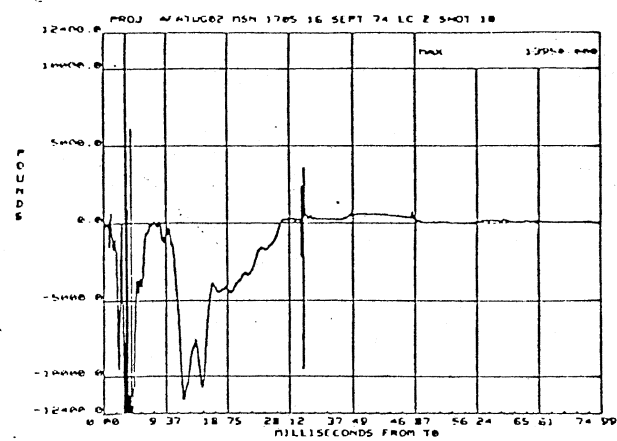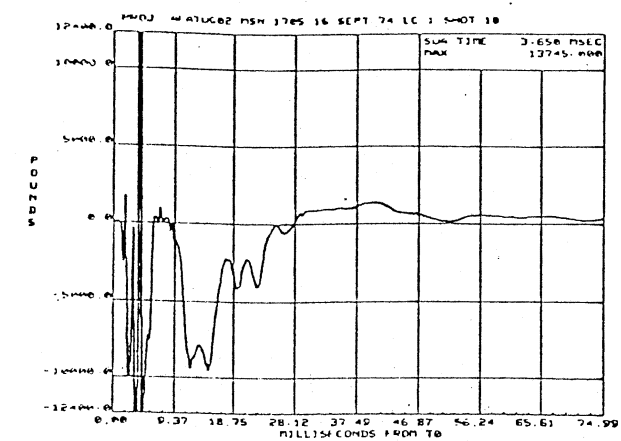
Figure 77. (Continued)
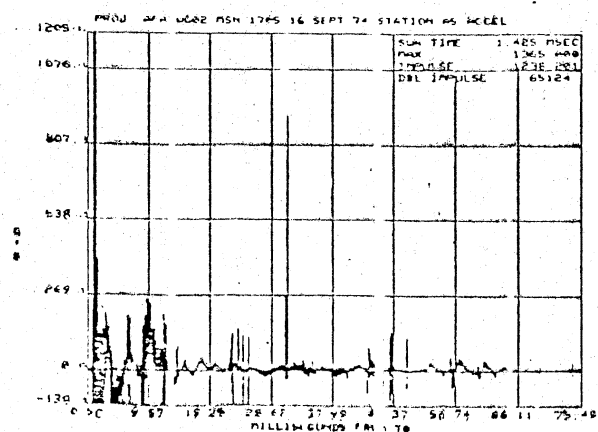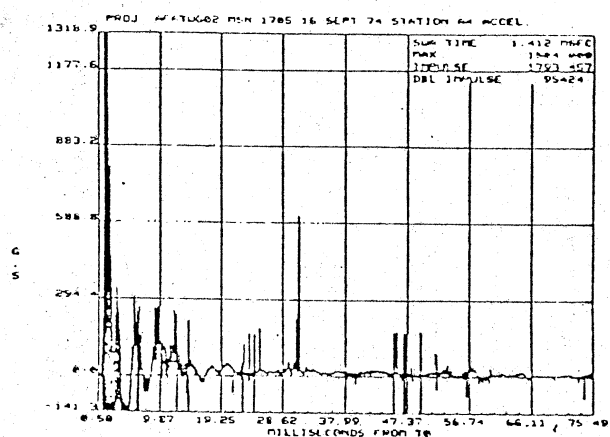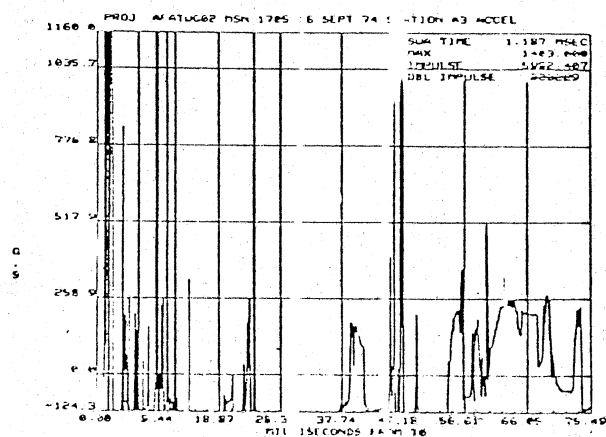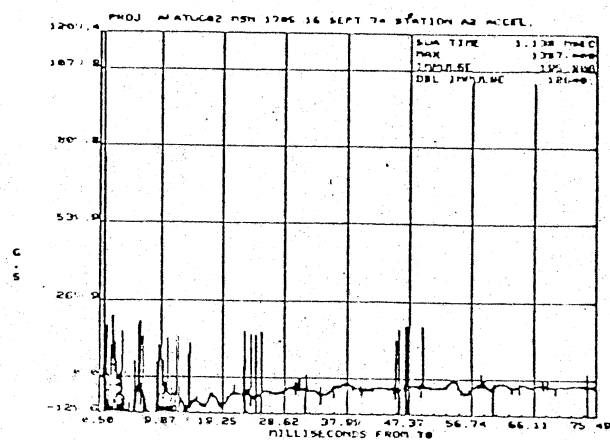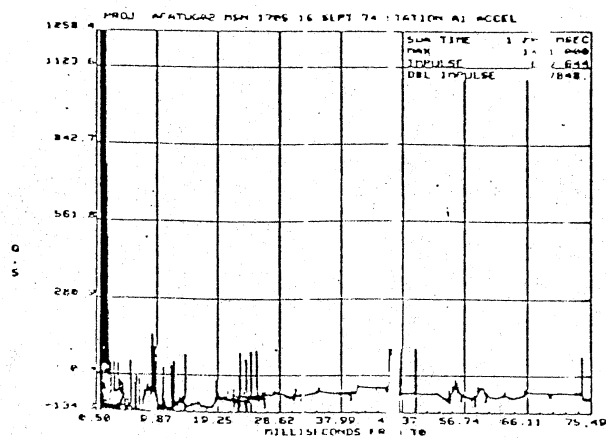
Figure 77. (Continued)
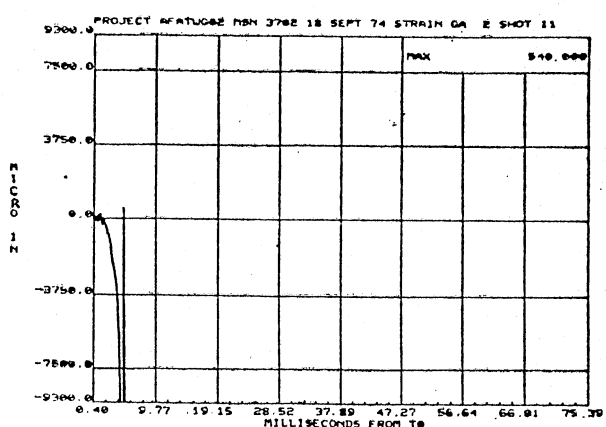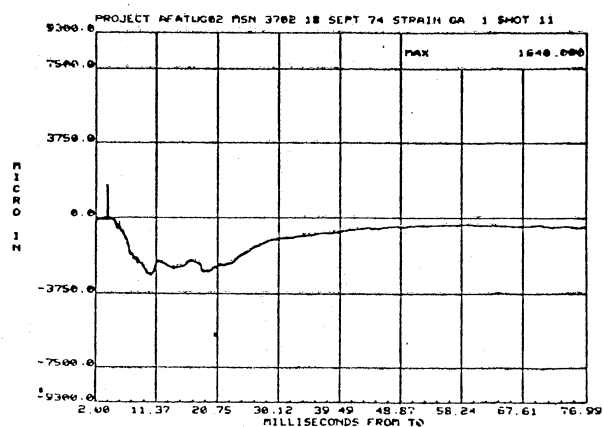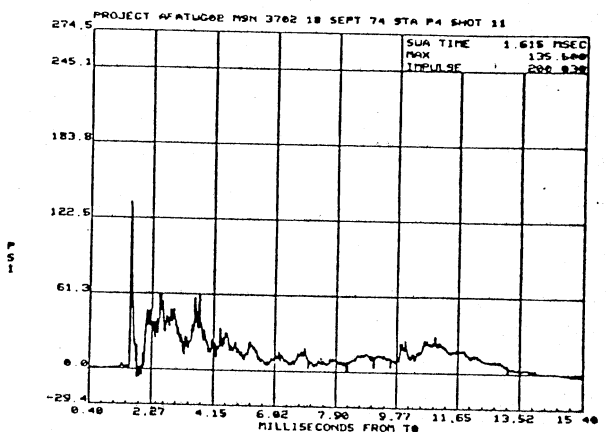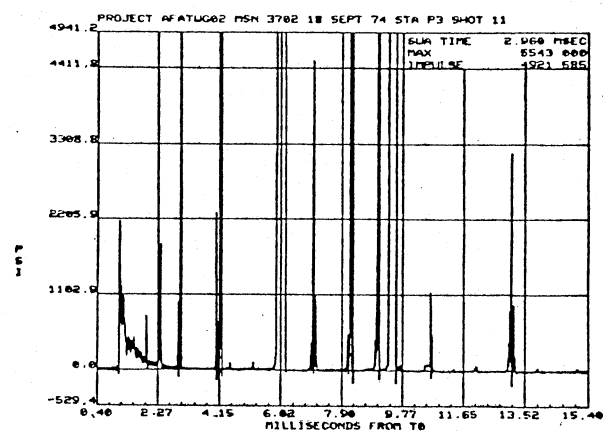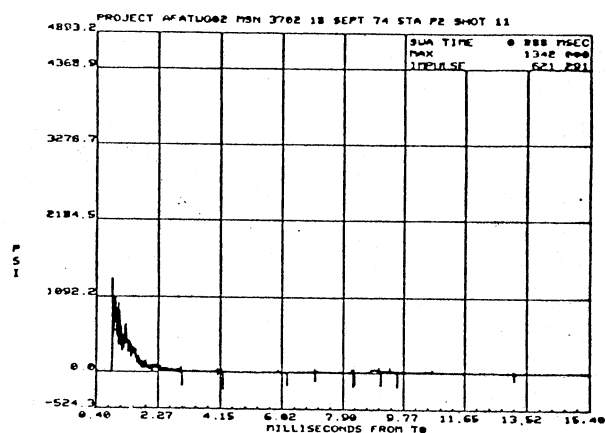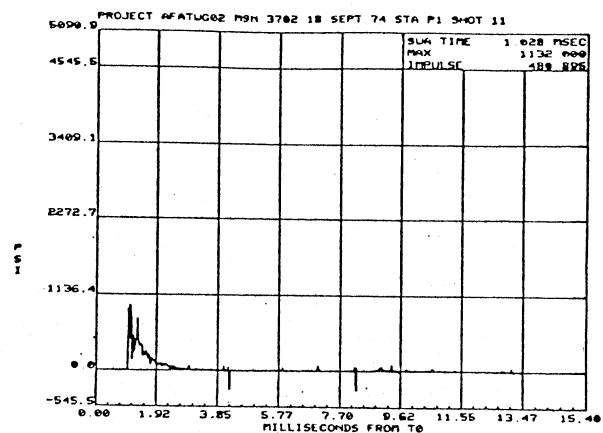
Figure 78. Data From Impulse Test 11, Beam 3, 18 September 1974
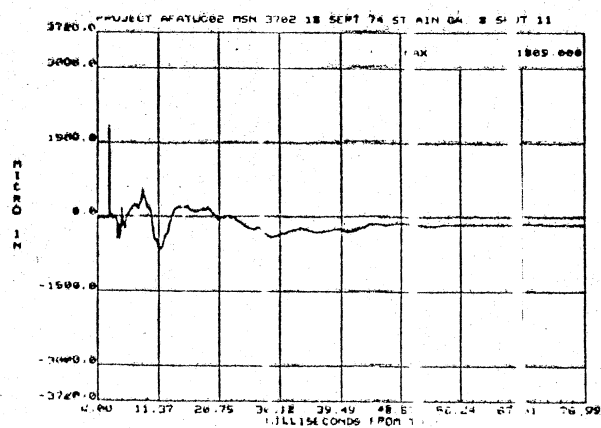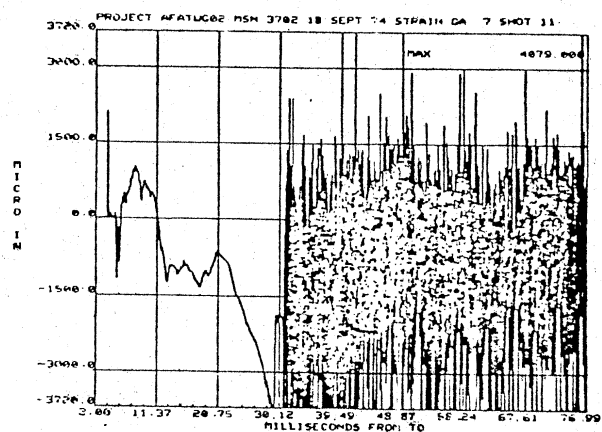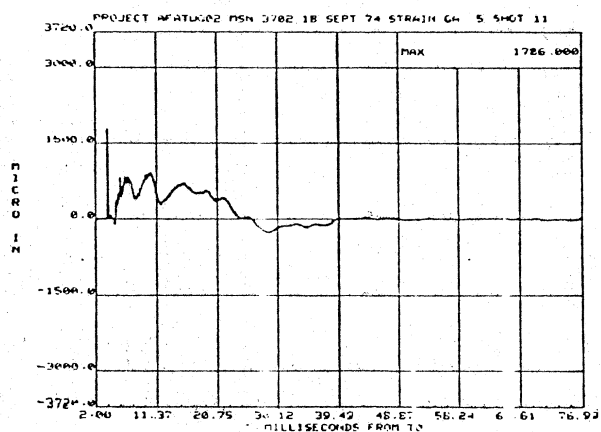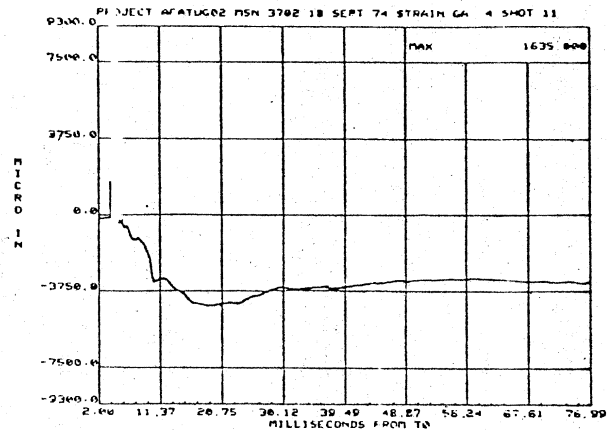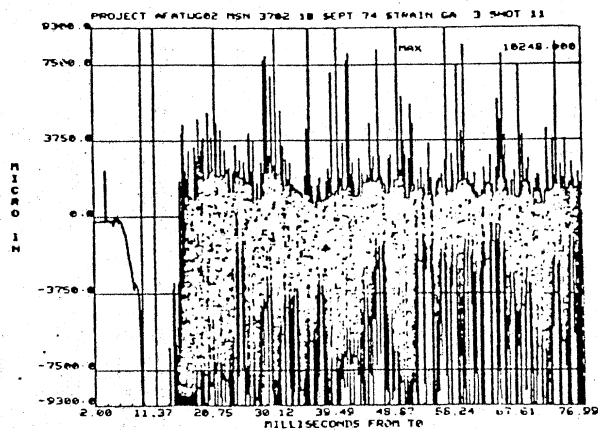
Figure 78. (Continued)
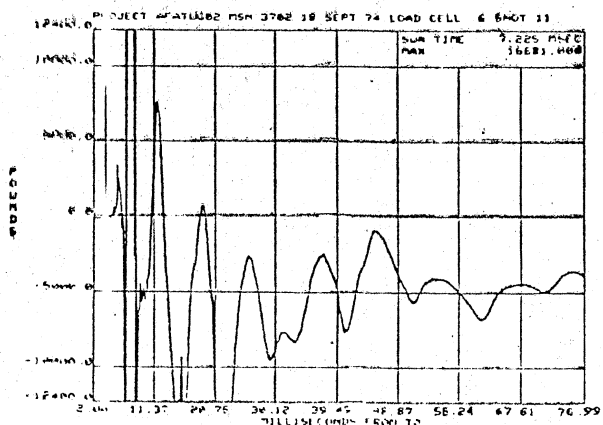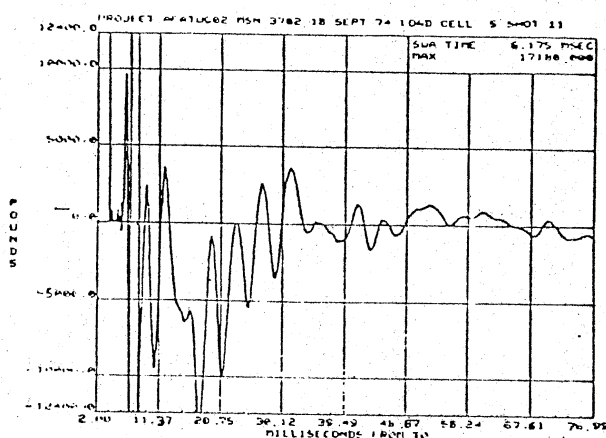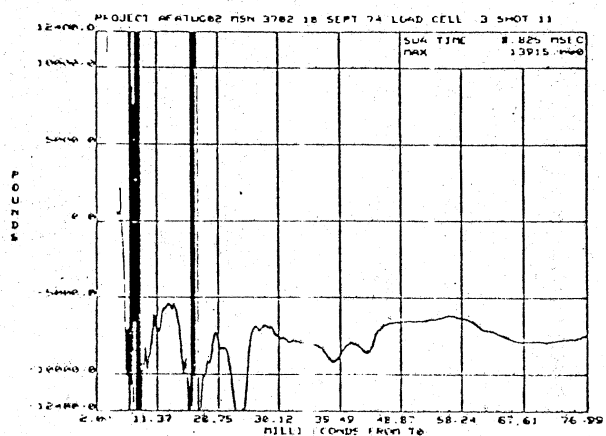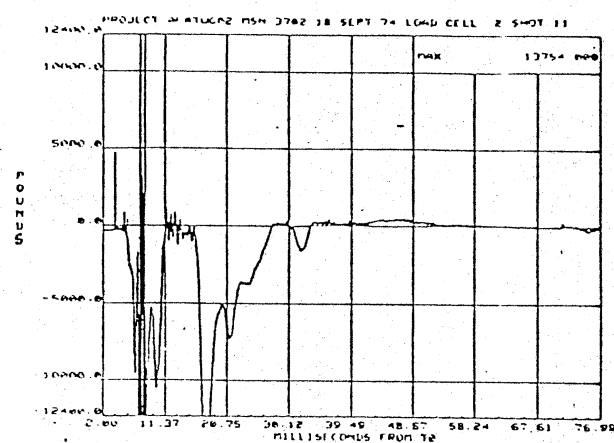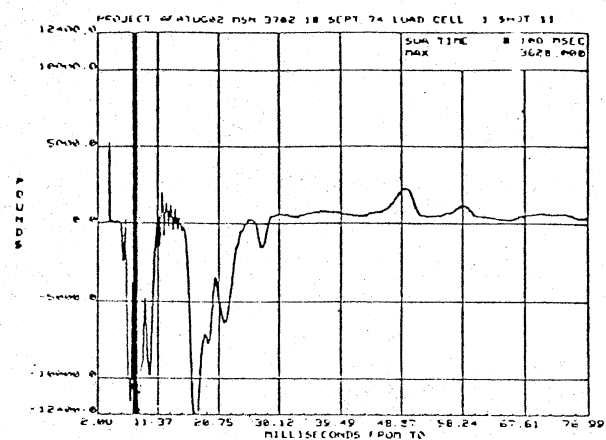
Figure 78. (Continued)
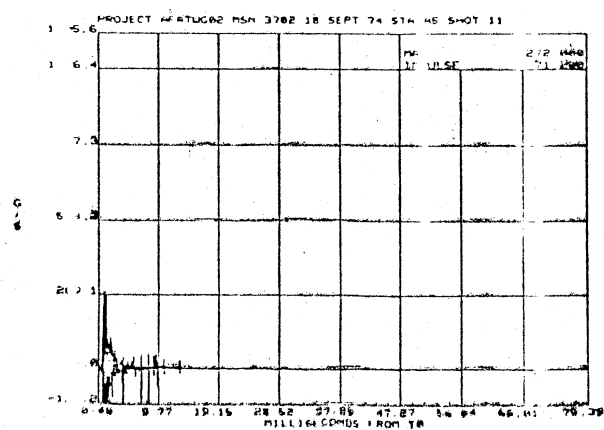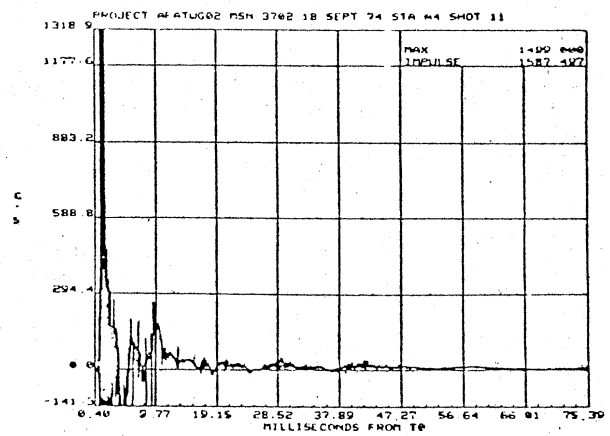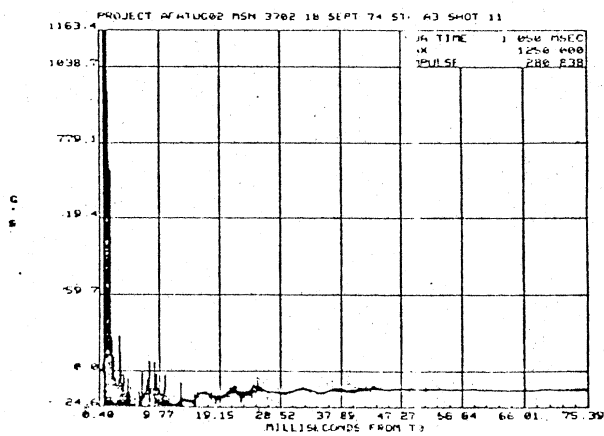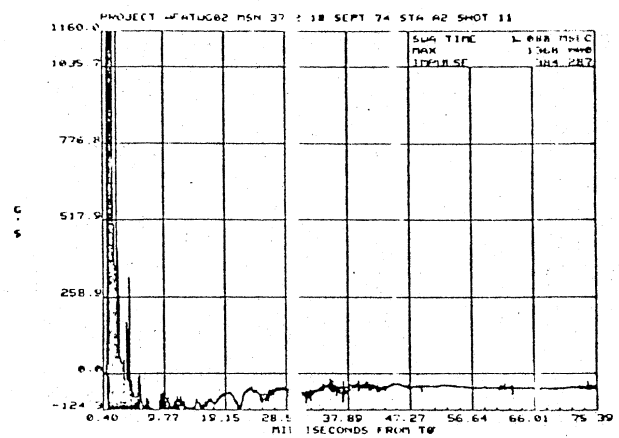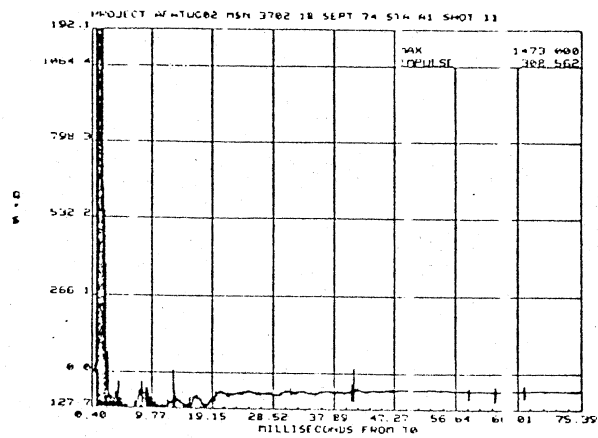
Figure 78. (Continued)
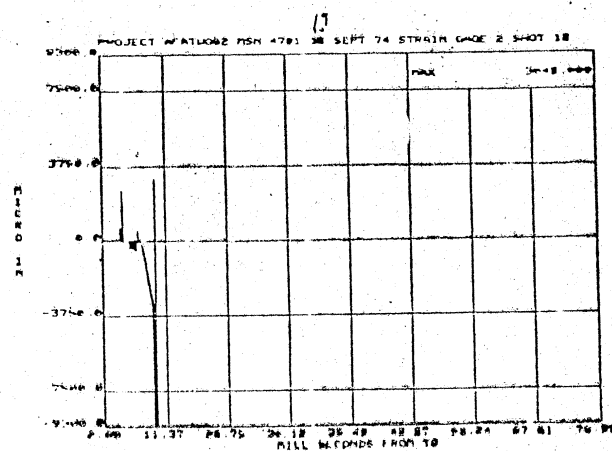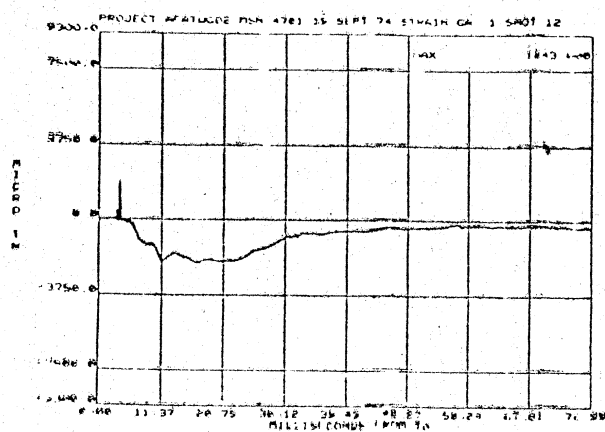
Figure 79.   Data From Impulse Test 12, Beam 11, 19 September 1974
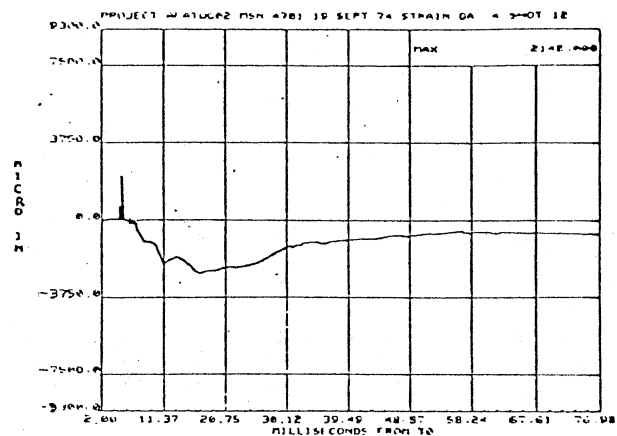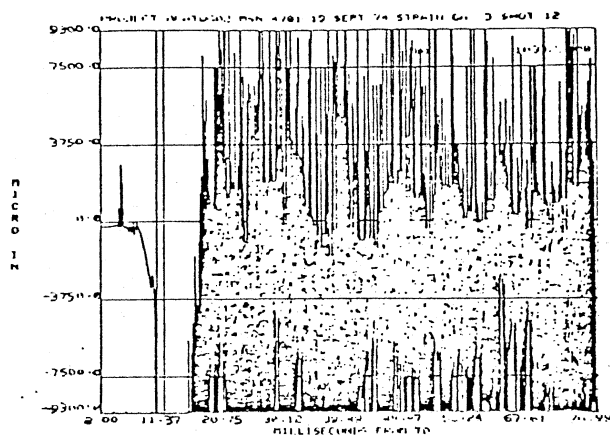
Figure 79. (Continued)
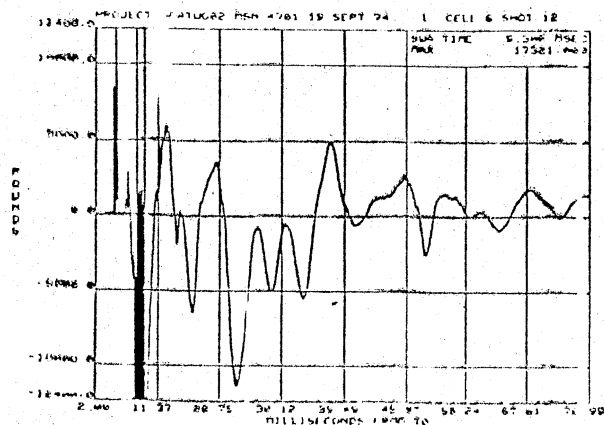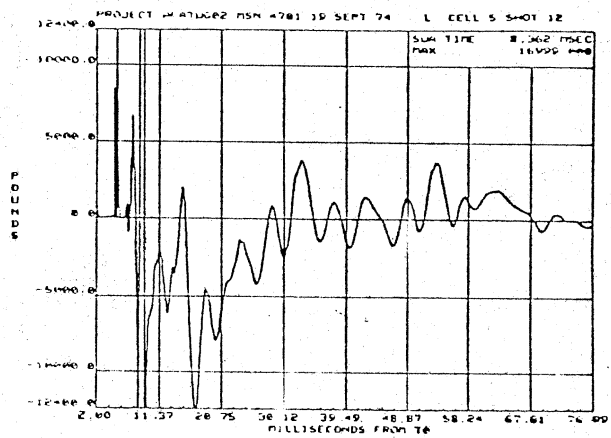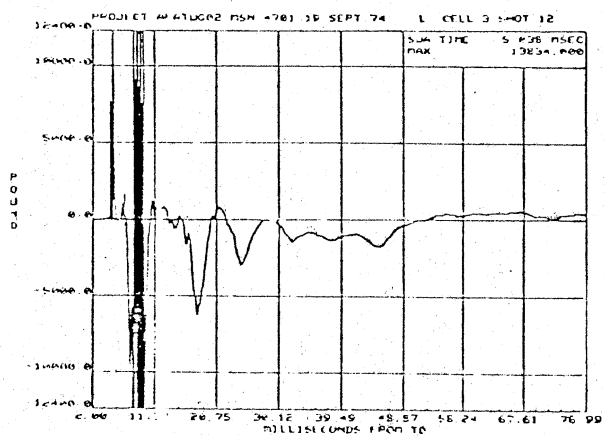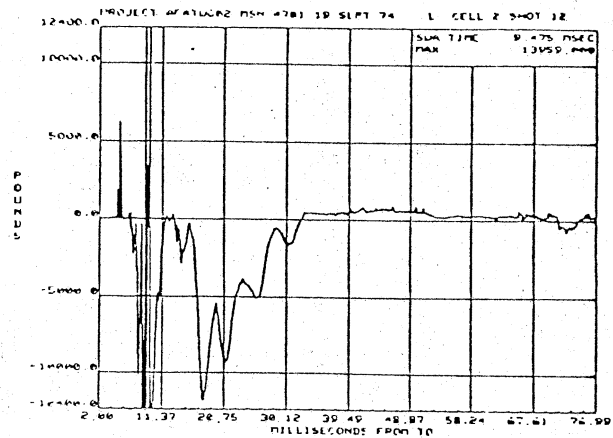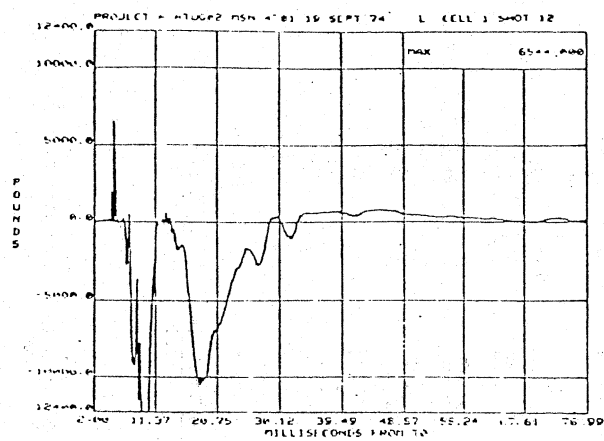
Figure 79. (Continued)
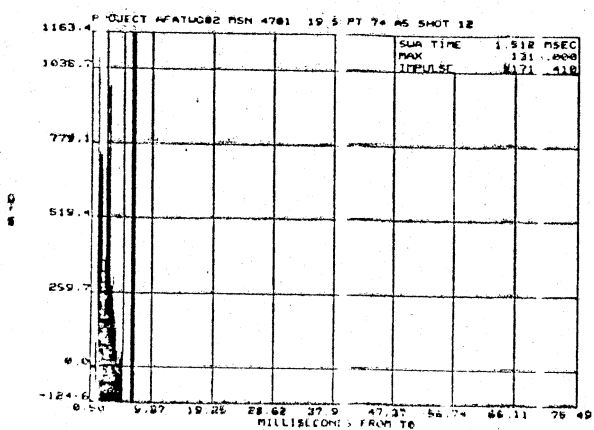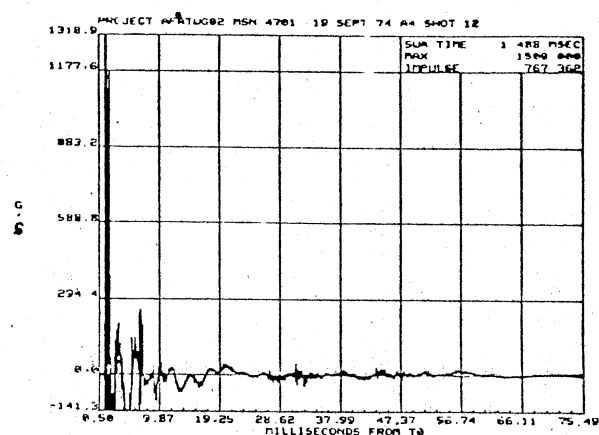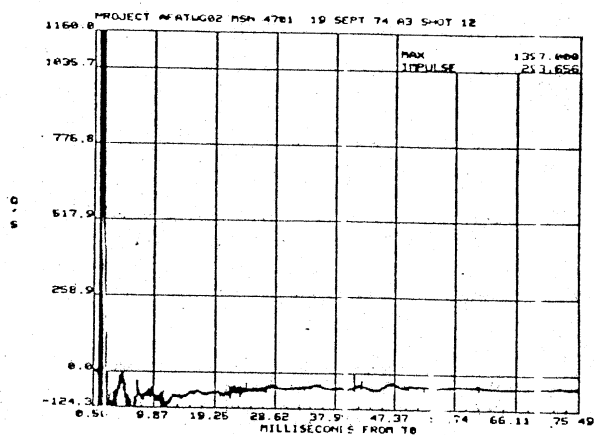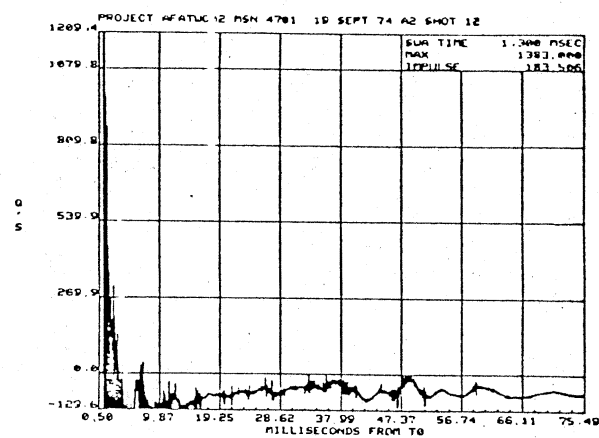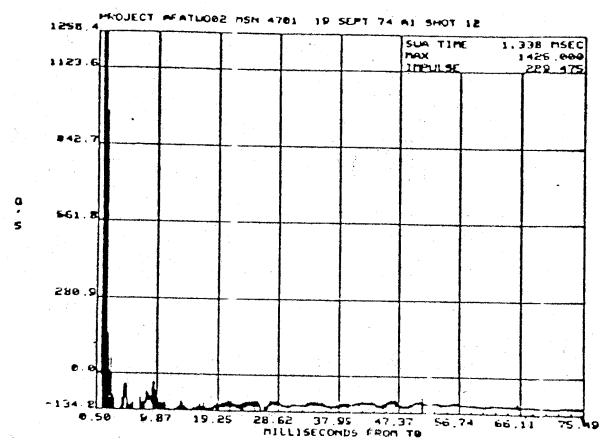
Figure 79. (Continued)

APPENDIX B

DESCRIPTION OF DYNAMIC MATERIAL PROPERTIES
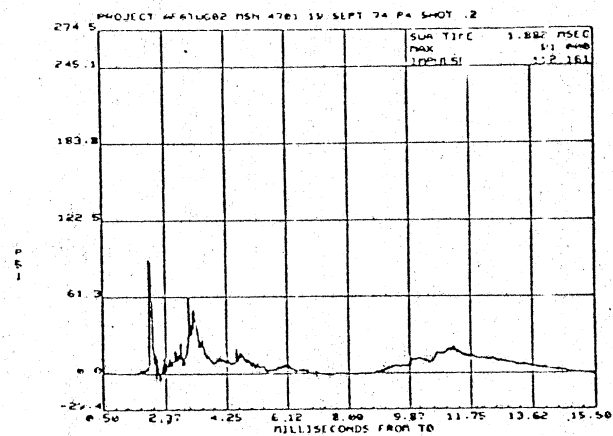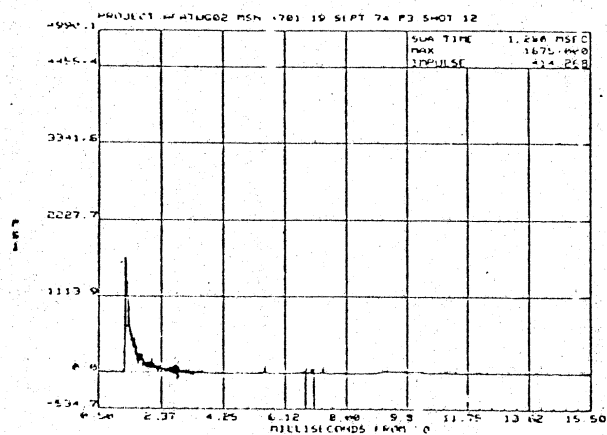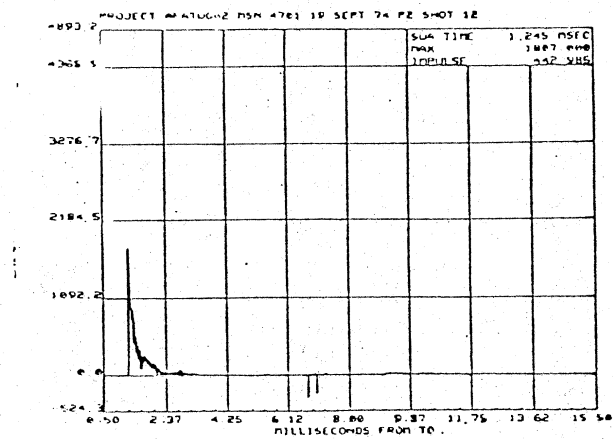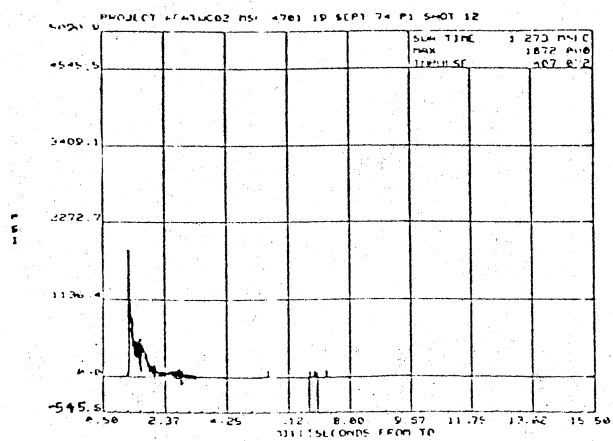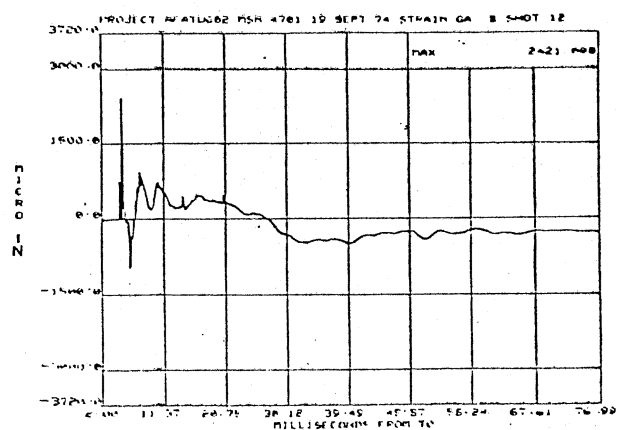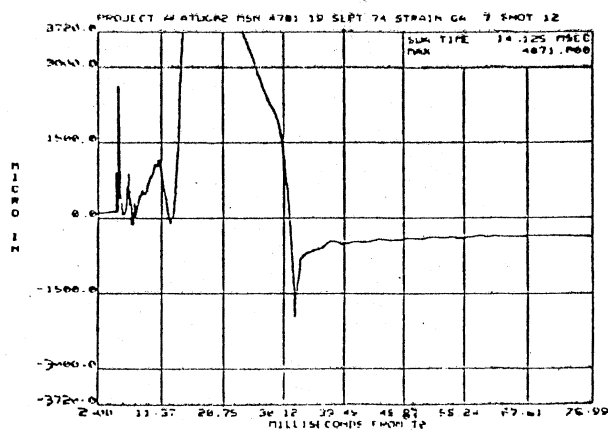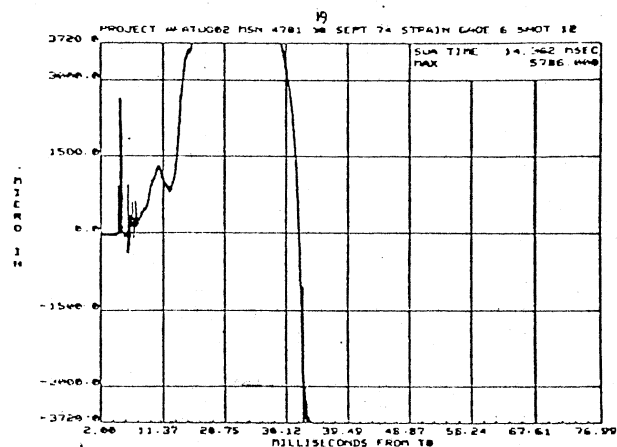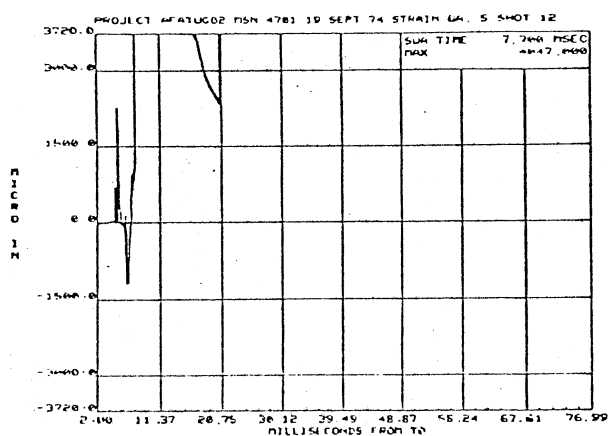
FOR IMPBC ANALYSIS

The discussion in this appendix pertains to the descriptions of material properties required as data for the computer simulation of impulse loaded beams. The digital computer program of Dawkins, IMPBC (2) was used for the analysis. Further details of the numerical method and the computer program are available in Reference (2).

B.1 Steel Dynamic Stress-Strain Curve

The dynamic stress-strain curve for the reinforcing steel was developed utilizing data from Manjoine (4). The dynamic yield stress, f_{Dy}, was estimated from the static yield stress of Table II, and the dynamic yield ratio, f_{Dy}/f_y from Figure 3. For the numerical study, a strain rate of 2.01/sec was selected. This value was predicted by the center steel gages on beam 11, test 12, and gave $f_{Dy}/f_y = 1.55$. The dynamic stress-strain curves for 40- and 60-grade steels are shown in Figure 80.

B.2 Concrete Dynamic Stress-Strain Curve

The concrete stress-strain curve was developed from static strength characteristics and a method proposed by Gupchup (31) to approximate the flexural behavior of a prismatic member at high strain
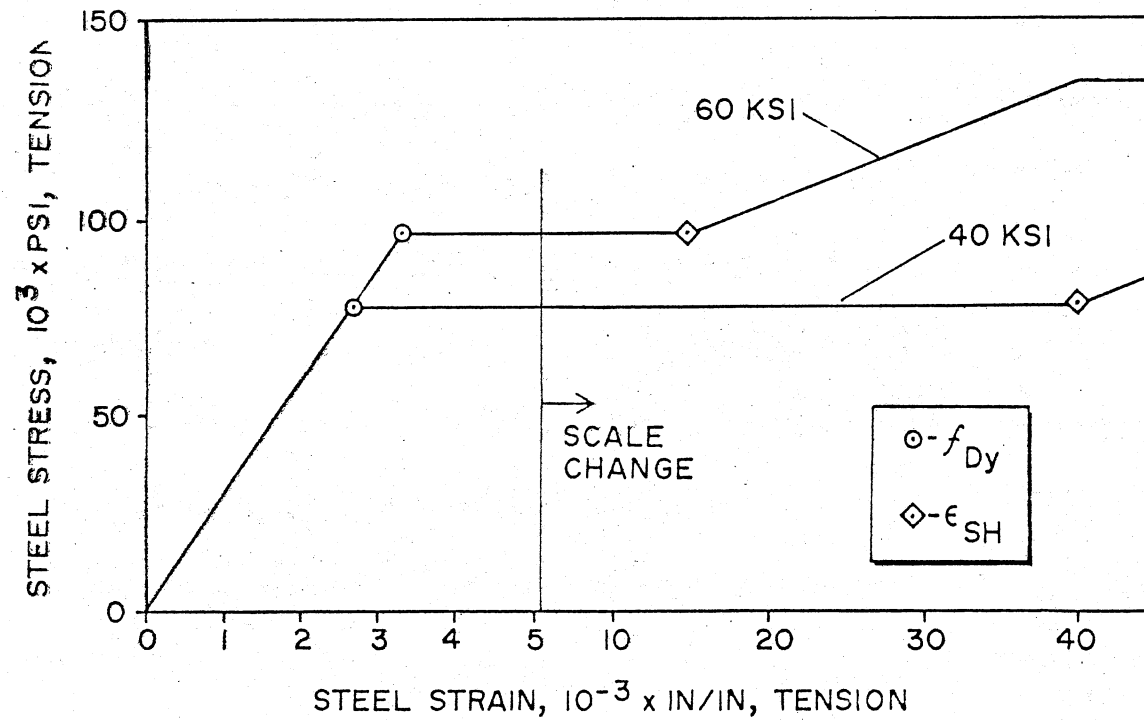
Figure 80. Steel Stress-Strain Curves Used in IMPBC Simulations

rates. As for steel, a single strain rate will be selected, although this quantity will vary with both vertical and longitudinal position on the beam.

The development of the concrete dynamic stress-strain curve is illustrated in Figure 81. Both the ultimate strength and corresponding strain are increased by α, a strain rate dependent quantity. The static stress strain curve, f_c, is increased proportionally to pass through f_{DC}' and ε_{DC}'. To account for flexural effects, the curve f_{DC} is reduced by .85 and yields f_{FDC}, the dynamic flexural stress-strain curve for concrete.

Also shown in Figure 81 is the shape of the stress-strain idealization used for computer simulation of the impulse-response phenomenon. In Figure 82 both the high strength and nominal dynamic concrete stress-strain curves are presented. These curves were constructed from averaged ultimate stress data of Table V, and an amplification factor α, from Figure 4. For a strain rate of 0.43/sec, $\alpha = 1.46$. This strain rate was observed at the center of beam 11 on test 12.

B.3 Moment-Curvature Characteristics

Beam dynamic flexural properties are shown in Figure 83. These curves were developed from stress-strain data of Figures 80 and 82. The symbols on the curves define

$\phi_{f_{Dy}}$ = the curvature related to onset of steel yield;

$\phi_{f_{DC}''}$ = the curvature producing ultimate concrete stress in the top fiber;

$\phi_{\varepsilon_{DC}'}$ = the curvature which produced failure strain in the concrete.

The points $\phi_{f_{DC}''}$ and $\phi_{\varepsilon_{DC}'}$ do not coincide because f_{DC}'' is reached at a

Figure 81. Adjustments of Concrete Cylinder Stress-Strain Curve to Account for Dynamic and Bending Effects
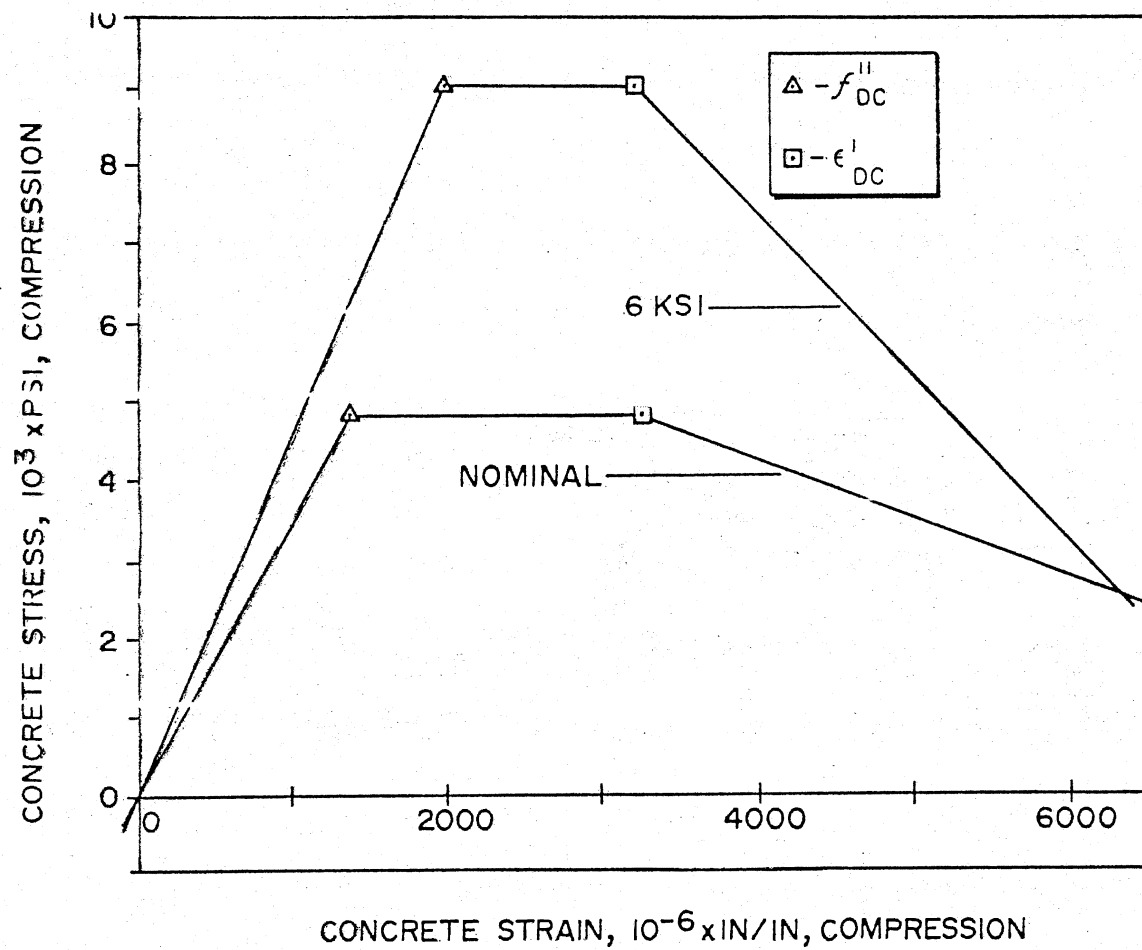
Figure 82. Concrete Stress-Strain Curves Used in IMPBC
Simulations
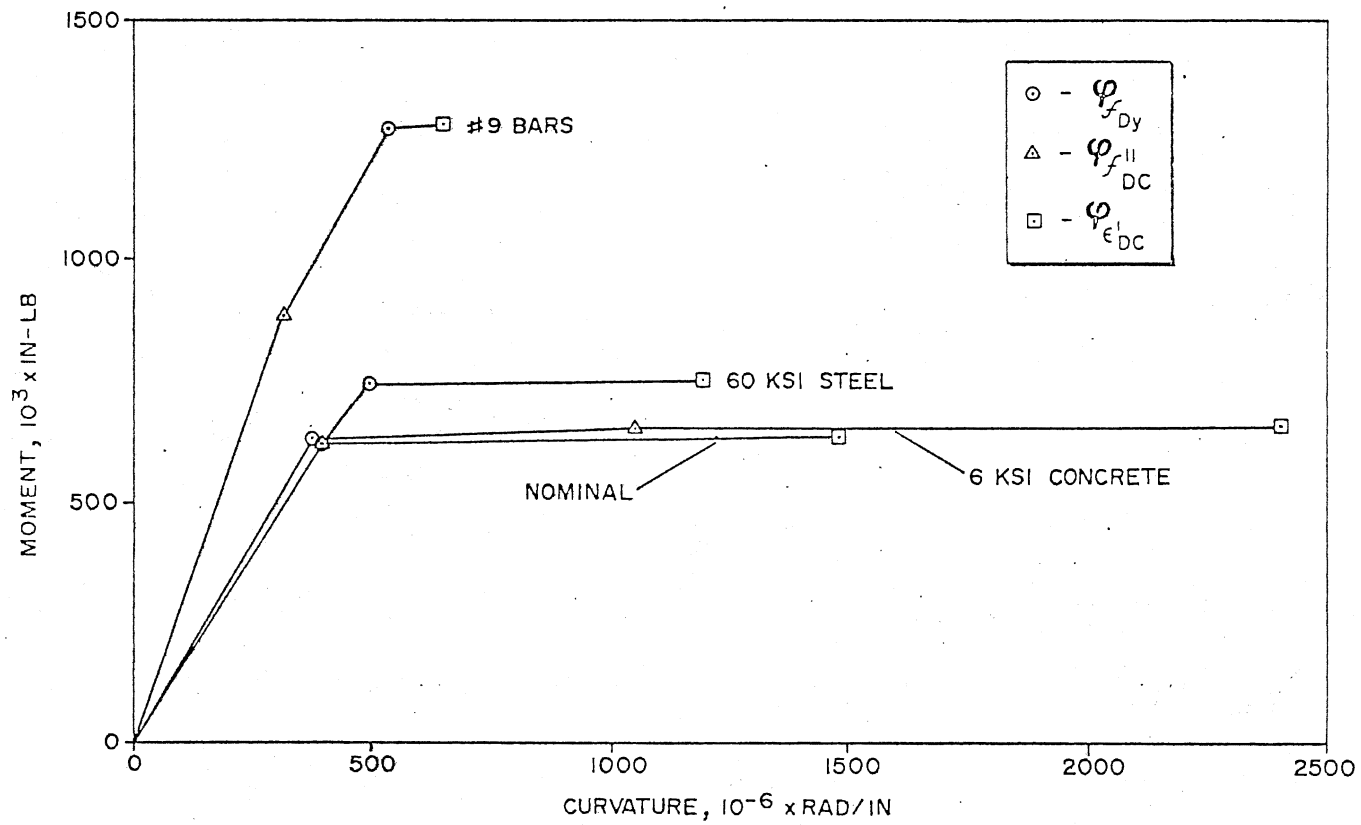
Figure 83. Predicted Variation of Moment With Curvature for IMPBC Model

strain which is less than the failure strain ϵ'_{DC}. This is clearly shown by the dashed line in Figure 81.

Several important features of these curves have been discussed in Chapters VII and VIII. First, the calculated flexural stiffness, EI, compares very favorably with measured values, Table VI. One notes that the measured flexural stiffness varies for beams 2, 3 and 7 through 16 have values of stiffness which vary from 1.32×10^9 to 1.53×10^{-9} lb-in^2. An exception is beam 13 with an average flexural stiffness of 1.17×10^9 lb-in^2. Examination of the data failed to yield the reason for the reduced stiffness when compared with the remaining beams. Included in this group are the nominal, high strength concrete, and high strength steel beams. In Figure 83 one notes little difference in the flexural stiffness of these members, and an average EI of 1.55×10^9 lb-in^2. This difference was anticipated and is due to the adjustment of concrete material properties to reflect increased strain rate. Furthermore, the calculated ultimate moment capacity of the nominal beam is 625 kip-in. compared with 462 kip-in. for beam 13. The 35 percent increase in the calculated over measured strength is anticipated due to increased strength of the concrete and steel for strain rate effects.

APPENDIX C

FREQUENCY ANALYSIS

Mass spring models of the test system were developed to study reaction vibrations observed in test data. Although IMPBC studies provided valuable curvature data, differences were noted between measured and calculated reactions. The oscillatory nature of the measured reactions indicated vibration of system components other than the test beam. The models presented in this section were developed to estimate frequencies associated with the soil foundation and the load reaction mechanism-load cell structure.

C.1 Beam Vibration

The lateral deflection of the beam was restricted to a sinusoidal shape as shown in Figure 84(a) and the deflection at any point is given by

$$y(x,t) = y_n(t) \sin \left(\frac{\pi x}{L}\right). \tag{C.1}$$

When support motion is present, Equation (C.1) is modified by the motion of the support, y_a (Figures 84(b) and 84(c))

$$y(x,t) = y_a(t) + y_n(t) \sin \left(\frac{\pi x}{L}\right). \tag{C.2}$$

C.2 Foundation Vibration

The effect of the foundation will be studied by the spring-mass models shown in Figures 84(b) and 84(c). In Figure 84(b) the stiffness of the support mechanism and the load cells are represented by an equivalent spring, K_e. To determine the effect of the soil foundation on the vibration of the system, the model shown in Figure 84(c) was developed. In addition to the stiffness of the load cells and support mechanism, a soil stiffness spring was required. Furthermore, the mass of the test frame was included in the model.

C.3 Model Parameters

Although weights of the beam and test frame components were known, it was necessary to estimate the weight of the foundation slab, as well as the stiffness of many of the system components.

A reasonable idealization of the support mechanism was possible due to its configuration. The support mechanism permitted a simple structural idealization as axially loaded bars and a simply supported beam while the load cell stiffness was calculated with reasonable accuracy from manufacturer's specifications. Stiffness values utilized in the frequency analysis are given below. The value of the beam flexural stiffness EI was taken from the analysis of moment curvature presented in Appendix B. However, attention is directed to Table VI. Note that the predicted flexural stiffness compares favorably with measured values given for nominal beams.

$EI = 1.55 \times 10^9$ lb/in^2 (beam stiffness);

$K_e = 0.58 \times 10^6$ lb/in (support mechanism and load cells);

$K_s = 1.9 \times 10^6$ lb/in (equivalent spring for soil);

$K_L = 1.1 \times 10^6$ lb/in (load cell);

$K_a = 1.2 \times 10^6$ lb/in (support mechanism).

The component masses are

$M_b = 2.72$ lb-sec^2/in (mass of beam);

$M_L = 1.17$ lb-sec^2/in (support mechanism mass);

$M_B = 227$ lb-sec^2/in (test frame and foundation).

To predict the stiffness of the foundation, K_s, a method proposed by Wu (34) was utilized:

$$K_s = \frac{4\ G}{1-\nu} \sqrt{\frac{BL}{\pi}} \qquad\qquad (C.3)$$

where

G = soil shear modulus (4000 psi);

B = width of footing (7 ft);

L = length of footing (14 ft);

ν = Poisson's ratio (0.4).

The structural idealization provided a valuable aid for the inter-pretation of test data. Further refinement of mass and stiffness properties is not warranted because of the nature of the idealization. Although plastic behavior of the beam is neglected, the effect will be one of damping, and will have little influence on the frequencies related to the test frame components.

C.4 Characteristic Equations

Equations of motion are formulated utilizing energy principles and Lagrange's equation,

$$\frac{d}{dt}\left(\frac{\partial T}{\partial \dot{y}_i}\right) - \frac{\partial T}{\partial y_i} + \frac{\partial U}{\partial y_i} = W_i \tag{C.4}$$

where

T = kinetic energy;

U = strain energy;

W_i = generalized force;

y_i = time dependent generalized coordinate, y_n, y_a, y_L, y_B.

For each mass spring model the characteristic equation will be presented.

C.4.1 Beam on Simple Supports, Model I

For the simply supported beam, Model I, one finds

$$\omega = \pi^2 \sqrt{\frac{EI}{M_b L^3}} \tag{C.5}$$

or

$$\omega \approx 179 \text{ rad/sec.}$$

C.4.2 Beam on Elastic Supports, Model II

The characteristic equation for the beam on elastic supports, Model II, is found from

$$\begin{vmatrix} \dfrac{EI\,\pi^4}{2L^3} - \omega^2\,\dfrac{M_b}{2} & -\omega^2\,\dfrac{2M_b}{\pi} \\[4mm] -\omega^2\,\dfrac{2M_b}{\pi} & 2K_e - \omega^2\,M_b \end{vmatrix} = 0 \tag{C.6}$$

which yields frequencies

$$\omega_1 = 174 \text{ rad/sec;}$$

$$\omega_2 = 1540 \text{ rad/sec.}$$

The frequency ω_2 is related to the vibration of the reaction mechanism and load cells.

C.4.3 Beam and Test Fixture on Elastic Supports, Model III

The characteristic equation for the beam and test frame mounted on elastic supports is found from:

$$\begin{vmatrix} \dfrac{EI \, \pi^4}{2L^3} - \omega^2 \dfrac{M_b}{2} & -\dfrac{2M_b}{\pi} & 0 \\[2ex] -\omega^2 \dfrac{M_b}{\pi} & 2K_e - \omega^2 M_b & -2K_e \\[2ex] 0 & -2K_e & K_s + 2K_e - \omega^2 M_b \end{vmatrix} = 0 \qquad (C.7)$$
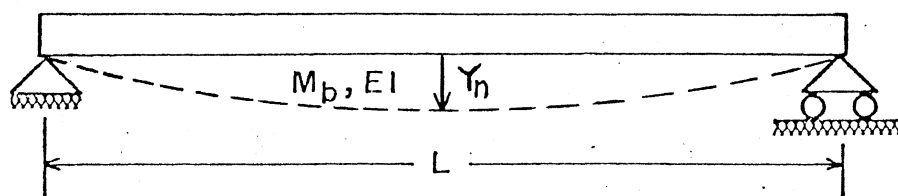
The frequencies of vibration for this system are

$$\omega_1 = 91 \text{ rad/sec;}$$
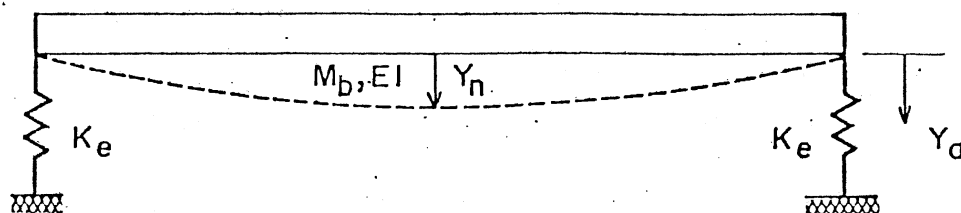
$$\omega_2 = 175 \text{ rad/sec;}$$

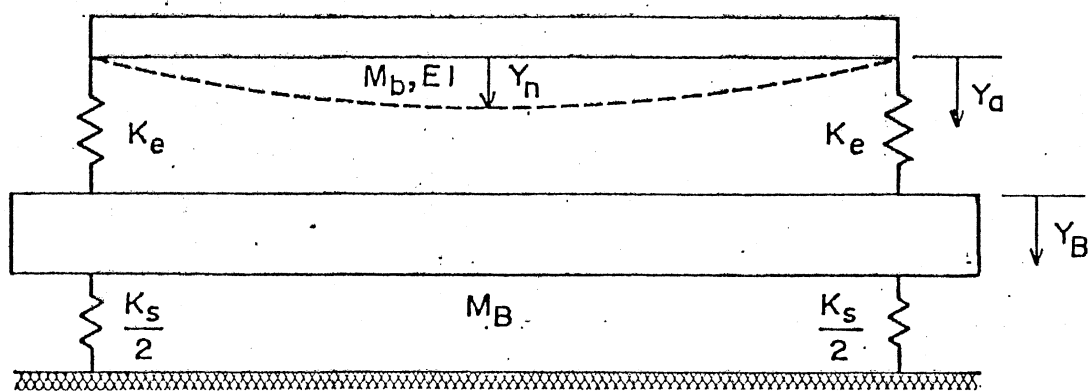$$\omega_3 = 1542 \text{ rad/sec.}$$

The lowest frequency, ω, is related to the vibration of the test structure on the soil spring. Note that it is significantly smaller than the beam frequency.

(a) Model I, Beam on Rigid Supports

(b) Model II, Beam on Elastic Supports

(c) Model III, Beam on Elastic Supports With Test
     Frame Motion

Figure 84. Spring Mass Models for Frequency Analysis

VITA

James Nelson Ingram

Candidate for the Degree of

Doctor of Philosophy

Thesis: AN INVESTIGATION OF THE EFFECTS OF HIGH INTENSITY IMPULSE
LOADS ON SIMPLY SUPPORTED REINFORCED CONCRETE BEAMS

Major Field: Civil Engineering

Biographical:

Personal Data: Born in Tucumcari, New Mexico, March 18, 1943, the
son of Mr. and Mrs. H. W. Ingram.

Education: Graduated from Tucumcari High School, Tucumcari, New
Mexico, in May 1961; graduated with a Bachelor of Aerospace
Engineering from the University of Kansas, Lawrence, Kansas, in
February, 1966; received the Master of Science degree from the
University of Kansas, Lawrence, Kansas, October, 1970; completed
the requirements for the Doctor of Philosophy degree from
Oklahoma State University in July, 1976.

Professional Experience: Student Engineer with Martin-Marietta
Aerospace Division, Denver, Colorado during the summers of 1963,
1964 and 1965 in the liaison engineering, computer science, and
loads and dynamics departments, respectively; Graduate Research
Assistant with the Center for Research in the Engineering
Sciences of the University of Kansas from January to September,
1967; Flight Dynamicist and, later, Aerodynamicist with the
Missile Systems Division of Beech Aircraft Corp., Wichita,
Kansas, from September, 1967 to January, 1973; and Graduate
Research Assistant, Oklahoma State University, Stillwater,
Oklahoma, from January, 1973 to May, 1975.

Professional and Honorary Societies: member of Chi Epsilon, member
of the American Concrete Institute; member of the American
Institute of Aeronautics and Astronautics.